Residential CO_2 Heat Pump System for Combined Space Heating and Hot Water Heating

by

Jørn Stene

Thesis submitted in partial fulfilment of the requirements for
the Degree of Doktor Ingeniør

NTNU - Norwegian University of Science and Technology
Faculty of Engineering Science and Technology
Department of Energy and Process Engineering

February 2004

EPT Report 2004:6

The purpose of technology should be to utilize:

- available material resources
- energy sources
- accumulated experience and know-how
- human creative power

for the best of mankind in a long-term perspective

Professor Gustav Lorentzen, Dr. Techn., 1915-1995

Preface

This thesis is a result of a doctoral study carried out at the Norwegian University of Science and Technology (NTNU), Department of Energy and Process Engineering during the period 2000-2004.

I am grateful to the following institutions and companies, which provided funding and granted various types of equipment for the experimental work:

- *The Research Council of Norway* – funded my doctoral scholarship through the doctoral programme "Energy for the Future".
- *SINTEF Energy Research*, Department of Energy Processes – funded the construction of the prototype CO_2 heat pump unit.
- *Sanyo Ltd (Japan)* – granted the rolling piston CO_2 compressor.
- *Satchwell Norge* AS – granted the Satchwell data acquisition system.
- *Høiax Norge AS* – granted several single-shell hot water tanks.
- *Båsum Boring Trøndelag AS* – drilled the energy well and installed the brine system for the pilot house.

I would like to thank my supervisors, Professor *Arne M. Bredesen*, Professor *Jostein Pettersen* and Associate Professor *Rolf Ulseth* at NTNU, Department of Energy and Process Engineering, for their assistance during my doctoral study. I am also grateful to the following colleagues at NTNU and SINTEF for their assistance (in alphabetical order):

- *Arvid Almenning* – for assistance during manufacturing of the CO_2 heat exchangers as well as other kinds of assistance.
- *Jostein Bakken* – for assistance regarding the measuring equipment.
- *Martin Bustadmo* – for assistance during manufacturing of the CO_2 heat exchangers as well as other kinds of assistance.
- *Stewart Clark* – for assistance in editing this thesis.
- *Trygve M. Eikevik* – for making it possible to fund and construct the prototype CO_2 heat pump unit.

- *Armin Hafner* – for all kinds for invaluable practical/technical assistance and for "accommodating" the prototype CO_2 heat pump system.
- *Helge J. Johansen* – for calibrating the measuring equipment.
- *Kjell Kolsaker* – for providing help regarding the NMF/IDA software.
- *Gunnar Lohse* and *Terje Strandheim* – for performing the electrical installation for the prototype CO_2 heat pump unit.
- *Harald S. Mæhlum* and *Knut Glasø* – for making helpful arrangements in the laboratory at NTNU/SINTEF.
- *Inge Håvard Rekstad* – for information regarding the compressors.
- *Christian Schorn* – for installing the Satchwell outstation and the programming of the Satchwell data acquisition system.
- *Geir Skaugen* – for making the thermodynamic and transport properties of CO_2 and other working fluids as well as heat transfer and pressure drop correlations available on Microsoft Excel.
- *Reidar Tellebon* – for constructing the prototype CO_2 heat pump unit, for modifying the hot water tank and for a lot of invaluable assistance when the CO_2 heat pump had to be modified or repaired.
- *Eugen Uthaug* – for assistance regarding software installation and computer troubleshooting.
- *Gholam R. Zakeri* – for providing help regarding the development of the computer model for the tripartite gas cooler.

I would also like to thank the rest of my colleagues for many interesting discussions, your encouragement and for making NTNU/SINTEF a inspiring and wonderful place to work.

Last but not least. I am deeply grateful to you my dear wife *Xiaoyun* for your love, patience and endless support during my doctoral work. And to my precious 7 year-old son *Michael*; I am very sorry that during longer periods I had to give priority to my doctoral work, and was unable to play with you as much as you (and I) wanted. Fortunately, you soon started to look forward to that day when my doctoral work would be finalised and I could be a 100% father again.

Trondheim February 2004

Jørn Stene

Summary and Conclusions

Carbon dioxide (CO_2, R-744) has been identified as a promising alternative to conventional working fluids in a number of applications due to its favourable environmental and thermophysical properties. Previous work on residential CO_2 heat pumps has been dealing with systems for either space heating or hot water heating, and it was therefore considered interesting to carry out a theoretical and experimental study of residential CO_2 heat pump systems for combined space heating and hot water heating – so-called integrated CO_2 heat pump systems. The scope of this thesis is limited to brine-to-water and water-to-water heat pumps connected to low-temperature hydronic space heating systems.

Gas Cooler Design and System Evaluation

Due to the low critical temperature of CO_2, an integrated CO_2 heat pump unit will give off heat by cooling of CO_2 at supercritical pressure in a gas cooler. In order to achieve a high coefficient of performance (COP), it is essential that useful heat is given off over a large temperature range, resulting in a relatively low CO_2 outlet temperature from the gas cooler.

A number of gas cooler configurations were evaluated. It was found that the application of *a tripartite gas cooler* for preheating of domestic hot water (DHW), low-temperature space heating and reheating of DHW, would enable production of DHW in the required temperature range from 60 to 85ºC, and contribute to the highest possible COP for the integrated CO_2 heat pump unit. In the investigated CO_2 heat pump system, the gas cooler units for heating of DHW were connected to a single-shell storage tank by means of a closed water loop.

Experimental Activities and Modelling

The Prototype Brine-to-Water CO_2 Heat Pump Unit

A test rig for a 6.5 kW residential brine-to-water CO_2 heat pump unit for combined space heating and hot water heating was built in order to document the performance and to study component and system behaviour over a wide range of operating conditions. The prototype heat pump was

equipped with a counter-flow tube-in-tube evaporator, a hermetic two-stage rolling piston compressor, a counter-flow tripartite tube-in-tube gas cooler, a low-pressure receiver (LPR) and a manual back-pressure valve.

The heat pump was tested in three different modes; Simultaneous space heating and DHW heating, DHW heating only and space heating only. The compressor was operated at 6000 rpm, and most tests were carried out at an evaporation temperature of -5ºC. The heat pump unit gave off heat to a low-temperature floor heating system at supply/return temperatures of 33/28, 35/30 or 40/35ºC. In the combined heating mode and the DHW heating mode, the set-point for the DHW temperature was 60, 70 or 80ºC. At each temperature programme for the space heating and DHW systems, the inlet gas cooler pressure was varied to check its impact on the heating capacity, the COP and the temperature profiles in the tripartite gas cooler.

A steady-state computer model for integrated CO_2 heat pump units using a tripartite counter-flow tube-in-tube gas cooler was developed in order to analyse and supplement the measurements from the prototype heat pump test rig. The model, which was established in Microsoft Excel/Visual Basic, was verified by means of measurements from the test rig.

The prototype CO_2 heat pump system was also analysed by means of the exergy method in order to document the thermodynamic losses in the components and sub-systems, and to check the possibilities for efficiency improvements.

The DHW Storage Tank and the Movable Insulating Plate

A test rig comprising a 200 litre cylindrical single-shell DHW tank was constructed, in order to measure the transient temperature development in the tank caused by conductive heat transfer through the tank walls and between the hot and cold water in the tank during the tapping and charging periods. The test rig was also used to examine the thermal performance and the functionality of a movable insulating plate, which was used to eliminate the mixing and to reduce the conductive heat transfer between the hot and cold water in the tank. Two different insulating plates made of 50 mm extruded polystyrene (XPS) and equipped with balancing weights were tested. During all tests, the tank was insulated with 40 mm fibre-glass, the city water temperature and the DHW temperature were around 5 and 55ºC, respectively, and the room temperature was between 20 and 22ºC.

A transient two-dimensional heat conduction model was developed in order to calculate the transient temperature profiles (thermoclines) in cylindrical single-shell DHW tanks at actual tank designs, temperature levels and gas cooler heating capacities. The model, which was established in the Neutral Model Format (Sahlin, 1996) and IDA (Equa Simulation Technology Group, 1996), was verified by means of measurements from the DHW test rig.

Results and Conclusions

Integrated CO_2 Heat Pumps

- Residential CO_2 heat pump systems for combined space heating and hot water heating may achieve the same or higher seasonal performance factor (SPF) than the most energy efficient state-of-the-art brine-to-water heat pumps as long as:
  - The CO_2 heat pump unit covers the entire DHW heating demand, and the annual heat delivered for DHW production is minimum 25 to 30% of the total annual heat delivered from the heat pump.
  - The CO_2 heat pump unit is operated in the combined heating mode when there is a simultaneous space heating and DHW heating demand.
  - The return temperature in the hydronic space heating system is about 30ºC or lower.
  - The city water temperature is about 10ºC or lower.
  - The thermodynamic losses in the DHW storage tank are low, i.e. negligible mixing losses and minimum conductive heat transfer between the hot and cold water during tapping and charging.
- In contrary to conventional heat pump systems for combined space heating and DHW heating, the integrated CO_2 heat pump system achieves the highest COP in the combined heating mode and the DHW heating mode, and the lowest COP in the space heating mode. Hence, the larger the annual DHW heating demand, the higher the SPF of the integrated CO_2 heat pump system.
- The lower the return temperature in the space heating system and the lower the DHW storage temperature, the higher the COP of the integrated CO_2 heat pump. A low return temperature in the space heating system also results in a moderate DHW heating capacity ratio, which

means that a relatively large part of the annual space heating demand can be covered by operation in the combined heating mode, where the COP is considerably higher than in the space heating mode.

- During operation in the combined heating mode and the DHW heating mode, the COP of the integrated CO_2 heat pump is heavily influenced by the inlet water temperature for the DHW preheating gas cooler unit. The lower the inlet temperature, the higher the COP. The CO_2 system will therefore achieve the highest COP at low city water temperatures, and when there is negligible mixing and minimum conductive heat transfer between the hot and cold water in the DHW tank during the tapping and charging periods.

- The COP for the integrated CO_2 heat pump is generally more sensitive to variations in the compressor efficiency than that of conventional brine/water-to-water heat pump systems. It is therefore of particular importance to apply a high-efficiency compressor.

- At each operating mode and temperature programme, there will be an optimum gas cooler (high-side) pressure that leads to a maximum COP for the integrated CO_2 heat pump. However, at moderate DHW temperatures, the heat pump can be operated at constant high-side pressure in all heating modes with only a minor reduction in the COP. This is favourable, since it simplifies the operation of the system and reduces the first cost.

- During operation in the combined heating mode, the COP for the integrated CO_2 heat pump may be higher than in the DHW heating mode due to similar temperature approaches at the cold outlet of the gas coolers and lower optimum high-side pressure. The higher the DHW temperature, the larger the COP difference for the operating modes.

- The integrated CO_2 heat pump system will be more complex than the state-of-the art residential heat pump systems due to the requirement for a tripartite gas cooler, extra valves and tubing for by-pass of fluids, an inverter controlled pump in the DHW circuit as well as an especially designed DHW storage tank. The application of optimum high-side pressure control will further increase the technical and operational complexity of the system.

Domestic Hot Water (DHW) Storage Tanks

- Conductive heat transfer between the DHW and the cold city water in the storage tank during the tapping and charging periods may result in a considerable increase in the inlet water temperature for the DHW preheating gas cooler. This will in turn reduce the COP of the integrated CO_2 heat pump. The thermodynamic losses are highest at large initial temperature differences for the DHW and the city water, small charging volumes and low gas cooler heating capacities. Inevitable mixing of hot and cold water in the tank will lead to further increase in the thermodynamic losses for the CO_2 heat pump system.

- One possible way to reduce internal conductive heat transfer and avoid the mixing in cylindrical single-shell DHW storage tanks, is to separate the DHW and the city water by means of a movable plate with low thermal conductivity. The concept proved to give satisfactory thermal performance and functionality at atmospheric operating conditions. However, definite conclusions regarding the functionality, thermal performance and optimum design can only be drawn after full-scale testing has been carried out in a pressurised tank. First-costs as well as the long-term reliability of the insulating plate are also important issues that need to be further addressed.

Suggestions for Further Work

On the basis of the results and conclusions from this thesis, the suggestions for further work are as follows:

- To develop a steady-state computer model for in-depth analyses and optimisation of integrated CO_2 heat pump systems, including the calculation of the SPF based on hourly time steps.

- To analyse the economic feasibility for an integrated brine-to-water CO_2 heat pump system for residential use.

- To study the operational characteristics and the performance of an integrated CO_2 heat pump system using ambient air as the heat source.

- To develop a low-cost and high-efficiency tripartite gas cooler.

- To carry out further analyses and tests on a movable insulating plate for cylindrical single-shell DHW tanks.

Table of Contents

1 Introduction

This chapter presents the background for the doctoral work, focusing on the main reasons for carrying out a theoretical and experimental study of residential brine-to-water and water-to-water CO_2 heat pump systems for combined space heating and hot water heating. The last part of the chapter presents the objectives and scope of the doctoral work as well as the structure of the thesis.

1.1 Background for the Doctoral Work

1.1.1 Working Fluids and the Environment

During the last fifteen to twenty years, the most pressing research issue within the field of refrigeration, air-conditioning and heat pump systems has been the search for environmentally acceptable working fluids which can replace the ozone-depleting ChloroFluoroCarbons (CFCs) and Hydro-ChloroFluoroCarbons (HCFCs). Most of the substances evaluated and tested have been new synthetic compounds, namely *HydroFluoroCarbons (HFCs)*. Although these compounds are non-toxic, non-flammable, non-carcinogenic and have zero ozone depletion potential (ODP), they have environmental drawbacks:

- The global warming potential (GWP factor) of the most commonly used HFCs is about 1300 to 3500 times higher than that of CO_2 (UNEP, 1998). Due to this fact, the HFCs have been implemented in the Kyoto Protocol[1] to the United Nations Framework Convention on Climate Change, together with CO_2, methane and NO_x.
- During production of HFCs, toxic and harmful wastes are released, including fluorinated materials, vinyl chloride, ethylene dichloride (carcinogenic), other chlorinated organics, HFCs and HCFCs (Banks and Sharrat, 1996).

[1] *The Kyoto Protocol - http://www.untreaty.un.org/English/notpubl/kyoto-en.htm*

Since the HFCs are foreign to nature, widespread use of these fluids will always include *a potential risk* of unexpected negative global environmental effects, as already experienced with the CFCs and the HCFCs.

An alternative to the HFCs is to apply naturally occurring and ecologically safe substances, so-called natural working fluids. The most important substances in this category are ammonia, hydrocarbons, carbon dioxide, water and air. From an environmental point of view, *carbon dioxide (CO_2, R-744)* can be regarded as an almost ideal working fluid since it is non-toxic, non-flammable and neither contributes to ozone depletion nor global warming[2]. In former days, CO_2 was used as a working fluid in many refrigerating and air conditioning applications. With the introduction of the CFCs in the 1930s and the HCFCs in the 1950s, the application of CO_2 was gradually reduced until it ceased completely during the 1960s. However, after several decades of ignorance, CO_2 was "rediscovered" as a working fluid by Lorentzen and Pettersen (1993), who initiated several projects regarding CO_2 heat pump and air conditioning systems. Due to considerable international research and development activities in recent years, CO_2 now appears as a viable long-term alternative to the HFCs in a number of residential, commercial and industrial applications.

1.1.2 Residential CO_2 Heat Pump Systems

Since virtually all residential heat pump units are charged with HFCs, it is relevant to examine whether CO_2 heat pumps can be successfully applied in the residential sector.

1.1.2.1 Research Projects on Residential CO_2 Heat Pump Systems

In recent years a number of universities, research institutions and companies have been evaluating and testing various types of residential CO_2 heat pump systems. The applications include CO_2 heat pump water heaters (Saikawa and Hashimoto, 2000), CO_2 heat pumps for the retrofitting of boilers in high-temperature radiator systems (Brandes and Kruse, 2000), CO_2 heat pumps in combination with low-temperature heat distribution systems (Kerherve and Clodic, 2002), air-to-air heat pump systems for the heating of ventilation air (Rieberer and Halozan, 1998), and reversible split-type air-to-air CO_2 heat pumps (Richter et al., 2002; Aarlien, 2002).

[2] *The CO_2 which is used as a working fluid is a by-product from industrial processes.*

1.1.2.2 A Residential CO_2 Heat Pump System for Combined Space Heating and Hot Water Heating

Previous work on residential CO_2 heat pumps has been dealing with systems for either space heating or hot water heating. It was therefore considered interesting to carry out a theoretical and experimental study of residential brine-to-water and water-to-water CO_2 heat pump systems for combined low-temperature space heating and hot water heating. The main reasons for selecting this heat pump concept were as follows:

- *Increasing Relative Heating Demand for Domestic Hot Water*

  Due to stricter building codes, the transmission and infiltration losses in houses have been considerably reduced in recent years, whereas the ventilation losses and the domestic hot water (DHW) heating demand have become more significant. Hence, the annual heating demand for DHW in new houses constitutes an increasing part of the total heating demand (Breembroek and Dieleman, 2001).

- *High-Efficiency Ground-Source and Water-Source Heat Pumps*

  The average seasonal performance factor (SPF) of ground-source and water-source heat pump systems is typically 25% higher than that of air-source systems (Gilly et al., 1999). They also maintain the heating capacity at low ambient temperatures, and have longer operational life-time due to relatively high and stable evaporation temperatures.

- *Low-Temperature Heat Distribution Systems*

  The lower the distribution temperature, the higher the SPF of the heat pump system. Residential low-temperature floor heating systems are now gaining an increasing market share in many European countries, while central low-temperature air heating systems are commonly used in the USA and Canada. (Breembroek and Dieleman, 2001).

1.2 Objectives of the Doctoral Work

The main objective of the doctoral work has been:

To carry out a theoretical and experimental study of residential brine-to-water and water-to-water CO_2 heat pump systems for combined low-temperature space heating and hot water heating, and to compare the performance with the state-of-the-art heat pump technology.

This objective had a number of sub-goals:

- Identify and evaluate possible system designs, and apply the most promising concept in the further work.
- Carry out a thermodynamic analysis for the selected system, and evaluate the most important factors that affect the energy efficiency.
- Design and test a prototype residential brine-to-water CO_2 heat pump system for combined space heating and hot water heating.
- Carry out computer simulations to analyse the CO_2 heat pump system and to supplement the measurements from the test rig.
- Compare the performance of the CO_2 heat pump system with the performance of state-of-the-art residential heat pump systems.

1.3 Structure of the Thesis

- **Chapter 2**, *Technological Status of Residential Heat Pumps for Space and Hot Water Heating*, provides an overview of the technological status for residential brine-to-water and water-to-water heat pump systems for combined space heating and hot water heating. A brief overview of the development in heating demands in houses as well as common design and temperature requirements for low-temperature hydronic space heating systems are also presented. The final part of the chapter summarizes the research and development work on residential CO_2 heat pump systems.
- **Chapter 3**, *Theoretical Background and System Evaluations*, provides a theoretical analysis of residential brine-to-water and water-to-water CO_2 heat pump systems for combined space heating and hot water heating. It focuses on the design, general operational characteristics and the performance of the CO_2 gas cooler and the hot water system. The application of a movable insulating plate, that reduces the conductive heat transfer inside the DHW storage tank and eliminates the mixing of hot and cold water, is also analysed.
- **Chapter 4**, *Test Rig Design and Experimental Methods*, presents the design, instrumentation and experimental procedures for two test rigs: A 6.5 kW residential brine-to-water CO_2 heat pump system for combined space heating and hot water heating (prototype), and a

cylindrical single-shell 200 litre DHW storage tank. A movable insulating plate, which was applied to reduce the exergy losses in the tank, was also tested in the latter test rig.

- **Chapter 5**, *Experimental Results*, provides a detailed presentation and analysis of the experimental results from the two test rigs described in Chapter 4.

- **Chapter 6**, *Modelling*, presents the thermodynamic background and mathematical basis for two computer models that were developed to study the performance of tripartite counter-flow tube-in-tube CO_2 gas coolers and cylindrical single-shell DHW tanks.

- **Chapter 7**, *Discussion and Analysis*, provides an overview and a discussion of the most important findings from the experiments and simulations regarding the CO_2 heat pump unit and the DHW tank. A thermodynamic (exergy) analysis of the prototype CO_2 heat pump as well as an overall estimate of the SPF for two CO_2 heat pump systems and a state-of-the-art heat pump system, are also presented.

- **Chapter 8**, *Conclusions and Suggestions for Further Work*, presents the main conclusions from the doctoral work and suggestions for further work.

- **Appendices**

  A) Outlines and discusses important properties and characteristics of CO_2 as a working fluid in heat pumps.

  B) Presents standards for testing of brine-to-water and water-to-water heat pumps and recent test results for residential units.

  C) Provides an overview of the test results for the prototype CO_2 heat pump unit.

  D) Presents the uncertainties in the single measurements and the computed values for the prototype CO_2 heat pump unit.

  E) Displays photos of the prototype CO_2 heat pump unit.

  F) Presents characteristic properties of DHW systems.

  G) Discusses the design of the balancing weight and the selection of plate material for a movable insulating plate in DHW tanks.

  H) Presents the test conditions for the movable insulating plates.

  I) Presents the NMF and IDA files for the transient two-dimensional heat conduction model for cylindrical DHW tanks.

2 Technological Status for Residential Heat Pumps for Space and Hot Water Heating

This chapter provides an overview of the technological status of residential ground-source and water-source heat pump systems for combined space heating and hot water heating – so-called integrated brine-to-water and water-to-water heat pumps.

The initial part of the chapter presents a classification of residential heat pump systems, and briefly describes the development in heating demands for houses as well as the main characteristics and typical temperature requirements for hydronic heat distribution systems. The state-of-the-art-technology for residential brine-to-water and water-to-water heat pump systems is presented, focusing on commonly used working fluids, component and system designs, energy efficiency and main operational characteristics. The final part of the chapter summarizes the research and development work on residential CO_2 heat pump systems.

2.1 Classification of Residential Heat Pump Systems

Figure 2.1 shows a possible way to classify *residential heating-only heat pump systems* according to the heating demand(s) that are covered by the heat pump, the type of heat source and heat distribution system(s) and whether the system is monovalent or bivalent. *Monovalent* heat pumps cover the entire annual space heating demand, whereas *bivalent* heat pumps are sized for 40 to 60% of the maximum heat load and cover about 50 to 90% of the annual space heating demand in the house. The remaining heat load is covered by an auxiliary heating system (peak load).

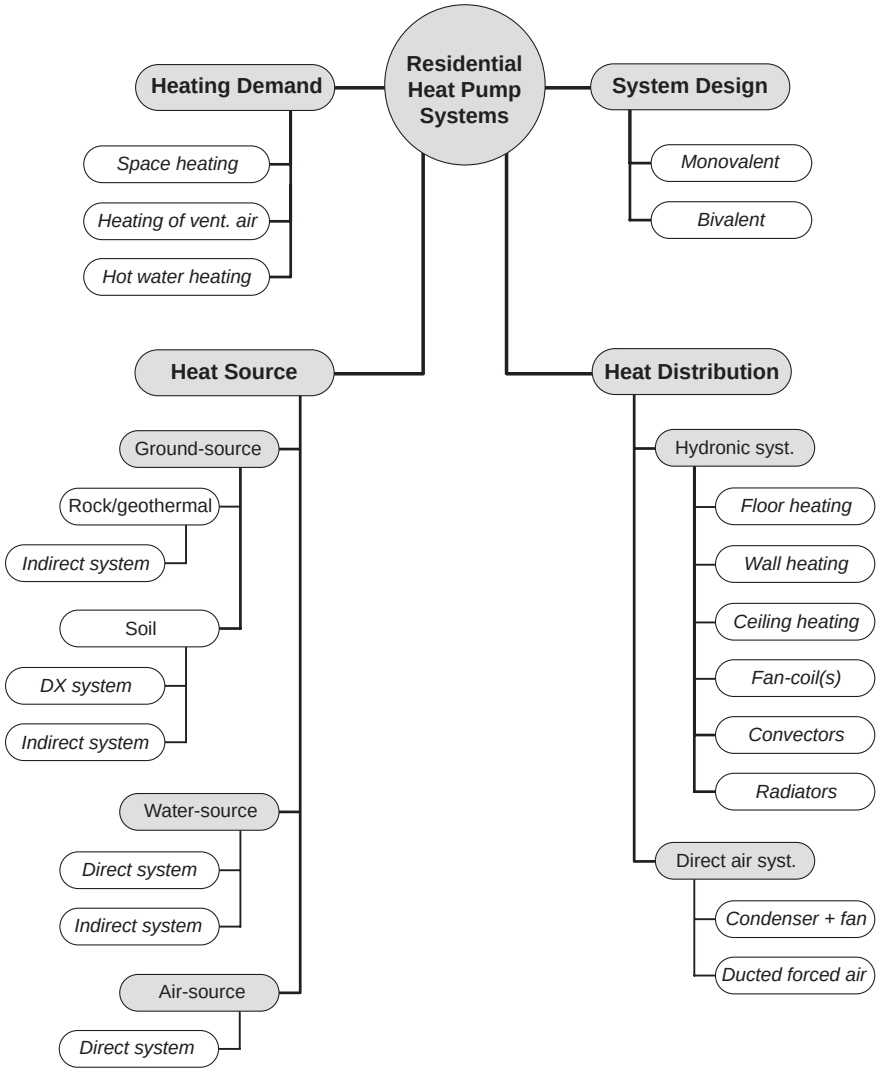

Figure 2.1 Classification of residential heating-only heat pump systems according to the heating demand(s), the type of heat source and heat distribution system(s) and monovalent/bivalent system design. "DX system" and "Indirect system" refer to direct expansion systems and brine systems, respectively.

Although Figure 2.1 classifies heating-only heat pump systems, a brine-to-water ground-source heat pump system can be utilized as *a combined heating and cooling system* by connecting one or several fan-coil units to the brine system.

2.2 Heating Demands in Houses

The heating demands in a house are caused by transmission and infiltration losses through the building envelope, ventilation losses when fresh air is supplied to the house by means of a ventilation system, and heating of domestic hot water (DHW). Owing to the implementation of more stringent building codes, the transmission and infiltration losses in new houses have been considerably reduced in recent years. Various standards for *low-energy houses* have also been established in Europe, the USA and Canada. The annual transmission and ventilation losses in these houses are typically 40 to 50% lower than that of new houses which are designed in accordance with prevailing building regulations (Breembroek and Dieleman, 2001).

Owing to the decreasing space heating demand and the fact that about 70% of the ventilation losses in balanced ventilation systems can be recovered by heat exchange, the annual heating demand for DHW constitutes an increasing share of the total heating demand in new houses. Figure 2.2 shows, as an example, the development of the different heating demands in German single-family houses (Breembroek and Dieleman, 2001). According to Afjei (1997) and Breembroek and Dieleman, the DHW ratio[1] typically ranges from 10 to 15% in existing houses and from 20 to 45% in new houses and low-energy houses.

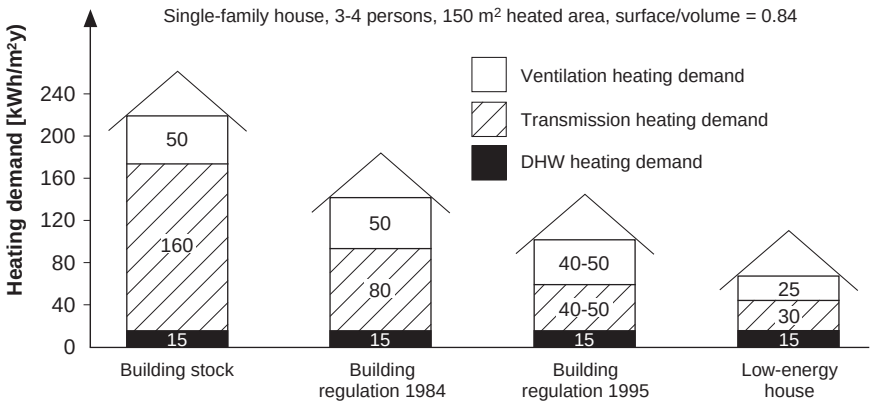

Figure 2.2 Development of the annual heating demand [kWh/(m²year)] for German single-family houses with 150 m² heated area and 3-4 residents (Breembroek and Dieleman, 2001).

[1] *The ratio of the annual DHW heating demand and the total annual heating demand of the house when heating of ventilation air is excluded.*

2.3 Hydronic Heat Distribution Systems

2.3.1 Main Characteristics

Heat distribution systems for residential heat pumps can be classified as *ductless air systems* (space conditioning), *central air systems* (space conditioning and ventilation) and *hydronic systems* (space heating and heating of ventilation air*)*. However, since the scope of this thesis is limited to brine-to-water and water-to-water heat pump systems, only hydronic heat distribution systems will be presented in more detail.

A hydronic heat distribution system comprises a closed-loop piping system, circulation pumps, an expansion system as well as terminal units for rejection of heat. Common terminal units are radiators, convectors, floor/wall/ceiling heating systems as well as fan-coil units. In contrary to ductless and central air systems, hydronic heat distribution systems can be connected to an accumulator tank (thermal storage), which can be used to shave electric peak loads and utilize off-peak electricity tariffs. The systems also enable separate temperature control in the rooms, and they generally have low parasitic energy demands and low distribution losses (Breembroek and Dieleman, 2001). However, a separate ventilation system is required in order to provide adequate indoor air quality in modern air-tight houses. With the exception of simple fan-coil systems, the state-of-the-art hydronic systems have relatively high investment and installation costs, and they are therefore mainly considered a viable option in new houses or houses that are being rehabilitated.

2.3.2 Temperature Requirements

Table 2.1 presents common temperature requirements for different types of terminal units in hydronic heat distribution systems installed in houses in Europe, the USA and Canada (Breembroek and Dieleman, 2001).

Table 2.1 Common temperature requirements for different types of terminal units in hydronic heat distribution systems (Breembroek and Dieleman, 2001).

System	Radiators	Convectors	Floor Heating	Fan-Coils
Temperature	60 – 80ºC	45 – 55ºC	35 – 45ºC	40 – 50ºC

According to Halozan (1997) and Afjei (1997), a supply temperature in the range from *28 to 32ºC* at design conditions is feasible for floor heating systems installed in low-energy houses.

2.3.3 Floor Heating Systems

Owing to the low distribution temperature, hydronic floor heating systems are particularly interesting in combination with brine-to-water and water-to-water heat pump systems, since a high seasonal performance factor (SPF) can be achieved (Afjei, 1997; Erb and Hubacher, 2001).

As long as draught from windows are prevented by means of windows with low U-values, floor heating systems contribute to superior thermal comfort and good indoor air quality due to moderate air temperatures, small vertical temperature gradients, low air speed and turbulence, little dust movement and no dust-burning (Breembroek and Dieleman, 2001).

Modern floor heating systems consist of diffusion-tight plastic tubes (OD 12 to 22 mm), which are embedded in concrete slabs, covered with concrete or gypsum on wooden sub-floors or installed on wooden sub-floors by means of thin profiled aluminium plates on prefabricated, insulating fibre boards, pressed wallboards or expanded polyester plates. In order to minimize the heat loss to the ground, 100 to 200 mm of non-compressible insulation (e.g. XPS) is recommended for basement installations (Breembroek and Dieleman, 2001; Woodson, 1999).

The optimum floor surface temperature when using a floor heating system ranges from about 24 to 27ºC, which corresponds to a heat transfer rate between 35 and 60 W/m^2 (Breembroek and Dieleman, 2001). The required distribution temperature is determined by the outside tube diameter, the tube (C-C) distance, the water flow rate, the thermal resistance below the tubes, the thermal resistance between the tubes and the ambient air, the required heat transfer rate and the room temperature. In order to obtain a relatively uniform floor surface temperature, the water flow is cooled down maximum 5 K (Woodson, 1999).

Floor heating systems are usually controlled by room thermostats and an outdoor air thermostat which control the supply temperature and the water flow (on/off) for the various tube sections. In floor heating systems with concrete or gypsum floors, the floor will act as a thermal storage, and the surface temperature will change very slowly when the water temperature changes (i.e. high inertia and large time constant). Floor heating systems

with a low thermal mass will correspondingly have a much lower time constant, which leads to more effective temperature control in the rooms. Due to the moderate temperature difference between the water in the tubes and the air, floor heating systems also have a self-regulating effect, and the lower the water temperature, the larger the reduction in the heat transfer rate at elevated room temperatures. Consequently, in low-temperature floor heating systems, the water temperature can be kept constant, and the heat emission from the system can be controlled solely by intermittent operation of the solenoid valves (Afjei, 1997).

2.4 The Heat Pump System

2.4.1 Design of the Heat Pump Unit

Residential brine-to-water and water-to-water heat pump units are generally equipped with the following main components:

- Plate heat exchangers (PHE) as evaporator and condenser
- Hermetic scroll or reciprocating compressor
- Thermostatic expansion valve (with external pressure equalization)
- Liquid receiver/accumulator (large capacity units only)
- Suction gas heat exchanger (propane and R-134a units)
- Subcooler (rarely included)
- De-superheater – tube coil or plate heat exchanger (rarely included)
- Expansion tank (brine systems only)
- Pumps for the secondary brine/water systems (not always included)
- Safety equipment, power supply, control/monitoring system

The heat pumps are using *R-404A*, *R-407C*, *R-410A*, *HFC-134a* (R-134a), *R-290* (propane) or *R-1270* (propene) as the working fluid. Table 2.2 presents some important physical and thermophysical properties for the most commonly used fluids.

Since R-134a has a considerably lower volumetric heating capacity than the other working fluids, R-134a heat pump units are mainly utilized in high-temperature radiator systems as well as in houses with a considerable DHW heating demand.

Table 2.2 Important physical and thermophysical properties for working fluids used in residential brine-to-water and water-to-water heat pump units (RnLib, 2003).

Property	R-290	R-407C	R-410A	R-134a
Normal boiling point [ºC]	-42.1	-43.8[1]	-51.6	-26.2
Critical temperature [ºC]	96.8	87.3	72.5	101.1
Critical pressure [MPa]	4.25	4.63	4.95	4.07
Condensation temp. at 2.5 MPa [ºC]	67.6	60.1	56.1[2]	77.6
Volumetric heating capacity at 0°C [kJ/m^3]	3880	4115	6737	2866

1) The mean of the bubble point and dew point has been used as the datum temperature

2) Condensation temperature at 3.5 MPa for R-410A

Figure 2.3 shows a typical design of a residential brine-to-water heat pump.

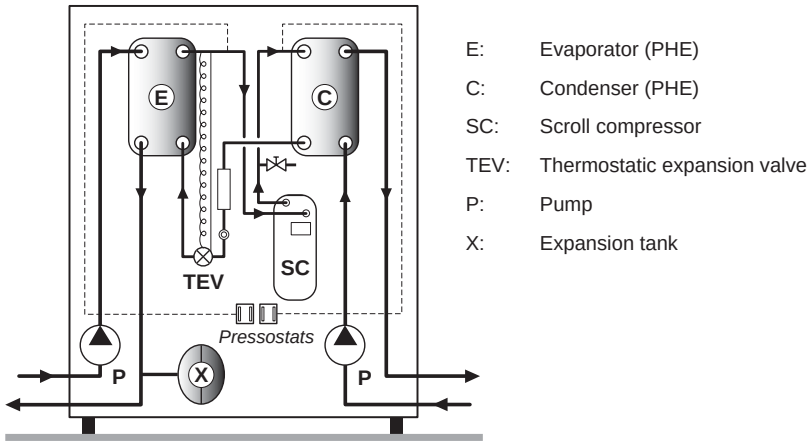

Figure 2.3 Typical design of a residential brine-to-water heat pump unit.

Recent test results from the heat pump test stations at WPZ Töss and TNO-MEP, demonstrates that the most energy efficient residential brine-to-water heat pumps on the market in the capacity range from about 5 to 7 kW, achieve a coefficient of performance (COP) of about 4.6 and 3.3 at inlet brine temperatures and outlet water temperatures of 0/35ºC and 0/50°C, respectively. Reference is made to Appendix B, *Performance Testing of Residential Brine-to-Water and Water-to-Water Heat Pumps*, for further details regarding performance testing of this kind of heat pump units.

2.4.2 Design of the Heat Pump System

2.4.2.1 Application of an Accumulator Tank

The heating capacity of residential brine-to-water and water-to-water heat pumps is controlled by *intermittent operation*, i.e. start and stop of the compressor. In hydronic heat distribution systems with moderate water volumes and/or limited thermal storage capacity, an accumulator tank is required in order to prevent frequent starts and stops of the compressor when heating demands are low. In countries offering low electricity tariffs at night-time or reduced electricity tariffs for heat pumps that can be switched off during peak hours at daytime, the storage volume of the accumulator tank will typically range from 800 to 1000 litres, and often be complemented by thermal storage in concrete floors.

2.4.2.2 Application of a DHW Storage Tank

In order to level the load for DHW heating during the day and night, virtually all residential stand-alone systems use a storage tank which is designed according to the momentary and average DHW demand in the house. In a residential heat pump system, the storage tank is either an integral part of the heat pump or a separate free-standing unit.

DHW systems are usually designed as *closed unvented systems*, where the storage tank is connected to the city water supply (cold mains). The static operating pressure inside unvented tanks typically ranges from 4 to 6 bars. In *open vented systems*, the storage tank has an open vent to the atmosphere. The DHW is then gravity fed to washbasins, bathtubs etc., and is distributed by means of booster pumps to showers and whirlpools.

The following types of DHW tanks are used together with residential brine-to-water and water-to-water heat pump units:

- *Single-shell DHW tanks* are usually cylindrical, and the tank volume typically ranges from 100 to 350 litres. The DHW is either preheated by the hot water from the heat pump condenser which circulates through an integrated tube-coil in the tank, or the water is heated to the set-point temperature by means of a de-superheater in a closed water-loop. Reheating and back-up heating of the DHW are usually provided by an electric immersion element.

- *Double-shell DHW tanks* are constructed from a cylindrical primary vessel for the DHW and a secondary vessel or water jacket. Typical water volumes for the primary/secondary vessels are 200/120 and 300/120 litres. The hot water from the heat pump condenser circulates through the secondary vessel and preheats the DHW. Reheating and back-up heating of the DHW are usually provided by an electric immersion element.

2.4.2.3 Examples of System Designs

Utilization of Condenser Heat for Hot Water Heating

The large majority of residential brine-to-water and water-to-water heat pumps preheat DHW by means of the condenser heat, and the higher the outlet water temperature from the condenser, the less reheating is required in order to meet the minimum DHW storage temperature of 55 to 60ºC. The minimum storage temperature is set to prevent growth of *the legionella bacteria* that cause the fatal legionnaires' disease (USHA, 2003).

Figure 2.4 shows the principle of two different residential pump systems for low-temperature space heating and DHW heating.

In *alternative A,* the system comprises an accumulator tank and a single-shell DHW tank with an integral tube-coil heat exchanger. Double-shell DHW tanks are also commonly used. The shuttle-valve directs the water flow either to the accumulator tank for the space heating system or the DHW tank, and heating of DHW is prioritized. When the heat pump unit supplies heat to the space heating system, the required supply temperature from the heat pump condenser is determined by the outdoor temperature and the return temperature in the space heating system, i.e. variable condensation temperature. During operation in the DWH mode, the water flow rate through the condenser will be lower and the return temperature will be higher than that of the space heating mode. Depending on the type of working fluid, the heat pump unit is able to preheat the DHW to a temperature of 45 to 60ºC.

In *alternative B,* the secondary vessel in the double-shell DHW tank acts as the thermal storage, and heat is transferred to the DHW through the bottom of the primary vessel. When the heat pump unit delivers heat to a low-temperature floor heating system, there will be an inevitable trade-off between the supply temperature from the condenser, which determines the COP of the heat pump unit and the degree of DHW preheating, and the need for supplementary heating in the DHW system. The lower the supply temperature, the more supplementary heating is required.

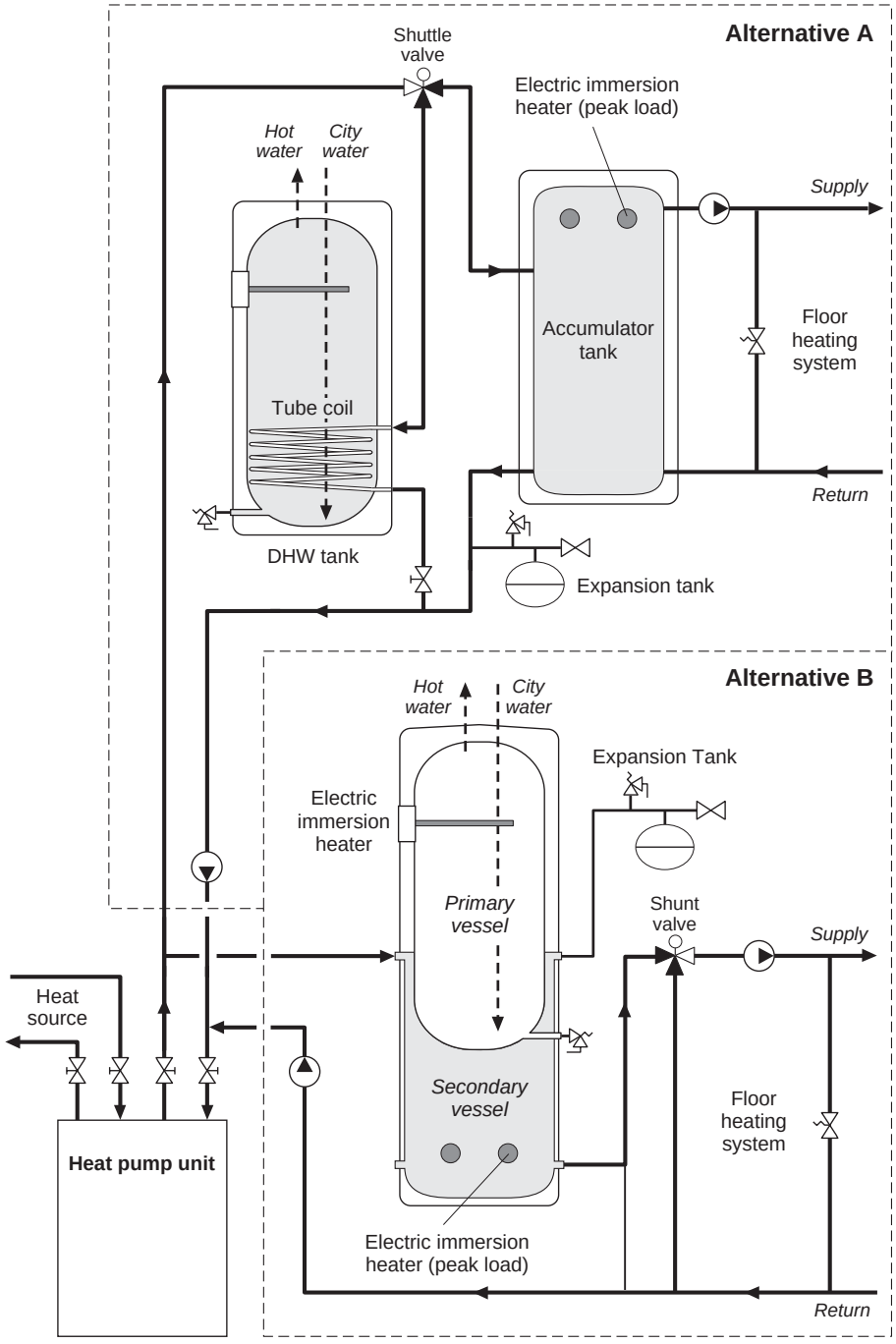

Figure 2.4 Principle of a residential heat pump system for space heating and DHW heating: A) Single-shell DHW tank with tube-coil and separate buffer tank, B) Double-shell DHW tank.

Table 2.3 shows, as an example, the relationship between the supply temperature and the COP for a high-efficiency residential brine-to-water heat pump unit (ref. Appendix B), and the relative need for external reheating of the DHW. In the calculations it has been assumed 0ºC inlet brine temperature to the evaporator, 10°C city water temperature, 60ºC DHW temperature and 2 K difference between the supply temperature and the DHW temperature at the bottom of the primary vessel.

Table 2.3 The relationship between the supply temperature from the condenser, the COP of the heat pump unit (Appendix B) and the relative need for supplementary heating for the DHW at 10ºC city water temperature and 60ºC DHW temperature.

Supply Temperature [°C]	COP	Preheating from Heat Pump [%]	Supplementary Heating [%]
35	4.6	45	**55**
45	3.7	65	**35**
55	2.9	85	**15**

Table 2.3 demonstrates that the larger the annual DHW heating demand, the higher the optimum supply temperature from the heat pump unit.

In *bivalent heating systems*, electric immersion heaters mounted in the accumulator tank or the secondary vessel are commonly used peak load units. Other peak load units of current interest include separate electric heaters and existing gas/oil-fired boilers which are installed in the hydronic heating system as well as wood fired stoves, oil/kerosene/gas/-electric stoves and electric baseboard heaters.

Utilization of a De-Superheater for Hot Water Heating

Some residential brine-to-water and water-to-water heat pump units are equipped with *a de-superheater*, which utilizes the high temperature discharge gas from the compressor for heating of DHW. The heat exchanger is either a finned or smooth tube-coil which is an integral part of a single-shell DHW tank, or a plate heat exchanger, which is connected to a single-shell DHW tank by means of a closed water-loop. A small inverter controlled pump is required for the latter system in order to circulate the water through the water-loop. Figure 2.5 shows the principle of a residential heat pump unit equipped with a de-superheater.

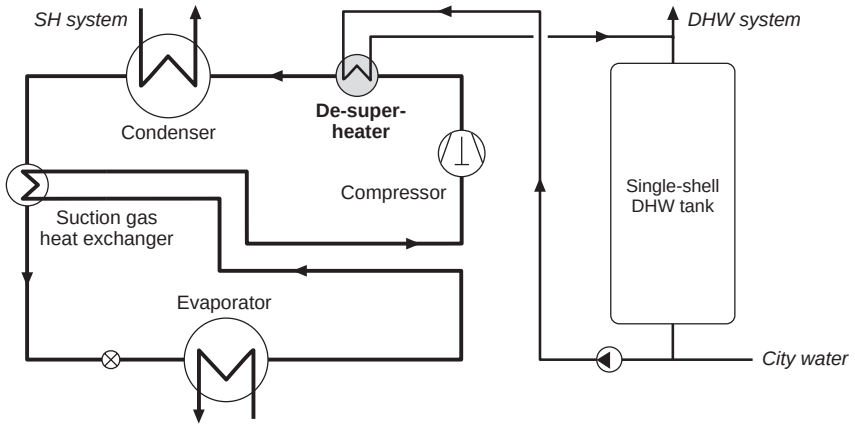

Figure 2.5 Principle of a residential heat pump unit equipped with a de-superheater for DHW heating.

The heating capacity of the de-superheater typically constitutes 15 to 20% of the total heating capacity of the heat pump unit. Since the temperature of the discharge gas for a residential brine-to-water or water-to-water heat pump unit is typically 30 to 40 K higher than the condensation temperature, a DHW temperature of 60 to 70ºC can be obtained even when the heat pump supplies heat to a low-temperature space heating system.

The *main drawback* of this system design is that heat can only be supplied from the heat pump unit to the DHW system as long as the compressor is running, and the DHW production is therefore inevitably linked to the space heating demand of the house. Under design conditions, the compressor will be running continuously, and cover the entire DHW demand. With a decreasing heating demand, however, the thermal storage capacity of the accumulator tank will lead to rather long off-periods for the compressor and limited DHW heating. Consequently, in modern well-insulated houses with moderate space heating demands, a heat pump unit equipped with a de-superheater will cover less of the annual DHW heating demand than that of a heat pump unit where the condenser heat is used for preheating of DHW.

Heat Pump System for Preheating and Reheating of DHW

A more energy efficient but more complex alternative to the heat pump systems presented in Figures 2.4 and 2.5, is to use the condenser for preheating of the DHW and a de-superheater for reheating. The principle of a possible system design is presented Figure 2.6.

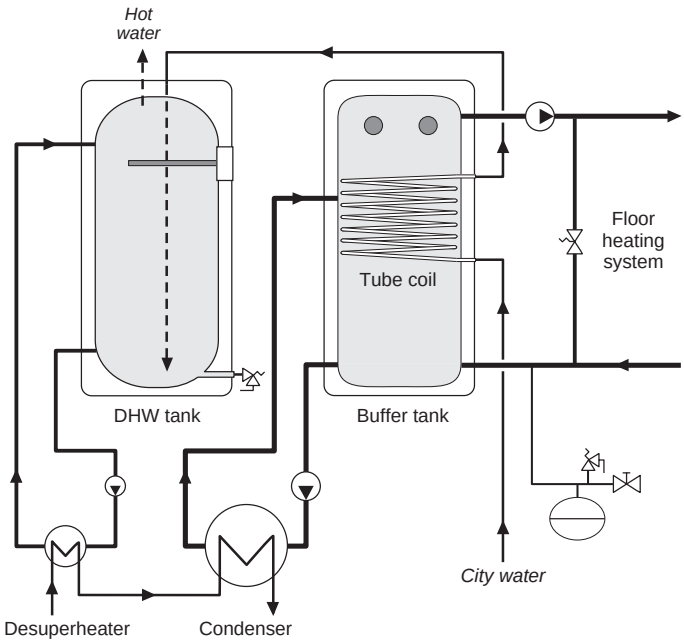

Figure 2.6 Principle of a residential heat pump system for space heating and DHW heating. The DHW is preheated and reheated by means of heat from the condenser and the de-superheater.

2.4.3 Technological Status of Residential CO_2 Heat Pumps

Owing to the favourable environmental and thermophysical properties of carbon dioxide (CO_2, R-744), many universities, research institutions and companies have in recent years been analysing and testing various types of residential CO_2 heat pump systems. The systems include heat pump water heaters, brine-to-water heat pumps for retrofitting in high-temperature radiator systems, air-to-water heat pumps in low-temperature heat distribution systems, monovalent air heating systems and reversible air-to-air heat pumps (air-conditioners).

2.4.3.1 CO_2 Heat Pump Water Heaters

Lorentzen (1994) reintroduced CO_2 as a working fluid, and demonstrated that the production of DHW is one of the most promising applications for the transcritical CO_2 heat pump process. The high energy efficiency of the CO_2 heat pump water heater is due to the good temperature fit between the CO_2 and the water in the counter-flow gas cooler, the excellent heat

transfer properties of CO_2 and the high compressor efficiency (ref. Appendix A, *CO_2 as a Working Fluid in Heat Pumps*). Another advantage of the CO_2 heat pump water heater is the capability of supplying high-temperature DHW, which eliminates the requirement for supplementary heating.

In recent years, a number of prototype CO_2 heat pump water heaters have been tested. Virtually all installations have been single-stage units using a low-pressure liquid receiver (LPR), a suction gas heat exchanger and a counter-flow tube-in-tube gas cooler. The principle of the CO_2 heat pump water heater is presented in Figure 2.7.

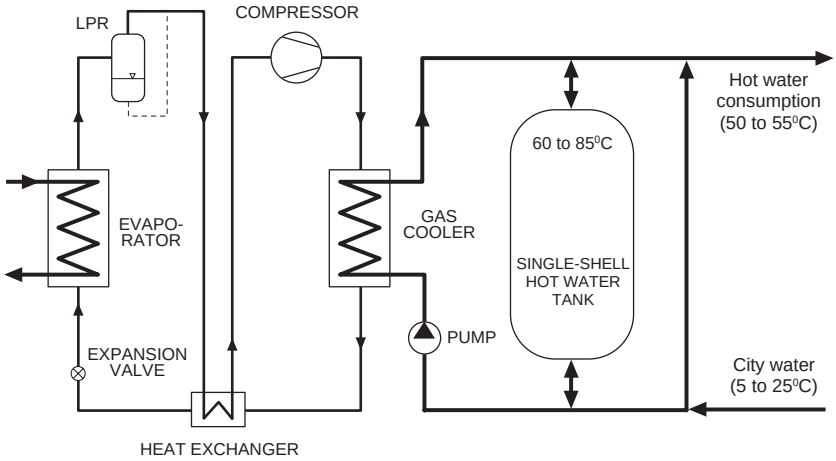

Figure 2.7 Principle of a CO_2 heat pump water heater.

Nekså et al. (1998) tested a 50 kW CO_2 heat pump water heater. The COP for the unit ranged from about 3.0 to 4.3 when the set-point for the DHW was 60°C and the evaporation temperatures ranged from -20 to 0ºC. At 80ºC DHW temperature and 0°C evaporation temperature, the measured COP was about 3.6. The optimum gas cooler (high-side) pressure ranged from about 9 to 11 MPa bar at DHW temperatures between 60 and 80°C.

CO_2 heat pump water heaters in the capacity range from 5 to 20 kW have been investigated by, among others, Rieberer and Halozan (1997), Hwang and Radermacher (1998) and Saikawa and Hashimoto (2000). The measured COPs of the prototype units are in the same range as for the CO_2 heat pump unit which was tested by Nekså et al.

In 2001, Denso Corporation Ltd. in Japan was the first company to start commercial production of a residential air-source CO_2 heat pump water heater. The 4.5 kW unit delivers 85ºC DHW, and the measured SPF in Tokyo climate is reported to be above 3 (Saikawa and Hashimoto, 2000). Due to the considerable market for heat pump water heaters in Japan, several other Japanese companies have also started production of CO_2 heat pumps based on the same type of technology (*www.shecco.com*).

2.4.3.2 CO_2 Heat Pumps for Retrofitting in High-Temperature Heat Distribution Systems

Brandes and Kruse (2000) investigated the possibility of using CO_2 heat pumps for retrofitting of residential oil-fired boilers installed in high-temperature radiator systems. In the theoretical study, both single-stage and two-stage CO_2 heat pumps were considered, but the 25% increase in COP could not be justified by the higher first costs of the two-stage system. A suction gas heat exchanger was not recommended owing to the marginal impact on the COP.

The performance of the CO_2 heat pump was calculated at different temperature regimes in the radiator system, including 90/70ºC, 70/50ºC, 50/40ºC and 35/30ºC. In Berlin climate, the estimated SPF for an air-to-water CO_2 heat pump installed in a 70/50°C system was about 2.8 when running the system at optimised high-side pressure, and about 2.6 when the high-side pressure was kept constant at 10.5 MPa. This was typically 10 to 25% lower than that of the state-of-the-art air-to-water heat pumps. However, by reducing the water flow rate in the heat distribution system by approximately 65%, the supply and return temperatures at design conditions were altered from 70/50ºC to 93/40ºC. Due to the reduced CO_2 outlet temperature from the gas cooler, the SPF increased by about 15%. For the 93/40ºC system, the optimum high-side pressure ranged from about 8.5 to 11.5 MPa at varying heat source and heat sink temperatures.

A prototype CO_2 air-to-water heat pump was designed and tested. The measured COP for the 93/40ºC system was about 10 to 18% higher that that of the theoretical system. Hence, *the CO_2 unit was more energy efficient than the best residential air-to-water heat pump on the market.* The main reason for the improved COP was that the prototype achieved a lower temperature approach $(\Delta T_A)_2$ than presupposed in the calculations.

[2] *The temperature approach is the difference between the CO_2 outlet temperature and the inlet temperature of the heat sink for a counter-flow gas cooler.*

2.4.3.3 CO_2 Heat Pumps in Combination with Low-Temperature Heat Distribution Systems

Kerherve and Clodic (2002) compared the performance of a state-of-the-art R-407C air-to-water heat pump unit with a prototype CO_2 heat pump unit. Heating capacities and COPs at various operating conditions for the R-407C unit were based on experimental data from the manufacturer. During testing of the CO_2 heat pump unit, the supply and return temperatures in the hydronic heat distribution system were either 32/28ºC (floor heating system) or 47/43°C (convector system). The inlet temperature to the evaporator was varied from -15 to +7ºC in each test series, and optimum high-side pressure control was used in all experiments.

The COP of the R-407C unit was higher than that of the CO_2 system at ambient air temperatures higher than -10ºC, and at +7ºC the difference was 25%. The main reason for the inferior energy efficiency of the CO_2 heat pump unit was the poor temperature fit in the gas cooler and the subsequent high CO_2 temperature before throttling. The only advantage of the CO_2 system was that the heating capacity diminished less rapidly than that of the R-407C system at ambient air temperatures below -5°C.

The test data were used to estimate the SPFs for the heat pump units when they were supposed to cover the heating demand of a typical 140 m^2 house situated in different climatic regions in France. In the calculations it was presupposed that the heat pumps were operated as monovalent systems. *The calculated SPF for the R-407C unit was in average 25% higher than that of the CO_2 unit*. Since the CO_2 heat pump had the highest heating capacity at lower ambient air temperatures, the difference in SPF would have been less pronounced if the units had been operated as bivalent heating systems using an external heater to cover the peak load demand.

2.4.3.4 A Monovalent Air-Heating System Using an Air-to-Air CO_2 Heat Pump Unit

Rieberer and Halozan (1998) investigated a monovalent air-heating system, which was designed to cover the transmission and ventilation losses in modern low-energy houses equipped with a balanced ventilation system. The heating system consisted of a ground heat exchanger, an air-to-air heat exchanger for heat recovery as well as an air-to-air CO_2 heat pump unit. Figure 2.8 shows the principle of the system.

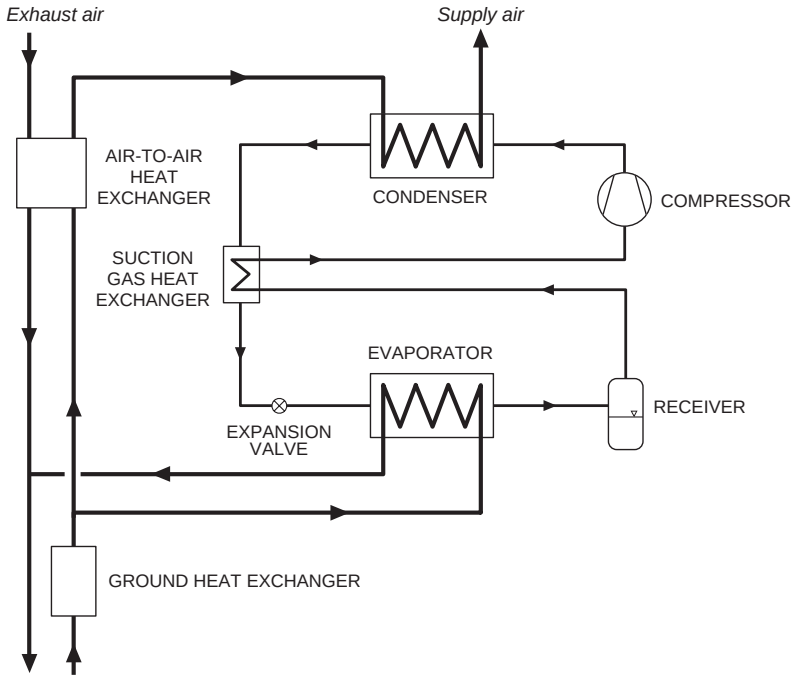

Figure 2.8 Principle of the residential monovalent air-heating system.

The ambient air is preheated in the ground heat exchanger before it enters the CO_2 evaporator and the exhaust air heat exchanger. The preheated air is then heated to the desired supply temperature in the CO_2 condenser. Depending on the specific transmission loss of the house, the air exchange rate and the outdoor temperature, the required supply temperature for the air will typically range from 25 to 50ºC. Owing to the low temperature of the inlet air, heat will be given off at a subcritical pressure.

The combination of a relatively low inlet air temperature in the condenser and a considerable temperature glide during heat rejection, results in an energy efficient heat pump cycle. When operating at a constant subcritical pressure of 7 MPa, *the calculated SPF for the air heating system was approximately 6.2 in an Austrian climate*. By utilizing optimum high-side pressure control the SPF increased about 5%.

Due to the high energy efficiency, the air heating system represents an interesting alternative to ground-coupled heat pumps in combination with low-temperature floor heating systems. However, the air heating system has several disadvantages:

- The DHW heating demand must be covered by a separate heating system.
- The thermal comfort will be less satisfactory than in houses equipped with low-temperature floor heating systems, since the warm supply air may create relatively large temperature gradients in the rooms.
- The ventilation efficiency will probably be reduced compared to conventional balanced ventilation systems, since the temperature of the supply air will be typically 5 to 30 K higher than the room temperature.
- There is a risk that bacteria and fungus in the ground heat exchanger may contaminate the inlet air. If the ground heat exchanger is omitted from the heating system, auxiliary heating will be required to maintain the room temperature at low ambient temperatures.

3 Theoretical Background and System Analysis

The initial part of this chapter provides a general analysis of the performance for the transcritical CO_2 heat pump cycle, and discusses operational characteristics for an integrated brine/water-to-water CO_2 heat pump unit using a tripartite gas cooler for preheating of domestic hot water (DHW), space heating and reheating of DHW. The theoretical framework for an exergy analysis of the heat pump system is also presented. The last part of the chapter presents the principle design and the main operational characteristics of the DHW system, and provides an analysis of the exergy losses in the DHW storage tank. The application of a movable insulating plate, that reduces the conductive heat transfer inside the DHW tank and eliminates the mixing of hot and cold water, is also analysed.

All calculations in this chapter have been performed by means of Microsoft Excel. The Span and Wagner (1996) equation of state was used for the thermodynamic properties of CO_2.

3.1 Introduction

Designing an integrated CO_2 heat pump system is a multi-variable problem, partly due to the strong interaction between the performance of the heat pump unit and the operational characteristics of the space heating and DHW systems. An integrated heat pump system can be designed for high energy efficiency, but in the design process there will always be a trade-off between first costs and technical solutions that reduce the thermodynamic losses in the system. In general, residential heat pump systems should have a simple design in order to be competitive with low-priced conventional heating systems. As a consequence, the theoretical analysis has been limited to *single-stage* heat pumps, since the higher coefficient of performance (COP) of a two-stage unit does not outweigh the additional investment costs (Brandes and Kruse, 2000).

Reference is made to Appendix A, *CO_2 as a Working Fluid in Heat Pumps*, regarding a presentation of important physical and thermophysical properties of CO_2, main design parameters, compressor and heat exchanger performance for residential CO_2 systems (literature review) and the effects of gas cooler (high-side) pressure control on system performance.

3.2 The CO_2 Heat Pump Unit

3.2.1 Theoretical Reference Cycles

3.2.1.1 The Modified Lorentz Cycle

For conventional heat pump cycles, where heat is absorbed and given off at practically constant temperatures, *the reversed Carnot cycle* is used as the theoretical reference cycle. However, for the transcritical CO_2 cycle, where heat is given off at a gliding temperature, *the modified Lorentz cycle* is more suitable as the theoretical reference cycle (Klöcker, 1998). This cycle is characterized by the following changes of state:

$1 – 2_s$	Isentropic compression
$2_s – 3$	Isobaric heat rejection (gliding temperature)
$3 – 4_s$	Isentropic expansion
$4_s – 1$	Isothermal heat absorption

Figure 3.1 shows the principle of the modified Lorenz cycle in a Temperature-entropy (T-s) diagram.

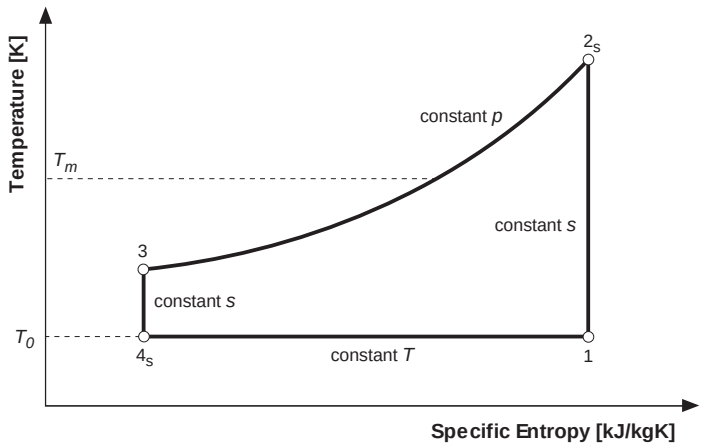

Figure 3.1 Illustration of the modified Lorenz cycle (Klöcker, 1998).

With reference to the definition of the COP of the reversed Carnot cycle (Gosney, 1982), the COP of the modified Lorentz cycle is defined as:

$$COP_{LZ} = \frac{T_m}{T_m - T_0} \quad \text{and} \quad T_m = \frac{T_{2s} - T_3}{\ln\left(\frac{T_{2s}}{T_3}\right)} \tag{3.1}$$

which gives

$$COP_{LZ} = \frac{T_{2s} - T_3}{(T_{2s} - T_3) - T_0 \cdot \ln\left(\frac{T_{2s}}{T_3}\right)} \tag{3.2}$$

where the subscripts *2s* and *3* refer to the inlet and outlet temperature of the heated fluid (heat sink), T_0 is the temperature of the heat source and T_m is the thermodynamic average temperature during heat rejection.

Whereas *the Carnot efficiency* is often used as a measure for the thermodynamic efficiency of conventional heat pump cycles, *the Lorentz efficiency* can be used for the transcritical CO_2 cycle. The Lorentz efficiency is defined as (Klöcker, 1998):

$$\eta_{LZ} = \frac{COP_{HP}}{COP_{LZ}} \tag{3.3}$$

where the subscript *HP* refers to the real CO_2 heat pump cycle.

Table 3.1 shows, as an example, the measured COP of residential CO_2 heat pumps for low-temperature space heating (Kerherve and Clodic, 2002) and hot water heating (Saikawa and Hashimoto, 2000) as well as the calculated Lorentz COP (COP_{LZ}) and the Lorentz efficiency (η_{LZ}) for the systems.

Table 3.1 clearly demonstrates that the thermodynamic losses in a CO_2 heat pump water heater are considerably smaller than in a CO_2 heat pump system for low-temperature space heating. The 25% higher Lorentz efficiency of the heat pump water heater is caused by the better temperature fit between the high-pressure CO_2 and the water in the counter-flow gas cooler (ref. Appendix A2.4, *Optimum High-Side Pressure when Incorporating Real Gas Cooler Performance*).

Table 3.1 Measured COPs as well as calculated Lorentz COPs and Lorentz efficiencies for residential CO_2 heat pumps for low-temperature floor heating (Kerherve and Clodic, 2002) and heating of DHW (Saikawa and Hashimoto, 2000).

Heating Demand	T_0	T_{2s}	T_3	COP_{HP}	COP_{LZ}	η_{LZ}
Space heating	0ºC	32ºC	28ºC	3.2	10.1	*0.32*
DHW heating	0ºC	85ºC	10ºC	3.0	6.9	*0.43*

3.2.1.2 The Ideal Lorentzen Cycle

For conventional heat pump systems with subcritical heat rejection, *the ideal Evans-Perkins cycle* is normally used as the ideal reference cycle. Halozan and Ritter (1994) proposed to use *the ideal Lorentzen cycle* as the ideal reference cycle for the transcritical CO_2 cycle. This cycle has the following changes of state:

- $1 – 2_s$ Isentropic single-stage compression to supercritical pressure
- $2_s – 3$ Isobaric supercritical heat rejection (gliding temperature)
- $3 – 4$ Isenthalpic expansion
- $4 – 1$ Isothermal heat absorption

Figure 3.2 shows the principle of the ideal Lorentzen cycle in a Temperature-entropy (T-s) diagram.

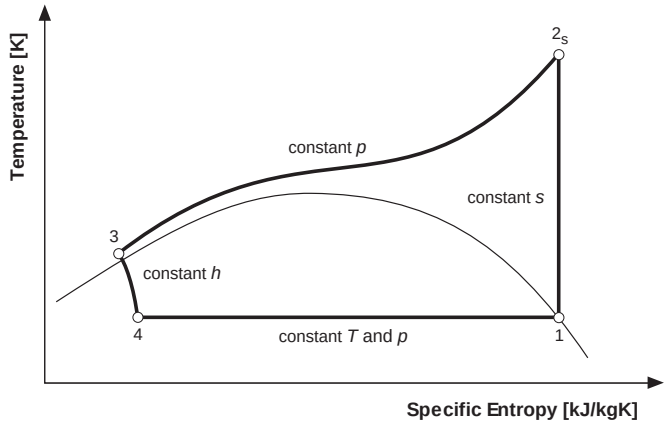

Figure 3.2 Illustration of the ideal Lorentzen cycle in a T-s diagram.

When comparing a real transcritical CO_2 heat pump cycle with the ideal Lorentzen cycle, the temperature approach[1] at the gas cooler outlet in the ideal cycle is assumed to be zero. A fundamental problem arises, however, regarding the selection of the gas cooler (high-side) pressure for the ideal cycle, since the CO_2 outlet temperature from the gas cooler, the heating capacity and the COP of a real transcritical CO_2 heat pump cycle are all affected by the high-side pressure (ref. Appendix A2.3 and A2.4). Since there is no acknowledged method for determining the required high-side pressure in an ideal Lorentzen cycle at fixed temperature conditions for the heat sink, the high-side pressure of the ideal cycle must be set as the high-side pressure of the real cycle.

Figure 3.3 shows the COP of *the ideal Lorentzen heat pump cycle* as a function of the CO_2 outlet temperature from the gas cooler and the high-side pressure. The evaporation temperature is 0ºC.

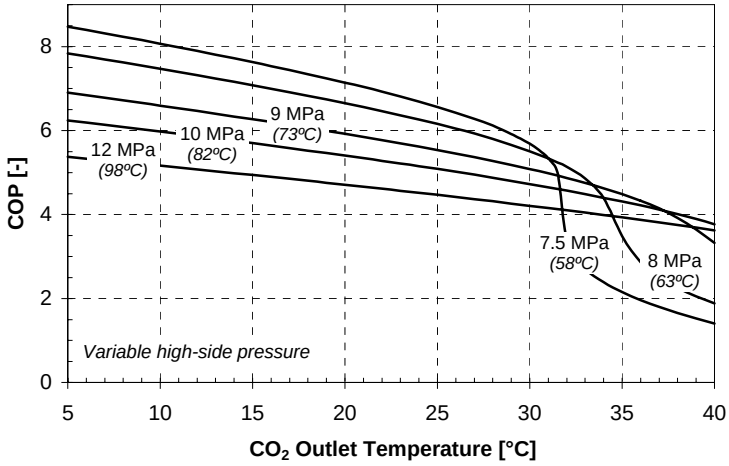

Figure 3.3 The COP for the ideal Lorentzen cycle as a function of the CO_2 outlet temperature from the gas cooler and the high-side pressure. The evaporation temperature is 0ºC.

3.2.2 The Transcritical CO_2 Heat Pump Cycle

The real transcritical CO_2 heat pump cycle, which is often referred to as *the Lorentzen Cycle*, is characterized by the following changes of state:

[1] *The difference between the CO_2 outlet temperature and the inlet air/water temperature in a counter-flow gas cooler is denoted the temperature approach (ΔT_A).*

1 – 2 Irreversible polytropic non-adiabatic compression

2 – 3 Non-isobaric supercritical heat rejection (gliding temp.)

3 – 4 Non-isenthalpic (non-adiabatic) expansion

4 – 1' Non-isobaric (i.e. non-isothermal) heat absorption

1' – 1 Non-isobaric superheating of the suction gas

3.2.2.1 The Coefficient of Performance (COP)

Figure 3.4 shows the calculated COP of a single-stage transcritical CO_2 heat pump cycle as a function of the CO_2 outlet temperature from the gas cooler and the high-side pressure. In the calculations it has been assumed -5ºC evaporation temperature, 5 K suction gas superheat, 60% isentropic compressor efficiency and 10% heat loss from the compressor. These are operating parameters that are typical for residential brine-to-water heat pump units. The temperatures in the brackets are the CO_2 inlet temperatures for the gas cooler.

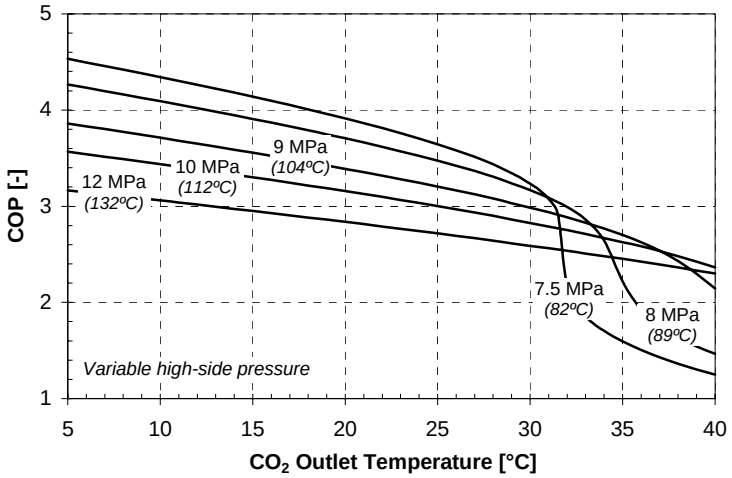

Figure 3.4 The COP for a single-stage transcritical CO_2 heat pump cycle as a function of the CO_2 outlet temperature from the gas cooler and the high-side pressure. The evaporation temperature is -5ºC.

From Figure 3.4 the following observation can be made:

- Compared to the ideal Lorentzen cycle, the discharge gas temperature has increased by 25 to 35 K, whereas the COP has dropped by roughly 40 to 45% at CO_2 outlet temperatures below 30ºC.

- In order to achieve a high COP for the transcritical CO_2 heat pump cycle, *useful heat* has to be rejected over a wide temperature range (i.e. a large temperature glide for the CO_2), and the resulting CO_2 outlet temperature from the gas cooler as well as the high-side pressure must be relatively low.

- At temperatures and high-side pressures relatively close to the critical values, the COP curves are very steep and even minor variations in the CO_2 outlet temperature from the gas cooler lead to a significant change in the COP (ref. Appendix A2.3, *Optimum High-Side Pressure at Constant CO_2 Outlet Temp. from the Gas Cooler*).

- At CO_2 outlet temperatures below 30ºC, the COP curves are virtually linear, and the COP increases on average by roughly 1% per degree Kelvin drop in the CO_2 outlet temperature.

- At CO_2 outlet temperatures below 30°C, the COP increases by roughly 1.5 to 3.5% per 0.1 MPa drop in the high-side pressure.

- In order to achieve a COP of 3.5, the CO_2 outlet temperature from the gas cooler must be lower than 8 to 24ºC at high-side pressures ranging from 8 to 10 MPa, respectively. When assuming a minimum CO_2 outlet temperature of 10ºC, a COP above 4 can only be achieved at high-side pressures below approximately 8.2 MPa.

The COP of a transcritical CO_2 heat pump is heavily affected by *the evaporation temperature* and *the isentropic efficiency* of the compressor. This is illustrated in Figures 3.5 and 3.6, where the high-side pressure is kept constant at 9 MPa and the other boundary conditions are as in Figure 3.4.

At CO_2 outlet temperatures below 30ºC, the COP increases by roughly 2.5% per degree Kelvin rise in the evaporation temperature, whereas the COP increases on average by 1.2% per percentage points rise in the isentropic compressor efficiency.

Since the COPs for the transcritical CO_2 heat pump cycle and the conventional subcritical heat pump cycle are depending on the temperature requirements and heating demands for the space heating and DHW systems, the component performance (ref. Appendix A1.5, *Compressor Performance*, and A1.6, *Heat Exchanger Performance*) as well as the system design, it is impossible to make a general comparison of the system performance for the cycles.

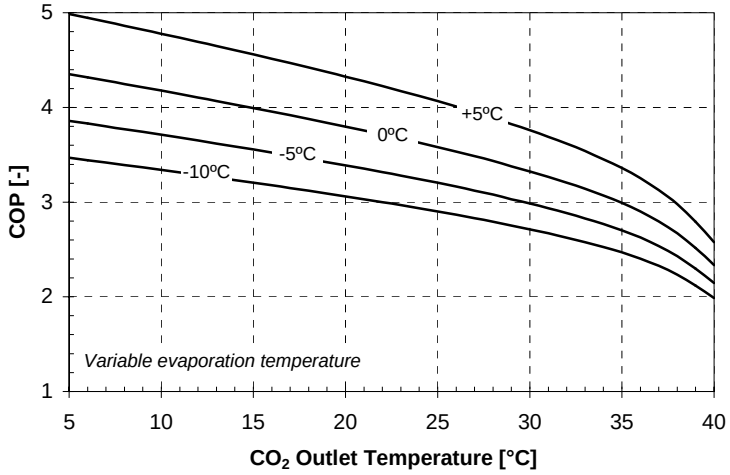

Figure 3.5 *The COP of a transcritical CO_2 heat pump as a function of the CO_2 outlet temperature from the gas cooler and the evaporation temperature. The high-side pressure is 9 MPa, and the other boundary conditions are as in Figure 3.4.*

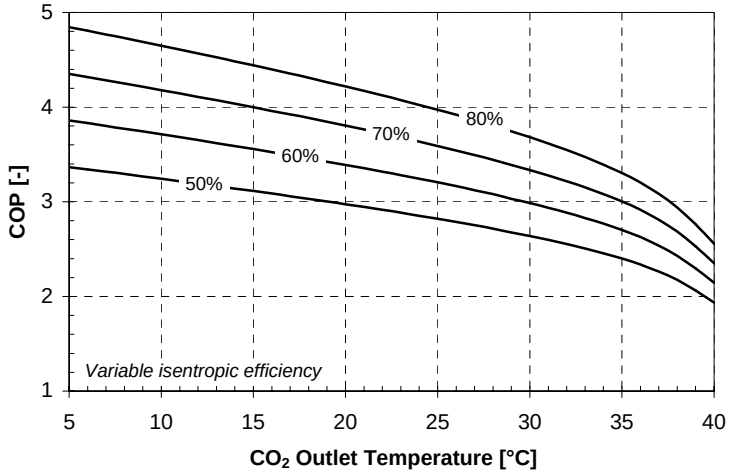

Figure 3.6 *The COP of a transcritical CO_2 heat pump as a function of the CO_2 outlet temperature from the gas cooler and the isentropic efficiency. The high-side pressure is 9 MPa, and the other boundary conditions are as in Figure 3.4.*

3.2.2.2 The Volumetric Heating Capacity

Figure 3.7 demonstrates how the volumetric heating capacity [kJ/cm^3] of a single-stage transcritical CO_2 heat pump cycle is affected by the CO_2 outlet temperature from the gas cooler and the high-side pressure. The temperatures in the brackets are the CO_2 inlet temperatures for the gas cooler, and the boundary conditions for the calculations are as in Figure 3.4.

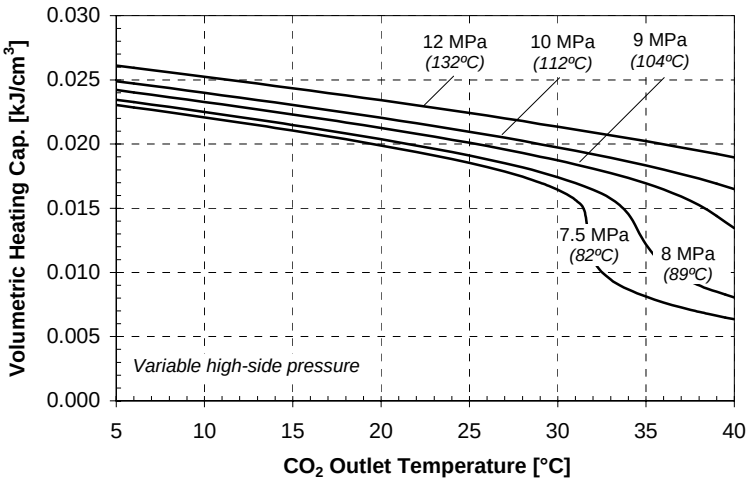

Figure 3.7 The volumetric heating capacity of a transcritical CO_2 heat pump cycle as a function of the CO_2 outlet temperature from the gas cooler and the high-side pressure. The boundary conditions are as in Figure 3.4.

At CO_2 outlet temperatures below 30°C the volumetric heating capacity of the heat pump increases by roughly 1% per degree Kelvin drop in the CO_2 outlet temperature.

Figure 3.8 shows how *the evaporation temperature* affects the volumetric heating capacity of the CO_2 heat pump when the high-side pressure is kept constant at 9 MPa and the other boundary conditions are as in Figure 3.4.

At CO_2 outlet temperatures below 30°C, the volumetric heating capacity increases on average by 2% per degree Kelvin rise in the evaporation temperature. The capacity variations are mainly due to the variations in the CO_2 vapour density at the compressor inlet. When incorporating the volumetric efficiency of the compressor, the relative variations in the absolute heating capacity will be even more pronounced than the variations in the volumetric heating capacity.

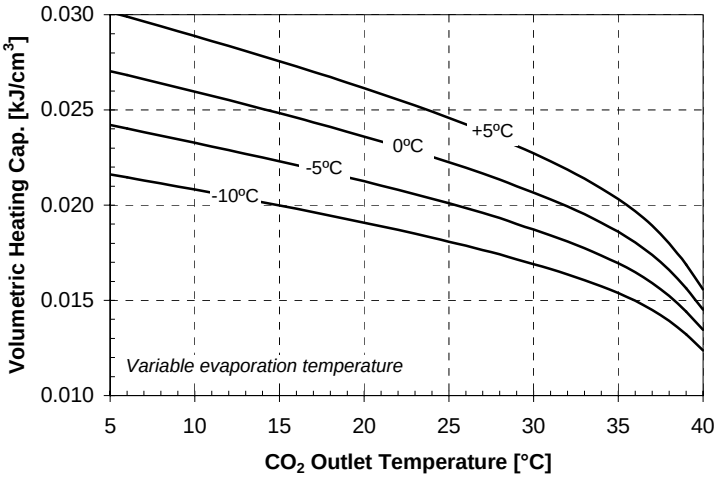

Figure 3.8 *The volumetric heating capacity as a function of the CO_2 outlet temperature from the gas cooler and the evaporation temperature. The high-side pressure is 9 MPa, and the other boundary conditions are as in Figure 3.4.*

3.2.3 Gas Cooler Configurations

The main operating modes of an integrated CO_2 heat pump system are:

- Simultaneous space heating and hot water heating (*combined mode*)
- Hot water heating only (*DHW mode*)
- Space heating only (*SH mode*)

The CO_2 outlet temperature after rejection of useful heat in the gas cooler should be as low as possible in order to achieve a high COP for the system. The CO_2 outlet temperature is mainly determined by:

- The characteristics of the fluids to be heated (heat sinks):
  - the inlet temperatures (or temperature set-points)
  - the CP-values (ref. Appendix A2.4)
- The design and configuration of the gas coolers
- The compressor discharge temperature:
  - the suction pressure and temperature
  - the high-side pressure
  - the isentropic efficiency and heat loss for the compressor

- The CO_2 mass flow rate:
  - the suction pressure and temperature
  - the compressor swept volume and rotational speed
  - the volumetric efficiency of the compressor
- The high-side pressure (ref. Appendix A2.4)

There is a close interaction between the operational characteristics of the space heating and DHW systems, the configuration of the gas cooler units and the performance of the CO_2 heat pump system. Figure 3.9 shows the principle of the following gas cooler configurations:

a) Parallel connection of two gas cooler units for space heating (SH) and hot water heating (DHW).

b) Serial connection of two gas cooler units for space heating (SH) and hot water heating (DHW), where the DHW gas cooler is located *before* the SH gas cooler.

c) Serial connection of two gas cooler units for space heating (SH) and hot water heating (DHW), where the DHW gas cooler is located *after* the SH gas cooler.

d) Serial connection of three gas cooler units for preheating of hot water (DHW-P), space heating (SH) and reheating of hot water (DHW-R).

The proposed gas cooler configurations will lead to the same CO_2 outlet temperature in the space heating (SH) mode and the DHW mode, as long as the operating conditions and the total heat transfer surfaces for the gas cooler units are identical. When applying *counter-flow heat exchangers*, the theoretical limit for the CO_2 outlet temperature for each gas cooler will be the inlet water temperature. For the parallel gas cooler configuration (a), the resulting CO_2 temperature T_d at the outlet of the gas coolers in *the combined heating mode* is calculated as:

$$h_d(T_d, p_d) = \frac{\dot{m}_2 \cdot h_b + \dot{m}_3 \cdot h_c}{(\dot{m}_2 + \dot{m}_3)} \tag{3.4}$$

where the subscripts refer to Figure 3.9, p is the supercritical pressure, h is the specific enthalpy, and $\dot{m}$ is the CO_2 mass flow rate. As an example, at equal mass flow rates, 10 MPa high-side pressure and CO_2 outlet temperatures of 30 and 10ºC for the SH and DHW gas cooler units, respectively, the resulting CO_2 temperature will be approximately 21ºC.

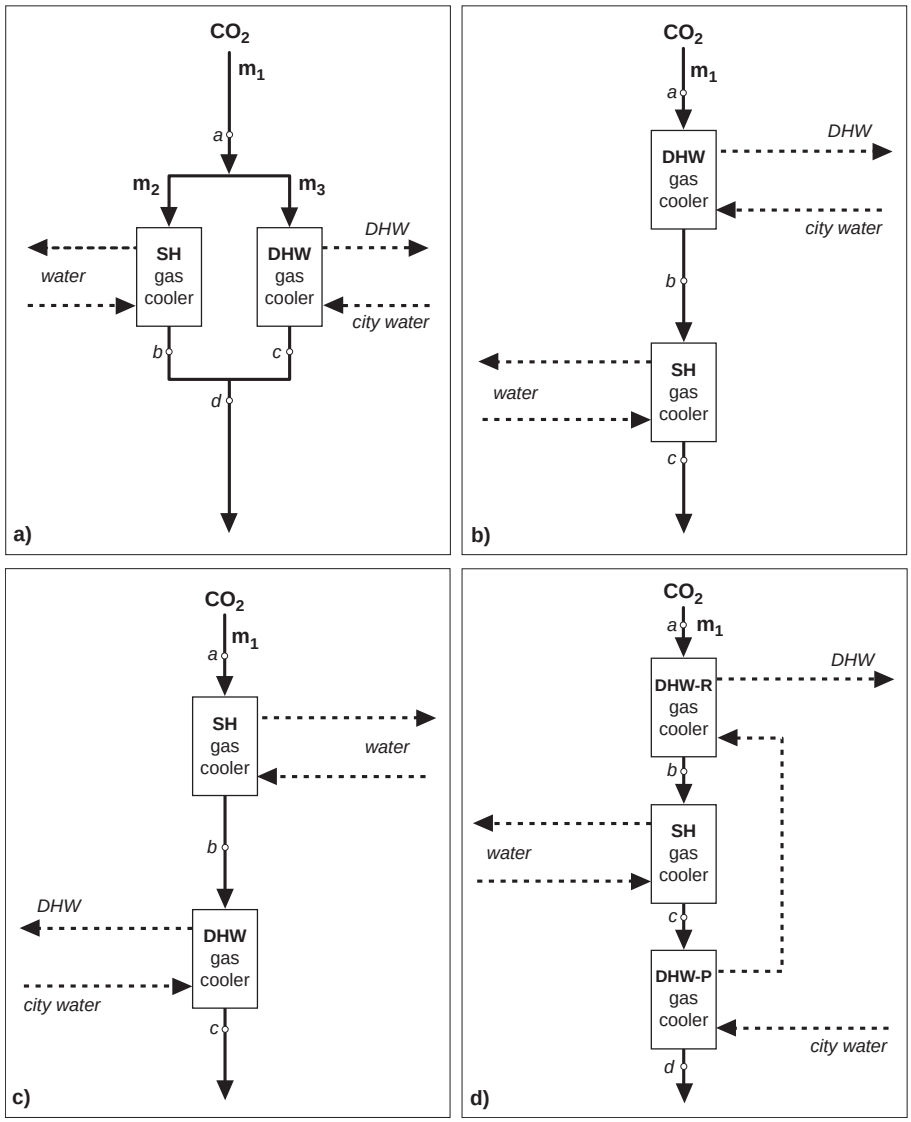

Figure 3.9 *Principle of the gas cooler configurations of current interest for an integrated CO_2 heat pump unit. SH=space heating, DHW=hot water heating, DHW-P=preheating of hot water and DHW-R=reheating of hot water.*

Table 3.2 summarizes the most important characteristics for the different gas cooler configurations with regard to design, thermal performance as well as capacity and temperature control.

Table 3.2 Presentation of important characteristics for the gas cooler configurations displayed in Figure 3.9.

	(a) Parallel	**(b) Serial**	**(c) Serial**	**(d) Serial**
High temperature space heating possible (>60ºC)?	Yes	No	Yes	No
Production of 60 to 80ºC DHW possible?	Yes	Yes	No	Yes
Theoretical minimum for the CO_2 outlet temp.	Minimum for Eq. 3.4	Return temp. SH system	City water temperature	City water temperature
No. of gas cooler units	2	2	2	3
Thermal interaction between the GC [1)] units?	No	Yes	Yes	Yes
Control valve(s) for CO_2 distribution required?	Yes	No/Yes	No/Yes	No/Yes
Means of capacity control for the CO_2 circuit(s)	Compressor and valves	Compressor	Compressor	Compressor
Means of temp. control for the secondary systems	Pumps, fans and valves	Pumps, fans and valves	Pumps, fans and valves	Pumps, fans and valves
Technical complexity	Lower	Lower	Lower	Higher

1) Gas cooler

The different gas cooler configurations have distinct advantages and drawbacks regarding the temperature limits for space heating and DHW heating as well as the maximum attainable COP for the CO_2 heat pump.

- Configuration a) enables simultaneous high-temperature space and DHW heating, but the COP will be lower than that of configurations c) and d).
- Configuration b) enables production of high-temperature DHW, but the COP will be lower than that of configurations c) and d). A low-temperature space heating system is also required.
- Configuration c) may lead to the same COP as configuration d), but it is incapable of producing high-temperature DHW.
- Configuration d) enables production of high-temperature DHW, and may lead to a high COP for the CO_2 heat pump due to the serial connection of three gas cooler units. The configuration is only applicable together with a low-temperature space heating system.

Only *the tripartite gas cooler configuration* (d) has been further analysed, since it is capable of producing high-temperature DHW and contributes to the highest possible COP for the CO_2 heat pump unit.

3.2.4 Application of a Tripartite Gas Cooler

3.2.4.1 Principle System Design

Figure 3.10 shows a possible design for an integrated CO_2 heat pump unit equipped with a counter-flow tripartite gas cooler for preheating of DHW (A), low-temperature space heating (B) and reheating of DHW (C).

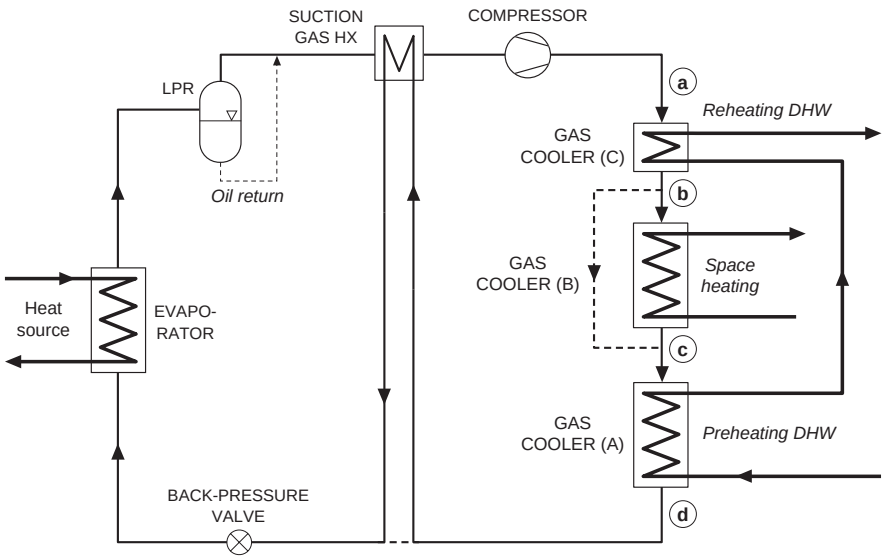

Figure 3.10 Principle of an integrated CO_2 heat pump unit for combined space heating and heating of DHW.

A low pressure receiver (LPR) system in combination with an automatic back-pressure valve can be used to control the supercritical pressure (ref. Appendix A2.2, *Methods of Controlling the High-Side Pressure*). The main purpose of the suction gas heat exchanger is to evaporate any CO_2 liquid from the oil return system and thus prevent liquid slugs in the compressor. The gas cooler units A and C are connected to a DHW system, which is described and analysed in Section 3.3. Gas cooler unit B is a water-cooled counter-flow heat exchanger, which is connected to a low-temperature hydronic heat distribution system with radiant floor heating, convectors or fan-coils.

3.2.4.2 Operational Characteristics

Simultaneous Space Heating and Hot Water Heating (Combined Mode)

An important parameter for the CO_2 heat pump unit in the combined mode is *the DHW heating capacity ratio*, which is defined as:

$$\xi_{DHW-HC} = \left[\frac{\dot{Q}_{DHW-P} + \dot{Q}_{DHW-R}}{\dot{Q}_{DHW-P} + \dot{Q}_{DHW-R} + \dot{Q}_{SH}} \right] \tag{3.5}$$

where the subscripts *SH*, *DHW-P* and *DHW-R* refer to space heating, preheating of DHW and reheating of DHW, respectively. The DHW heating capacity ratio is determined by the temperature levels and mass flow rates for the space and DHW systems, the discharge gas temperature from the compressor, the high-side pressure, the CO_2 mass flow rate and the heat transfer area and geometry for the three gas cooler units.

In Figure 3.11, the supercritical heat rejection process in the combined mode is illustrated in a temperature-enthalpy (T-h) diagram. At 8.5 MPa high-side pressure, heat is supplied to a low-temperature floor heating system at 35/30°C supply/return temperatures and a DHW system where the inlet water temperature and set-point temperature are 6.5ºC and 70ºC, respectively. At the actual gas cooler design and operating conditions, the DHW heating capacity ratio is about 45%.

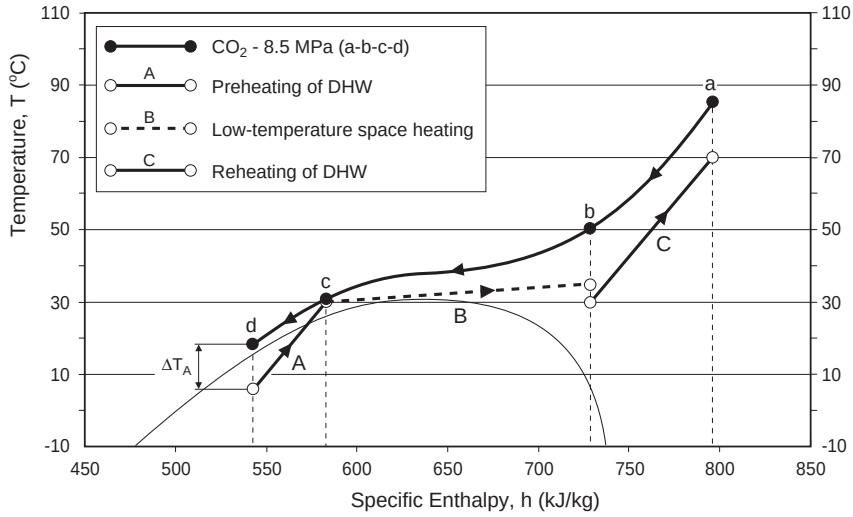

Figure 3.11 Illustration of the heat rejection process for a tripartite gas cooler operating in the combined mode. The high-side pressure is 8.5 MPa.

The slope of the CO_2 isobar $(\partial T/\partial h)_p$ in the T-h diagram is the inverse of the isobaric specific heat capacity of the CO_2, whereas the slope of the process lines for preheating of DHW (A), low-temperature space heating (B) and reheating of DHW (C) are calculated as:

$$\frac{\partial T}{\partial h} = \left(\frac{\dot{m}_{CO2}}{\dot{m}_W} \right) \cdot \frac{1}{c_p} \tag{3.6}$$

where $\dot{m}_{CO2}$ and $\dot{m}_W$ are the mass flow rates for the CO_2 and water, respectively, and c_p is the average specific heat capacity of water at the actual temperature range.

The heat rejection process in the tripartite gas cooler can alternatively be displayed in a temperature-heat (T-Q) diagram as illustrated in Figure 3.12 (ref. Appendix A2.4). In the example, the high-side pressure is 9.5 MPa, the supply/return temperatures for the space heating system are 40/35ºC, and the inlet city water temperature and set-point temperature for the DHW system are 6.5ºC and 70ºC, respectively.

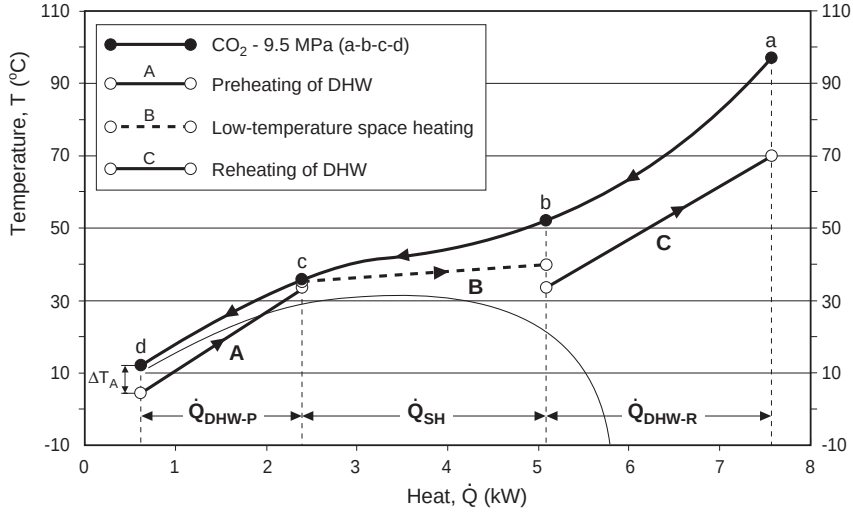

Figure 3.12 Illustration of the heat rejection process for a tripartite gas cooler operating in the combined mode. The high-side pressure is 9.5 MPa.

The main advantage of the T-Q diagram is that the heating capacities of the three gas cooler units, the evaporator capacity and the compressor power input can be read directly off from the abscissa.

From Figures 3.11 and 3.12 as well as Appendix A2, *The Transcritical CO_2 Heat Pump Cycle*, the following observations and comments can be made:

- At moderate high-side pressures, the CO_2 isobar has a sway-backed shape, and the heat rejection process is quite similar to a conventional heat pump cycle with de-superheating (a-b), condensation (b-c) and sub-cooling (c-d) of the working fluid.

- The counter-flow tripartite gas cooler enables production of high-temperature DHW, and the CO_2 outlet temperature before throttling may be considerably lower than the return temperature in the space heating system.

- For a fixed gas cooler design, the CO_2 outlet temperature from the tripartite gas cooler, and with that the heating capacity and COP of the heat pump unit, is heavily affected by the temperature levels in the space heating and DHW systems.

- Due to the serial connection of the counter-flow gas cooler units, changes in heat transfer areas or boundary conditions for one of the gas cooler units will influence the heating capacity and the temperature profiles for the two other units.

- As a result of the variation in the specific heat capacity at pressures and temperatures near to the critical point, the high-side pressure will affect on the temperature differences between the supercritical CO_2 and the fluids to be heated, and with that the heating capacity of each of the three gas cooler units. Consequently, for an integrated CO_2 heat pump system there is *an optimum high-side pressure* that will lead to a maximum COP (ref. Appendix A2.4).

- By using a tripartite gas cooler, a small temperature approach (ΔT_A) may be achieved at a moderate high-side pressure, which in turn will lead to a large heating capacity and a moderate power input to the compressor. As a consequence, the COP of an integrated CO_2 heat pump in the combined mode may be even higher than that of the DHW mode, where the optimum high-side pressure typically ranges from 10 to 12 MPa (Nekså et al., 1998).

Hot Water Heating Only (DHW Mode)

The heat rejection process in the DHW mode is illustrated in a T-h diagram in Figure 3.13. The high-side pressure is 10 MPa, while the city water and DHW set-point temperature are 6.5ºC and 70ºC, respectively.

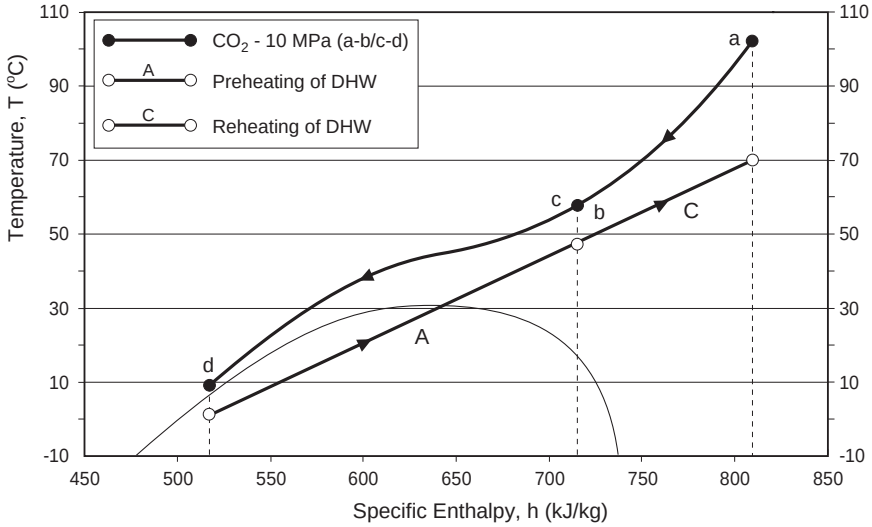

Figure 3.13 Illustration of the heat rejection process for a tripartite gas cooler operating in the hot water heating (DHW) mode. The high-side pressure is 10 MPa.

The two gas cooler units for preheating and reheating of DHW will perform as a single unit since no heat is delivered to the space heating system. The high-side pressure must be higher than that of the combined mode in order to move the pinch-point to the CO_2 outlet of the gas cooler, and with that obtain a small temperature approach. Reference is made to Appendix A2.4 and Nekså et al. (1998) for a further discussion on operational characteristics of CO_2 heat pump water heaters.

Space Heating only (SH Mode)

The heat rejection process in the SH mode is illustrated in a T-h diagram in Figure 3.14. The high-side pressure is 8.5 MPa, and heat is given off to a low-temperature floor heating system at 35/30ºC supply and return temperatures.

Whereas the theoretical minimum CO_2 outlet temperature from the tri-partite gas cooler in the combined mode and the DHW mode is *the inlet water temperature* for the DHW system, the CO_2 outlet temperature in the SH mode is limited by *the return temperature* in the space heating system. A low-temperature floor heating system may achieve a minimum return temperature in the order of 28 to 30ºC (ref. Section 2.3, *Hydronic Heat Distribution Systems*).

Due to the bad temperature fit between the supercritical CO_2 and the water in the floor heating system and the consequent high average temperature difference, the COP will be lower than that of a conventional heat pump cycle where heat is given off at constant temperature by condensation of the working fluid (Kerherve and Clodic, 2002).

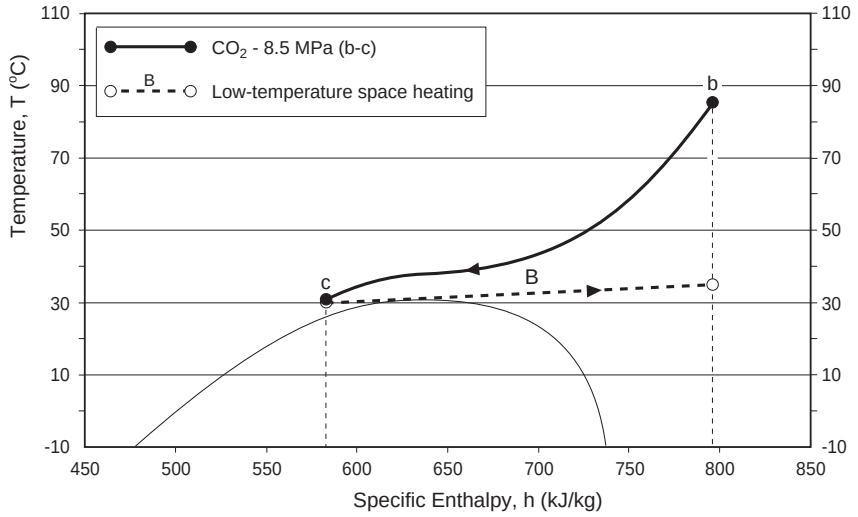

Figure 3.14 Illustration of the heat rejection process for a tripartite gas cooler operating in the SH mode. The high-side pressure is 8.5 MPa.

3.2.4.3 Design of the Tripartite Gas Cooler

Designing a tripartite gas cooler for an integrated CO_2 heat pump unit is an iterative optimization process, since there are tight reciprocal connections between the set-point temperatures for the secondary systems and the heat transfer surfaces for the three gas cooler units on one hand, and the required heating capacity, the DHW heating capacity ratio, the high-side pressure and finally the COP on the other hand. One of the main goals in the design process, is to obtain the largest possible temperature glide during heat rejection (i.e. a large enthalpy difference) at the lowest possible high-side pressure (i.e. a moderate compressor power input) during operation in the different modes.

Figure 3.15 shows the principle of the heat rejection process in the tripartite gas cooler as well as an overview of the main variables and input parameters.

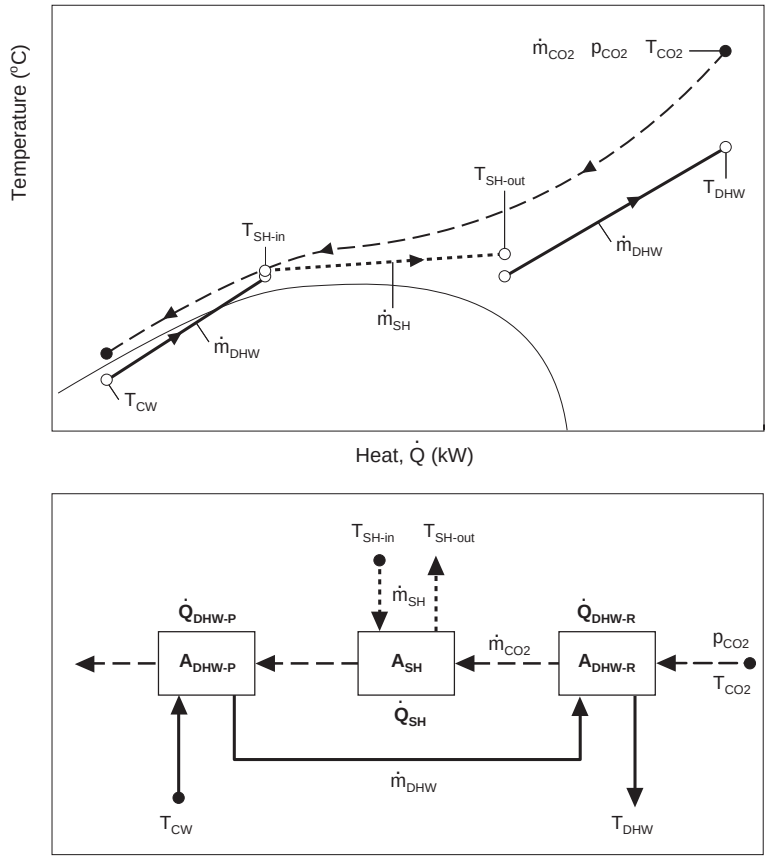

Figure 3.15 Principle of the heat rejection process in the tripartite gas cooler in the combined mode and an overview of the main variables and input parameters.

When the suction state and the compressor characteristics are known, the main input parameters and variables in the design process comprise:

The main input parameters at design conditions are:

- the operating mode (Combined mode, DHW mode or SH mode)
- the required space heating capacity ($\dot{Q}_{SH}$)
- the required DHW heating capacity ($\dot{Q}_{DHW}$)
- the supply temperature in the space heating system ($T_{SH\text{-}out}$)
- the return temperature in the space heating system ($T_{SH\text{-}in}$)
- the set-point for the DHW temperature (T_{DHW})
- the city water temperature (T_{CW})

The main variables are:

- the high-side pressure (p_{GC})
- the inlet CO_2 temperature (T_{CO2})
- the CO_2 mass flow rate ($\dot{m}_{CO2}$)
- the water flow rate in the space heating circuit ($\dot{m}_{SH}$)
- the water flow rate in the DHW circuit ($\dot{m}_{DHW}$)
- the heat transfer surface for space heating gas cooler (A_{SH})
- the heat transfer surface for the DHW preheating gas cooler ($A_{DHW\text{-}P}$)
- the heat transfer surface for the DHW reheating gas cooler ($A_{DHW\text{-}R}$)

3.2.4.4 Testing of a Prototype Heat Pump – Modelling

In order to document the performance and study the operational characteristics of an integrated CO_2 heat pump, a 6.5 kW prototype brine-to-water heat pump system was constructed and tested. The design of the test rig and the test programme are described in Section 4.1, *Testing of a Residential Brine-to-Water CO_2 Heat Pump Unit*, whereas the results are presented and analysed in Section 5.1, *Testing of a Residential Brine-to-Water CO_2 Heat Pump Unit*, and Section 7.1, *Main Findings from the Experiments and the Simulations*.

A steady-state computer model for a tripartite counter-flow tube-in-tube CO_2 gas cooler was also developed in order to analyse and supplement the measurements from the heat pump test rig. The thermodynamic basis and the mathematical background for the model as well as the simulation results are presented in Section 6.1, *Modelling of CO_2 Heat Pumps Using a Tripartite Gas Cooler*.

3.2.5 Exergy Analysis

3.2.5.1 Theoretical Framework

The thermodynamic losses for an integrated CO_2 heat pump system can be quantified by employing an exergy analysis (Haukås, 1992). The total exergy loss in W for each component or subsystem is calculated as:

$$\Delta\dot{E}_{tot} = \left(\dot{E}_{H,in} - \dot{E}_{H,out}\right) + \left(\dot{E}_{Q,in} - \dot{E}_{Q,out}\right) + \left(\dot{E}_{P,in} - \dot{E}_{P,out}\right) \quad (3.7)$$

where the subscripts *in* and *out* refer to exergy transfer in and out of the component or sub-system. The variables refer to exergy transfer due to fluid flows (E_H), heat transfer (E_Q) and transmission of electric power or mechanical work (E_P) across the component/system boundary.

The exergy losses in W for the evaporator, the hermetic/semihermetic compressor, the tripartite gas cooler, the expansion valve and the space heating system are calculated as shown in Eqs. (3.8) to (3.13). In the equations, the subscripts *H* and *C* refer to the "hot" CO_2 flow and the "cold" secondary flow (water), respectively. Here $\dot{m}_H$ is the CO_2 mass flow rate, $\dot{Q}$ is the heating capacity or heat load, *P* is the compressor power input, T_0 is the reference (ambient) temperature and $\overline{T}_C$ is the logarithmic average temperature for the secondary flow.

The exergy loss for *the evaporator* (*E*) is calculated as:

$$\Delta\dot{E}_E = \dot{m}_H \cdot \left[\left(h_{H,in} - h_{H,out}\right) - T_0 \cdot \left(s_{H,in} - s_{H,out}\right)\right] \quad (3.8)$$

The exergy loss for *the hermetic/semi-hermetic compressor* (*C*) including the motor efficiency and the heat loss from the compressor shell, is calculated as:

$$\Delta\dot{E}_C = P - \dot{m}_H \cdot \left[\left(h_{H,out} - h_{H,in}\right) - T_0 \cdot \left(s_{H,out} - s_{H,in}\right)\right] - \left[P - \dot{m}_H \cdot \left(h_{H,out} - h_{h,in}\right)\right] \cdot \frac{\overline{T}_{HL} - T_0}{\overline{T}_{HL}} \quad (3.9)$$

where $\overline{T}_{HL}$ is the resulting average air temperature when heat is given off from the compressor shell due to non-adiabatic compression.

The total exergy loss for *the tripartite gas cooler* (*GC*) is calculated as:

$$\Delta\dot{E}_{GC} = \sum_{n=1}^{n=3} \left[\dot{m}_H \cdot \left[\left(h_{H,in} - h_{H,out}\right) - T_0 \cdot \left(s_{H,in} - s_{H,out}\right)\right] - \dot{Q} \cdot \frac{\overline{T}_C - T_0}{\overline{T}_C}\right]_n \quad (3.10)$$

where *n* is the number of the gas cooler unit. The average temperature for the cold flow (water) during the heat transfer process is calculated as:

$$\overline{T}_{C,n} = \frac{\left(T_{C,in} - T_{C,out}\right)_n}{\ln\left(\frac{T_{C,in}}{T_{C,out}}\right)_n} \tag{3.11}$$

The exergy loss for *the expansion valve* (*EX*) is calculated as:

$$\Delta\dot{E}_{EX} = \dot{m}_H \cdot T_0 \cdot \left(s_{H,out} - s_{H,in}\right) \tag{3.12}$$

The exergy loss for *the space heating system* (*SH*) is calculated as follows, when the room temperature is denoted T_R.

$$\Delta\dot{E}_{SH} = \dot{Q}_{SH} \cdot \left[\left(\frac{\overline{T}_C - T_0}{\overline{T}_C}\right) - \left(\frac{T_R - T_0}{T_R}\right)\right] \tag{3.13}$$

The exergy loss for the DHW supply is regarded to be zero, since the DHW from the CO_2 heat pump is pumped directly to the DHW tank and stored. Reference is made to Section 3.3.3, *Exergy Losses in the DHW Storage Tank*, for a description of the exergy losses in the DHW tank due to heat loss through the tank walls, mixing of hot and cold water during tapping and charging of the tank and conductive heat transfer inside the DHW tank.

The exergy analysis can also be extended to include the electric power input to *the circulation pumps* for the heat source and heat distribution systems, and the power input to *the peak load unit(s)* if the heat pump system is designed as a bivalent heating system.

With reference to Eq. (3.7), *the total exergy balance* for the integrated CO_2 heat pump system is expressed as:

$$\sum \Delta\dot{E}_{tot} = P_{tot} - \left(\dot{E}_{Q-SH} + \dot{E}_{Q-DHW} + \dot{E}_{Q-HL}\right) \tag{3.14}$$

where P_{tot} is the total power input to the compressor, pumps and peak load unit(s), and $\dot{E}_{Q-SH}$, $\dot{E}_{Q-DHW}$ and $\dot{E}_{Q-HL}$ represent the exergy content in W for the space heating load, the DHW heating load and the heat loss from the compressor, respectively. The exergy balance is illustrated in Figure 3.16.

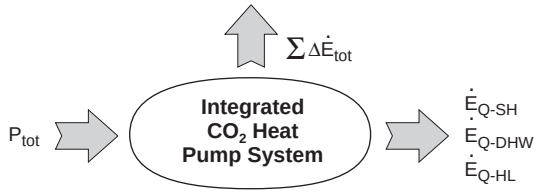

Figure 3.16 Illustration of the exergy balance for the entire system.

The different exergy losses for the integrated CO_2 heat pump system can also be expressed as *relative values* by dividing the individual losses by the total exergy loss of the entire system. As an example, the relative exergy loss of the compressor is expressed as:

$$\Delta \dot{E}_{C-rel} = \left(\frac{\Delta E_C}{\Delta \dot{E}_E + \Delta \dot{E}_C + \Delta \dot{E}_{GC} + \Delta \dot{E}_{EX} + \Delta \dot{E}_{SH}} \right) \cdot 100\% \qquad (3.15)$$

It should be emphasized that the different exergy losses in the integrated CO_2 heat pump system are *mutually dependent*, which means that modifications in one part of the system will effect the absolute and relative exergy losses in other components or sub-systems.

3.2.5.2 Exergy Analysis of the Prototype CO_2 Heat Pump

Section 7.2, *Exergy Analysis of the Prototype CO_2 Heat Pump System*, presents the results from an exergy analysis of the prototype brine-to-water CO_2 heat pump system during operation in the three different operating modes at 33/28 and 40/35ºC supply/return temperatures for the space heating system and 60 and 80ºC DHW temperature. The analysis includes, among other things, a discussion of the possibilities for efficiency improvements of the prototype CO_2 heat pump system.

3.3 The Hot Water System

3.3.1 Overall Design Criteria

With reference to Section 2.4.2.2, *Application of a DHW Storage Tank*, modern domestic hot water (DHW) systems are equipped with unvented single-shell or double-shell storage tanks, which are designed to cover the momentary and daily DHW demand in the house. The storage temperatures typically range from 60 to 85ºC.

When designing the DHW system for an integrated CO_2 heat pump unit, the main goal is to attain a large temperature glide for the supercritical CO_2 during heat rejection, and with that *a low CO_2 outlet temperature* from the DHW preheating gas cooler. Since a double-shell DHW tank cannot utilise the thermodynamic benefit of two separate gas cooler units operating at different temperature levels, the DHW system should be equipped with a *single-shell storage tank*. In principle there are two ways of integrating the two gas cooler units and the storage tank:

- The gas cooler units are made an *integral part* of the storage tank, which means that the heat exchangers are designed as tube-coils and mounted inside the tank as shown in Figure 3.17.
- The gas cooler units are *separated* from the storage tank, and connected to the tank by means of a closed water loop.

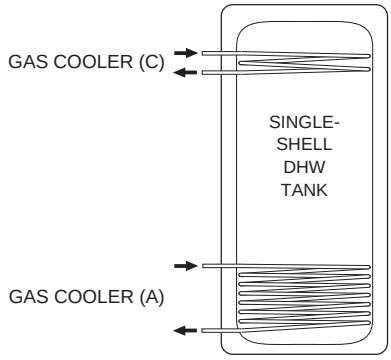

Figure 3.17 Principle of a single-shell DHW tank, where the CO_2 gas cooler units A and C are an integral part of the tank.

Although an integral design eliminates the need for a pump and a water loop, externally mounted counter-flow gas coolers will lead to a lower CO_2 outlet temperature. This is the main reason why virtually all CO_2 heat

pump water heaters that have been developed and tested in recent years have been using counter-flow gas coolers and a closed water loop (ref. Section 2.4.3.1, *CO_2 Heat Pump Water Heaters*). Figure 3.18 shows how the gas cooler units for preheating and reheating of DHW should be connected to the single-shell storage tank. The other main components in the DHW system include a small inverter controlled pump for circulation of water through the DHW gas cooler units and an electric immersion element for backup heating. The start and stop sequences for the pump is activated by a temperature sensor at the bottom of the tank (T_{CW}), whereas the set-point temperature for the DHW (T_S) is controlled by adjusting the rpm of the pump and with that the water flow rate through the gas coolers.

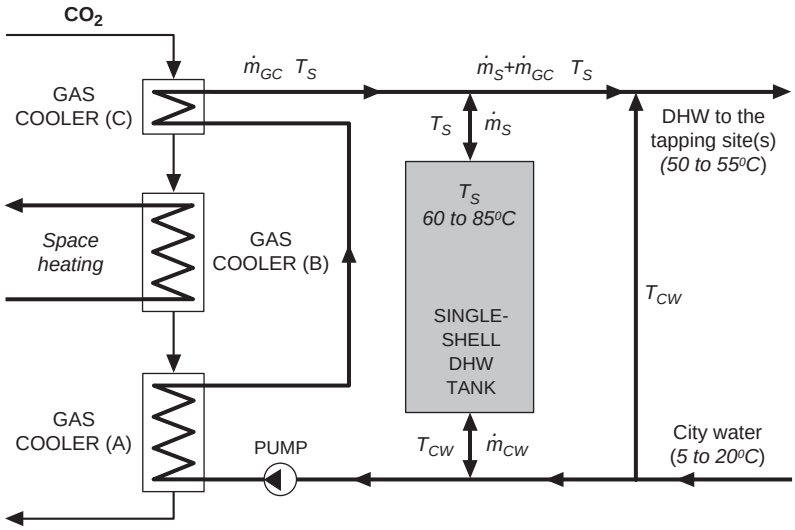

Figure 3.18 Principle of the tripartite CO_2 gas cooler connected to an unvented single-shell DHW tank and city water supply.

An integrated CO_2 heat pump is designed to cover the entire DHW demand, and the total heating capacity of the two gas cooler units is expressed as:

$$\dot{Q}_{GC-DHW} = \dot{m}_{GC} \cdot c_p \cdot (T_S - T_{CW}) \qquad (3.16)$$

Due to the considerable difference between the set-point (storage) temperature for the DHW in the tank (T_S) and the inlet city water temperature (T_{CW}), the water flow rate though the gas cooler units ($\dot{m}_{GC}$) becomes quite small. Figure 3.19 shows the relationship between the total heating capacity of the DHW gas cooler units, and the resulting water flow rate at different DHW temperatures. The inlet water temperature is 10ºC.

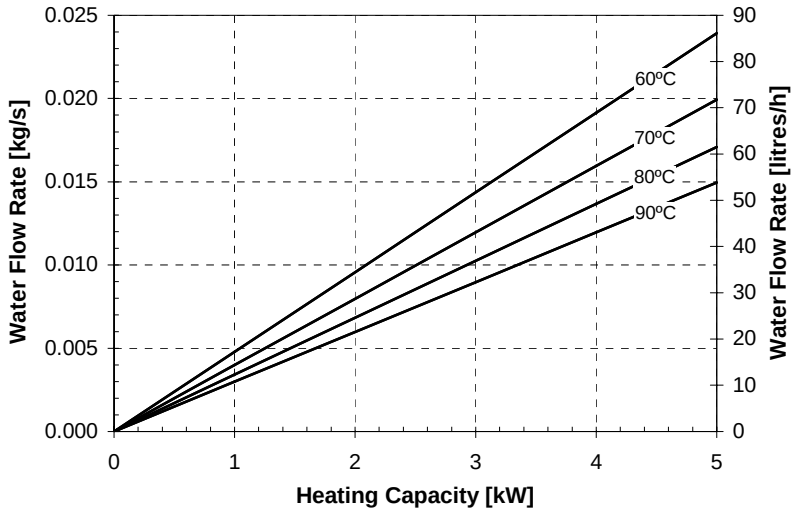

Figure 3.19 The relationship between the total heating capacity of the DHW gas cooler units and the water flow rate at different DHW temperatures. The inlet water temperature is 10ºC.

At equal heat loads, the mass flow rate in a floor heating system with 5 K temperature difference between the supply and return line will be roughly 10 to 15 times higher than that of the DHW system.

3.3.2 Operating Modes

The DHW system will be operating in three different modes:

- Tapping mode
- Charging (heating) mode
- Reheating mode

3.3.2.1 The Tapping Mode

Figure 3.20 shows the principle of the DHW system during the tapping mode. DHW at typically 60 to 85ºC (T_S) is drained from the top of the tank at a flow rate $\dot{m}_S$, premixed with city water to avoid risk of scolding, distributed to the tapping site(s) and finally mixed with city water to reach the desired tapping temperature T_T. City water at typically 5 to 20ºC (T_{CW}) is supplied at a flow rate $\dot{m}_{CW}$ at the bottom of the tank. The CO_2 heat pump unit is operative during the tapping mode, and the relatively small water flow $\dot{m}_{GC}$ is heated to the set-point temperature T_S.

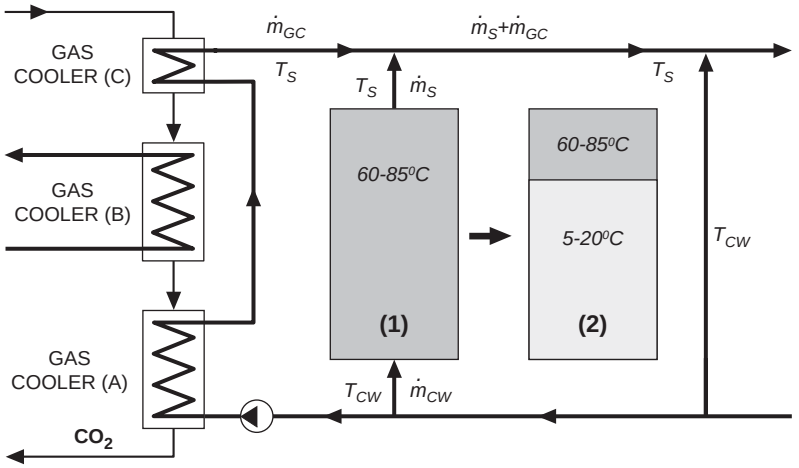

Figure 3.20 Principle of the DHW system during the tapping mode. (1) Tapping started, (2) Tapping ceased.

The total water flow rate from the DHW tank and the two CO_2 gas cooler units during the tapping period is:

$$\dot{m}_{tot} = \dot{m}_T \cdot \left(\frac{T_T - T_{CW}}{T_S - T_{CW}} \right) \tag{3.17}$$

where $\dot{m}_T$ and T_T are the total flow rate and water temperature at the tapping site(s), respectively. At 70ºC storage temperature, 10ºC city water temperature and 40ºC tap water temperature, the total water flow rate from the DHW system is 50% of the water flow rate at the tapping site(s).

3.3.2.2 The Charging (Heating) Mode

Figure 3.21 shows the principle of the DHW system during the charging (heating) mode. The cold water is pumped at a flow rate $\dot{m}_{GC}$ from the bottom of DHW the tank through the two gas cooler units, heated to the set-point temperature T_S, and delivered at the top of the tank. The required charging period for the DHW tank is:

$$\tau = \left[\frac{V_T \cdot \rho \cdot c_p \cdot (T_T - T_{CW})}{\dot{Q}_{GC-DHW}} \right] \tag{3.18}$$

where V_T is the total water consumption at the tapping site(s), and ρ and c_p are the density and the specific heat capacity of water, respectively.

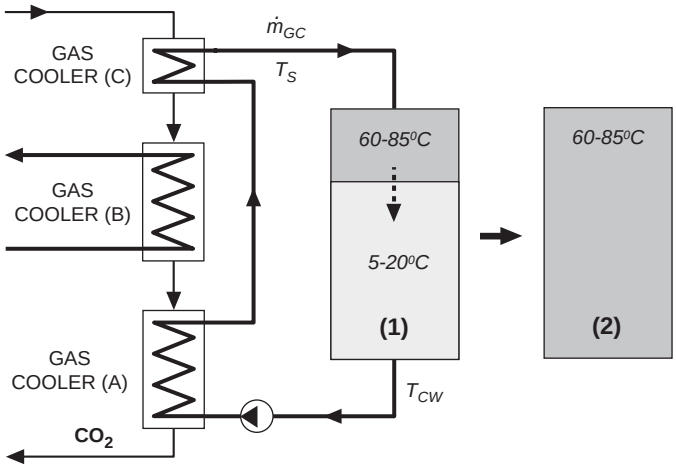

Figure 3.21 Principle of the DHW system during the charging (heating) mode. (1) Charging started, (2) Charging ceased.

Eq. (3.18) describes the theoretical minimum charging period, since the effects of mixing of hot and cold water, conductive heat transfer inside the tank and heat loss from the tank have not been taken into account (ref. Section 3.3.3). Figure 3.22 shows the minimum required charging period at different DHW consumptions V_T and gas cooler heating capacities.

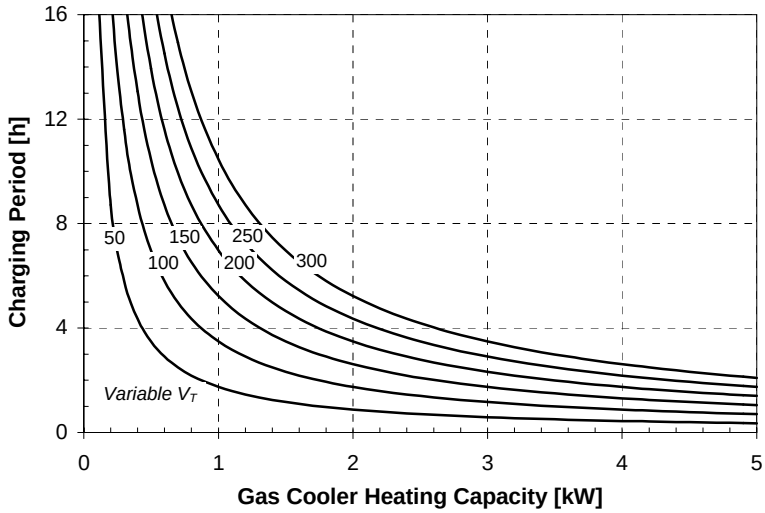

Figure 3.22 The minimum required charging period for the DHW system at different DHW consumption [litres] and gas cooler heating capacities. The DHW and city water temperatures are 70 and 10ºC, respectively.

Table 3.3 presents the required charging periods at typical DHW demands when the total heating capacity of the DHW gas cooler units ranges from 1 to 3 kW. For the calculations it has been assumed a city water temperature of 10ºC and a DHW temperature of 70ºC. The water consumption data are from Appendix F, *Characteristic Properties of DHW Systems*.

Table 3.3 The required charging period τ [hours] at different DHW demands and gas cooler heating capacities.

Tapping Sites	m_T [1)] [l/s]	Time [min]	V_T [2)] [litres]	τ_1 [h] *at 1 kW*	τ_2 [h] *at 2 kW*	τ_3 [h] *at 3 kW*
Washbasin x 3	0.1 x 3	1.1	20	0.7	0.4	0.2
Shower x 2	0.2 x 2	5.0	120	4.2	2.1	1.4
Bath-tub x 1	0.3	7.8	140	4.9	2.4	1.6
Aggregated demand	-	-	*280*	*9.8*	*4.9*	*3.2*

1) DHW flow rate (40ºC) 2) Total DHW demand (40ºC)

The duration of the charging period at the actual operating conditions is about 10 to 50 times longer than the duration of the tapping period.

3.3.2.3 The Reheating Mode

In periods with little or no DHW demand in the house, the water temperature in the tank may drop below the set-point due to heat loss from the tank shell, and the water needs to be reheated. Owing to the relatively high temperature level in the tank, only the DHW reheating gas cooler unit (C) can be used during the reheating mode. The DHW preheating gas cooler unit (A) can be by-passed either on the water side or the CO_2 side. When by-passing on the water side, two solenoid valves and a temperature sensor are required. Figure 3.23 shows the principle of the by-pass arrangement. The extra tubing and components will ensure proper operation of the tripartite gas cooler, but will increase the cost and complexity of the system. An alternative solution for the reheating mode is to use the electric immersion element located near the bottom of the tank for reheating of the DHW.

When the heat pump unit is operated in the combined heating mode, the by-pass arrangement will be needed if the inlet water temperature from the DHW tank exceeds the CO_2 outlet temperature from the space heating gas cooler (B).

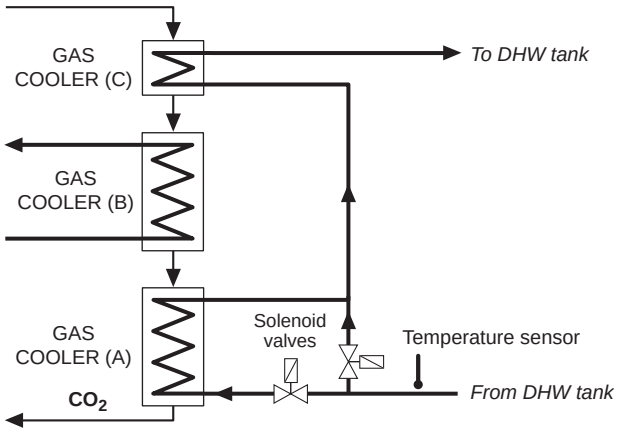

Figure 3.23 Principle of a valve arrangement which by-pass the water flow to gas cooler C during the reheating mode.

3.3.3 Exergy Losses in the DHW Storage Tank

The main exergy losses in the DHW storage tank are related to heat loss through the tank walls, mixing of hot and cold water during the tapping and charging modes and conductive heat transfer inside the tank.

3.3.3.1 Heat Loss Through the Tank Walls

Standard-sized cylindrical DHW tanks are normally insulated with 40 mm fibre glass or expanded polystyrene (EPS), having a thermal conductivity of typically 0.045 and 0.035 W/(mK) respectively. At an ambient temperature of 20ºC and DHW temperatures ranging from 60 to 90ºC, the mean heat flux from the tanks will range from about 35 to 60 W/m^2 for glass-wool insulation and 30 to 50 W/m^2 for EPS insulation.

The temperature drop in the DHW tank can be estimated by the following differential equation when assuming uniform water temperature in the tank:

$$-\left(M_W \cdot c_{p-W} + M_T \cdot c_{p-T}\right) \cdot d\theta = \left(U \cdot A \cdot \theta\right) \cdot d\tau \qquad (3.19)$$

where M_W and M_T are the total mass of the water and the stainless DHW steel tank, $c_{p\text{-}W}$ and $c_{p\text{-}T}$ are the specific heat capacity of the water and the tank, U is the overall heat transfer coefficient for the tank wall, A is the total outside surface area of the tank, and θ is the temperature difference between the water and the ambient air.

By integrating Eq. (3.19), the DHW temperature T_S in the tank after a period τ is calculated as follows:

$$T_S = T_R + \theta_0 \cdot e^{-\kappa \cdot \tau} \tag{3.20}$$

where

$$\kappa = \left[\frac{U \cdot A}{\left(M_W \cdot c_{p-W} + M_T \cdot c_{p-T} \right)} \right] \tag{3.21}$$

where T_R is the room temperature and θ_0 is the initial temperature difference between the DHW and the ambient air.

Figure 3.24 shows the calculated mean temperature drop in a 200 litre glass-wool insulated DHW tank during 48 hours storage time. The initial DHW temperature ranges from 60 to 90ºC and the room temperature is 20ºC. In the calculations the convective heat transfer coefficient between the tank wall and the ambient air was estimated to be 10 W/(m^{2}K).

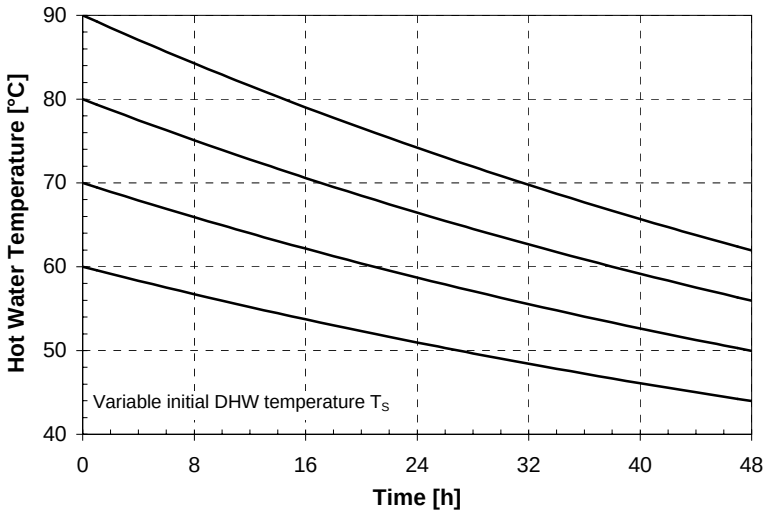

Figure 3.24 The mean temperature drop in a 200 litre glass-wool insulated DHW tank at different initial DHW temperatures.

At 70ºC initial DHW temperature, the temperature drop is about 10 K during a period of 24 hours, which corresponds to an average temperature drop of about 0.4 K per hour. Hence, during normal operation of the DHW system with regular tapping and charging, reheating of the water in the tank is not required. However, reheating will be necessary if there is no tapping during longer periods, e.g. during weekends and holidays.

The mean temperature drop in the tank during a 24 hour period is also influenced by the insulation standard, the tank volume and the ambient air temperature. Table 3.4 shows the estimated annual heat loss from a 200 litre DHW tank at different temperatures when using different insulation materials. The boundary conditions are as in Figure 3.24.

Table 3.4 The annual heat loss from a 200 litre DHW tank at different DHW temperatures and insulation types.

Insulation type	Annual Heat Loss [kWh/year]			
	60°C	**70°C**	**80°C**	**90°C**
Glass-wool	880	1110	1320	1550
XPS	700	880	1060	1230

By replacing the glass-wool with expanded polystyrene (EPS), the annual heat loss from the DHW tank will be reduced by about 20%.

The annual exergy loss in J due to the heat loss through the tank wall is calculated as:

$$\Delta E = \left(E_{in} - E_{out}\right) = Q \cdot \left(\frac{T_S - T_0}{T_S} - \frac{T_R - T_0}{T_R} \right) \qquad (3.22)$$

where Q is the annual heat loss from the tank, T_S is the DHW storage temperature in the tank, T_R is the room temperature and T_0 is the reference temperature (e.g. the outdoor temperature). At 70ºC storage temperature, 20ºC ambient air temperature and 0ºC reference temperature, the exergy loss constitutes about 15% of the heat loss from the tank.

3.3.3.2 Mixing of Hot and Cold Water

During the tapping and charging (heating) periods, the inlet water flows will lead to inevitable mixing of some of the hot and cold water in the DHW tank. This will in turn increase the average inlet water temperature to the DHW preheating gas cooler unit during the charging period, and with that reduce the COP of the CO_2 heat pump (ref. Figure 3.4 in Section 3.2.2.1). Figure 3.25 illustrates an idealized mixing process, where T_m and V_M refer to the average temperature and the water volume of the mixing zone, respectively.

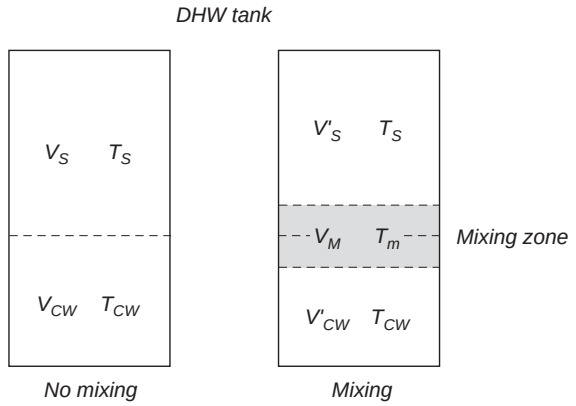

Figure 3.25 Principle of the mixing of hot and cold water in a DHW tank during the tapping and charging modes.

Since the water flow rate during the tapping period is in the order of 10 to 50 times higher than that of the charging period, the mixing is mainly a problem during tapping. In an idealized mixing process, the cold city water volume will be reduced by ½ V_M, and the total water volume that has to be heated by the CO_2 heat pump, will increase by ½ V_M.

The exergy loss in J due to the mixing can be estimated as follows, when using average values for the density ρ and the specific heat capacity c_p:

$$\Delta E = \frac{V_M}{2} \cdot \rho \cdot c_p \cdot (T_m - T_{CW}) \cdot \left[\frac{T_S - T_0}{T_S} + \frac{T_{CW} - T_0}{T_{CW}} - 2 \cdot \left(\frac{T_m - T_0}{T_m} \right) \right] \quad (3.23)$$

where

$$T_m = \frac{T_S + T_{CW}}{2} \quad (3.24)$$

According to the first law of thermodynamics, the mixing process will not affect the total heating demand during the charging period, i.e.:

$$V_{CW} \cdot \rho \cdot c_p \cdot (T_S - T_{CW}) = V'_{CW} \cdot \rho \cdot c_p \cdot (T_S - T_{CW}) + V_M \cdot \rho \cdot c_p \cdot (T_S - T_m) \quad (3.25)$$

However, the mixing of hot and cold water will increase the energy consumption for the CO_2 heat pump unit, since the COP is heavily affected by the inlet water temperature to the DHW preheating gas cooler unit. Hence:

$$\frac{V_{CW} \cdot \rho \cdot c_p \cdot (T_S - T_{CW})}{COP_{T-CW}} \leq \frac{V'_{CW} \cdot \rho \cdot c_p \cdot (T_S - T_{CW})}{COP_{T-CW}} + \frac{V_M \cdot \rho \cdot c_p \cdot (T_S - T_m)}{COP_{T-m}} \quad (3.26)$$

where the subscripts *T-CW* and *T-m* refer to the COP of the CO_2 heat pump at the inlet water temperatures T_{CW} and T_m for the gas cooler. The equality sign is only valid when $V'_{CW}=V_{CW}$, i.e. when $V_M=0$.

Figure 3.26 shows, as an example, the estimated percentage reduction in the COP for a residential CO_2 heat pump water heater operating at different DHW temperatures, 10ºC city water temperature and varying extent of the mixing zone. The COP data for the CO_2 heat pump unit are from Figure 3.4 in Section 3.2.2.1. A relative extent of the mixing zone of 0.5, means that 50% of the city water volume has been mixed with an equal amount of DHW, and reached an intermediate temperature T_m.

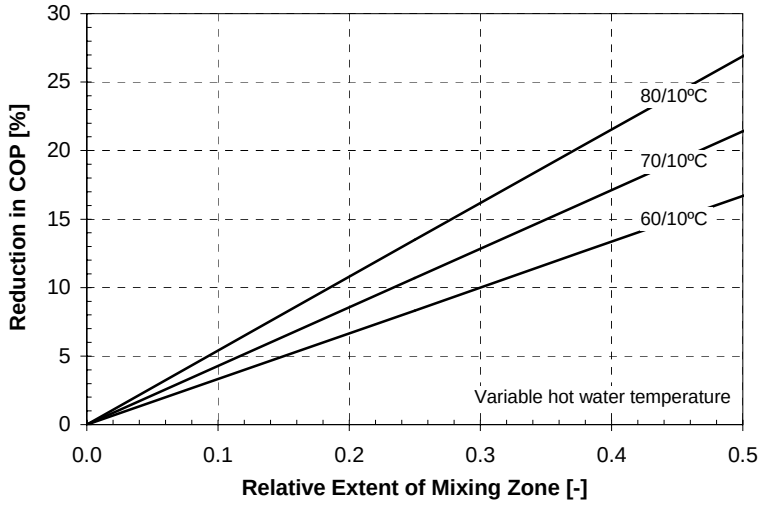

Figure 3.26 Percentage reduction in the COP for a residential CO_2 heat pump as a function of the relative extent of the mixing zone and the DHW temp. The city water temp. is 10ºC .

The mixing loss can be greatly reduced by installing adequate diffusers that decrease the inlet water velocities. A device that eliminates the mixing is presented in Section 3.3.4.

3.3.3.3 Conductive Heat Transfer Inside the DHW Tank

Owing to the direct contact and the relatively high initial temperature difference between the hot and cold water reservoirs in the DHW tank during the tapping and charging periods, there will be considerable conductive heat transfer between the reservoirs. This will in turn increase the average inlet water temperature for the DHW preheating gas cooler unit during the charging period, and reduce the COP of the heat pump.

The temperature gradient between the water reservoirs is denoted *the thermocline*, and the extent of the thermocline zone is mainly depending on the initial temperature difference (T_S-T_{CW}) and the duration of the tapping and charging periods. Figure 3.27 shows the principle of a thermocline in a DHW tank, where $V_{TC\text{-}CW}$ is the city water volume that has been heated by the DHW reservoir, $V_{TC\text{-}S}$ is the DHW volume that has been cooled by the city water reservoir, V_{TC} is the total volume of the thermocline zone and T_m is the average thermocline temperature.

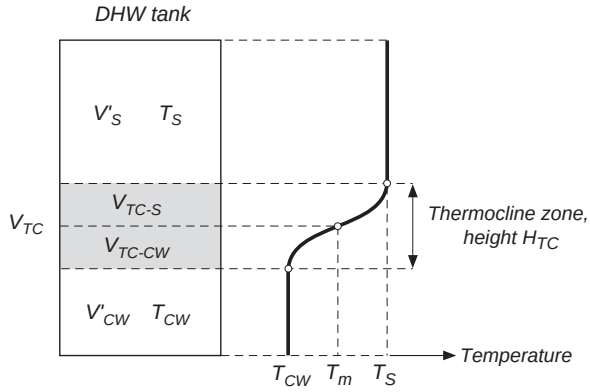

Figure 3.27 Principle of the thermocline, i.e. the temperature gradient, between the hot and cold water reservoirs in a DHW tank.

$V_{TC\text{-}CW}$ and $V_{TC\text{-}S}$ are identical as long as there is no mixing of hot and cold water, the heat transfer through the tank walls is neglected and the density, the specific heat capacity and the thermal conductivity of water are regarded independent of temperature. At temperatures ranging from 10 to 80ºC, these properties will deviate by less than ±1.5%, ±0.2% and ±6.5% from their average values, respectively (NIST, 2000).

The total volume of the thermocline zone is calculated as:

$$V_{TC} = \left(V_{TC-CW} + V_{TC-S}\right) = A_{DHW} \cdot H_{TC} \qquad (3.27)$$

were A_{DHW} is the cross-sectional area of the DHW tank and H_{TC} is the total height of the thermocline zone.

The general conduction equation (Kreith and Black, 1980) can be used to determine the transient temperature gradient between the hot and cold water reservoirs, and ultimately the extent and the average temperature of the thermocline zone:

$$\frac{\partial^2 T}{\partial x^2} + \frac{\partial^2 T}{\partial y^2} + \frac{\partial^2 T}{\partial z^2} = \frac{1}{\alpha} \cdot \frac{\partial T}{\partial t} \tag{3.28}$$

and

$$\alpha = \frac{k}{\rho \cdot c_p} \tag{3.29}$$

where α is the thermal diffusivity of water.

Figure 3.28 shows the estimated heat flux across a thermocline as a function of the thickness of the thermocline zone (H_{TC}) and the initial temperature difference (ΔT) between the hot and cold water reservoirs. Constant thermal conductivity for the water was assumed.

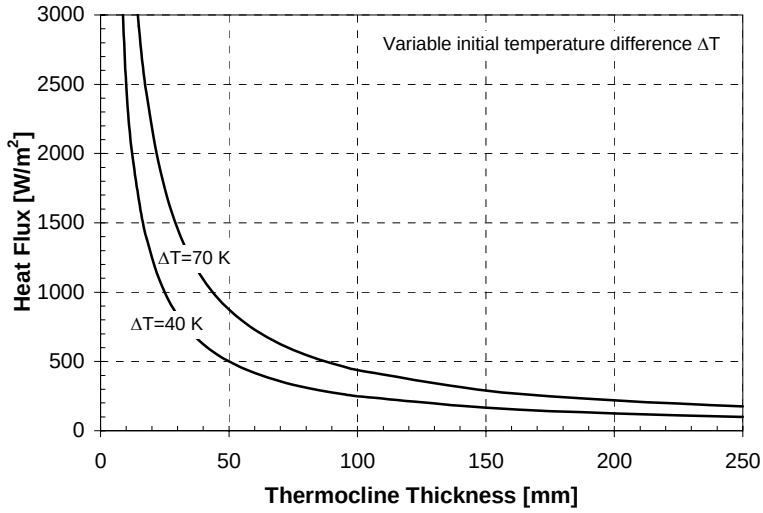

Figure 3.28 The heat flux across the thermocline as a function of the thermocline thickness H_{TC} and the initial temperature difference ΔT.

Since the heat flux between the reservoirs is inversely proportional to the thickness of the thermocline zone, the growth rate of the zone ($\partial H_{TC}/\partial t$) will drop off gradually during the tapping and charging periods.

When the average temperature T_m and the volume of the thermocline zone V_{TC} are known, the exergy loss in the DHW tank and the reduction in COP for the CO_2 heat pump can be estimated according to Eq. (3.23) and (3.26), respectively.

3.3.4 Application of a Movable Insulating Plate Inside the DHW Tank

One way to reduce the internal conductive heat transfer and to eliminate the mixing in cylindrical single-shell DHW tanks, is to separate the water volumes by means of *a plate with low thermal conductivity*. Since the contact surface between the hot and cold water is moving up and down during the tapping and charging periods, respectively, the plate has to be movable. The simplest method to ensure proper function of the plate at all operating conditions is to utilize the density difference between the hot and cold water. Figure 3.29 shows the density of pure water at 6 bar as a function of temperature.

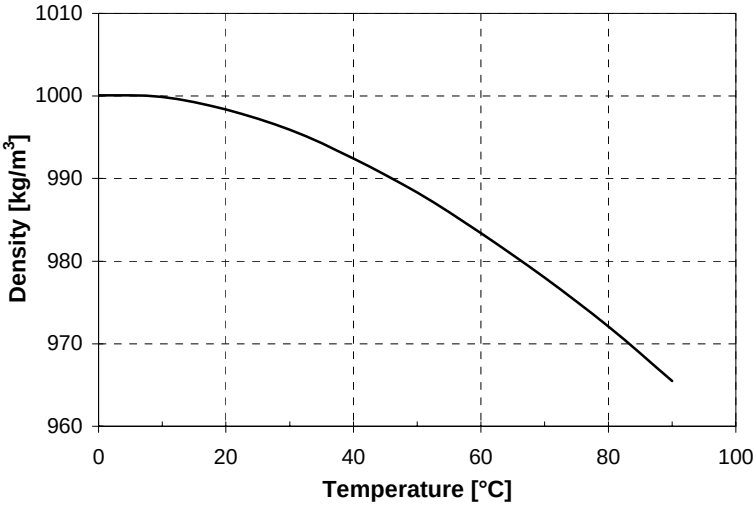

Figure 3.29 The density of pure water at 6 bar (NIST, 2000).

By employing an insulating plate which average density is lower than that of the cold city water (5 to 20ºC) and higher than that of the DHW (60 to 85ºC), the plate will always be located between the water reservoirs due to the hydrostatic force balance (Nozomi, 1986).

The hydrostatic force balance of a submerged plate can be expressed as:

$$p + (\rho_1 \cdot g \cdot H_1) + \rho_{IP} \cdot g \cdot (H_2 + H_3) = p + \rho_1 \cdot g \cdot (H_1 + H_2) + (\rho_2 \cdot g \cdot H_3) \quad (3.30)$$

and

$$\rho_{IP} = \left(\frac{\rho_1 \cdot H_2 + \rho_2 \cdot H_3}{H_2 + H_3} \right) \quad (3.31)$$

where g is the acceleration due to gravity, p is the static pressure in the tank, ρ is the density of the hot and cold water, ρ_{IP} is the average density of the insulating plate and H are the heights as illustrated in Figure 3.30.

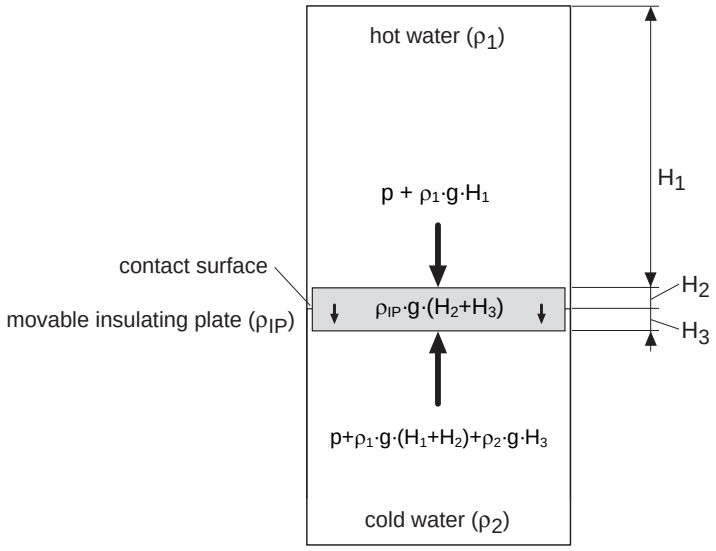

Figure 3.30 Principle of the hydrostatic force balance of a movable insulating plate in a circular DHW tank.

With reference to Eq. (3.31), *the underside* of the insulating plate will be located at the contact surface between the water reservoirs (i.e. $H_3 \rightarrow 0$) when the average density of the plate (ρ_{IP}) approaches the density of the DHW (ρ_1). On the other hand, when the average density of the plate approaches the density of the cold water (ρ_2), *the upper side* of the plate will be located at the contact surface (i.e. $H_2 \rightarrow 0$).

The diameter of the insulating plate should be roughly 5 to 10 mm less than the inner diameter of the DHW tank in order to avoid undesirable friction forces between the plate and the tank wall, which could alter the hydrostatic balance of the plate. When the plate reaches the top or bottom position in the tank during the tapping and charging periods, the water can flow freely through the cylindrical gap.

Figure 3.31 shows the fundamental function of the movable insulating plate during the tapping and charging modes.

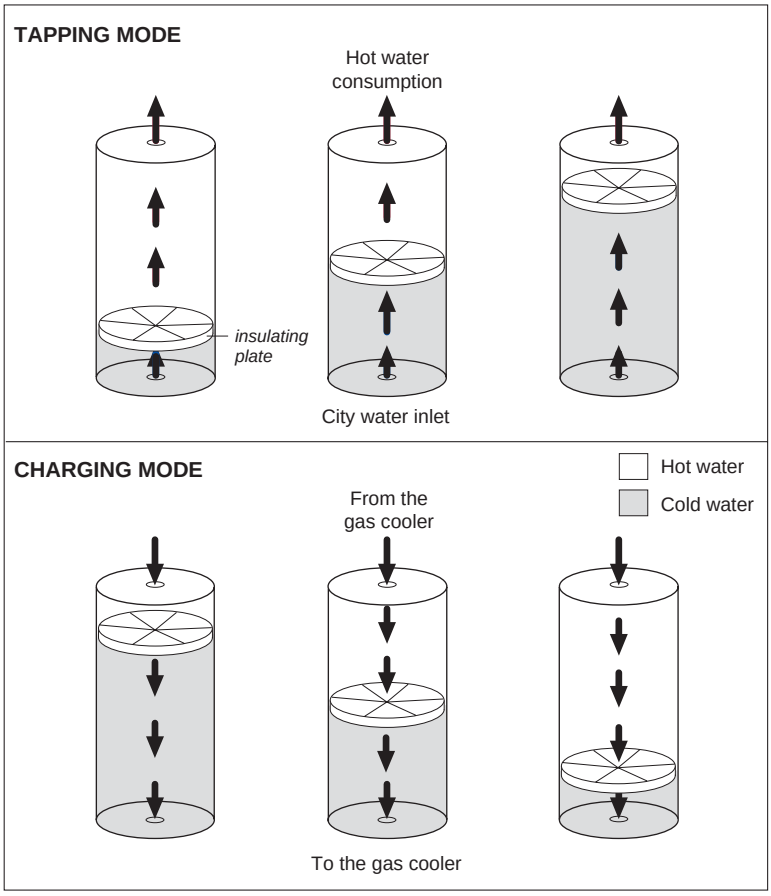

Figure 3.31 Principle of a cylindrical DHW tank equipped with a movable insulating plate for separation of the hot and cold water reservoirs.

Since the density of solid insulators of current interest are considerably lower than that of water, *a balancing weight* must be attached to the plate. The required mass (M_{BW}) of the balancing weight is calculated on the basis of the mass of the insulating plate (M_{IP}), the density of water (ρ_W) at an intermediate temperature (e.g. 35-40ºC), and the volumes of the insulating plate (V_{IP}) and the balancing weight (V_{BW}):

$$M_{BW} = \left(V_{IP} + V_{BW}\right) \cdot \rho_W - M_{IP} \tag{3.32}$$

Details regarding the design of the balancing weight and the selection of plate material are discussed in Appendix G, *Application of a Movable Insulating Plate in Cylindrical Single-Shell DHW Tanks*.

3.3.5 Testing and Modelling of DHW Tanks and Movable Insulating Plates

A full scale DHW tank test rig was constructed to study the transient temperature development in cylindrical single-shell DHW tanks caused by internal and external heat transfer. The tank was also used to examine the feasibility of using a movable insulating plate to reduce the exergy losses in the tank. The design of the test rig and the test programme are presented in Section 4.2, *Testing of a DHW Tank and a Movable Insulating Plate*, whereas the results are presented and discussed in Section 5.2, *Testing of a DHW Tank and a Movable Insulating Plate*, and Section 7.1.2.4, *The COP vs. the Thermodynamic Losses in the DHW Tank*.

A transient two-dimensional heat conduction model was also developed in order to enable tailor-made calculations of the transient temperature development in cylindrical single-shell DHW tanks at topical tank designs, temperature levels, DHW demands and gas cooler heating capacities. The thermodynamic basis and the mathematical background for the model as well as the simulation results are presented in Section 6.2, *Modelling of Cylindrical Single-Shell DHW Tanks*.

4 Test Rig Design and Experimental Methods

This chapter expands on Chapter 3, *Theoretical Background and System Evaluations*, and provides a detailed presentation of the design, instrumentation and experimental methods for the following test rigs:

- A 6.5 kW residential brine-to-water CO_2 heat pump unit for combined space heating and hot water heating (prototype).
- A 200 litre cylindrical single-shell domestic hot water (DHW) tank, including two movable insulating plates (prototypes).

The main purpose of the heat pump test rig was to document the energy efficiency and operational characteristic in order to evaluate the technical potential of integrated CO_2 heat pump systems in residential applications. The objective of the second test rig was to measure the transient temperature development in cylindrical single-shell DHW tanks caused by internal and external heat transfer, and to examine the feasibility of using an insulating plate between the hot and cold water volumes to reduce the exergy losses in the tank.

4.1 Testing of a Residential Brine-to-Water CO_2 Heat Pump Unit

4.1.1 Introduction

A residential brine-to-water CO_2 heat pump unit for combined space heating and hot water heating was constructed in order to measure the heating capacity and COP as well as to study component and system behaviour over a wide range of operating conditions. Since it was considered as interesting to run the unit at realistic operating conditions and obtain long-term operational experience, the prototype CO_2 heat pump was installed in a detached pilot house situated in Trondheim, Norway.

The prototype heat pump system comprised the following sub-systems:

1) An integrated brine-to-water CO_2 heat pump unit
2) A heat source system (energy well, indirect system)
3) A space heating (SH) system – hydronic floor heating
4) A domestic hot water (DHW) system.

The heat pump system was operated in two different modes:

- In the *Auto mode*, the CO_2 heat pump unit utilized a 150 m deep rock well as heat source, and supplied heat to a 200 m^2 low-temperature floor heating system and a 300 litre single-shell DHW tank. A Satchwell data acquisition system was used to control the overall system and the individual components, and to collect and process data from the temperature sensors, pressure transducers, volume/mass flow meters and watt meters.
- In the *Test mode*, the CO_2 heat pump unit was operated independently of the heat source system, the floor heating system and the DHW tank in order to measure the performance at specified operating conditions. In this mode, all components, such as the CO_2 compressor, pumps, and control valves were controlled manually, and the data from the data acquisition system were transferred to tailor-made Excel spreadsheets for further processing and analysis.

Virtually all experiments were carried out in the Test mode, and the few results from the Auto mode were mainly used to compare the performance of the evaporator and the tripartite gas cooler with the design data.

4.1.2 Design of the CO_2 Heat Pump Unit

4.1.2.1 General

The prototype brine-to-water CO_2 heat pump unit was designed for a total heating capacity of approximately 6.5 kW in the combined heating mode. The CO_2 process as well as the individual components were analysed and designed by using MS Excel, Coolpack (Rasmussen, 2001) and software for heat exchanger design and analysis developed at NTNU-SINTEF, Department of Energy and Process Engineering. The integrated CO_2 heat pump unit was constructed from the following components:

- A hermetic two-stage rolling piston compressor
- A tripartite counterflow tube-in-tube gas cooler for:
  - Preheating of hot water (*DHW preheating gas cooler unit*)
  - Low-temperature space heating (*SH gas cooler unit*)
  - Reheating of hot water (*DHW reheating gas cooler unit*)
- A counterflow tube-in-tube suction gas heat exchanger
- A cross-flow subcooler
- Manual throttling valves (back-pressure valve and needle valve)
- A low-pressure receiver (LPR)
- An oil return system including filter
- Control valves, closing valves and safety valves (8 and 12 MPa)

The design conditions for the heat pump unit are presented in Table 4.1.

Table 4.1 Design conditions for the residential CO_2 heat pump unit.

Component/Mode	**Parameter**	**Value**
Compressor	Suction pressure (-5ºC)	3.046 MPa
	Suction temperature	0ºC
	Discharge pressure	8.5 to 9.0 MPa
	CO_2 mass flow rate	~1.40 kg/min
Evaporator	Evaporation temperature	-5ºC
	LMTD	~5 K
Tripartite Gas Cooler	SH – Water temperatures	**35/30ºC**
Combined mode	SH – Heating capacity	~3.0 kW
	SH – Temperature approach	< 0.2 K
	DHW – Water temperatures	**5/60ºC**
	DHW – Heating capacity	~3.5 kW
	DHW – Temperature approach	< 3 K
DHW Gas Coolers Units	Water temperatures	**5/60ºC**
DHW mode	Heating capacity	~7.0 kW
	Temperature approach	< 3 K
SH Gas Cooler Unit	Water temperatures	**35/30ºC**
SH mode	Heating capacity	~5.5 kW
	Temperature approach	< 0.2 K

Figure 4.1 shows the principle of the integrated CO_2 heat pump unit including the instrumentation.

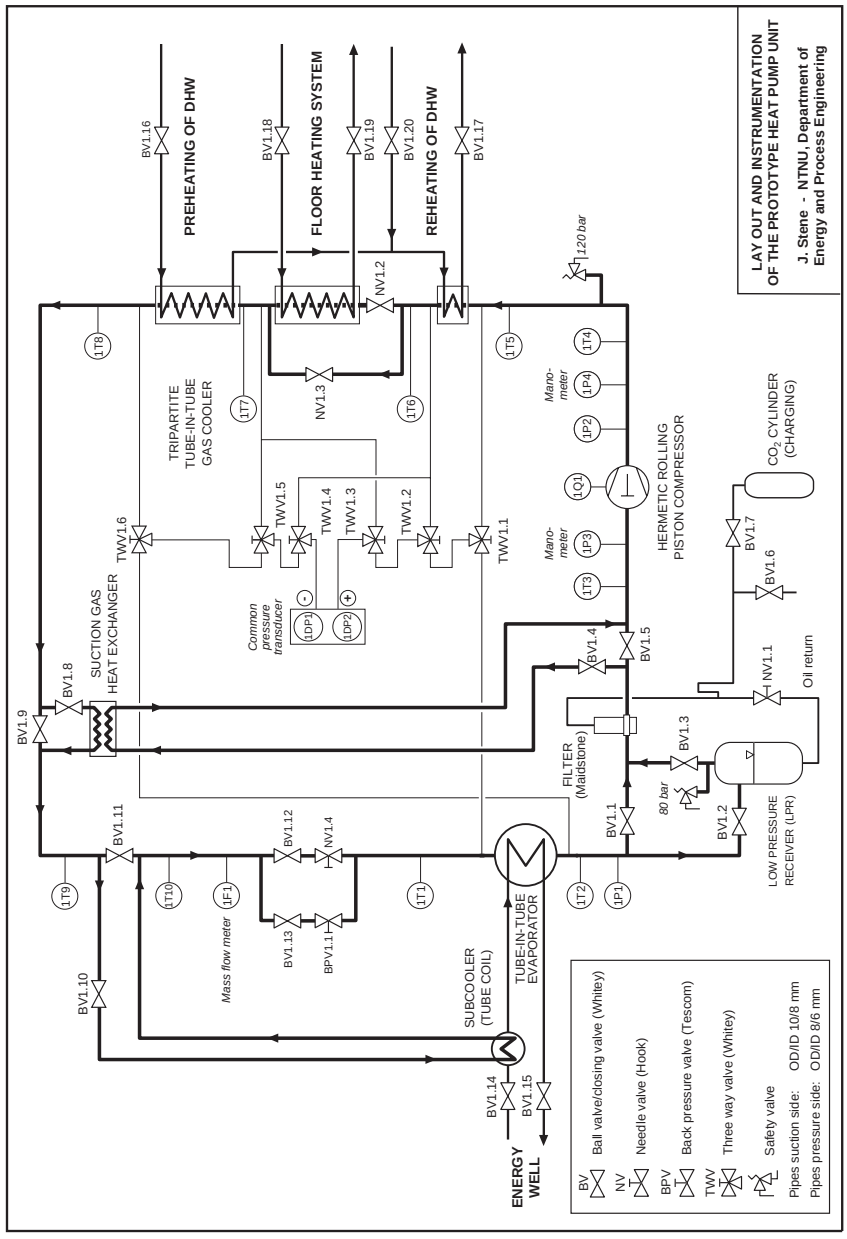

Figure 4.1 Principle of the integrated CO_2 heat pump unit.

Figures 4.2 and 4.3 show the prototype CO_2 heat pump unit before it was installed in the pilot house (reference is also made to Appendix E).

Figure 4.2 Front view of the prototype CO_2 heat pump unit.

Figure 4.3 Rear view of the prototype CO_2 heat pump unit.

4.1.2.2 The Compressor

The prototype CO_2 heat pump unit was initially equipped with a Dorin CD5.0175 compressor, Figure 4.4. This is a semi-hermetic single-stage reciprocating unit with two cylinders. At a rotational speed of 1450 rpm, the swept volume is 1.75 m^3/h. This corresponds to a heating capacity of approximately 6 kW at +5ºC suction temperature and 35 and 85 bar suction and discharge pressure, respectively.

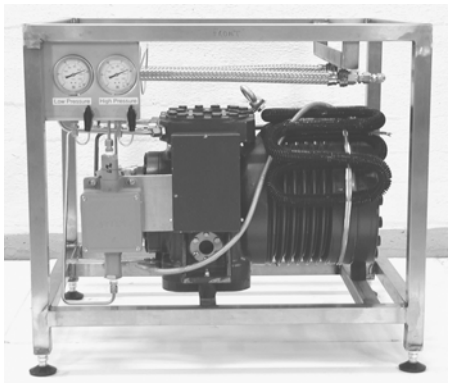

Figure 4.4 The Dorin single-stage reciprocating CO_2 compressor.

During the function testing of the CO_2 heat pump, the CO_2 mass flow rate dropped gradually due to extensive wear and tear in the bearing for the connecting rod between the crankshaft and the piston. The compressor was therefore replaced by *a prototype hermetic two-stage rolling piston compressor* from Sanyo (Tadano et al., 2000), Figure 4.5.

Figure 4.5 The Sanyo two-stage rolling piston compressor (prototype).

The rotational speed, and with that the heating capacity of the Sanyo compressor, was controlled by a tailor-made AC inverter from Sanyo.

The specifications of the prototype compressor are presented in Table 4.2.

Table 4.2 Specifications for the rolling piston compressor (prototype).

Compressor	
Type:	Hermetic two-stage rolling piston unit Operated as a single-stage unit (LP + HP)
Operating range:	1800 to 7200 rpm (30 to 120 Hz)
Displacement volume:	3.33 cm^3/rev (LP) and 1.88 cm^3/rev (HP)
Swept volume:	1.439 m^3/h at 7200 rpm
Max. operating pressure:	14 MPa
Max. discharge temperature:	125ºC at continuous operation
Motor	
Type:	Digitally controlled brushless motor – 4 poles
Maximum power input:	2500 W
Lubricant	
Type:	Polyalkylene glycol (PAG)
Viscosity:	100 cSt
Properties:	- Non-soluble with CO_2 - Heavier than saturated CO_2 liquid above -15°C - Excellent thermal and chemical stability - High viscosity index - High flash point – low pour point - Hygroscopic
Oil discharge:	- Approximately 6 to 9% of total mass flow rate (100 Hz). Oil discharge rate increases with rpm and lower suction/discharge pressure (Hubacher and Groll, 2002)

Figure 4.6 shows the principle compressor arrangement with gas flows at suction pressure, intermediate pressure and discharge pressure.

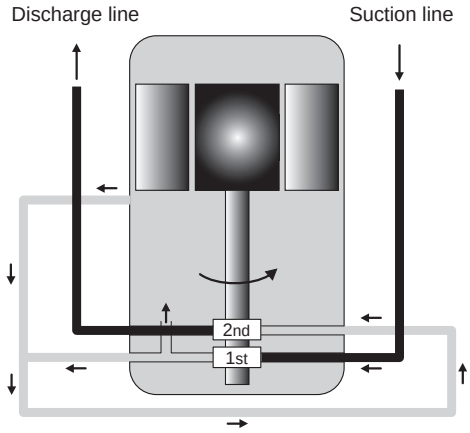

Figure 4.6 Principle of the Sanyo hermetic two-stage rolling piston compressor (Bouma, 2002).

The compressor was charged with about *400 g of PAG oil*. Although the oil discharge from the rolling piston compressor was quite high (ref. Table 4.2), it was decided to operate the unit without an oil separator. The main reason for this was that the construction of the prototype heat pump unit was considerably overdue, and construction and testing of a tailor-made oil separator would have delayed the project further. Reference is made to Section 5.1.3.7, *Evaporator Performance*, and 5.1.3.8, *Performance and Main Operating Characteristics of the Tripartite Gas Cooler*, regarding the impact of the lubricant on heat transfer in the evaporator and the tripartite gas cooler. The estimated overall isentropic efficiency and the relative heat loss for the compressor at various operating conditions are presented in Section 5.1.3.6, *Compressor Performance*.

4.1.2.3 The Evaporator

The evaporator was a helical counter-flow tube-in-tube heat exchanger. The main reason for selecting this type of heat exchanger was the moderate costs, and the fact that the heat exchanger could be easily constructed at the engineering workshop of NTNU, Department of Energy and Process Engineering. Table 4.3 shows the specifications of the evaporator.

A copper wire with suitable thickness was wrapped as a spiral around the inner CO_2 tube in order to maintain uniform distance between the CO_2 tube and the brine tube. Figure 4.7 shows a sketch of the cross section of the tubes and the centring wire, whereas Figure 4.8 shows the evaporator mounted in the test rig before the plant was insulated.

Table 4.3 Technical specifications for the evaporator.

Type:	Tube-in-tube heat exchanger
Number of circuits:	One
Material:	Stainless steel, both tubes
Diameters, inner tube (CO_2):	D_i = 8 mm D_o = 10 mm
Diameters, outer tube (brine):	D_i = 20 mm D_o = 24 mm
Tube length:	12 m
Average coil diameter:	450 mm
Approximate weight:	17 kg
Heat transfer area, inner tube (CO_2): Heat transfer area, inner tube (brine): Ratio, heat transfer areas (A_o/A_i):	A_i = 0.302 m^2 A_o = 0.377 m^2 1.25
Cross-sectional area, inner tube (CO_2): Cross-sectional area, annuli (brine):	$A_{c,i}$ = 50 mm^2 $A_{c,o}$ = 236 mm^2

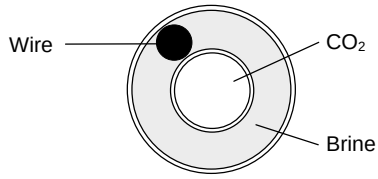

Figure 4.7 Principle of the cross section of the evaporator.

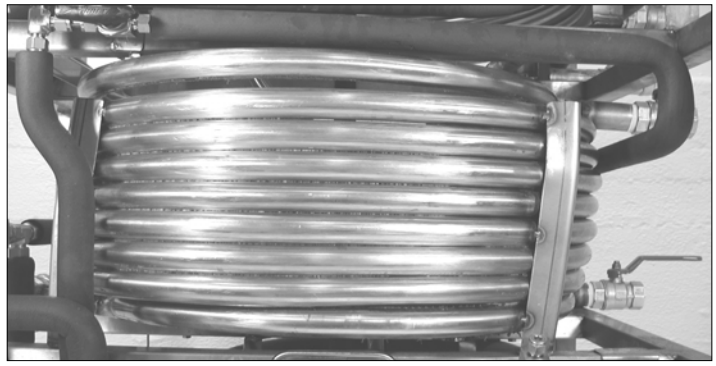

Figure 4.8 The tube-in-tube evaporator mounted in the test rig.

The evaporator was insulated with 25 mm Armaflex (k=0.032 W/(mK)), and aluminium tape was used as diffusion block.

4.1.2.4 The Tripartite Gas Cooler

The CO_2 gas cooler for preheating of DHW, low-temperature space heating and reheating of DHW, was designed as three separate helical counter-flow tube-in-tube heat exchangers. Figure 4.9 illustrates the principle for the tripartite gas cooler with superimposed CO_2 flows and water flows.

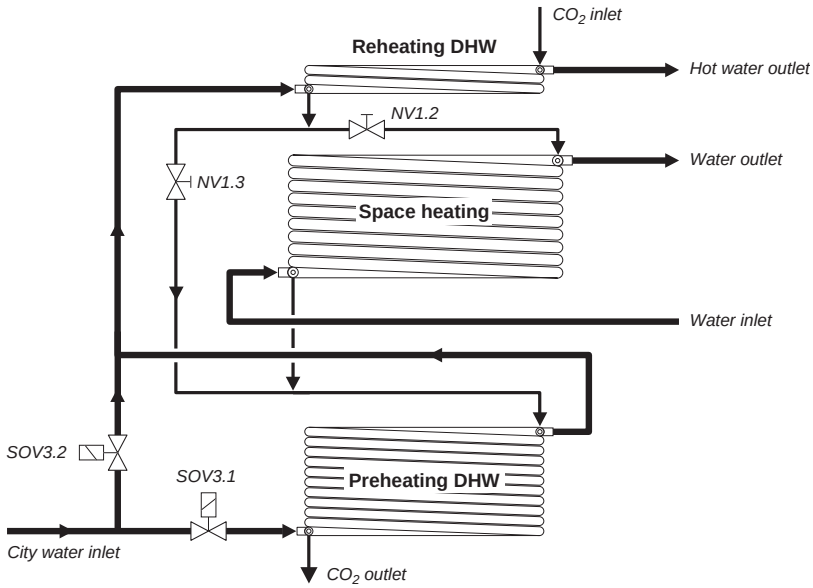

Figure 4.9 Principle configuration for the tripartite gas cooler.

When the unit was operated as a heat pump water heater, the CO_2 flow was bypassed the space heating gas cooler by closing needle valve NV1.2 (*Hook*) and opening needle valve NV1.3 (*Hook*). In order to ensure proper oil return, the counter-flow heat exchangers were operated with the CO_2 flowing downwards and the water flowing upwards. Under normal operation conditions, solenoid valve SOV3.1 (*Danfoss*) was open and solenoid valve SOV3.2 (*Danfoss*) was closed. However, in special cases when the inlet water temperature to the DHW preheating gas cooler exceeded the CO_2 outlet temperature from the space heating gas cooler, SOV3.1 was closed and SOV3.2 was opened to avoid heating of the CO_2 and subsequent operational problems. Reference is made to Section 3.3.2.3, *The Reheating Mode*, for further details on this topic.

Tables 4.4 to 4.6 present the technical specifications for the tripartite tube-in-tube gas cooler.

Table 4.4 Technical specifications for the tube-in-tube gas cooler for preheating of domestic hot water (DHW).

Type:	Tube-in-tube heat exchanger
Number of circuits:	One
Material:	Stainless steel, both tubes
Diameters, inner tube (CO_2):	D_i = 6 mm D_o = 8 mm
Diameters, outer tube (water):	D_i = 12 mm D_o = 16 mm
Tube length:	14 m
Average coil diameter:	350 mm
Approximate weight:	13 kg
Heat transfer area, inner tube (CO_2 side): Heat transfer area, inner tube (brine side): Ratio, heat transfer areas (A_o/A_i):	A_i = 0.264 m^2 A_o = 0.352 m^2 1.33
Cross-sectional area, inner tube (CO_2 side): Cross-sectional area, annuli (brine side): Ratio, cross-sectional areas ($A_{c,o}/A_{c,i}$):	$A_{c,i}$ = 28 mm^2 $A_{c,o}$ = 63 mm^2 2.2

Figure 4.10 shows the tube-in-tube gas cooler for preheating of DHW mounted in the test rig. The insulated suction gas heat exchanger (SGHX) can be seen above the gas cooler.

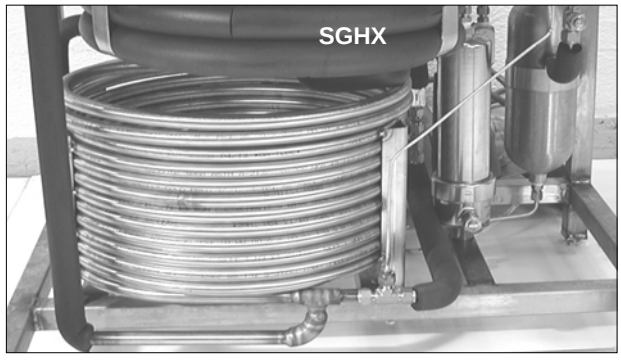

Figure 4.10 The tube-in-tube gas cooler for preheating of DHW.

Table 4.5 Technical specifications for the tube-in-tube gas cooler for reheating of domestic hot water (DHW).

Type:	Tube-in-tube heat exchanger
Number of circuits:	One
Material:	Stainless steel, both tubes
Diameters, inner tube (CO_2):	D_i = 6 mm D_o = 8 mm
Diameters, outer tube (water):	D_i = 12 mm D_o = 16 mm
Tube length:	3.5 m
Average coil diameter:	350 mm
Approximate weight:	3 kg
Heat transfer area, inner tube (CO_2 side): Heat transfer area, inner tube (water side): Ratio, heat transfer areas (A_o/A_i):	A_i = 0.067 m^2 A_o = 0.088 m^2 1.33
Cross-sectional area, inner tube (CO_2 side): Cross-sectional area, annuli (water side): Ratio, cross-sectional areas ($A_{c,o}/A_{c,i}$):	$A_{c,i}$ = 28 mm^2 $A_{c,o}$ = 63 mm^2 2.2

Figure 4.11 shows the tube-in-tube gas cooler for reheating of DHW before it was mounted in the test rig.

Figure 4.11 The tube-in-tube gas cooler for reheating of hot water.

Table 4.6 Technical specifications for the space heating gas cooler.

Type:	Tube-in-tube heat exchanger
Number of circuits:	One
Material:	Stainless steel, both tubes
Diameters, inner tube (CO_2):	D_i = 6 mm D_o = 8 mm
Diameters, outer tube (water):	D_i = 18 mm D_o = 22 mm
Tube length:	15 m
Average coil diameter:	450 mm
Approximate weight:	18 kg
Heat transfer area, inner tube (CO_2 side): Heat transfer area, inner tube (water side): Ratio, heat transfer areas (A_o/A_i):	A_i = 0.283 m^2 A_o = 0.377 m^2 1.33
Cross-sectional area, inner tube (CO_2 side): Cross-sectional area, annuli (water side): Ratio, cross-sectional areas ($A_{c,o}/A_{c,i}$):	$A_{c,i}$ = 28 mm^2 $A_{c,o}$ = 204 mm^2 7.3

Figure 4.12 shows the tube-in-tube gas cooler for space heating mounted in the test rig. The small tube-in-tube gas cooler for reheating of DHW (DHW-RH) can be seen above the floor heating heat exchanger.

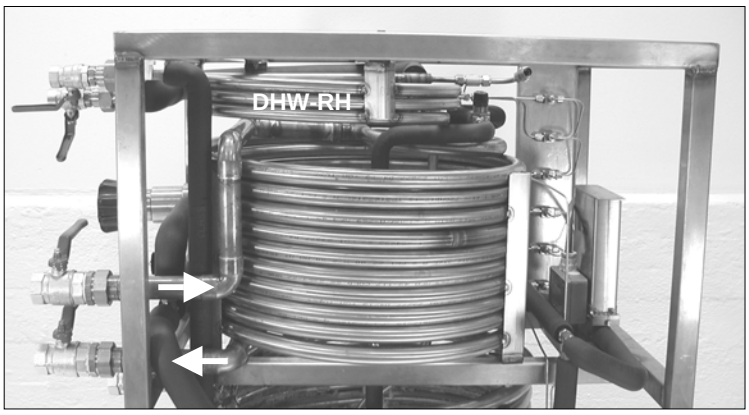

Figure 4.12 The tube-in-tube gas cooler for space heating.

A stainless steel wire with suitable thickness was wrapped as a spiral around the inner CO_2 tube in order to maintain uniform distance between the CO_2 tube and the water tube. The gas coolers units for space heating and preheating of DHW were insulated with 12 mm Armaflex, whereas 25 mm insulation was used for the DHW reheating gas cooler unit due to the high operational temperature.

4.1.2.5 The Suction Gas Heat Exchanger

The main purpose of the suction gas heat exchanger was to superheat the suction gas to the compressor. The heat exchanger was designed as a counterflow tube-in-tube unit, and the heating capacity was controlled by means of ball-valves at the inlet and outlet of the heat exchanger tubes.

Table 4.7 presents the technical specifications for the heat exchanger, whereas Figure 4.13 shows the heat exchanger before it was installed in the heat pump test rig.

Table 4.7 Technical specifications for the suction gas heat exchanger.

Type:	Tube-in-tube heat exchanger
Number of circuits:	One
Material:	Stainless steel, both tubes
Diameters, inner tube (low pressure CO_2):	D_i = 8 mm D_o = 10 mm
Diameters, outer tube (high pressure CO_2):	D_i = 12 mm D_o = 16 mm
Tube length:	2.3 m
Average coil diameter:	350 mm
Approximate weight:	2.5 kg
Heat transfer area, inner tube (low pressure side): Heat transfer area, inner tube (high pressure side): Ratio, heat transfer areas (A_o/A_i):	A_i = 0.058 m^2 A_o = 0.072 m^2 1.25
Cross-sectional area, inner tube (low pres. side): Cross-sectional area, annuli (high pressure side): Ratio, cross-sectional areas ($A_{c,o}/A_{c,i}$):	$A_{c,i}$ = 50 mm^2 $A_{c,o}$ = 35 mm^2 0.7

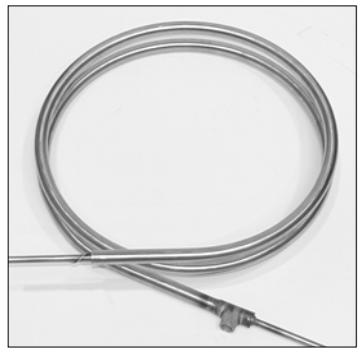

Figure 4.13 The tube-in-tube suction gas heat exchanger.

As with the gas cooler units, a stainless steel wire with suitable thickness was wrapped around the inner tube in order to maintain uniform distance between the tubes. The heat exchanger was insulated with 12 mm Armaflex before it was mounted in the test rig.

4.1.2.6 The Subcooler

A subcooler was installed after the suction gas heat exchanger in order to lower the CO_2 temperature before throttling and to reduce the amount of flash gas at the evaporator inlet. The capacity of the subcooler was controlled by means of a number of ball valves.

The simple cross-flow subcooler was made of a 6 m long ID 8 mm stainless steel tube that was twisted around the inlet pipeline to the evaporator. The total heat transfer area of the heat exchanger was about 0.05 m^2. Figure 4.14 shows the subcooler installed in the test rig.

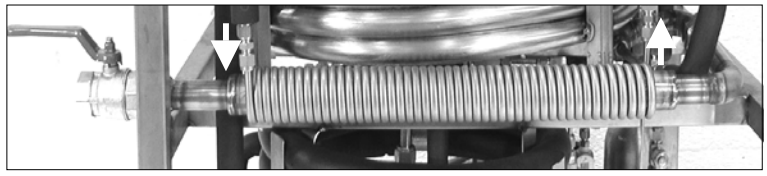

Figure 4.14 The cross-flow subcooler in the rest rig.

4.1.2.7 The Low-Pressure Receiver and Oil Return System

A low-pressure receiver (LPR) was installed between the evaporator outlet and the inlet of the suction gas heat exchanger. The main purpose of the LPR was to supply and absorb liquid for control of the gas cooler pressure

at all operating conditions (liquid reservoir), and to prevent droplets from entering the compressor. The heat pump was originally equipped with a one litre LPR. However, at certain operating conditions the LPR turned out to be too small, and was therefore replaced by a 4 litre vessel. Reference is made to Appendix A2.2, *Methods of Controlling the High-side Pressure*, for further details about the design and operation of the LPR.

The heat pump unit was charged with approximately 2.5 kg of CO_2. In order to ensure proper oil return and to provide liquid overfed in the evaporator, an ID 4 mm stainless steel tube was installed between the bottom of the LPR and the top of the filter (*Maidstone*). A needle valve (*Hook*) was used to control the oil flow rate. Reference is made to Section 5.1.1, *Function Testing*, for details regarding function testing and operation of the oil return system.

Figure 4.15 shows the one litre LPR and the oil return system. The filter is placed behind the control valve NV1.1

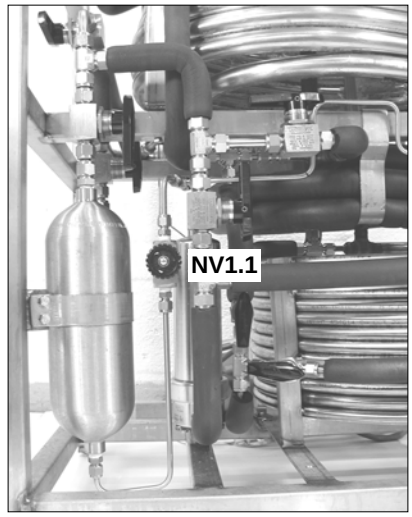

Figure 4.15 The LPR, the oil return pipeline/valve and the filter.

4.1.2.8 The Expansion Valves

The test rig was equipped with two manually operated expansion valves, i.e. a needle valve (*Hook*) and a back-pressure valve (*Tescom*). The latter valve, which maintained a constant high-side pressure at each set point, was used in virtually all the experiments. Figure 4.16 shows the expansion valves installed in the test rig.

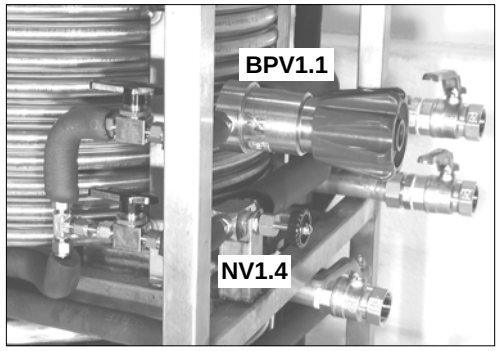

Figure 4.16 The expansion valves in the test rig.

4.1.2.9 Pipelines

The pipelines at the low-pressure side of the test rig were round OD/ID 10/8 mm stainless steel tubes, whereas round OD/ID 8/6 mm stainless steel tubes were used for the high-pressure side. The tubes and components were joined by means of *Swage Lock* fittings.

4.1.3 Design of the Other Sub-Systems

4.1.3.1 The Heat Source System

The main purpose of the heat source system was to supply heat to the CO_2 evaporator as well as to provide cooling of the space heating system whenever required (ref. Section 4.1.3.3).

Figure 4.17 sketches the heat source system. The system consisted of a 150 m deep ID 135 mm borehole (energy well), which was connected to the evaporator by means of a round OD/ID 40/32 mm PEM pipeline. Potassium formate (*Hycool 20*), with a freezing point of -20°C, was used as the secondary fluid (brine). The main circuit was equipped with an inverter controlled pump (*Pump2.1*), a 5 kW electric heater connected to a variable resistance (Variac) as well as a brine vessel and an expansion system. The evaporator was either directly connected to the energy well, or operated in a closed loop together with the pump and the electric heater. The parallel circuit, which comprised a plate heat exchanger (*PEH2.1*), a hand control valve (*HCV2.1*) and a pump (*Pump2.2*) with fixed rpm, was used to cool the return flow in the space heating system whenever required. The maximum cooling capacity was about 10 kW.

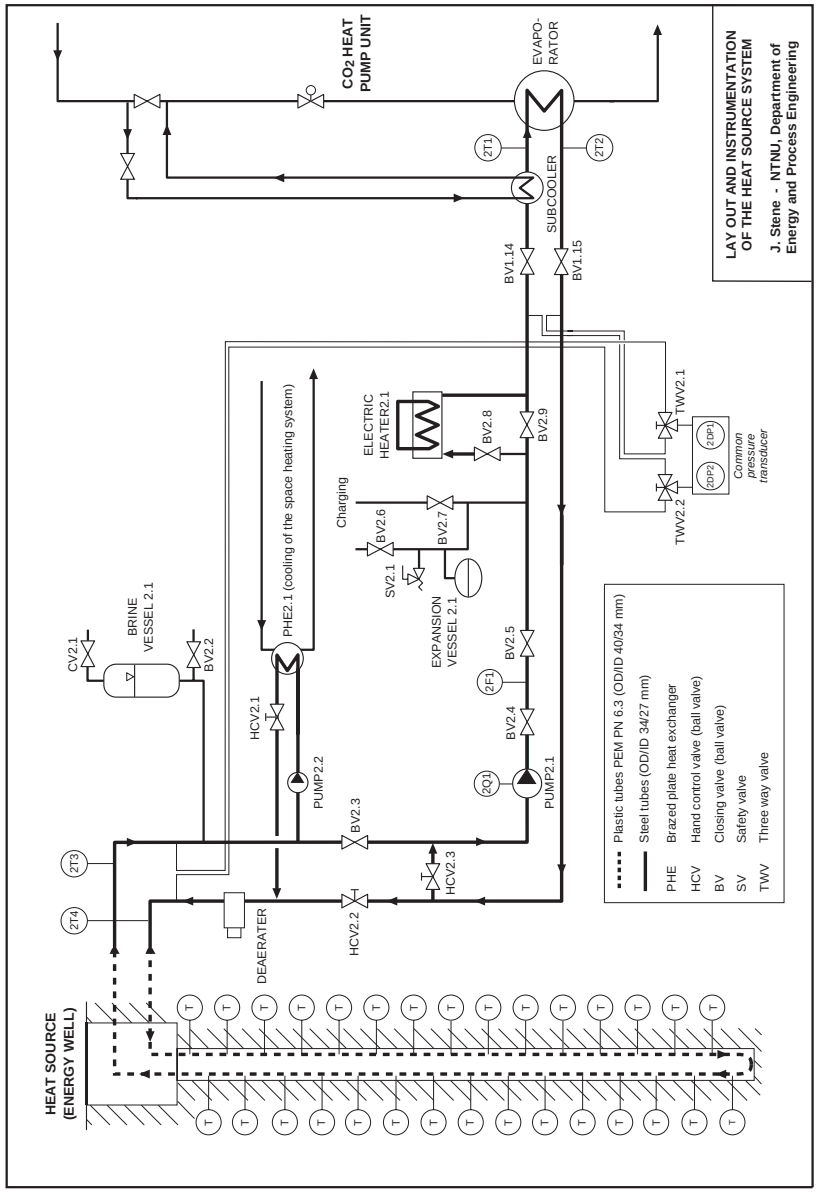

Figure 4.17 Principle of the heat source system.

4.1.3.2 The Hot Water System

The hot water system was connected to the gas coolers units for pre-heating and reheating of DHW. The main component in the system was a standard 300 litre single-shell DHW tank (*Høiax*). The inner diameter and height of the stainless steel tank were 500 and 1250 mm, respectively, and it was insulated with 40 mm glass-wool.

In order to meet the special requirements for the prototype CO_2 heat pump unit, the DHW tank was modified as follows:

- Stainless steel tubes for the hot and cold water inlet and outlet were mounted at the top and bottom of the tank, respectively.
- A simple diffuser was mounted at the end of the tube inside the tank in order to reduce the water velocity and consequent mixing of hot water and cold city water during tapping. The diffuser directed the water flow downwards in the tank, and reduced the water velocity by approximately 80%.
- Five 250 mm long stainless steel pockets for Pt1000 sensors were installed to enable measurements to be made of the vertical temperature gradient in the centre of the tank. The same type of pockets was also installed at the inlet and outlet pipelines.
- Five ID 80 mm inspection glasses (PN 10) were mounted in the front and the back of the tank wall in order to study the water flow inside the tank.
- A back-up heating system was made from a 4 kW electric heater and stainless steel tubes with OD/ID of 54/48 mm and 34/28 mm. The tubes were connected to the bottom and the top of the tank as seen in Figure 4.18. In order to control the water flow rate and with that the outlet temperature from the thermosyphon heating system (max. 80°C), a round disk with an ID 6 mm orifice was mounted inside the upper part of the tube.

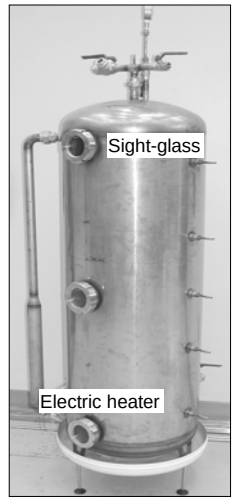

Figure 4.18 The modified 300 litre single-shell hot water tank.

In addition to the DHW tank, the hot water system comprised a pump in stainless steel (*Pump3.1*), a needle control valve in bronze (*ACV3.1*) and two solenoid valves (*SOV3.1, SOV3.2*). Figure 4.19 sketches the principle of the hot water system connected to the gas coolers units for preheating (A) and reheating (C) of DHW.

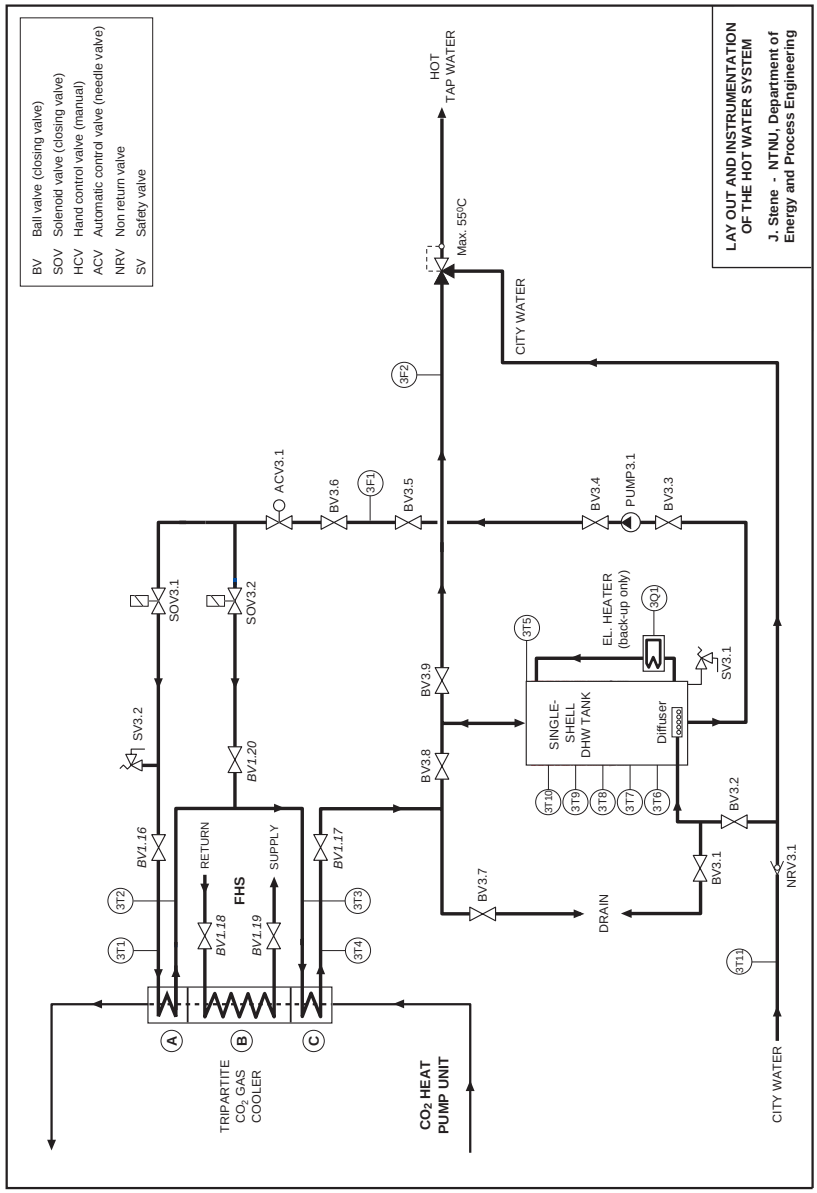

Figure 4.19 Principle of the hot water system.

As described in Section 4.1.2.4, the purpose of the two solenoid valves was to direct the inlet water flow to either the gas cooler units for pre-heating or reheating of DHW, depending on the temperature level of the water.

The hot water system was designed to be operated as a closed loop or as an open system. During closed loop operation (*Auto mode*), cold or tempered water from the bottom of the DHW tank was pumped through the gas cooler(s) by means of *Pump3.1* and returned to the top of the tank. The needle valve *ACV3.1* was used to control the mass flow rate, and with that the outlet hot water temperature. In open mode (*Test mode*), cold city water was circulated through the diffuser and the bottom of the DHW tank, heated in the gas cooler units and poured into a drain through a ball valve (*BV3.7*). It was not necessary to use the pump in open mode, since the hot water system was pressurized (5 bar).

4.1.3.3 The Space Heating System

The space heating system, which was connected to the space heating gas cooler (B), comprised two circuits that could be operated together or as independent systems. Figure 4.20 shows the layout of the space heating system.

Circuit 1 was a specially designed test circuit, which was equipped with an expansion tank, an inverter controlled pump (*Pump4.1*), a hand control valve (*bypass – HCV4.1*) and a cooling system. The latter system, which was used to cool the return water flow in the space heating system whenever required, comprised a pump (*Pump4.3*), a hand control valve (*HCV2.1*) and a plate heat exchanger (*PEH2.1*) connected to the heat source system.

Circuit 2 was connected to a 200 m^2 state-of-the-art low-temperature floor heating system. The circuit was equipped with an inverter controlled pump (*Pump4.2*), an expansion tank, a 120 litre accumulator and a 12 kW electric back-up system. When operating the two circuits together, it was possible to increase the inlet water temperature to the gas cooler by adjusting the by-pass valve (*HCV4.2*) between the supply and return pipelines.

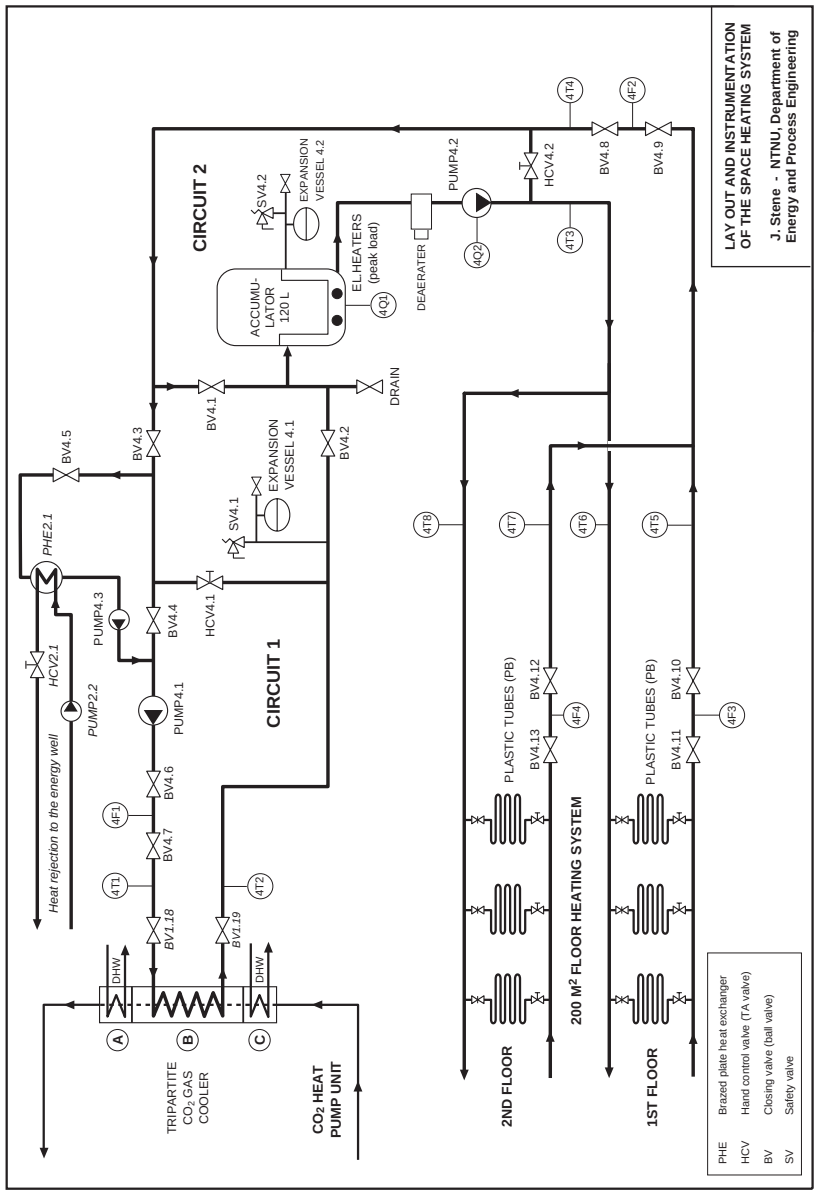

Figure 4.20 Principle of the space heating system.

4.1.4 Instrumentation

Temperature sensors, pressure transducers, volume/mass flow meters and watt meters with high accuracy, were installed in order to measure the performance and operating conditions of the prototype heat pump system.

The signals from the sensors/instruments were continuously processed and logged by an advanced *Satchwell* data acquisition system, consisting of a Satchwell UNC596 Outstation (hardware) and BAS 2800+ software. Selected measurement data from the Outstation were processed, analysed and displayed by means of tailor-made Excel spreadsheets. In the Excel calculations, the thermophysical properties of CO_2 were supplied by the library *xlco2lib.dll* (Skaugen 2002), where the data are based on correlations from Span and Wagner (1996). The thermodynamic properties of water and potassium formate (Hycool) were based on data from the VDI Heat Atlas (1993) and Melinder (2000), respectively.

The absolute and relative uncertainties of the readings from the sensors/-instruments and for the computed values are shown in Table 4.11 in Section 4.1.4.5 and in Tables 4.12 to 4.16 in Section 4.1.4.6, respectively.

4.1.4.1 Temperature

Selected temperatures in the four sub-systems were measured with calibrated platinum resistance (Pt1000) sensors from *Kundo*, since the Satchwell Outstation was not capable of processing low voltage signals from thermocouples. Table 4.8 shows an overview of the temperature measurements in the four sub-systems. The tag no. *xTy*, refers to the number of the sub-system *x* (Sections 4.1.2 and 4.1.3) and the number of the sensor *y*.

The measurements from the Pt1000 sensors in the heat source, hot water the space heating systems were used when calculating the heating capacity of the tripartite gas cooler and the COP of the heat pump unit. In order to measure the bulk temperature, the sensors were placed in specially designed metal pockets that were installed vertically inside the tubes. The sensors that were used to measure temperature differences, were calibrated both individually and as pairs since this improved the accuracy of the measurements.

The temperature measurements from the CO_2 heat pump unit were used for system and component analysis. Due to the relatively large diameter of the Pt1000 sensors (5 mm), they had to be installed at the outside of the OD 8 and 10 mm CO_2 tubes. Each sensor was mounted by means of plastic strips, thermal mass and aluminium tape. In order to achieve isothermal conditions for the sensor, about 10 cm of the wire was clamped to the tube and insulated with 12 mm Armaflex.

Table 4.8 Overview of the temperature measurements.

Tag. No.	Range	Sensor Placement	Fluid
1T1	-20 to +5ºC	Expansion valve – outlet Evaporator – inlet	CO_2
1T2	-20 to +10ºC	Evaporator – outlet	CO_2
1T3	-20 to +30ºC	Suction gas heat exchanger – outlet Compressor – inlet	CO_2
1T4	75 to 125ºC	Compressor – outlet	CO_2
1T5	75 to 125ºC	Gas cooler – inlet (reheating DHW)	CO_2
1T6	40 to 125ºC	Gas cooler – outlet (reheating DHW) Gas cooler – inlet (space heating)	CO_2
1T7	25 to 40ºC	Gas cooler – outlet (space heating) Gas cooler – inlet (preheating DHW)	CO_2
1T8	5 to 40ºC	Gas cooler – outlet (preheating DHW) Suction gas heat exchanger – inlet	CO_2
1T9	-10 to 40ºC	Suction gas heat exchanger – outlet Subcooler – inlet	CO_2
1T10	-15 to +35ºC	Subcooler – outlet Expansion valve –inlet	CO_2
2T1	-15 to +10ºC	Evaporator – inlet	Brine
2T2	-15 to +10ºC	Evaporator – outlet	Brine
3T1	2 to 15ºC	Gas cooler – inlet (preheating DHW)	Water
3T2	20 to 35ºC	Gas cooler – outlet (preheating DHW)	Water
3T3	20 to 35ºC	Gas cooler – inlet (reheating DHW)	Water
3T4	60 to 80ºC	Gas cooler – outlet (reheating DHW)	Water
3T5-10	50 to 80ºC	Inside DHW tank	Water
4T1	25 to 40ºC	Gas cooler – inlet (space heating)	Water
4T2	30 to 45ºC	Gas cooler – outlet (space heating)	Water

Calibrated thermocouples of type T (Cu/K) were installed to measure the transient temperature response at the compressor inlet/outlet, the gas cooler inlet/outlet and the outlet of the suction gas heat exchanger. The thermocouples were connected to a *Fluke Hydra 2625* data logger.

4.1.4.2 CO_2 Pressure

The CO_2 pressure at the evaporator outlet and the compressor outlet was measured by *Druck* PTX 521-00 and *Druck* PTX 510 piezoelectric pressure transducers. The pressure transducers were calibrated to measure the absolute pressure. A *Rosemount* G1151 DP5 pressure transducer was used to measure the differential pressure in the evaporator, the entire gas cooler and the individual gas cooler units. Six three-way valves were used to switch between the measurement signals.

The pressure transducers were mounted above the heat pump unit, and the connecting pipelines were designed with the purpose of preventing liquid and oil hold up since this would affect the accuracy of the measurements. Table 4.9 presents an overview of the pressure measurements.

Table 4.9 Overview of the pressure measurements.

Tag. No.	Range	Sensor Placement	Fluid
1P1	2 to 6 MPa	Evaporator Compressor – inlet	CO_2
1P2	0 to 16 MPa	Compressor – outlet Gas cooler – inlet (reheating DHW)	CO_2
1DP1/2	10 to 150 kPa	Evaporator Gas cooler – reheating DHW Gas cooler – space heating Gas cooler – preheating DHW Entire gas cooler	CO_2

4.1.4.3 Mass and Volume Flow Rates

The CO_2 mass flow rate was measured by a Coriolis-type *Rheonic* sensor RHM 015 GET2 connected to a *Rheonic* RHE 08 signal converter. The sensor was installed between the suction gas heat exchanger and the expansion valves. Figure 4.21 shows the sensor installed in the test rig.

The volume flow rates in the heat source, space heating and hot water systems were measured by ultrasonic volume flow meters of type *Kundo* G03. Due to the very low flow rate in the hot water system (< 2 l/min), the measurements during most of the tests were carried out by means of a 2000 ml can and a stop watch in order to improve the accuracy of the measurements.

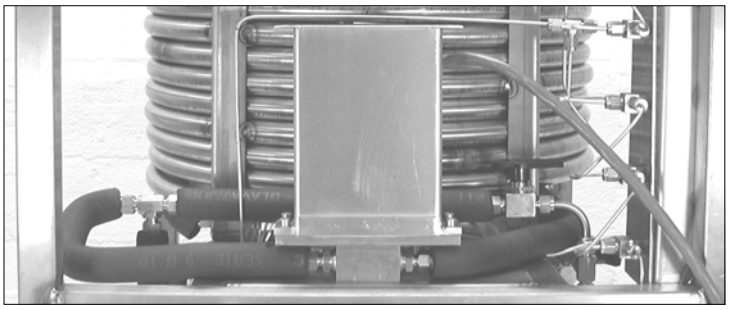

Figure 4.21 The Coriolis CO_2 mass flow meter.

Table 4.10 presents an overview of the mass and volume flow rate measurements in the heat pump system.

Table 4.10 Overview of the mass/volume flow rate measurements.

Tag. No.	Range	Sensor Placement	Fluid
1F1	0.5 – 2.0 kg/min	Heat pump unit	CO_2
2F1	0.1 – 0.5 l/s	Heat source system (evaporator)	Brine
3F1	0.2 – 2.0 l/min	Hot water system	Water
4F1	0.1 – 0.5 l/s	Space heating system	Water

4.1.4.4 Power Input to the Compressor

The electric power input to the compressor was measured by a *Norma* 1704GB3D (class 0.5) analogue wattmeter. The measurements were corrected for the power consumption and the efficiency of the inverter in order to find the net power consumption of the compressor. The power consumption and the efficiency of the inverter at various operating conditions were measured in separate compressor tests.

4.1.4.5 Uncertainty of the Single Measurements

Table 4.11 provides an overview of the relative and absolute uncertainties in the readings from the different sensors/instruments. The uncertainties are based on calibration data or manufacturer data, and represent $\pm 2\sigma$, i.e. with a confidence level of 95%. The relative uncertainties refers to the measured value in percent of full scale (FS) or measured value (MV).

Table 4.11 Relative and absolute uncertainties of the sensors/instruments for the prototype CO_2 heat pump unit. FS=full scale, MV=measured value (ref. Section 4.1.4.1 to 4.1.4.4).

Sensor	Range	Relative Uncertainty	Absolute Uncertainty
Temperature *Pt1000*	-20 to 140ºC	*	± 0.085ºC ± 0.5ºC[1]
Temperature *TC Type T (Cu/K)*	-20 to 140ºC	*	± 0.5ºC[1]
Absolute pressure *Druck*	2 to 6 MPa	± 0.2% FS	± 12 kPa
Absolute pressure *Druck*	0 to 16 MPa	± 0.2% FS	± 32 kPa
Pressure difference *Rosemount*	10 to 150 kPa	± 0.09% FS	± 135 Pa
CO_2 mass flow meter *Rheonic*	0.5 to 2.0 kg/min	± 0.3% MV	± 0.0015 – 0.006 kg/min
Volume flow meter *Kundo*	5 to 30 l/min	± 0.5% MV	± 0.025 – 0.15 l/min
Volume flow meter *Bucket, stop watch*	0.2 to 2 l/min	± 1% MV	± 0.002 – 0.02 l/min
Wattmeter *Norma*	500 to 2500 W	± 1% FS	± 25 W

1) Estimated uncertainty in the CO_2 temperature measurement, when taking into account that the sensor measured the tube wall temperature and not the CO_2 bulk temperature.

4.1.4.6 Uncertainty of the Computed Values

The uncertainty of the computed values was calculated on the basis of the individual uncertainties propagation analysis, i.e. a root-sum-square combination of the effects of individual measurements. The principles of the uncertainty analysis are presented in Appendix D, *Uncertainty Analysis of the Measurements for the Prototype CO_2 Heat Pump*.

Tables 4.12 to 4.16 show the calculated absolute uncertainty of the evaporation temperature as well as the relative uncertainty of the gas cooler heating capacity and the COP of the CO_2 heat pump unit. The uncertainties for the heating capacity and the COP are based on measurements from both the water circuits and the CO_2 circuit. Details regarding the calculations are presented in Appendix D.

Table 4.12 The absolute uncertainty in the evaporation temperature.

T [ºC]	-10	-5	0
δT [K]	±0.16	±0.14	±0.13

Table 4.13 The relative uncertainty in the total heating capacity of the tripartite CO_2 gas cooler. The calculations are based on measurements from the water circuits.

	SH	**DHW**	**SH + DHW**
αQ [%]	±2.5	±1.0	±1.3

SH=Space heating mode DHW=hot water heating mode SH+DHW=combined mode

Table 4.14 The relative uncertainty in the total heating capacity of the tripartite CO_2 gas cooler. The calculations are based on measurements from the CO_2 circuit.

Heating Mode	**SH**		**DHW**		**SH + DHW**	
High-Side Pressure	8 MPa	9 MPa	9 MPa	10 MPa	8 MPa	9 MPa
αQ [%]	±2.2	±2.0	±2.4	±2.0	±1.9	±1.9

SH=Space heating mode DHW=hot water heating mode SH+DHW=combined mode

Table 4.15 The relative uncertainty in the COP of the CO_2 heat pump unit. The heating capacities are based on measurements from the water circuits.

	SH	**DHW**	**SH + DHW**
αCOP [%]	±2.8	±1.7	±1.9

SH=Space heating mode DHW=hot water heating mode SH+DHW=combined mode

Table 4.16 The relative uncertainty in the COP of the CO_2 heat pump unit. The heating capacities are based on measurements from the CO_2 circuit.

Heating Mode	**SH**		**DHW**		**SH + DHW**	
High-Side Pressure	8 MPa	9 MPa	9 MPa	10 MPa	8 MPa	9 MPa
αCOP [%]	±2.6	±2.2	±2.1	±2.6	±2.6	±2.5

SH=Space heating mode DHW=hot water heating mode SH+DHW=combined mode

4.1.5 Test Procedures and Test Programme

Since all components were manually controlled, a period of 1 to 3 hours was required to stabilize the heat pump system at the selected set-points. Logging was carried out 15 minutes after the system had stabilised.

Figure 4.22 provides an overview of all controllable components and the set-points for each sub-system. The component (Tag) numbers refer to the sketches in Figures 4.1, 4.17, 4.19 and 4.20.

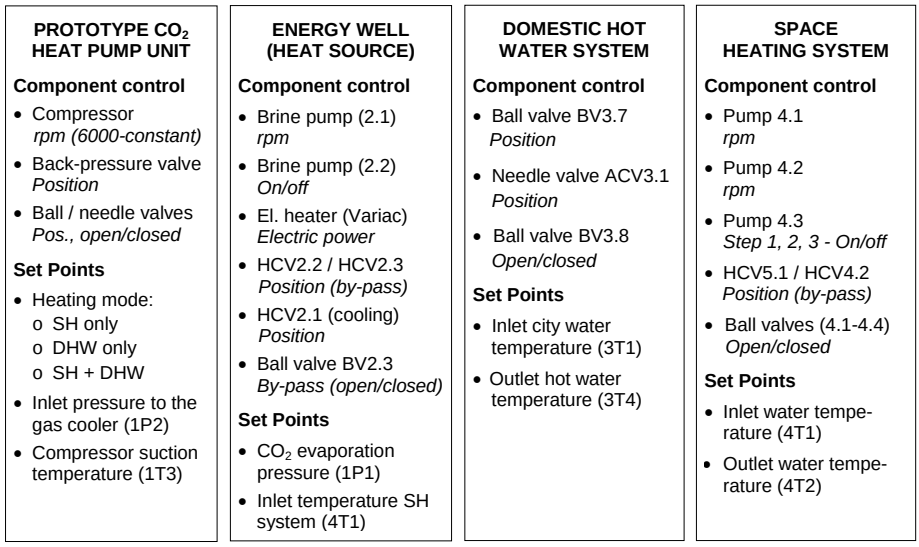

Figure 4.22 Overview of controllable components and set-points.

Table 4.17 shows the ranges for the different set-points and the maximum tolerable deviation.

The heat pump system was run in three different modes: 1) Space heating mode (SH), 2) Hot water heating mode (DHW) and 3) Combined heating mode (SH+DHW). When the system was operated in the space heating mode, the circulation in the hot water system was stopped. In the DHW mode, the CO_2 flow was by-passed the space heating gas cooler unit.

For all test series, the evaporation temperature and the superheating of the suction gas were kept constant in order to provide constant inlet conditions for the compressor. The suction gas superheat and the mass flow rate were controlled by adjusting the ball valves for the suction gas heat exchanger and the oil return valve. The latter valve determined the inlet vapour quality to the suction gas heat exchanger.

Table 4.17 Overview of the operating modes and range for the set-points.

System – Component	Set Points	Variation
Evaporation temperature	-10, -5 and 0ºC	± 0.1ºC
Superheating of suction gas[1)]	2.5 and 5 K	± 0.5 K
Gas cooler – supercritical pressure	7.5 to 11 MPa	± 0.03 MPa
DHW system – inlet water temp.[2)]	Approx. 6ºC	± 1.5ºC
DHW system – outlet water temp.	60, 70 or 80ºC	± 0.5ºC
SH system – outlet temperature	33ºC, 35ºC or 40ºC	± 0.1ºC
SH system – temp. difference	5 K	± 0.1 K
Compressor – rotational speed	6000 rpm (100 Hz)	Constant
CO_2 mass flow rate[3)]	1.210 to 1.630 kg/min	± 3%

1) 5 K for the space heating mode and 2.5 K for the other modes

2) Depended on the city water temperature and heat transfer through the supply pipe

3) Depended on the pressure and temperature of the suction gas

Most of the tests were carried out at an evaporation temperature of -5°C, since this represents a typical temperature level for a ground-coupled heat pump operating in a cold climate. The heat pump unit rejected heat to a typical floor heating system, where the supply temperature ranged from 33 to 40°C, and the temperature difference was kept constant at 5 K.

At fixed inlet and outlet temperatures for the space heating and hot water systems, the inlet gas cooler pressure was varied between 7.5 and 11 MPa in order to see its impact on the heating capacity and the COP of the heat pump unit as well as the temperature fit in the tripartite gas cooler.

Before the actual test series were conducted, the heat pump system was run for a longer period in order to gain general operational experience and to carry out preliminary tests. The purpose of these tests was, among other things, to evaluate the quality of the measurements by means of repeated experiments at equal set-points, and to compare the measurements carried out at the water circuits and the CO_2 circuit.

About *80 tests* were accomplished during the experimental period. Table 4.18 provides an overview of the set-points for each test series.

Table 4.18 Overview of the test series.

Evap.-temp.	**Super-heat**	**Gas cooler pressure**	**Hot water (DHW) Inlet/outlet temp.**		**Floor heating Inlet/outlet temp.**	
[°C]	**[K]**	**[MPa]**	**[°C]**		**[°C]**	
-5	5	7.5 – 9.0	*	*	28	33
-5	5	8.0 – 9.5	*	*	30	35
-5	5	8.5 – 10.0	*	*	35	40
0	5	8.0 – 9.5	*	*	30	35
-10	5	8.0 – 9.5	*	*	30	35
-5	2-3	8.0 – 9.5	5.4 – 6.0	60	*	*
-5	2-3	8.5 – 10.0	5.8 – 6.1	70	*	*
-5	2-3	9.5 – 10.8	6.2 – 6.5	80	*	*
-10	2-3	8.0 – 9.5	6.8	60	*	*
-5	2-3	7.5 – 9.0	6.6 – 6.9	60	28	33
-5	2-3	8.0 – 9.5	7.1 – 7.4	70	28	33
-5	2-3	8.0 – 9.5	6.4 – 6.6	80	28	33
-5	2-3	7.5 – 9.0	6.7 – 7.4	60	30	35
-5	2-3	8.0 – 9.5	6.4 – 7.1	70	30	35
-5	2-3	8.5 – 10.0	7.4 – 8.0	80	30	35
-5	2-3	8.0 – 9.5	6.1 – 7.0	60	35	40
-5	2-3	8.5 – 10.0	6.4 – 6.6	70	35	40
-5	2-3	8.5 – 10.0	6.6 – 7.0	80	35	40
-10	2-3	7.5 – 9.0	5.9 – 7.1	60	30	35

4.2 Testing of a DHW Tank and a Movable Insulating Plate

With reference to Section 3.3.3, *Exergy Losses in the DHW Storage Tank*, and Section 3.3.4, *Application of a Movable Insulating Plate Inside the DHW Tank*, a test rig, comprising a cylindrical single-shell DHW storage tank, two movable insulating plates (prototypes) and auxiliary equipment, was constructed in order to:

- Measure the transient temperature development in the tank at various operating conditions.
- Measure the thermal performance and test the functionality of a movable insulating plate.

4.2.1 Construction of the Test Rig

A standard-sized 200 litre cylindrical DHW tank was constructed from transparent polycarbonate plates. The dimensions of the tank were as follows:

- Internal diameter: 500 mm (standard diameter)
- Height: 1000 mm (standard height)
- Thickness, wall: 2 mm
- Thickness, cover: 10 mm
- Thickness, bottom: 10 mm

The bottom of the tank was mounted on a wooden frame, and the polycarbonate cover was reinforced with an 8 mm steel plate and tightened with six M8 steel rods in order to enable testing under slightly pressurized conditions. A special device was constructed in order to lift and lower the 15 kg steel plate. The tank was connected to city water, a hot water system and a drain by means of rubber and plastic hoses, and the water flows were controlled by means of ball valves, hand control valves and a pump. A 1 kW electric heater was used to heat the city water from the tank. Sketches and photos of the test rig are presented in Figures 4.23 to 4.26.

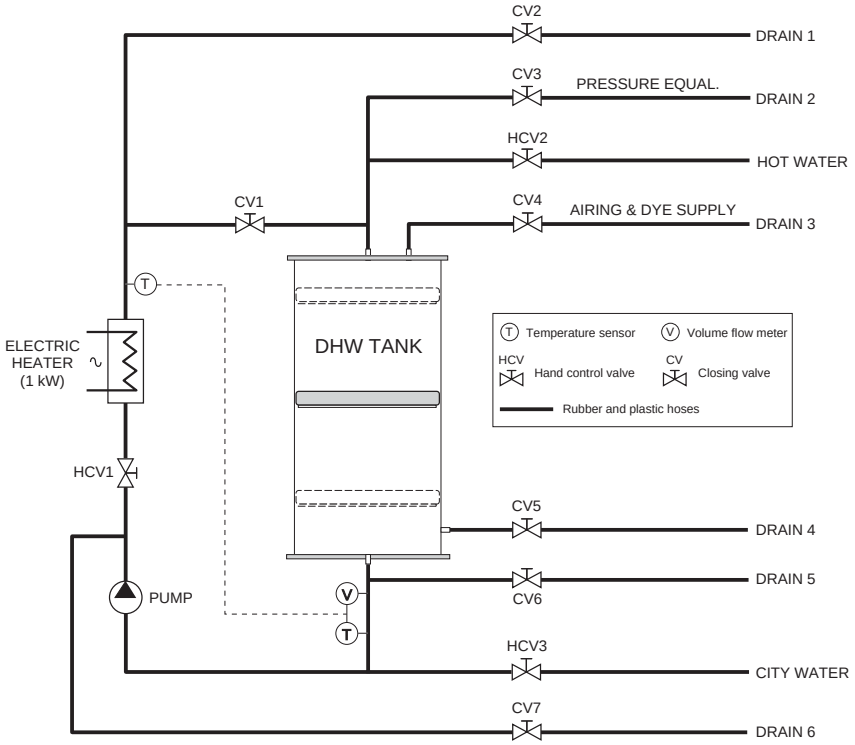

Figure 4.23 Principle of the test rig.

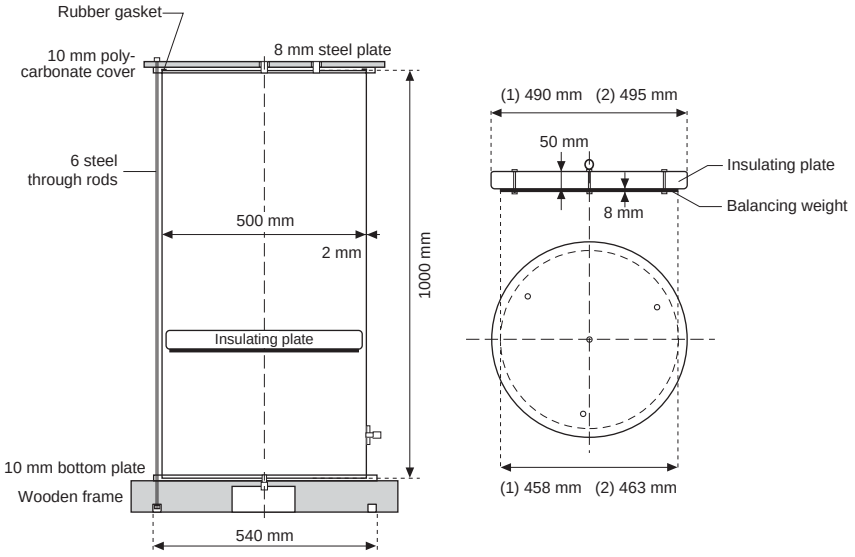

Figure 4.24 Principle of the DHW tank and the insulating plates.

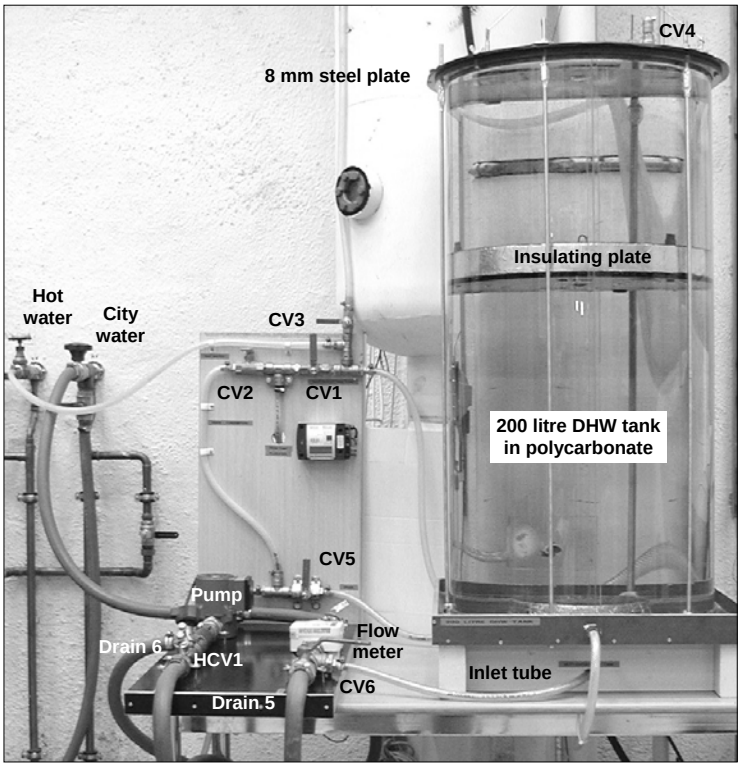

Figure 4.25 The DHW tank and the auxiliary equipment in the test rig.

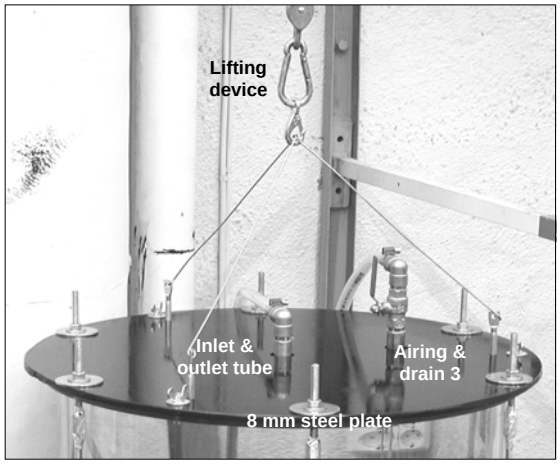

Figure 4.26 The steel cover and the lifting device in the test rig.

A simple diffuser was mounted at the ID 10 mm inlet pipeline at the bottom of the tank. The purpose was to reduce the water velocity during testing of the insulating plates, since strong currents could alter the hydrostatic balance of the plates. The diffuser reduced the average flow rate by a factor of 50.

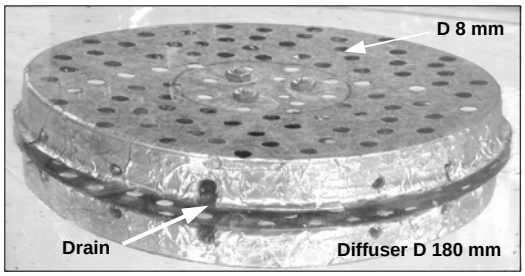

Figure 4.27 The diffuser.

Two *movable insulating plates* with different diameters were constructed, and the specifications were as follows:

- Material: Extruded polystyrene, painted to avoid water absorption
- Density: Approx. 43 kg/m^3
- Thickness: 50 mm
- Diameter: 495 mm 490 mm
- Volume: 9.622 litres 9.423 litres
- Weight: 0.409 kg 0.400 kg

The balancing weights, which were clamped to the underside of the insulating plates, had the following specifications:

- Material: Steel
- Density: Approx. 7700 kg/m^3
- Thickness: 8 mm
- Diameter: 463 mm 458 mm
- Volume: 1.347 litres 1.318 litres
- Weight: 10.543 kg 10.318 kg (incl. 170 g for bolts/nuts)

The average density of the insulating plates and the balancing weights was the same as the density of water at 40°C (i.e. approx. 992 kg/m^3).

Figure 4.28 shows the largest insulating plate with the balancing weight.

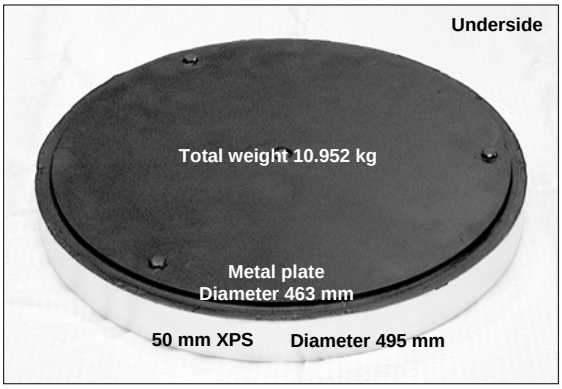

Figure 4.28 The underside of the largest insulating plate.

4.2.2 Temperature Measurements

4.2.2.1 Introduction

The purpose of these experiments was to measure the transient temperature drop in the DHW tank at various operating conditions. All temperature measurements were carried out with Type T (Cu/K) thermocouples, which were connected to a *Fluke Hydra 2625* data logger. The data logger was equipped with an accurate internal reference point using a Pt100 sensor, and the thermocouples were calibrated by means of melting crushed ice. The absolute uncertainty of the thermocouples was ±0.2ºC. During all tests the tank was insulated with a 40 mm glass-wool mat.

4.2.2.2 Transient Temperature Drop in a DHW Tank

With reference to Section 3.3.3.1, *Heat Loss Through the Tank Walls*, the overall heat transfer coefficient (U-value) of the prototype DHW tank was estimated on the basis of the measured transient temperature drop [ºC/s] for the hot water at specified boundary conditions.

Experimental Procedure

The 200 litre polycarbonate tank was filled with 56ºC water from the common hot water system in the building. The temperatures at the centre of the tank and at the tank wall were measured by means of 16 thermocouples attached to an OD 8 mm plastic tube, Figure 4.29. The average room temperature during the 24 hour test period was about 22ºC.

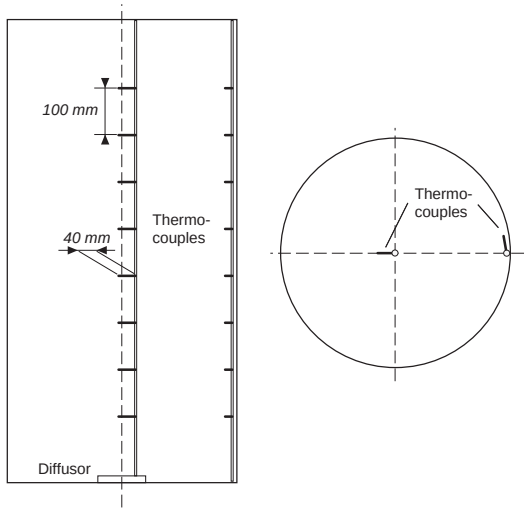

Figure 4.29 The positions of the thermocouples for measuring the water temperatures at the centre and the rim of the DHW tank.

4.2.2.3 Transient Temperature Gradients in a DHW Tank Filled with Hot and Cold Water

With reference to Section 3.3.3.3, *Conductive Heat Transfer Inside the DHW Tank*, there will be considerable conductive heat transfer between the hot and cold water reservoirs during the tapping and charging periods. By measuring the transient temperature gradient (*thermocline*) between the reservoirs in the *static mode* (static thermocline) and the outlet water temperature from the tank during the *charging mode* (dynamic thermocline), the reduction in the COP for an integrated CO_2 heat pump due to the conductive heat transfer inside the DHW tank can be estimated (ref. Eq. 3.26, Section 3.3.3.2).

Experimental Set-Up

In order to separate the hot and cold water reservoirs without hampering the conductive heat transfer, a thin circular stainless steel plate with a 50 mm centre hole was installed 400 mm above the bottom of the tank. The plate was supported by three plastic sticks, and the slit between the plate and the tank wall was sealed by means of aluminium tape.

20 thermocouples were attached to an OD 8 mm plastic tube, which was installed at the centre of the tank and fixed to the diffuser and the polycarbonate cover. The installation of the thermocouples is shown in Figure 4.30.

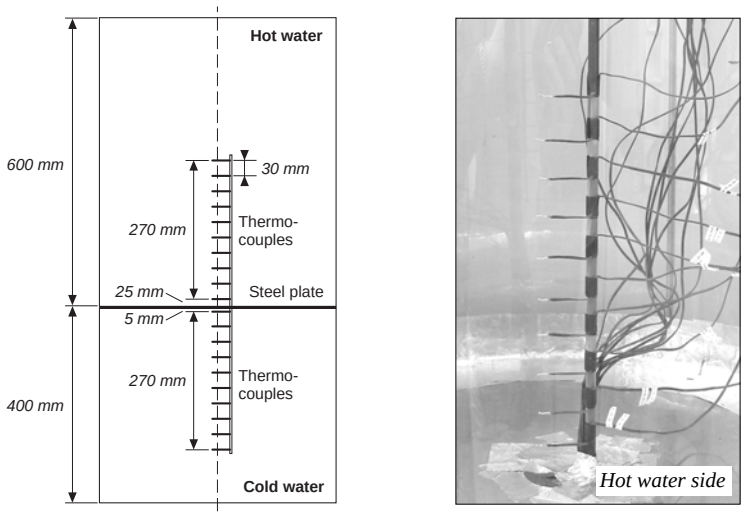

Figure 4.30 The experimental set-up when measuring the temperature gradient between the hot and cold water reservoirs.

The sensors were spaced 30 mm apart. In order to minimize heat conduction along the wires, 40 mm of each wire end was mounted horizontally.

Experimental Procedure – Static Mode (*Static Thermocline*)

The tank volume below the steel plate was filled with 5ºC city water through the diffuser. When the cold water barely flooded the steel plate, all water bubbles were removed, and the centre hole in the plate was closed. The upper tank volume was then filled with 53ºC hot water from the common hot water system in the building. During filling, the hot water was heavily mixed in order to achieve a uniform temperature in the reservoir. The temperature in the tank was measured during a period of 24 hours, and there was no water flow through the tank during testing. The average room temperature was about 22ºC.

Experimental Procedure – Charging Mode (*Dynamic Thermocline*)

In order to measure the outlet temperature from the tank during draining (charging) of the tank, an additional thermocouple was installed inside the diffuser at the bottom of the tank. During testing, the tank was filled with hot and cold water as described in the previous section, and the 50 mm circular hole at the centre of the plate was opened. Water was then drained from the bottom of the tank, whereas hot water was supplied at the same flow rate at the top of the tank. The initial hot water temperature ranged

from about 55 to 57ºC, the initial city water temperature was approximately 5ºC, and the average room temperature during testing was about 21ºC. The water flow rate, which ranged from about 0.6 to 2.5 l/min, was measured by means of a 2000 ml can and a stop watch.

4.2.2.4 Thermal Performance of an Insulating Plate

The application of a movable insulating plate in cylindrical DHW tanks will eliminate the mixing losses and lead to a considerable reduction in the conductive heat transfer between the hot and cold water reservoirs (ref. Section 3.3.4, *Application of a Movable Insulating Plate Inside the DHW Tank*). The thermal performance of an insulating plate was documented by measuring the transient temperature gradient at each side of the plate.

Experimental Set-Up

Only the insulating plate with the largest diameter was tested, since the two plates had nearly identical designs. Owing to the additional weight of the temperature sensors and the required auxiliary equipment, it was only possible to measure the thermal performance of the plate in the static mode, i.e. when the plate was kept at a fixed position in the middle of the tank during testing.

20 thermocouples were mounted on four vertical plastic coated metal rods that were attached to the centre and the rim of the plate. In order to minimize heat conduction along the wires, 40 mm of each wire end was mounted horizontally (isothermally). The positioning and installation of the thermocouple wires are shown in Figures 4.31 and 4.32.

Experimental Procedure

The initial temperature of the insulating plate and the 200 litre polycarbonate tank was about 22ºC. When the tank was empty, the insulating plate was resting on a metal cylinder in order to protect the thermocouples at the underside of the plate. During testing, the tank was filled with 6ºC city water through the diffuser until the plate was floating in the middle of the tank. The plate was then fixed to the tank wall in order to avoid any movement of the plate and subsequent mixing of hot and cold water when the hot water was supplied to the tank. The tank volume above the plate was filled with 55ºC water, the polycarbonate cover was mounted, and the tank was insulated with a 40 mm glass-wool mat. The average room temperature during the 12 hour test period was about 22ºC.

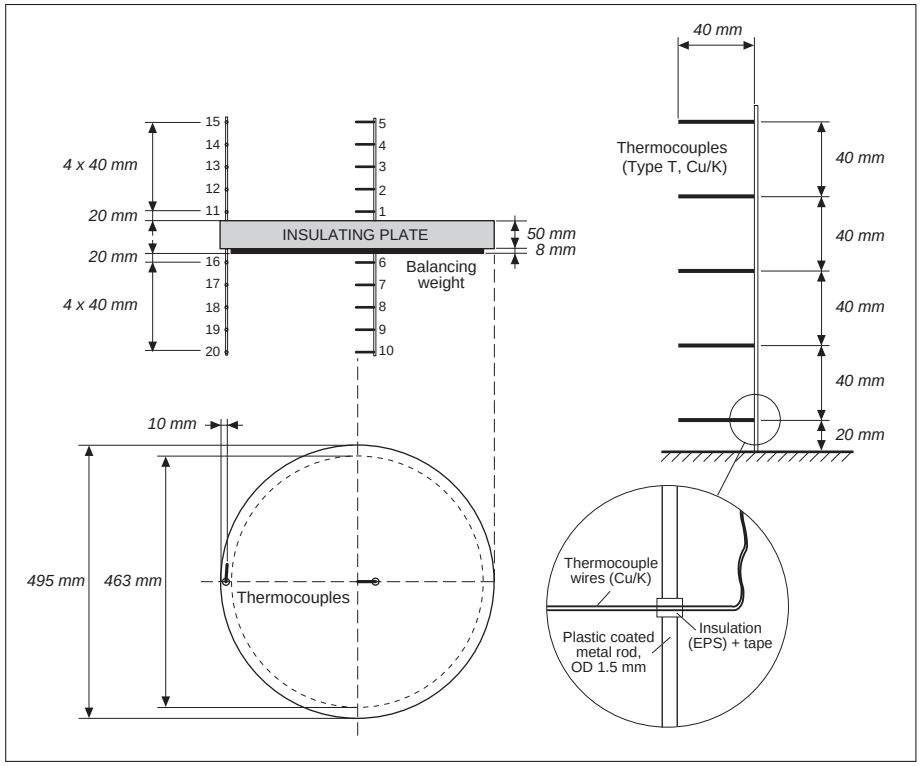

Figure 4.31 Positioning of the thermocouples at the insulating plate.

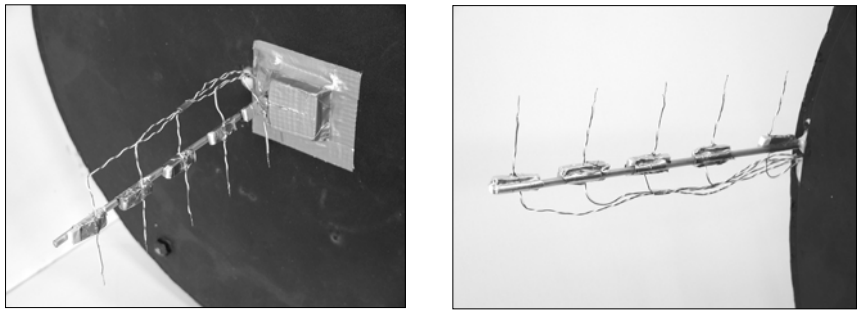

Figure 4.32 Installation of the thermocouple wires at the centre and the rim of the insulating plate.

4.2.3 Flow Studies

4.2.3.1 Introduction

The flow studies were carried out in order to test the hydrostatic balance and functionality of the insulating plates. The tank was mainly operated at atmospheric pressure (open tank), but experiments with a closed tank were also carried out. In order to pressurize the tank (maximum 1.3 bar), a 4 mm wide rubber gasket was mounted in a slot in the polycarbonate cover. However, it was impossible to attain a 100% efficient tightening between the thin tank wall and the cover at water flow rates above 10 l/min. The base of the tank was therefore equipped with a water draining system.

By dissolving a dye (*Brilliant Green*, hydrogen sulphate) in the hot water reservoir, it was possible to observe any flow of hot or cold water through the cylindrical gap between the insulating plate and the tank wall and subsequent mixing of the water reservoirs. About 2 grams of dye was sufficient to create a very deep turquoise colouring in 200 litres of water.

The test programme is presented in Appendix H, *Test Conditions for the Prototype Movable Insulating Plates*.

4.2.3.2 Experimental Procedures

Testing of the insulating plates was carried out in the tapping mode, the charging mode and the static mode, using 5ºC city water and 55ºC hot water. During the relatively long-lasting charging and static modes, the tank was insulated with 40 mm glass-wool, which is standard insulation for DHW tanks.

Tapping Mode – Open Tank

The insulating plate was placed at the bottom of the tank, and city water was fed through the diffuser until the plate was floating just above the diffuser. Dyed 55°C water was then carefully supplied above the plate until the height of the hot water reservoir was about 40 cm (80 litres). During testing, the water flow rates through the diffuser ranged from 5 to 30 l/min, which corresponds to typical water flow rates in DHW tanks (ref. Appendix F, *Characteristic Properties of DHW Systems*). The tests were stopped when the hot water surface was about 5 cm from the top of the tank. Figure 4.33 shows the principle of the DHW tank and the movement of the insulating plate during testing in the tapping mode.

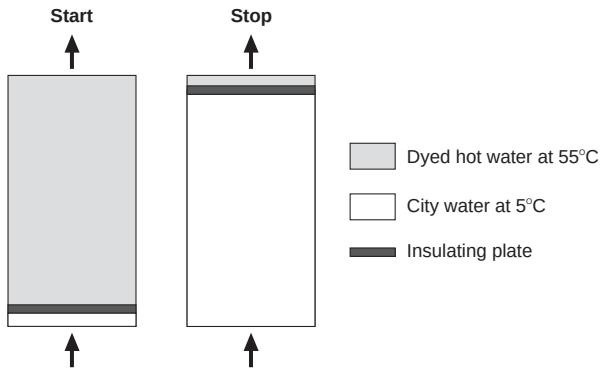

Figure 4.33 Movement of the insulating plate during the tapping mode.

The average water flow rate through the diffuser was calculated by measuring the position of the plate every 30 seconds. Figure 4.34 shows the relationship between the velocity of the plate and the water flow rate.

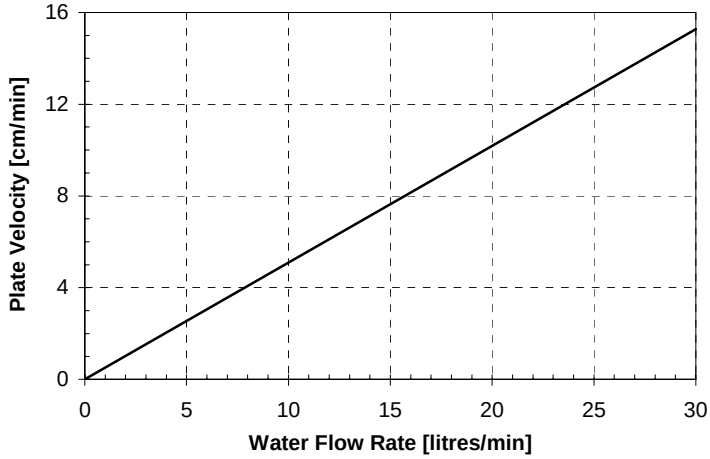

Figure 4.34 The relationship between the velocity of the movable insulating plate and the water flow rate through the diffuser.

Tapping Mode – Closed Tank

The tank was filled with city water and dyed hot water as described in the previous section. The polycarbonate cover and the metal plate were mounted by using the lifting device, and the six steel rods were tightened. During testing, city water was fed through the diffuser, and the hot water above the insulating plate was drained through the outlet hose at the top of the tank (drain 2). Due to unwanted deformation of the tank walls (oval shape), the maximum water flow rate was limited to about 20 l/min.

Charging Mode – Open Tank

The insulating plate was placed at the bottom of the tank, and city water was fed through the diffuser until the plate was about 15 cm below the top of the tank. Dyed 55°C water was then supplied above the plate until the height of the hot water reservoir was about 10 cm. After mounting the cover, the cold water below the insulating plate was pumped through the electric heater at a flow rate of approximately 0.3 l/min, heated to about 60ºC, and returned at the top of DHW tank. The required charging period to heat the entire water volume of 190 litres was about 11 hours, and the testing was stopped when the insulating plate reached the diffuser. Figure 4.35 shows the principle of the DHW tank and the movement of the insulating plate during testing in the charging mode.

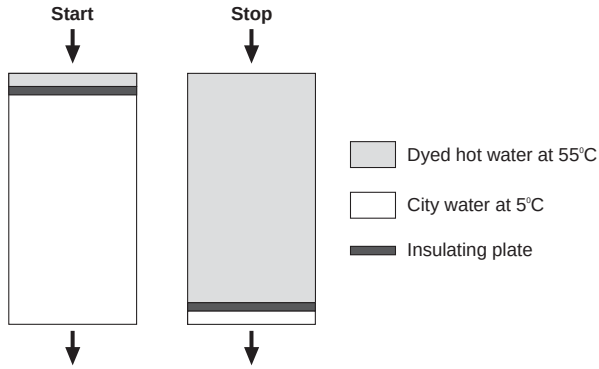

Figure 4.35 Movement of the insulating plate during the charging mode.

Static mode – Open Tank

The insulating plate was placed at the bottom of the tank, and 5°C city water was fed through the diffuser until the plate was floating in the middle of the tank. Dyed 55°C water was then supplied above the plate until the hot water surface was about 1 cm from the top of the tank. The position of the insulating plate was measured over a period of 8 hours.

5 Experimental Results

This chapter expands on Chapter 4, *Test Rig Design and Experimental Methods*, and provides a detailed presentation of the experimental results from the following test rigs:

- A 6.5 residential brine-to-water CO_2 heat pump unit for combined space heating and hot water heating (prototype).
- A 200 litre cylindrical single-shell domestic hot water (DHW) tank including two movable insulating plates (prototypes).

5.1 Testing of a Residential Brine-to-Water CO_2 Heat Pump Unit

5.1.1 Function Testing

The experimental set-up, the instrumentation and the experimental procedures for the prototype CO_2 heat pump are described in Section 4.1, *Testing of a Residential Brine-to-Water CO_2 Heat Pump.*

Before the CO_2 heat pump unit was insulated and connected to the secondary systems in the pilot house, extensive function testing and troubleshooting was carried out in order to:

- Detect possible leakages in the CO_2 and water circuits.
- Discover operational problems and component malfunction, and repair or replace components, valves and tubing if necessary.
- Tune the set-point for the control valve in the oil return system.
- Find the optimum CO_2 charge that ensured sufficient liquid feed to the evaporator and prevented wet suction gas at the compressor inlet at all operating conditions.

- Estimate the compressor performance as well as the heating or cooling capacities of the different heat exchangers, and compare the results with the design values.

The CO_2 mass flow rate dropped gradually during the test period due to wear and tear in the bearing for the connecting rod between the crankshaft and the piston. The Dorin reciprocating compressor was therefore replaced by a hermetic two-stage rolling piston compressor from Sanyo (prototype). Due to the very compact design, it was possible to mount the new compressor on the same frame as the rest of the CO_2 heat pump unit.

The rolling piston compressor was designed to use a PAG lubricant which was insoluble with CO_2. Since the oil return pipeline was connected to the bottom of the low pressure receiver (LPR), the density of the PAG had to be higher than that of the CO_2 liquid in order to ensure proper oil return (ref. Appendix A2.2, *Methods of Controlling the High-Side Pressure*). Since there was no available density data for the lubricant, the density was measured and compared with the density of saturated liquid CO_2 (RnLib, 2003). The results are presented in Figure 5.1.

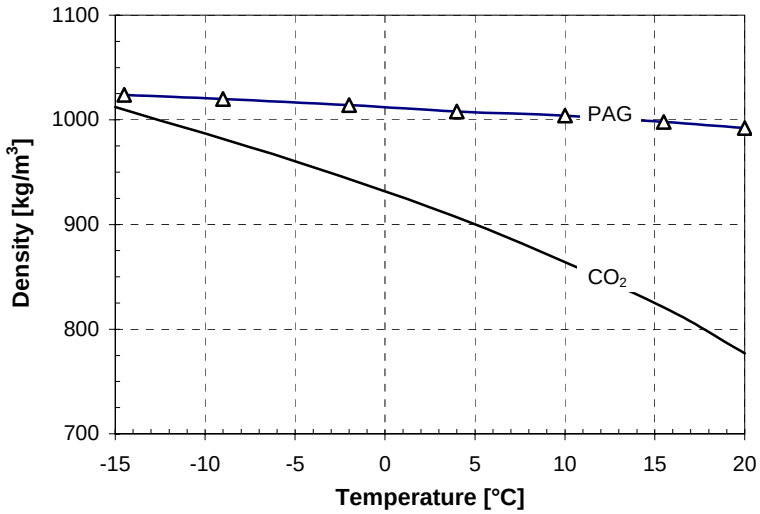

Figure 5.1 The measured density of the PAG lubricant and the calculated density of saturated CO_2 liquid (RnLib, 2003).

Figure 5.1 demonstrates that the LPR oil return system would work satisfactorily at evaporation temperatures down to roughly -15°C.

The function testing revealed that the one litre LPR was too small, since it was impossible to avoid droplets from the receiver at 7.5 MPa high-side pressure and with the same CO_2 charge achieve sufficient liquid feed to the evaporator at 11 MPa high-side pressure. The wet suction reduced the suction gas temperature considerably, while insufficient liquid feed resulted in a lower evaporation temperature and excessive superheating of the suction gas. The receiver was therefore replaced by a 4 litre vessel.

5.1.2 Preliminary Testing

The following tasks were performed prior to the experimental period:

- Testing and validation of the measuring equipment.
- Comprehensive preliminary testing of the CO_2 heat pump unit and the secondary systems in order to gain experience with the test rig, the control system and the data acquisition system.
- Repeatability testing, i.e. comparison of measurements from independent experiments carried out under identical operating conditions.
- Testing of energy balances, i.e. comparison of the heating capacities of the gas cooler units based on measurements in the secondary (water) circuits and the CO_2 circuit.

The repeatability tests documented negligible variations in the measurement values. The calculated deviation between the gas cooler heating capacities measured in the water circuits and the CO_2 circuit is presented and discussed in Section 5.1.3.9.

5.1.3 Experimental Results

5.1.3.1 Introduction

With reference to Section 3.2.4.2, *Operational Characteristics*, the integrated CO_2 heat pump unit was run in three different modes during the experimental period; space heating only (SH mode), hot water heating only (DHW mode) and simultaneous space heating and hot water heating (combined mode). The compressor was always operated at 6000 rpm (100 Hz), and virtually all tests were carried out at an evaporation temperature of -5ºC, since this represents a typical temperature level for a ground-coupled heat pump operating in a cold climate. The heat pump unit gave off heat to a low-temperature floor heating system where the supply

temperature ranged from 33 to 40°C, and the temperature difference was kept constant at 5 K. In the combined heating mode and the DHW heating mode, the set-point for the hot water temperature was 60, 70 or 80ºC.

At fixed inlet and outlet temperatures for the space heating and hot water systems, the inlet gas cooler pressure was varied between 7.5 and 11 MPa in order to see its impact on the heating capacity and the COP of the heat pump unit as well as the temperature fit in the tripartite gas cooler.

The calculation of the heating capacity for the tripartite gas cooler and the COP of the CO_2 heat pump unit were carried out as follows:

- The heating capacities of the three gas cooler units for preheating of DHW, space heating and reheating of DHW were calculated on the basis of temperature and flow measurements in the water circuits.
- The measured power input to the compressor was corrected for the inverter efficiency when calculating the COP of the heat pump unit. The inverter efficiency at 100 Hz (6000 rpm) was approx. 0.95.
- The total power input to the pumps in the evaporator, space heating and hot water circuits was not included when calculating the COP of the heat pump unit.

The measured values from each test series were processed by means of Microsoft Excel. Figures 5.2 and 5.3 illustrate one of the tailor-made spreadsheets as well as the T-h and T-Q diagrams that were used to display and analyse the measured values.

About *80 tests* were done during the experimental period. In the following sections, the COP, the heating capacity and the operational characteristics of the CO_2 heat pump unit at 1) Simultaneous space heating and hot water heating (*combined mode*), 2) Hot water heating only (*DHW mode*) and 3) space heating only (*SH mode*) are presented and analysed. A comparison of the optimum high-side pressure during operation in the different modes (ref. Appendix A2.4, *Optimum High-Side Pressure when Incorporating Real gas Cooler Performance*) is also presented, and the performance of the compressor, the evaporator and the tripartite gas cooler is presented and analysed.

The detailed test results are presented in Appendix C, *Test Results for the Prototype CO_2 Heat Pump*.

MEASURED VALUES						CALCULATED VALUES				
Tag#	**Fluid**	**Component**	**Measurement**	**Unit**	**Value**	**Enthalpy [kJ/kg]**	**Capacity [W]**		**Capacity [W]**	**Deviation [%]**
1S1	Electr.	Inverter	Frequency	Hz	**100**					
1Q1	Electr.	Compressor	Electric power	W	**1900**		**1793**	P_{COMP}		
1P1	CO_2	Evaporator	Pressure	kPa	**3048**					
1P2	CO_2	Gas cooler	Pressure	kPa	**8500**					
1F1	CO_2	Heat pump	Mass flow rate	kg/min	**1.455**					
1T2	CO_2	Evaporator	Inlet temp.	ºC	**-4.5**	534.3				
1T3	CO_2	Evaporator	Outlet temp.	ºC	**-4.4**	736.1				
1T4	CO_2	Compressor	Inlet temp.	ºC	**-2.3**	740.6				
1T5	CO_2	Compressor	Outlet temp.	ºC	**88.6**	801.9				
1T7	CO_2	Gas cooler	Inlet temp.	ºC	**86.1**	798.2				
1T8	CO_2	Gas cooler	Interm. temp. 1	ºC	**49.4**	726.6	**1737**	Q_{DHW-RH}		
1T9	CO_2	Gas cooler	Interm. temp. 2	ºC	**30.4**	583.2	**3477**	Q_{SH}		
1T10	CO_2	Gas cooler	Outlet temp.	ºC	**17.7**	541.5	**1013**	Q_{DHW-PH}	**6227**	Q_{GC-TOT}
1T12	CO_2	SGHX	Outlet temp.	ºC	**15.0**	533.7	**188**	Q_{SGHX}		
1T13	CO_2	Subcooler	Outlet temp.	ºC	**14.8**	534.3	**0**	$Q_{SUBCOOL}$		
2F1	Hycool	Evaporator	Volume flow rate	l/s	**0.333**					
2T1	Hycool	Evaporator	Inlet temp.	ºC	**4.4**					
2T1	Hycool	Evaporator	Outlet temp.	ºC	**0.8**	*3.6 K*	**4303**	Q_{EVAP}		
3F1	DHW	Gas cooler	Volume flow rate	l/min	**0.635**					
3T2	DHW	Gas Cooler	Inlet temp.	ºC	**6.7**					
3T3	DHW	Gas cooler	Interm. temp. 1	ºC	**30.2**	*23.7 K*	**1046**	Q_{DHW-PH}	ΔQ_{DHW-RH}	-0.5 %
3T4	DHW	Gas cooler	Interm. temp. 2	ºC	**30.2**				ΔQ_{DHW-PH}	3.1 %
3T6	DHW	Gas cooler	Outlet temp.	ºC	**70.0**	*39.6 K*	**1729**	Q_{DHW-RH}	ΔQ_{SH}	4.4 %
4F1	Water	Gas cooler	Volume flow rate	l/s	**0.175**				ΔQ_{GC-TOT}	**2.8 %**
4T3	Water	Gas cooler	Inlet temp.	ºC	**30.0**					
4T4	Water	Gas cooler	Outlet temp.	ºC	**35.0**	*5.0 K*	**3635**	Q_{SH}	**6410**	Q_{GC-TOT}
									3.58	**COP**

Figure 5.2 Illustration of one of the tailor-made Excel spreadsheets that was used to display and process the measured values.

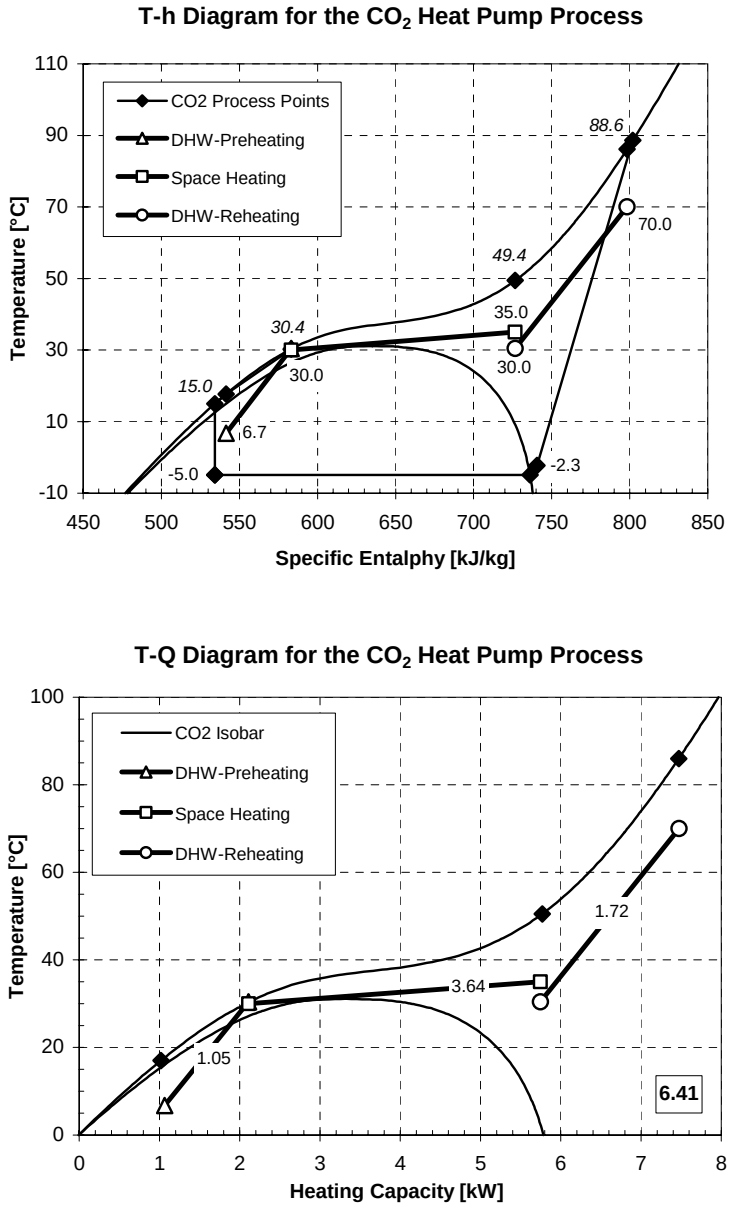

Figure 5.3 Illustration of the T-h and T-Q diagrams that were used to display and process the measured values.

The heating and cooling curves in the diagrams in Figure 5.3 indicate the overall temperature levels, and do not display the actual temperature development for the fluids as a function of the relative length of the gas cooler units.

5.1.3.2 Simultaneous Space and Hot Water Heating

The Maximum COP vs. the Optimum High-Side Pressure

For each measuring series at fixed set-point temperatures for the space heating and hot water systems, there was a maximum COP that corresponded to an optimum gas cooler (high-side) pressure (ref. Appendix A2.4). This is demonstrated in Figure 5.4, where the heating capacity of the tripartite gas cooler (Q_{GC}), the power input to the compressor (P_C) and the COP of the heat pump are shown as a function of the high-side pressure. For the selected measuring series, the evaporation temperature was -5ºC (3.046 MPa), and the set-point temperatures for the space heating and hot water system were 35/30ºC and 60ºC, respectively.

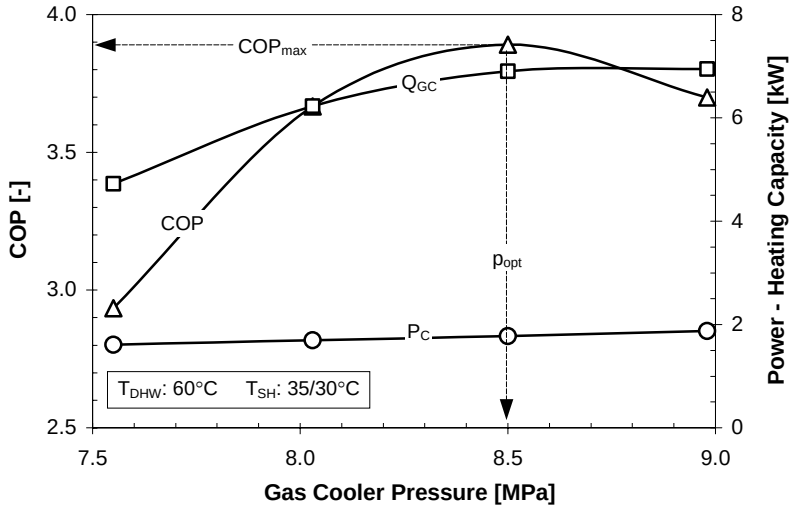

Figure 5.4 The measured heating capacity of the gas cooler (Q_{GC}), the compressor power input (P_C) and the COP at varying gas cooler (high-side) pressure in the combined mode.

Whereas the power input to the compressor was virtually proportional to the high-side pressure, there was a significant change in the heating capacity of the tripartite gas cooler when the pressure was gradually increased from 7.5 to 9.0 MPa. This is further demonstrated in Figure 5.5, where the heat rejection process in the tripartite gas cooler for the selected test series is displayed by means of T-Q diagrams. An overview of the power input to the compressor, the heating capacities for the three gas cooler units as well as selected temperatures for the heat rejection process is presented in Table 5.1.

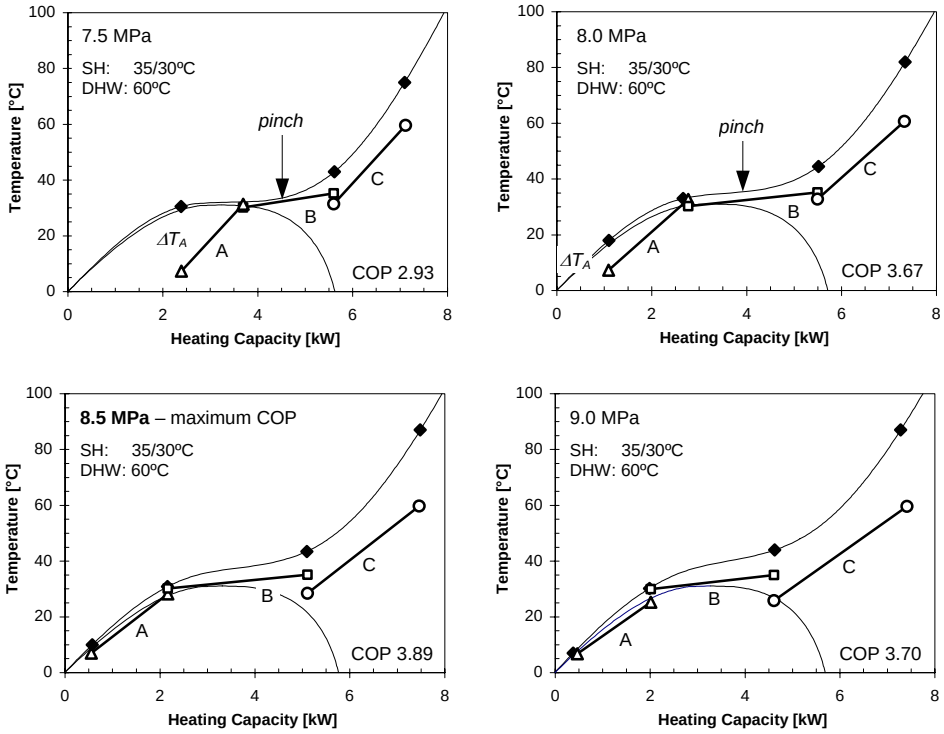

Figure 5.5 The heat transfer process for the tripartite gas cooler in the combined mode illustrated in T-Q diagrams at 35/30ºC (SH), 60ºC (DHW) and varying high-side pressure.

At 7.5 MPa high-side pressure, the minimal temperature difference between the CO_2 and the water and the *pinch point* inside the gas cooler led to a very small heating capacity for the space heating gas cooler (B). Furthermore, the moderate discharge gas temperature from the compressor and the consequent low temperature difference in the DHW reheating gas cooler (C), limited the water flow rate in the hot water circuit. Owing to the latter and the high specific heat capacity of the CO_2 in the near critical region, the CO_2 was cooled down only a few degrees in the DHW preheating gas cooler (A). As a result, the temperature approach (ΔT_A)[1] was almost 25 K, and the total heating capacity of the tripartite gas cooler was less than 5 kW.

By increasing the high-side pressure to 8 MPa, the heating capacity of the space heating gas cooler (B) increased considerably as a result of the larger temperature difference between the CO_2 and the water. The 6 K

[1] *The difference between the CO_2 outlet temperature and the inlet air/water temperature in a counter-flow gas cooler is denoted the temperature approach.*

higher discharge gas temperature from the compressor led to a 20% larger water flow rate in the hot water circuit, and since the specific heat capacity of the CO_2 in the near critical region was considerably lower than at 7.5 MPa, the temperature approach dropped by 13 K.

Table 5.1 Measured values for the CO_2 heat pump unit at 60ºC DHW temperature, 35/30ºC supply/return temperatures for the SH system and variable high-side pressure.

Measured Values	**7.5 MPa**	**8.0 MPa**	**8.5 MPa**	**9.0 MPa**
Evaporation temperature [ºC]	-5.0	-5.1	-5.1	-5.0
Compressor discharge gas temp. [°C]	75.5	81.6	86.4	90.6
Inlet temperature expansion valve [ºC]	30.5	18.0	9.8	8.5
Compressor input power [W]	1610	1700	1775	1880
Heating capacity - Space heating [W]	1910	2730	2940	2600
Heating capacity - DHW preheating [W]	1300	1670	1610	1550
Heating capacity - DHW reheating [W]	1510	1830	2360	2800
Total heating capacity [W]	4722	6230	**6907**	6947
DHW heating capacity ratio [-] [1)]	0.60	0.56	0.57	0.63
COP [-]	2.93	3.67	**3.89**	3.70
Temperature approach [K]	23.4	10.6	2.8	1.8

1) The ratio of the heating capacity for heating of DHW and the total heating capacity of the tripartite gas cooler (ref. Eq. 3.5, Section 3.2.4.2, Operational Characteristics).

At 8.5 MPa, the temperature approach dropped off by another 8 K, and an additional 0.5 MPa rise in the high-side pressure had only a marginal effect of the temperature approach and the total heating capacity of the tripartite gas cooler. Hence, for this particular test series *the maximum COP* of 3.89 was measured at 8.5 MPa high-side pressure.

Figure 5.6 provides an overview of the measured maximum COPs and the respective optimum high-side pressures for all the measuring series in the combined mode. Since the measurements were carried out at 0.5 MPa intervals, the indicated optima for the high-side pressures for each measurement series should only be regarded as *approximate values*. For the same reason, the maximum COP for the heat pump at the different operating conditions may be slightly higher than the measured values.

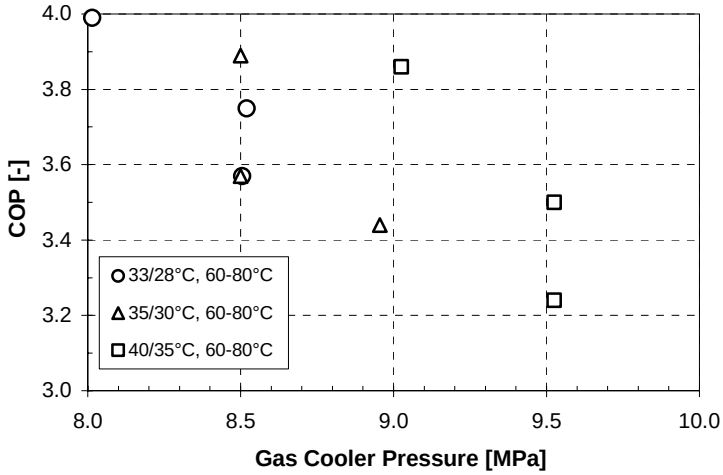

Figure 5.6 *Overview of the measured maximum COP as a function of the high-side pressure at varying temperature levels for the SH and DHW systems.*

The COP vs. the Hot Water Temperature

Figures 5.7 through 5.9 show the measured COP for the CO_2 heat pump unit at fixed supply/return temperatures for the space heating system and varying hot water temperature. The evaporation temperature was -5ºC (3.046 MPa), the suction gas superheating was 2.4 K ±0.4 K, the CO_2 mass flow rate was 1.42 kg/min ±2% and the city water temp. was 6.7ºC ±0.8 ºC.

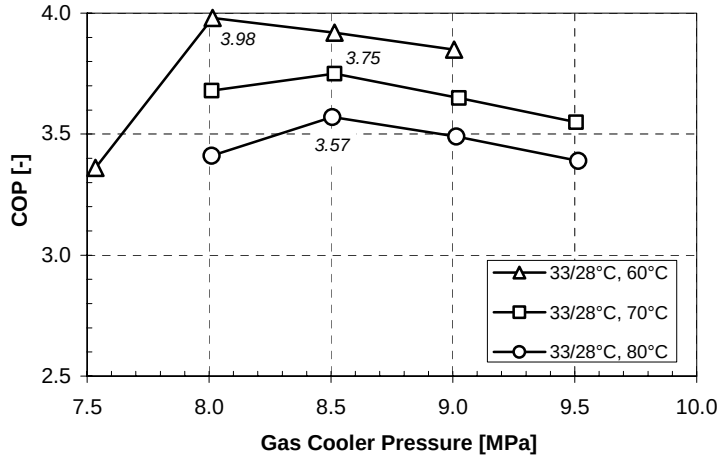

Figure 5.7 *The measured COP at 33/28ºC supply/return temperatures for the SH system and varying DHW temperature.*

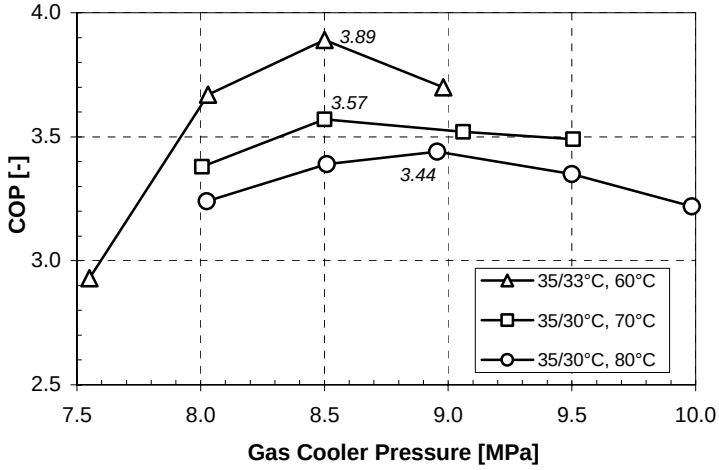

Figure 5.8 The measured COP at 35/30ºC supply/return temperatures for the SH system and varying DHW temperature.

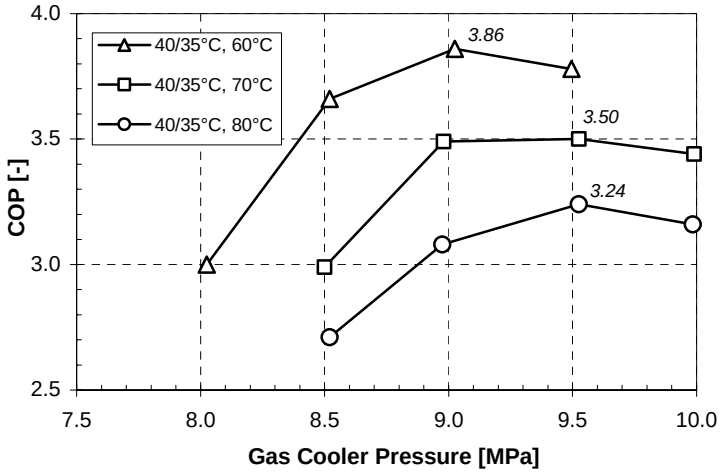

Figure 5.9 The measured COP at 40/35ºC supply/return temperatures for the SH system and varying DHW temperature.

At constant supply/return temperatures for the space heating system, the maximum COP for the heat pump unit decreased quite rapidly when the hot water temperature was increased from 60 to 80ºC. The measured average reduction of the maximum COP at 33/28, 35/30 and 40/35ºC supply/return temperatures were about 0.5, 0.6 and 0.8%, respectively, per K rise in the hot water temperature. The falling COP was mainly a result of decreasing water flow rate at increasing set-point temperature, which led to less cool-down of the CO_2 in the DHW preheating gas cooler and thus a higher temperature approach. The variation in the power input to

the compressor also affected the maximum COP, since the optimum high-side pressure rose by about 0.5 MPa when the set-point for the hot water temperature was increased from 60 to 80ºC.

The set-point for the hot water temperature had a significant impact on *the DHW heating capacity ratio*. This is demonstrated in Figure 5.10, where the heat rejection process in the tripartite gas cooler is displayed in T-Q diagrams at optimum high-side pressures, 60 and 80ºC hot water temperatures and 35/30ºC supply/return temperatures for the space heating system.

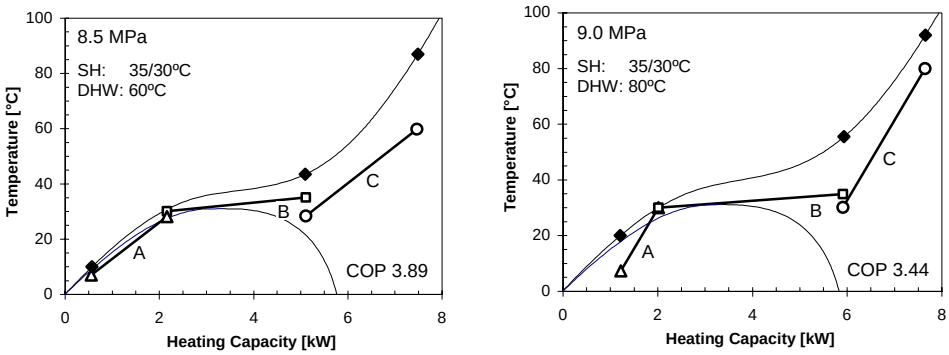

Figure 5.10 Illustration of the heat transfer process in the tripartite gas cooler in the combined mode at optimum high-side pressures, 35/30ºC supply/return temperatures for the SH system and 60℃ and 80ºC DHW temperatures.

According to Figure 5.10, the optimum high-side pressure rose from 8.5 to 9.0 MPa when the hot water temperature was increased from 60 to 80ºC, and the water flow rate in the hot water circuit had to be reduced by nearly 55%. As a result the heating capacity of the DHW preheating (A) and re-heating (C) gas coolers dropped off by approximately 14%, whereas the heating capacity of the space heating gas cooler (B) increased by 22% due to the higher average temperature difference. All in all the elevated set-point temperature reduced the DHW heating capacity ratio from 57 to 39%.

Figure 5.11 shows the measured maximum COP as a function of *the DHW heating capacity ratio* at varying supply/return temperatures for the space heating system and varying set-point temperature for the hot water system. At 33/28, 35/30 and 40/35ºC supply/return temperatures in the space heating system, the DHW heating capacity ratio dropped by approximately 18 percentage points when the set-point temperature for the hot water was increased from 60 to 80ºC.

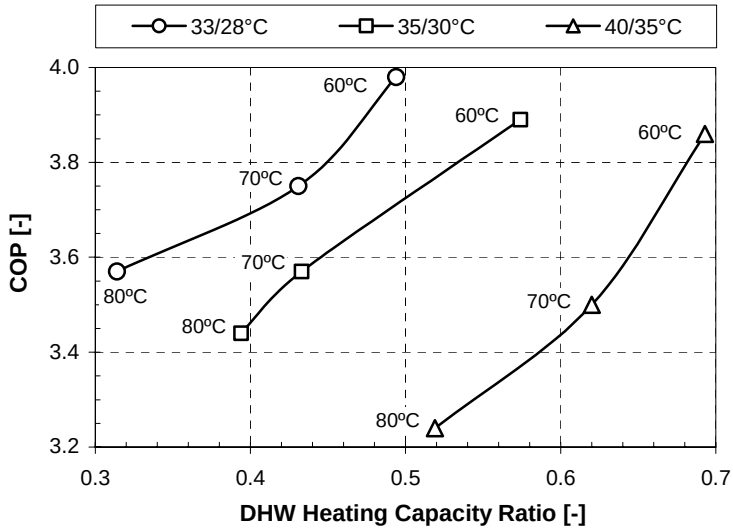

Figure 5.11 The relationship between the maximum COP and the DHW heating capacity ratio in the combined mode.

Figures 5.12 through 5.14 show the measured COP for the CO_2 heat pump unit as a function of *the temperature approach* at fixed supply/return temperatures for the space heating system and varying hot water temperature.

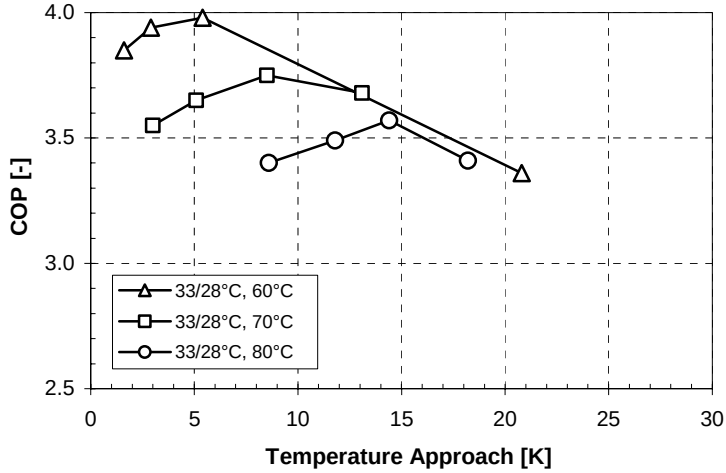

Figure 5.12 The measured COP as a function of the temperature approach at 33/28ºC supply/return temperatures for the SH system and varying DHW temperature.

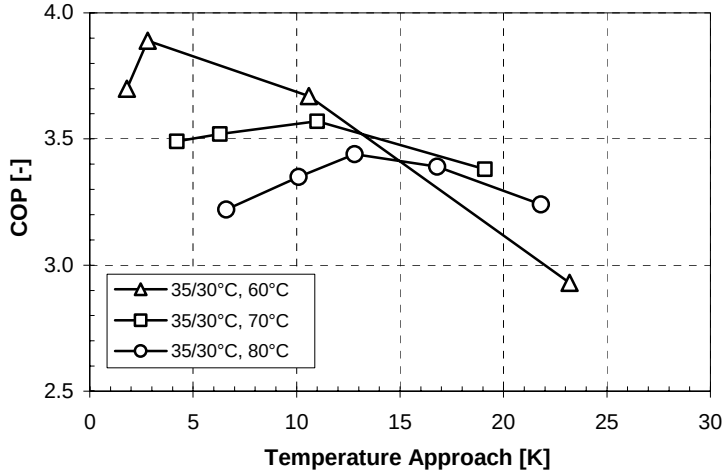

Figure 5.13 The measured COP as a function of the temperature approach at 35/30ºC supply/return temperatures for the SH system and varying DHW temperature.

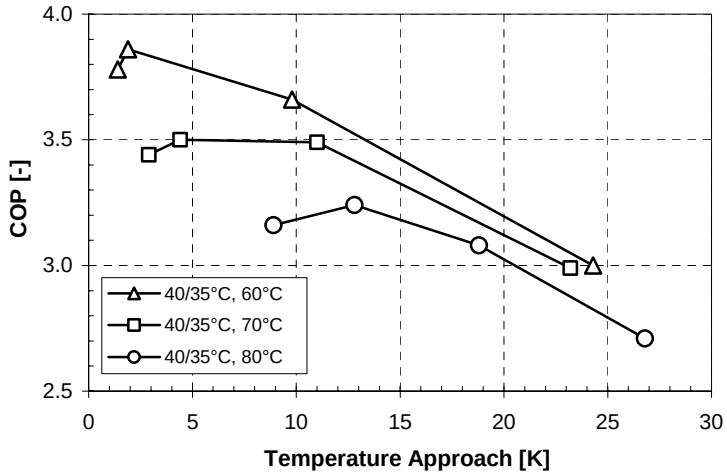

Figure 5.14 The measured COP as a function of the temperature approach at 40/35ºC supply/return temperatures for the SH system and varying DHW temperature.

The maximum COP was virtually proportional to the temperature approach at constant temperature level in the space heating system and varying set-point temperature for the hot water system. The lower the hot water temperature, the smaller the temperature approach at the maximum COP (i.e. at the optimum high-side pressure).

The COP vs. the Temperature Level in the Space Heating System

Figures 5.15 through 5.17 show the measured COP for the CO_2 heat pump unit as a function of the high-side pressure at fixed set-point for the hot water temperature and varying supply/return temperatures for the space heating system. The measured values come from the same measuring series as presented in Figures 5.7 through 5.9.

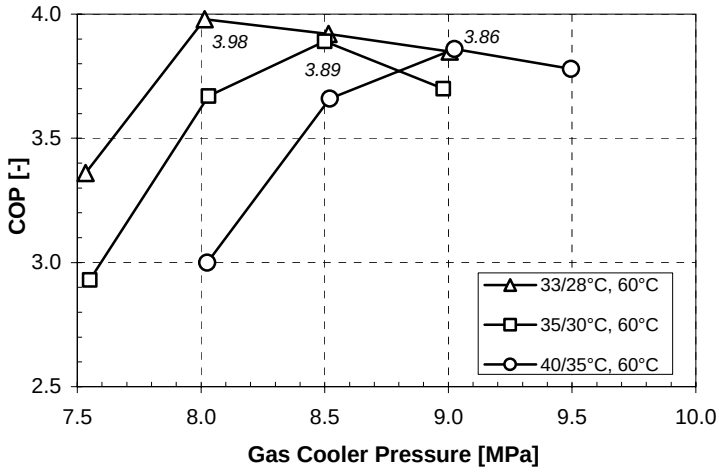

Figure 5.15 The measured COP at 60ºC DHW temperature and varying supply/return temperatures for the SH system.

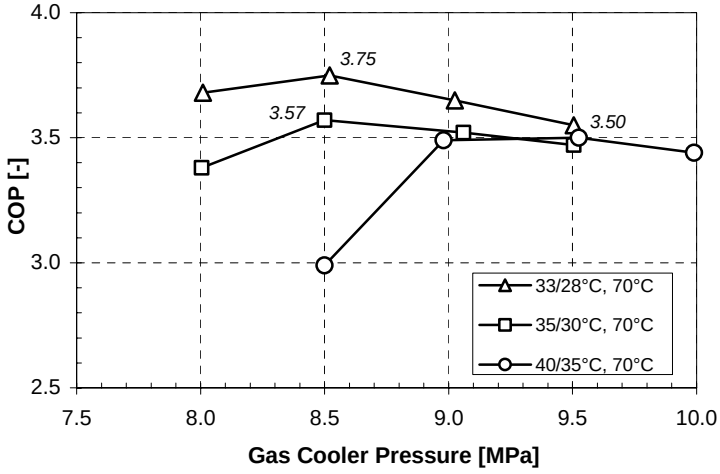

Figure 5.16 The measured COP at 70ºC DHW temperature and varying supply/return temperatures for the SH system.

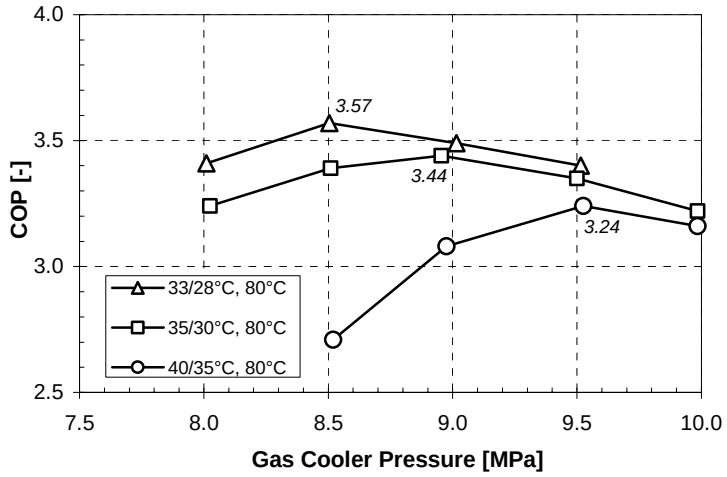

Figure 5.17 The measured COP at 80ºC DHW temperature and varying supply/return temperatures for the SH system.

The high-side pressure had a considerable impact on the average temperature difference between the CO_2 and the water in the space heating gas cooler, which in turn affected the heating capacity and the CO_2 outlet temperature. By increasing the high-side pressure, the total heating capacity of the tripartite gas cooler increased, but at the cost of a higher power input to the compressor. For the measuring series displayed in Figures 5.15 through 5.17, *the optimum high-side pressure* rose by approximately 1 MPa when the hot water temperature was kept constant and the supply/return temperatures for the space heating system was altered from 33/28ºC to 40/35°C. With the exception of the measuring series at 33/28°C supply/return temperatures and 60ºC hot water temperature, the COP curves were relatively flat near the maximum values, and the COP decreased by about 2.5 to 5.5% at ±0.5 MPa deviation from the optimum high-side pressure.

Although the highest COP was measured at the lowest supply/return temperatures, the maximum COP at the optimum high-side pressure was relatively insensitive to variations in the temperature level in the space heating system. At 60°C hot water temperature, the maximum COP dropped off by approximately 3% when the supply/return temperatures was increased from 33/28ºC to 40/35ºC. At 70 and 80ºC hot water temperature, the corresponding figures were about 6% and 9%, respectively. According to Figure 5.11, the main reason for the relatively constant COP was the considerable variations in *the DHW heating capacity ratio* at different temperature levels in the space heating system. By altering the supply/return temperatures from 33/28ºC to 40/35ºC, the DHW heating

capacity ratio increased by approximately 18 percentage points. Hence, *the higher the temperature level in the space heating system, the larger the hot water heating capacity for the CO_2 heat pump unit*. This aspect is illustrated in Figure 5.18, where the heat rejection process in the tripartite gas cooler is displayed by means of T-Q diagrams at optimum high-side pressures, 32/28ºC and 40/35ºC supply/return temperatures for the space heating system and 60ºC hot water temperature.

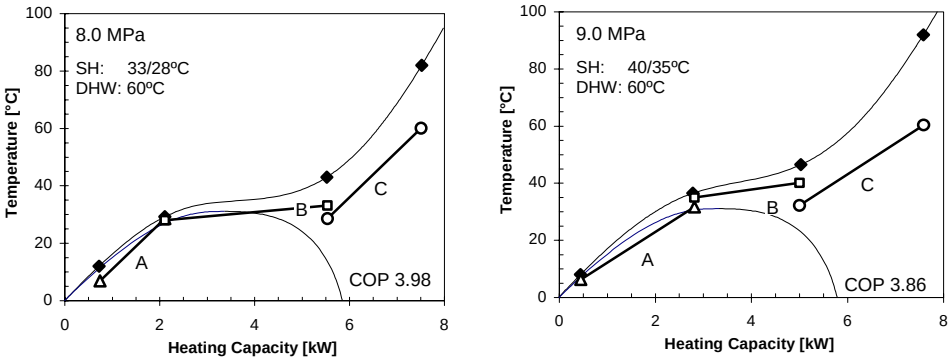

Figure 5.18 Illustration of the heat transfer process in the tripartite gas cooler in combined mode at optimum high-side pressures, 33/28ºC and 40/35ºC supply/return temperatures for the SH system and 60ºC DHW temperature.

According to Figure 5.18, the total heating capacity of the tripartite gas cooler at 40/35ºC supply/return temperatures, exceeded the heating capacity at 33/28°C by approximately 6%. This was due to the 8 K higher CO_2 outlet temperature from the compressor and the 3.5 K lower temperature approach. The latter was in turn a result of the nearly 50% larger water flow rate in the hot water circuit. Since the power input to the compressor was about 9% higher at 40/35ºC, the COPs for the two measuring series were virtually identical.

Figures 5.19 through 5.21 show the measured COP for the CO_2 heat pump unit as a function of *the temperature approach* at fixed set-point for the hot water temperature and varying supply/return temperatures for the space heating system.

The higher the temperature level in the space heating system, the higher the DHW heating capacity ratio and the lower the approach temperature. The difference was, however, on average less than 3 K at 33/28ºC and 40/35ºC supply/return temperatures.

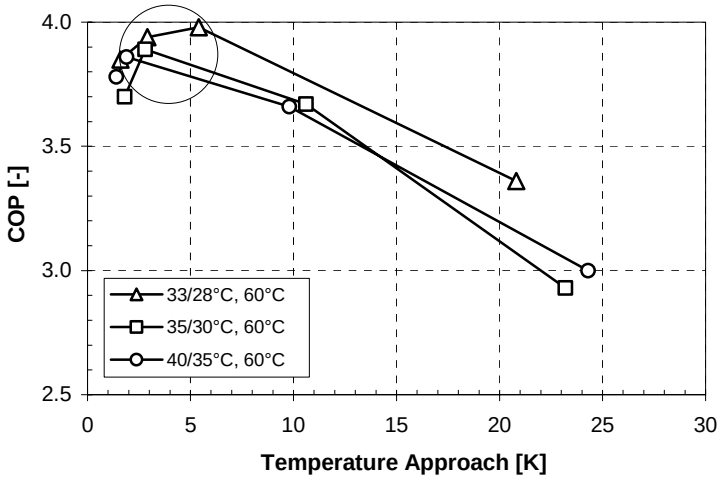

Figure 5.19 The measured COP as a function of the temperature approach at 60ºC DHW temperature and varying supply/-return temperatures for the SH system.

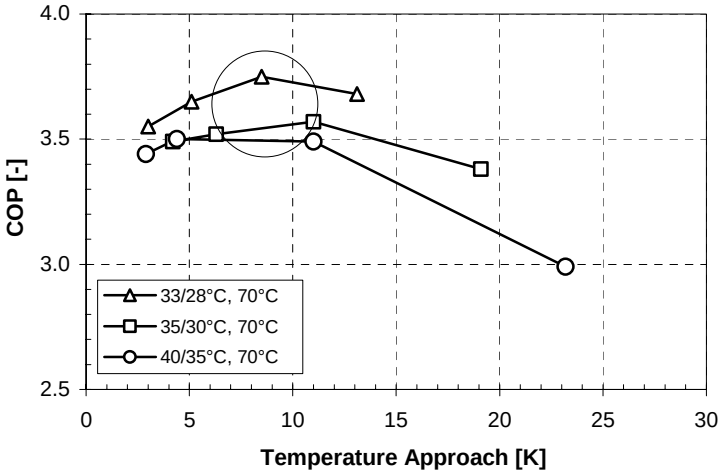

Figure 5.20 The measured COP as a function of the temperature approach at 70ºC DHW temperature and varying supply/-return temperatures for the SH system.

According to Figure 5.20, the temperature approaches at 35/30°C were higher than that of the 33/28ºC measuring series. The most likely explanation to this inconsistent result is that the optimum high-side pressure in reality was between 8.5 and 9 MPa and not at the measuring point of 8.5 MPa, since a slightly elevated high-side pressure would have lowered the temperature approach and increased the COP of the heat pump.

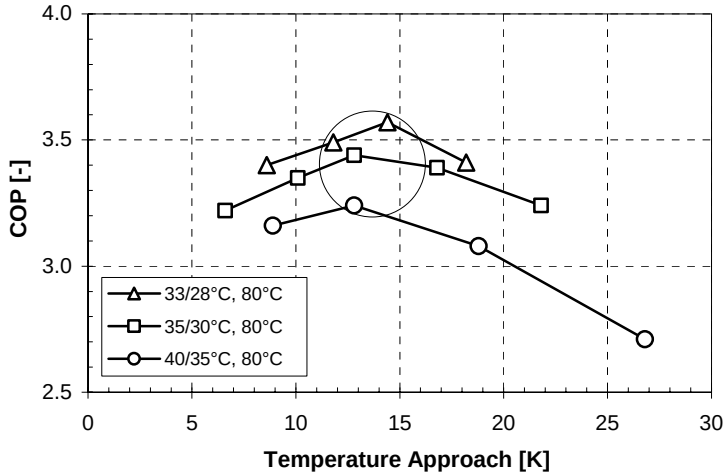

Figure 5.21 The measured COP as a function of the temperature approach at 80ºC DHW temperature and varying supply/-return temperatures for the SH system.

The COP vs. the Evaporation Temperature

Figure 5.22 shows the measured COP for the CO_2 heat pump unit at varying evaporation temperature, 60ºC hot water temperature and 35/30ºC supply/return temperatures for the space heating system. At -10ºC evaporation temperature (2.649 MPa), the suction gas superheating was 2.1 K ±0.5 K, the CO_2 mass flow rate was 1.22 kg/min ±1.5% and the inlet city water temperature was 6.5ºC ±0.6ºC. Unfortunately, the test at 0ºC evaporation temperature had to be cancelled due to operational problems (leakage) and consequent plant shut-down.

By changing the evaporation temperature from -5ºC to -10ºC, the mass flow rate dropped off by 15%, whereas *the optimum high-side pressure* decreased from 8.5 to 8 MPa. Since the measurements were carried out at 0.5 MPa intervals, the indicated optima for the high-side pressures should only be regarded as approximate values. At optimum high-side pressure, the total heating capacity of the tripartite gas cooler and the power input to the compressor dropped off by approximately 11% and 5%, respectively, resulting in a *6% lower COP* at -10°C evaporation temperature. The DHW heating capacity ratio of the heat pump unit was virtually unaffected by the evaporation temperature.

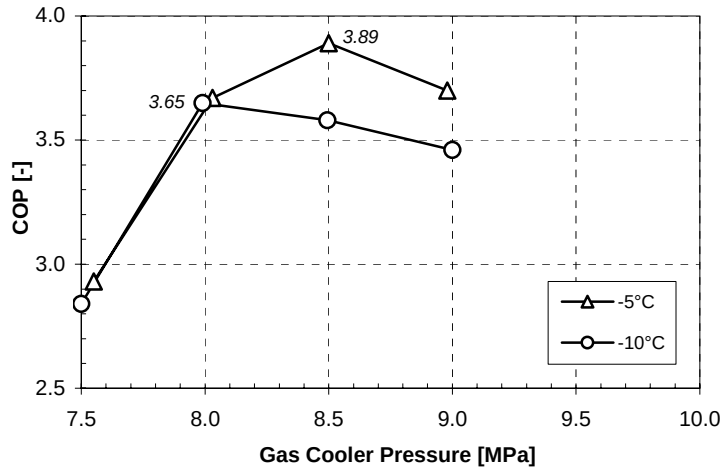

Figure 5.22 The measured COP in the combined mode at varying evaporation temperature, 60ºC DHW temperature and 35/30ºC supply/return temperatures for the SH system.

The High-Side Pressure vs. the Temperature Approach

Figure 5.23 shows an overview of the relationship between the high-side pressure and *the temperature approach* at varying hot water temperature and temperature level in the space heating system.

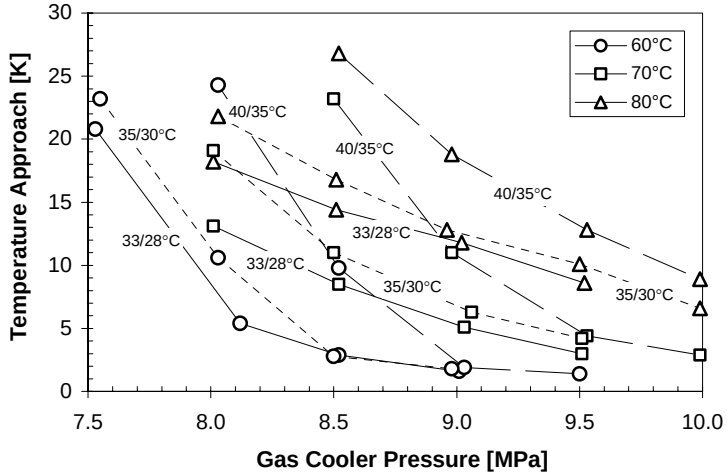

Figure 5.23 The measured temperature approach as a function of the high-side pressure at varying DHW temperature and supply/return temperatures for the SH system.

Due to the relatively small temperature difference, the curves at 33/28°C and 35/30°C supply/return temperatures for the space heating system were virtually coincident. Moreover, the lower the hot water temperature, the steeper the average gradient ($\partial\Delta T_A/\partial p_{GC}$), where ΔT_A is the temperature approach and p_{GC} the gas cooler (high-side) pressure.

The Heating Capacity of the Tripartite Gas Cooler

Despite the relatively large variations in the set-point temperatures for the space heating and hot water systems, the total heating capacity of the tripartite gas cooler at optimum high-side pressure did not change much, and ranged from about 6.4 to 7.2 kW (6.8 kW ±6%). Figure 5.24 shows *the relative heating capacity* for each of the three gas cooler units at optimum high-side pressure and varying temperature levels in the space heating and hot water systems. The numbers above the columns represent *the DHW heating capacity ratio* in percent for the CO_2 heat pump unit.

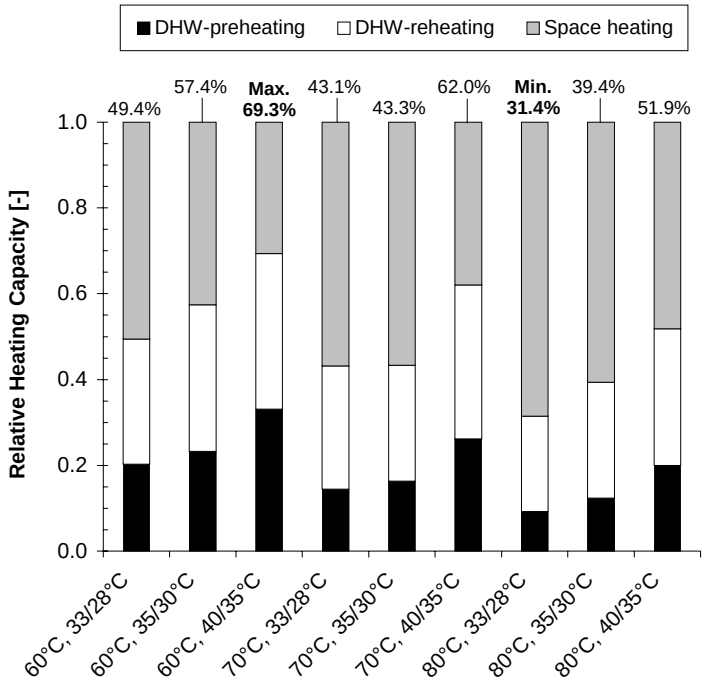

Figure 5.24 The measured relative heating capacity for the three gas cooler units at optimum high-side pressure and varying temperature levels in the SH and DHW systems.

The heat transfer surface of the DHW reheating gas cooler unit was less than 10% of the total heat transfer area for the tripartite gas cooler. However, due to the relatively large average temperature difference between the CO_2 and the water, the heating capacity of the gas cooler unit constituted as much as 22 to 36% of the total heating capacity for the tripartite gas cooler. The lowest heating capacity was measured at 33/28ºC supply/return temperatures for the space heating system and 80°C hot water (31.4% DHW heating capacity ratio), whereas the largest heating capacity was measured at 40/35°C supply/return temperatures and 60ºC hot water temperature (69.3% DHW heating capacity ratio).

Temperature Characteristics of the Tripartite Gas Cooler

Figure 5.25 shows the principle of the tripartite gas cooler for preheating of hot water (*DHW-P*), low-temperature space heating (*SH*) and reheating of hot water (*DHW-R*). The variables T_1, T_2, T_3 and T_4 represent the inlet and outlet CO_2 temperatures for the three gas cooler units.

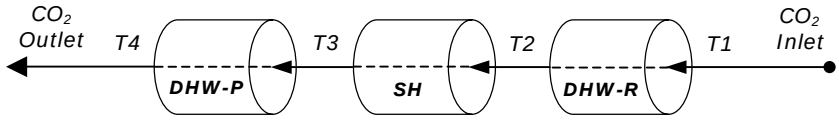

Figure 5.25 Principle of the tripartite gas cooler.

For each measuring series at fixed set-point temperatures for the space heating and DHW systems, both the inlet and outlet CO_2 temperature from the space heating gas cooler (T2 and T3) remained virtually constant when the high-side pressure was gradually increased. Table 5.2 presents an overview of the CO_2 temperatures for the different measuring series.

Table 5.2 Overview of the measured CO_2 temperatures at the inlet (T2) and outlet (T3) of the space heating gas cooler unit during operation in the combined mode.

DHW Temperatures	**Inlet – Outlet CO_2 Temperatures for the SH Gas Cooler**		
	SH 33/28ºC	**SH 35/30ºC**	**SH 40/35ºC**
60ºC	44 – 29ºC	44 – 31ºC	46 – 36ºC
70ºC	49 – 29ºC	50 – 31ºC	51 – 36ºC
80ºC	55 – 29ºC	56 – 31ºC	56 – 36ºC

The virtually constant inlet and outlet CO_2 temperatures for the space heating gas cooler are illustrated in Figure 5.26, where the heat rejection process in the tripartite gas cooler is displayed by means of T-Q diagrams at 33/28ºC supply/return temperatures for the space heating system and 70ºC hot water temperature.

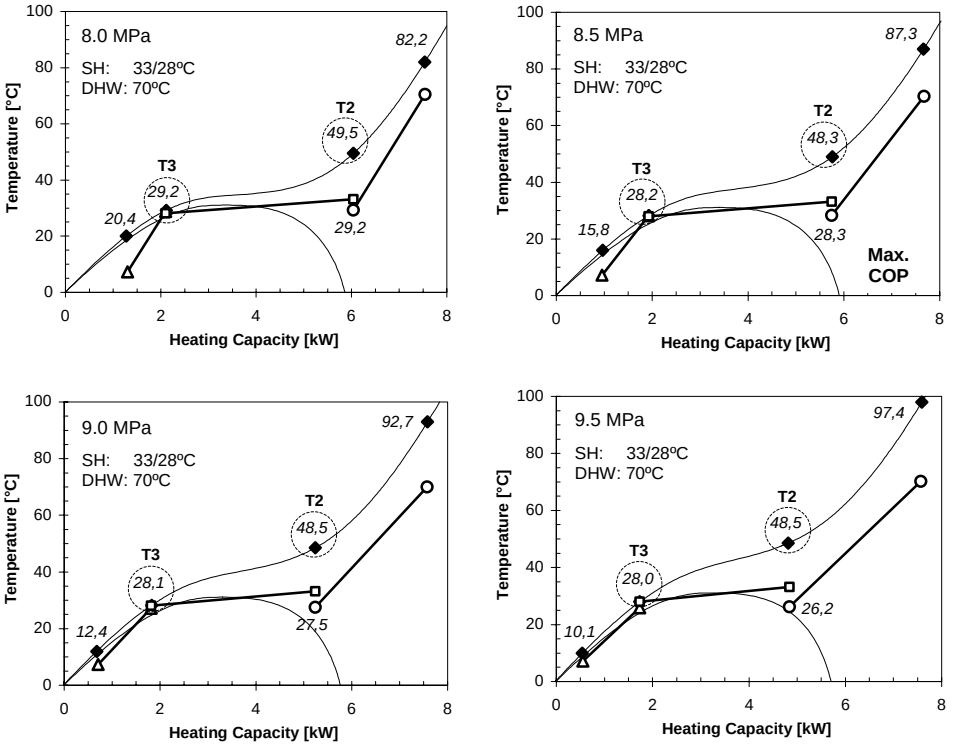

Figure 5.26 The heat transfer process for the tripartite gas cooler in the combined mode illustrated in T-Q diagrams at varying high-side pressure. The supply/return temperatures and the DHW temperature was 33/28ºC and 70ºC.

The outlet CO_2 temperature *T3* from the space heating gas cooler was limited by the return temperature in the space heating system. Due to the relatively large heat transfer surface and the excellent heat transfer conditions, the temperature approach was small and the CO_2 outlet temperature remained virtually constant when the high-side pressure was increased.

Since the CO_2 mass flow rate was virtually constant and the set-point temperatures for the space heating and hot water systems were set at 33 and 70°C, respectively, the outlet CO_2 temperature *T2* from the DHW

reheating gas cooler was mainly determined by the discharge gas temperature from the compressor, the outlet water temperature from the DHW preheating gas cooler and the water flow rate (i.e. the CP-value[2]). Due to the large heat transfer surface of the DHW preheating gas cooler, the outlet water temperature dropped off only 3 K when the mass flow rate was increased from 0.53 l/min at 8 MPa high-side pressure to 0.90 l/min at 9.5 MPa. The cooling effect of the increasing water flow rate was more or less offset by the rise in the discharge gas temperature from the compressor, and the outlet CO_2 temperature from the DHW reheating gas cooler *T2* was therefore practically constant at varying high-side pressure.

5.1.3.3 Hot Water Heating Only

The Maximum COP vs. the Optimum High-Side Pressure

With reference to Figure 3.10 in Section 3.2.4.1, *Principle System Design*, the space heating gas cooler (B) was by-passed, and heat was delivered solely from the DHW preheating (A) and reheating (C) gas coolers units in the DHW mode.

Whereas the power input to the compressor was virtually proportional to the high-side pressure, there was a significant change in the total gas cooler heating capacity when the high-side pressure was increased. Hence, for each measuring series with fixed set-point for the hot water temperature, there was a maximum COP which corresponded to an optimum high-side pressure. This is demonstrated in Figure 5.27, where the heat rejection process in the two gas cooler units is displayed by means of T-Q diagrams. For the selected measuring series, the evaporation temperature was -5ºC and the hot water temperature was 70ºC.

At 9 and 9.5 MPa high-side pressure, the heat transfer process was considerably hampered by *a pinch point* inside the gas cooler units, which in turn limited the water flow rate in the hot water circuit and led to a very large temperature approach. By increasing the high-side pressure to 10 MPa, the temperature fit between the CO_2 and the water was greatly improved, and the temperature approach of the DHW preheating gas cooler unit dropped off to 3.5 K. Since an additional 0.5 MPa rise in the high-side pressure only had a marginal effect on the temperature approach and the total heating capacity of the gas cooler units, the maximum COP of 3.58 was measured at 10 MPa high-side pressure.

[2] *The product of the specific heat capacity and the mass flow rate.*

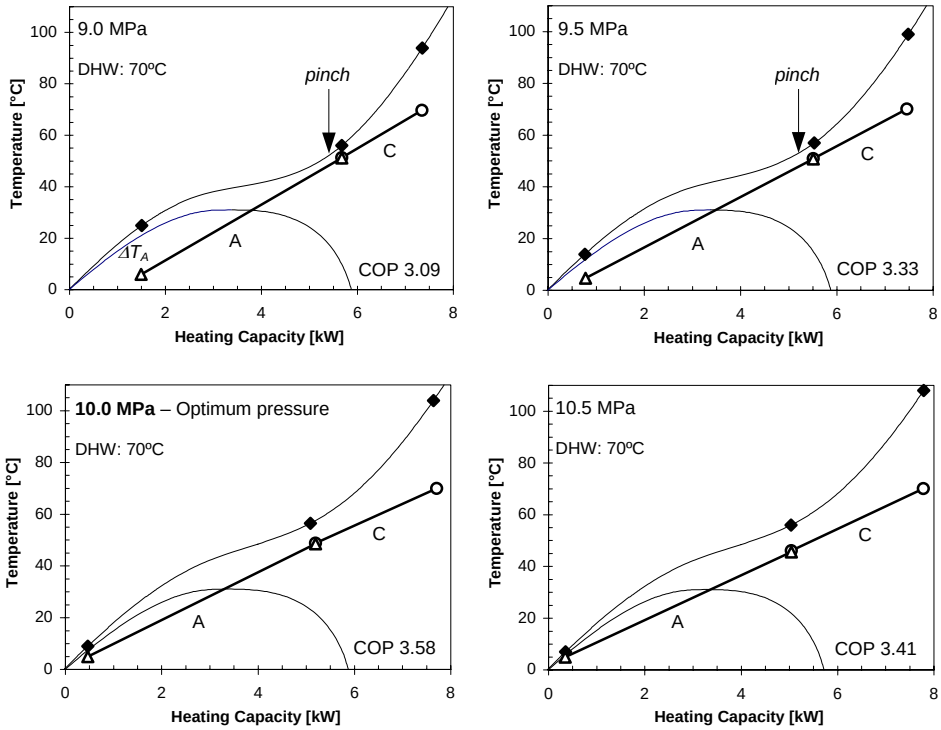

Figure 5.27 The heat transfer process for the gas cooler in the DHW mode illustrated in T-Q diagrams at 70ºC DHW temperature and varying high-side pressure.

COP vs. the Hot Water Temperature

Figure 5.28 presents the measured COP for the CO_2 heat pump unit at varying hot water temperature. The evaporation temperature was -5ºC (3.046 MPa), the suction gas superheating was 1.8 K ±0.6 K, the CO_2 mass flow rate was 1.40 kg/min ±1.5% and the city water temperature was 5.7ºC ±0.7ºC.

The maximum COP at the optimum high-side pressure dropped off by approximately 6% when the set-point for the hot water temperature was changed from 60 to 70ºC. This was a result of the 13% reduction in the water flow rate and the roughly 1 MPa higher optimum high-side pressure at 70ºC. The heat transfer processes at optimum high-side pressures are displayed by means of T-Q diagrams in Figure 5.29.

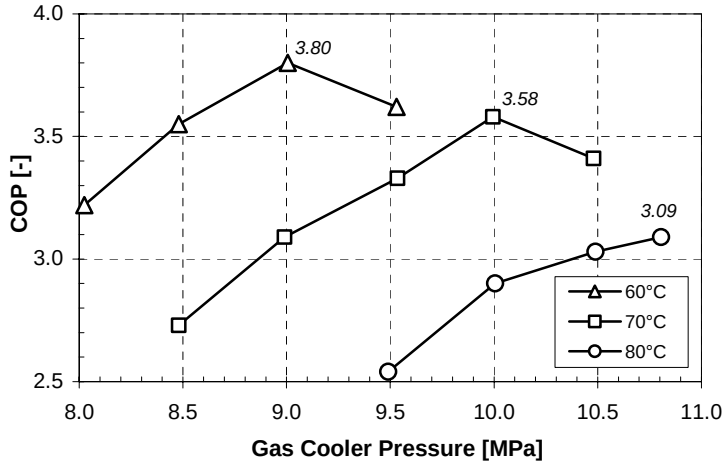

Figure 5.28 The measured COP in the DHW mode as a function of the high-side pressure at varying DHW temperature.

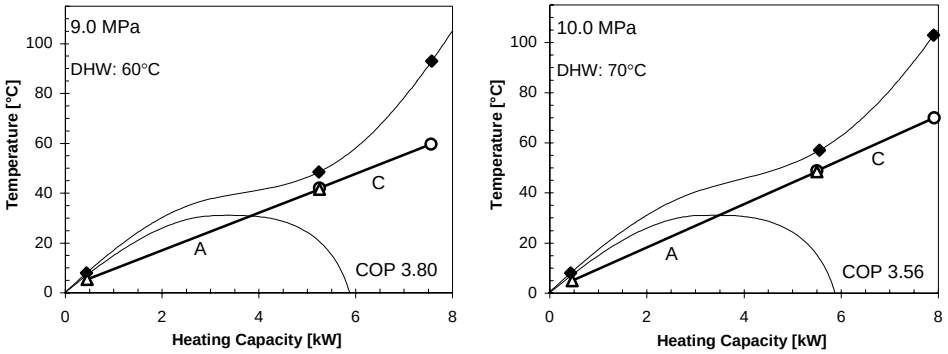

Figure 5.29 The heat transfer process for the gas cooler in the DHW mode illustrated in T-Q diagrams at 60 and 70ºC DHW temperature and optimum high-side pressure.

According to Figure 5.28, the maximum COP and the corresponding optimum high-side pressure were not determined for the 80ºC hot water measuring series, since the CO_2 heat pump unit could not be operated above 10.8 MPa high-side pressure due to motor load limitations.

Figure 5.30 shows the measured COP for the CO_2 heat pump unit as a function of *the temperature approach* at varying hot water temperature, while Figure 5.31 demonstrates the relationship between the high-side pressure and the temperature approach.

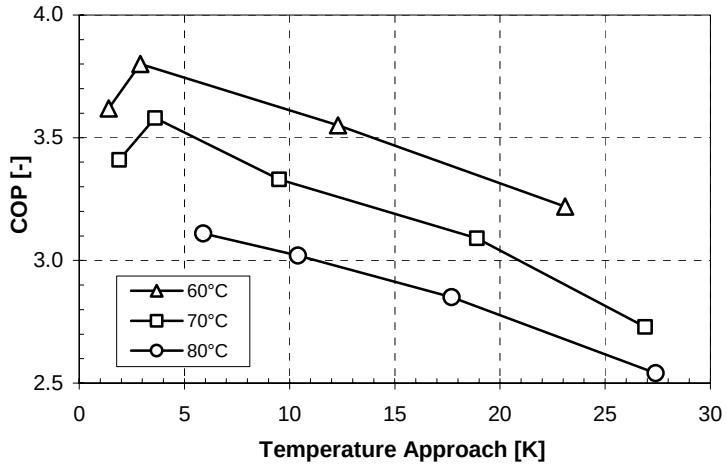

Figure 5.30 The measured COP in the DHW mode as a function of the temperature approach at varying DHW temperature.

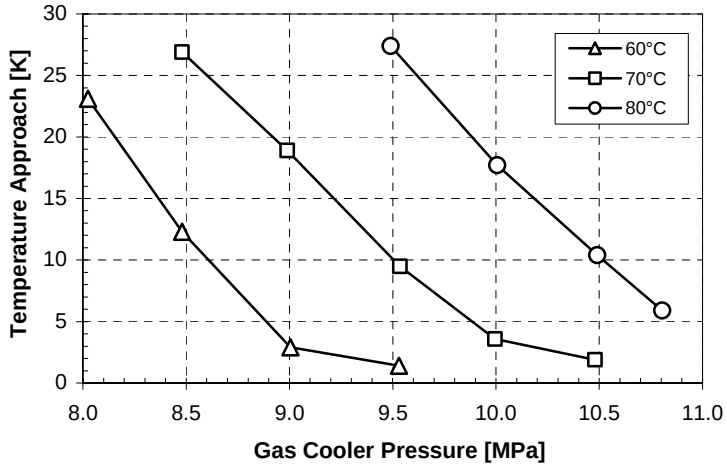

Figure 5.31 The measured temperature approach as a function of the high-side pressure at varying DHW temperature.

The maximum COPs at 60 and 70ºC hot water temperature were measured at approximately 9 and 10 MPa high-side pressure, respectively. At high-side pressures below the optimum values, there was virtually a linear relationship between the COP and the temperature approach as well as between the temperature approach and the high-side pressure. On the other hand, there was only a marginal reduction in the temperature approach when the high-side pressure was increased above the optimum level. By analysing the results in Figure 5.30, it is most likely that the optimum high-side pressure for the 80ºC measuring series was above 11 MPa, and that the corresponding temperature approach was around 5 K.

The COP vs. the Evaporation Temperature

Figure 5.32 shows the measured COP for the CO_2 heat pump unit at varying evaporation temperature and 60ºC hot water temperature. At -10ºC evaporation temperature (2.649 MPa), the suction gas superheating was 2.2 K ±0.1 K, the CO_2 mass flow rate was 1.21 kg/min ±2% and the inlet city water temperature was 6.9ºC. The test at 0°C evaporation temperature had to be cancelled due to operational problems with the test rig.

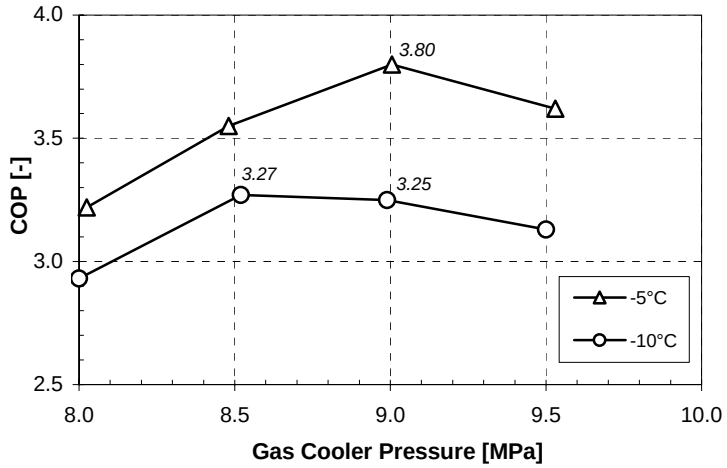

Figure 5.32 The measured COP in the DHW mode at varying evaporation temperature and 60ºC DHW temperature.

Since the COP at -10ºC evaporation temperature was virtually identical at 8.5 and 9 MPa high-side pressure, the optimum high-side pressure was probably located between 8.5 and 9 MPa, and the maximum COP was therefore higher than 3.27. Hence, assuming a maximum COP of 3.4, the COP decreased by approx. 10% when the evaporation temperature was altered from -5 to -10ºC. This is about 4 percentage points more than that of the combined mode, which indicates that the COP was more sensitive to variations in the evaporation temperature in the DHW mode.

The Heating Capacity of the Gas Cooler Units

The total heating capacity at optimum high-side pressure and 60 and 70ºC hot water temperature was 7.1 to 7.5 kW, respectively. This was about 5% higher than that of the total average heating capacity in the combined mode. The difference was mainly a result of the higher optimum high-side pressure and the lower average temperature approach.

Figure 5.33 shows that *the relative heating capacities* for the two gas cooler units were identical at optimum high-side pressure and varying set-point temperature for the hot water.

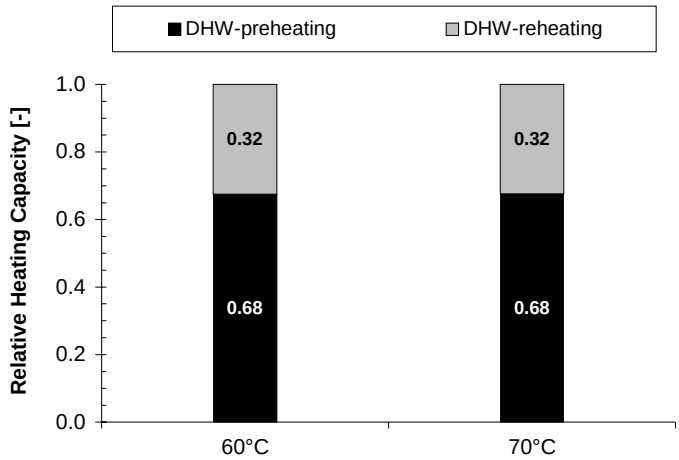

Figure 5.33 The measured relative heating capacity for the gas cooler units in the DHW mode at optimum high-side pressure and varying DHW temperature.

Although the heat transfer surface of the DHW preheating gas cooler unit was nearly 5 times larger than that of the DHW reheating gas cooler unit, the heating capacity of the latter at optimum high-side pressure constituted about 30% of the total heating capacity. According to Figure 5.27, this was mainly due to a larger average temperature difference.

5.1.3.4 Space Heating Only

The Maximum COP vs. the Optimum High-Side Pressure

During testing in the space heating mode (*SH mode*), there was no water flow in the hot water circuit, and the supercritical CO_2 passed through the DHW reheating gas cooler before it entered the space heating gas cooler.

For each measuring series with fixed supply/return temperatures for the space heating system, there was a maximum COP that corresponded to an optimum high-side pressure. This is demonstrated in Figure 5.34, where the heat rejection process in the two gas cooler units is displayed by means of T-Q diagrams. For the selected measuring series, the evaporation temperature was -5ºC and the supply/return temperatures in the space heating system were 35/30ºC.

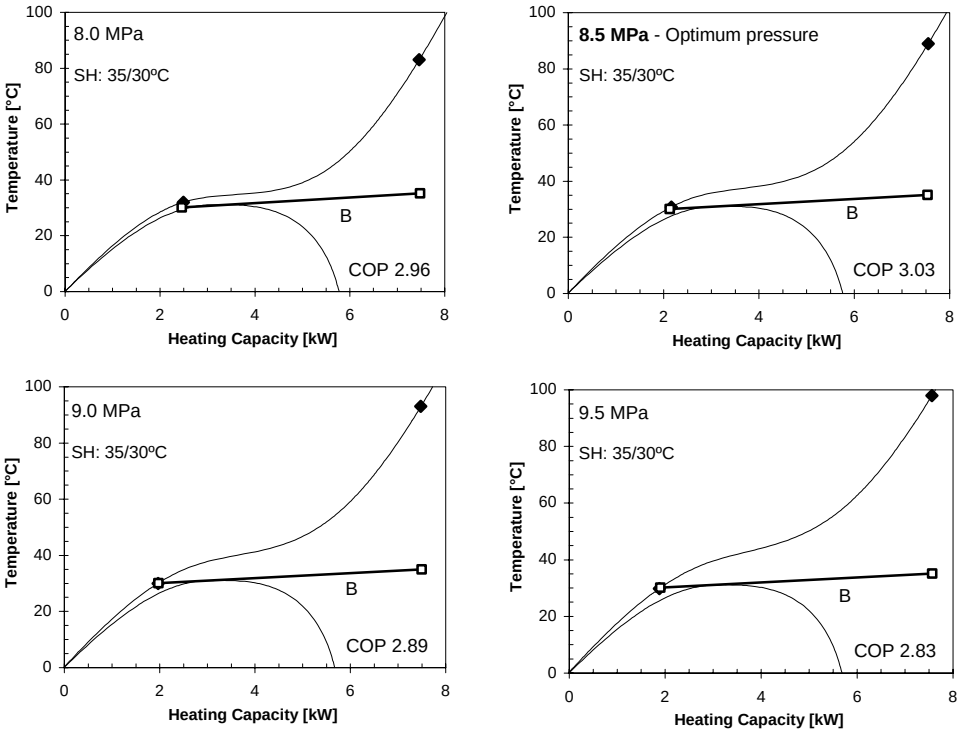

Figure 5.34 The heat transfer process for the tripartite gas cooler in the SH mode illustrated in T-Q diagrams at 35/30°C supply/-return temperatures and varying high-side pressure.

The COP vs. the Temperature Level in the Space Heating System

Figure 5.35 shows the measured COP for the CO_2 heat pump unit as a function of the high-side pressure at varying supply/return temperatures for the space heating system. The evaporation temperature was -5ºC (3.046 MPa), the suction gas superheating was 4.8 K ±0.2K and the CO_2 mass flow rate was 1.44 kg/min ±1%.

The optimum high-side pressure rose by approximately 1 to 1.5 MPa when the supply/return temperatures for the space heating system was altered from 33/28ºC to 40/35ºC. The COP dropped off on average 1.7% per K temperature rise when the supply temperature was increased from 33 to 40ºC. Whereas the COP curves were relatively flat around the optimum high-side pressure at the two lowest temperature levels, there was a distinct maximum at 40/35ºC.

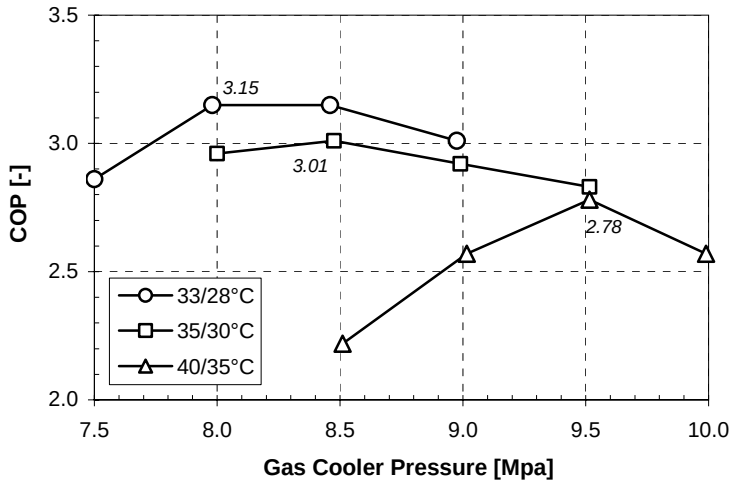

Figure 5.35 The measured COP as a function of the high-side pressure at varying supply/return temperatures for the SH system.

Figure 5.36 presents the relationship between the high-side pressure and the temperature approach.

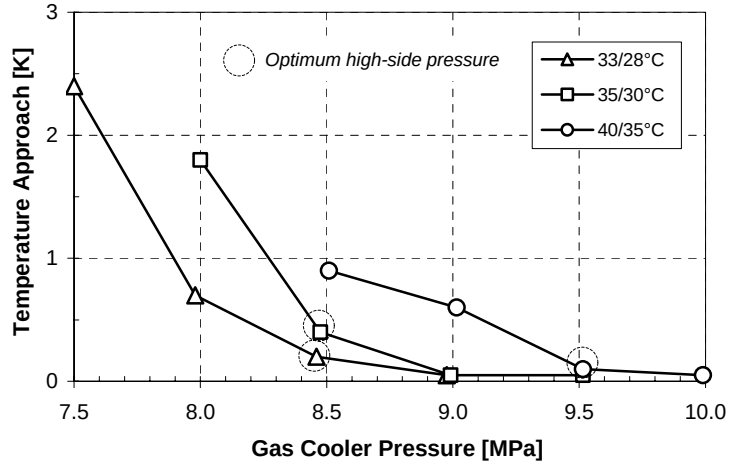

Figure 5.36 The measured temperature approach as a function of the high-side pressure at varying supply/return temperatures.

As a result of the large average temperature difference, there were only minor variations in the temperature approach when increasing the high-side pressure. Hence, the optimum high-side pressure was mainly determined by the marginal rise of the CO_2 outlet temperature from the compressor and the marginal power input the compressor.

The COP vs. the Evaporation Temperature

Figure 5.37 shows the measured COP for the CO_2 heat pump unit at varying evaporation temperature and 35/30ºC supply/return temperatures for the space heating system. At -10ºC evaporation temperature, the CO_2 mass flow rate was 1.21 kg/min ±2% and the suction gas superheating was 4.8 K ±0.5 K. At 0ºC evaporation temperature the corresponding numbers were 1.63 kg/min ±0.3% and 4.5 K ±0.5K.

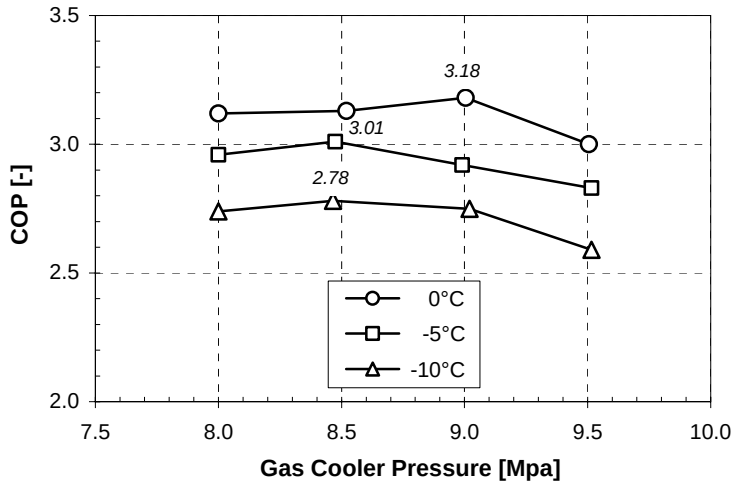

Figure 5.37 The measured COP at varying evaporation temperature and 35/30ºC supply/return temperatures for the SH system.

The COP curves were relatively flat around the optimum high-side pressure, and the optimum high-side pressure was rather invariable with the evaporation temperature. The COP decreased on average by approximately 1.3% per K drop in the evaporation temperature, which is the same order of magnitude as in the combined mode.

5.1.3.5 Comparison of the Measurements in the Different Heating Modes

The Coefficient of Performance (COP)

Figure 5.38 compares the maximum COPs at the optimum high-side pressures for the three heating modes at varying hot water temperature and supply/return temperatures for the space heating system. Since the maximum COP at 80ºC hot water temperature in DHW mode could not be experimentally determined due to pressure limitations for the CO_2 heat pump unit, the value was estimated to be about 3.20.

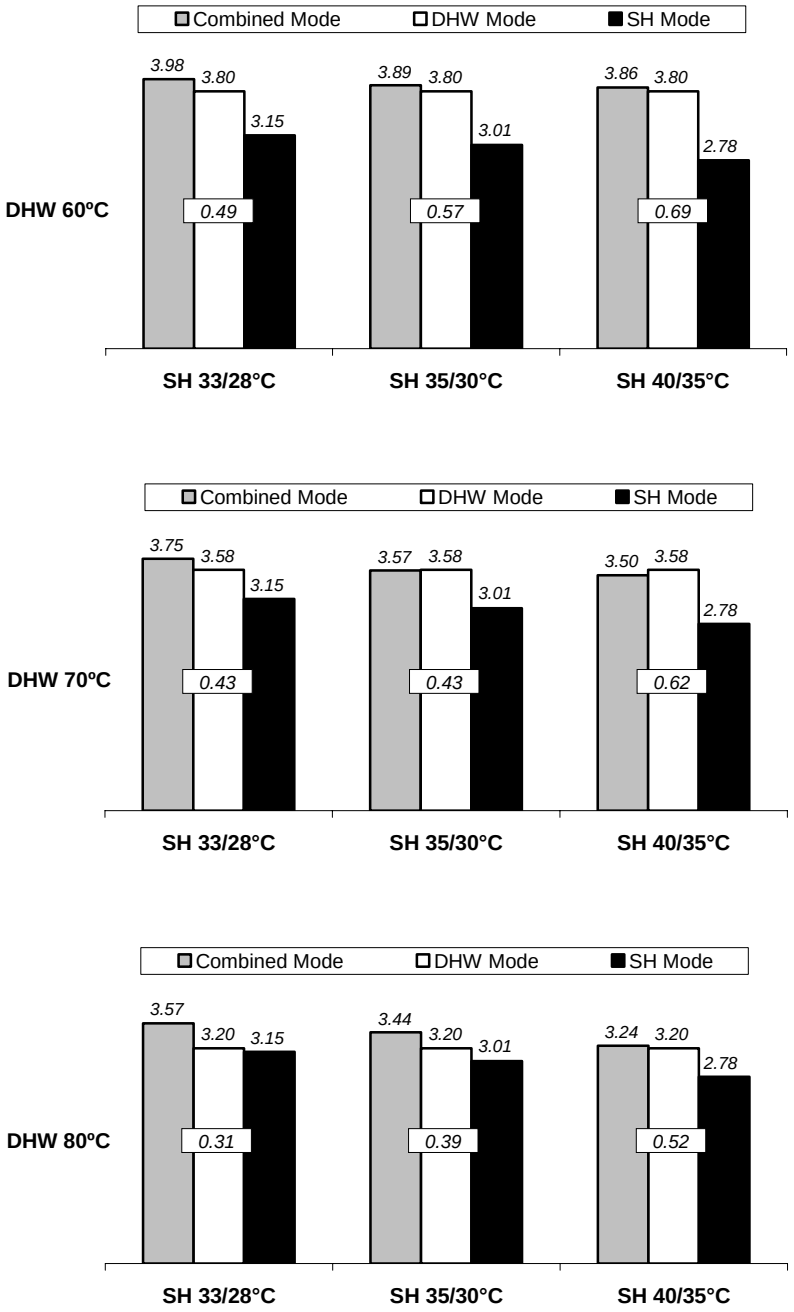

Figure 5.38 The measured maximum COP for the CO_2 heat pump unit at varying temperature levels for the space heating and hot water systems. The DHW heating capacity ratio for each temperature programme is shown in the middle of the bars.

According to Figure 5.38, the comparison of the measured COPs for the different heating modes can be summarized as follows:

- At 33/28°C supply/return temperatures in the space heating system and 60 to 80ºC DHW temperature, the COP in the combined mode was about 5 to 10% higher than that of the DHW mode, and the higher the hot water temperature, the larger the difference. This was mainly a result of the 1 to 2.5 MPa lower optimum high-side pressure and with that 10 to 20% less power input to the compressor.

- At 35/30ºC supply/return temperatures and 60 to 70ºC hot water temperature, the COPs in the combined mode and the DHW mode were virtually the same. However, at 80ºC hot water temperature the COP was about 7% higher in the combined mode.

- At 40/35ºC supply/return temperatures, the COP in the combined mode and the DHW mode were practically identical at all hot water temperatures. This was owing to similar optimum high-side pressures at 60ºC hot water temperature, and the fact that the negative impact of the higher high-side pressure in the DHW mode at 70 to 80ºC hot water temperature was outweighed by a lower temperature approach.

- The COP in the SH mode was considerably lower than that of the COP in the combined mode, due to a very bad temperature fit in the gas cooler and a relatively high CO_2 outlet temperature (ref. Figure 5.34). The higher the temperature level in the space heating system, the larger the relative difference in COP. At 60ºC hot water temperature and 33 to 40ºC supply temperature, the COP in the space heating mode was 21 to 28% lower than that of the combined mode. The corresponding figures at 70 and 80ºC hot water temperature were 16 to 21% and 12 to 14%, respectively.

Optimum High-Side Pressure

As demonstrated in the previous sections, the temperature levels in the space heating and hot water systems had a major impact on the optimum high-side pressure for the different heating modes. Figure 5.39 presents the COP as a function of the high-side pressure at 60, 70 and 80°C hot water temperature and 33/28, 35/30 and 40/35ºC supply/return temperatures for the space heating system.

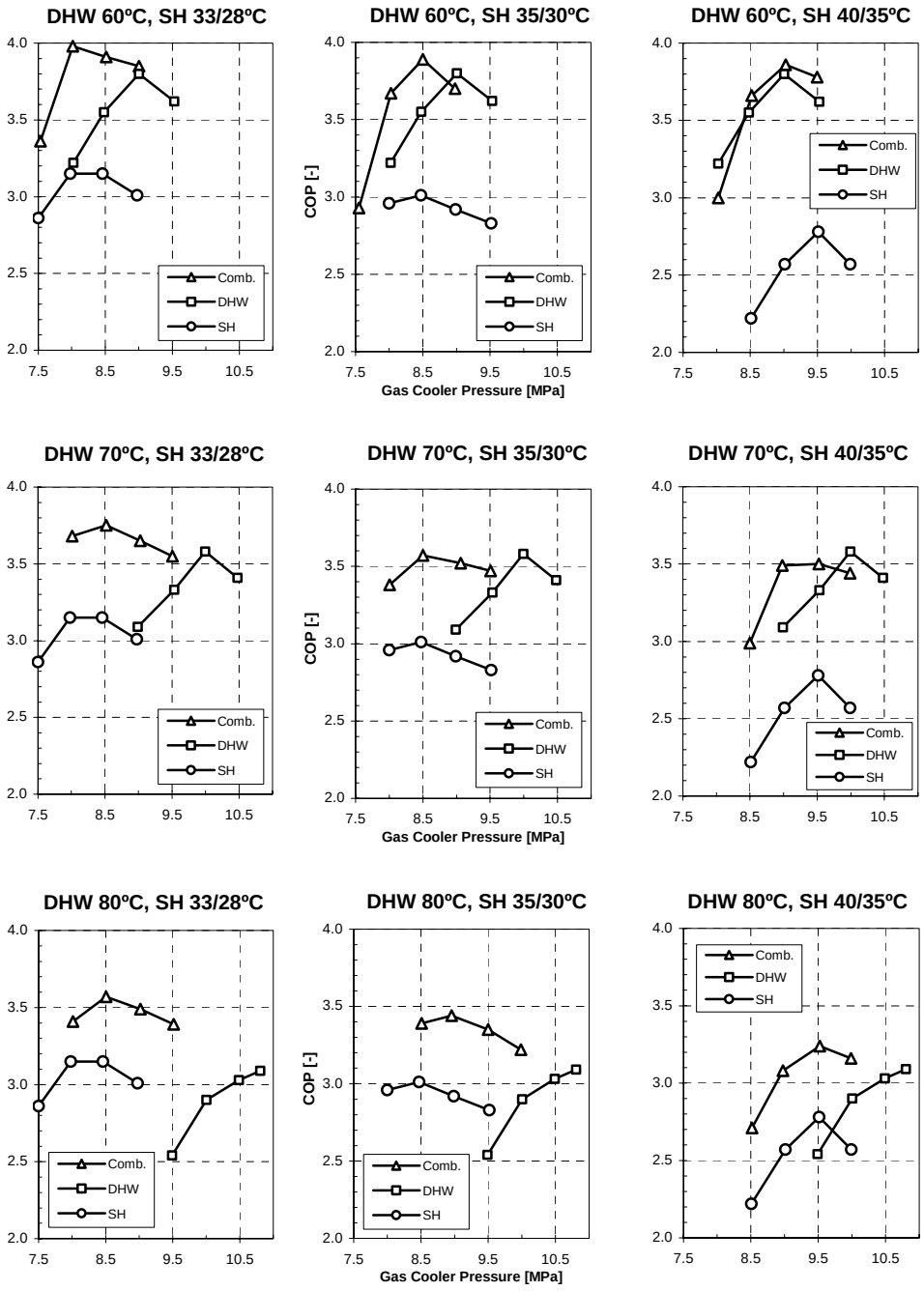

Figure 5.39 The relationship between the measured COP and the high-side pressure at varying DHW temperature and supply/-return temperatures for the SH system. Comb. = Combined mode, DHW = DHW mode, and SH = SH mode.

According to Figure 5.39, the impact of the high-side pressure on the COP during the different heating modes and temperature programmes can be summarized as follows:

- By using active pressure control, it was feasible to run the integrated CO_2 heat pump unit at optimum high-side pressure over a relatively wide range of operating conditions, and thus achieve the highest possible COP.

- For each of the nine temperature programmes, the optimum high-side pressures in the combined mode and the SH mode were maximum 0.5 MPa apart. Hence, by operating the CO_2 heat pump unit at a constant high-side pressure, the actual COPs would have been more or less identical with the maximum COPs as long as the temperature levels in the space heating and hot water systems were constant and the entire hot water demand was covered by operation in the combined mode.

- At 60ºC hot water temperature, the COP was about 5% (combined mode), 0% (DHW mode), and 7.5% (SH mode) less than the maximum COP when CO_2 heat pump unit was run at a constant high-side pressure of 9 MPa.

- At 70ºC hot water temperature and the two highest temperature levels in the space heating system, the COP was about 3% (combined mode), 7% (DHW mode), and 6% (SH mode) less than the maximum COP when the CO_2 heat pump unit was run at a constant high-side pressure of 9.5 MPa.

- At 80ºC hot water temperature, the difference between the average COP at varying temperature levels in the space heating system and the maximum COP was about 7% (combined mode), 10% (DHW mode) and 18% (SH mode) when the CO_2 heat pump unit was run at a constant high-side pressure of 10 MPa.

The Heating Capacity of the Space Heating Gas Cooler Unit

Figure 5.40 shows the ratio between the heating capacity of the space heating gas cooler unit during operation in the SH mode and the combined mode at optimum high-side pressure and varying set-point temperatures.

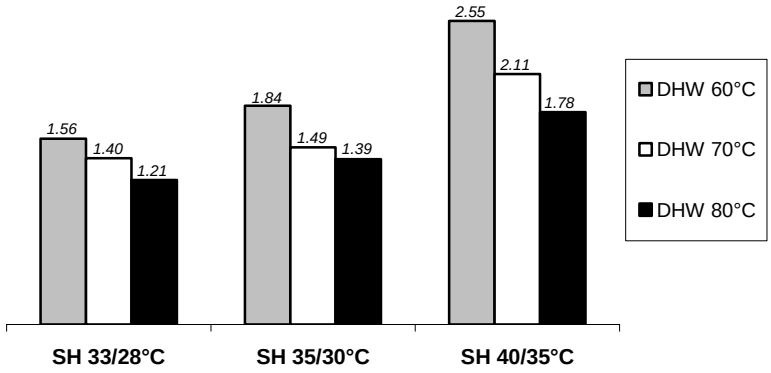

Figure 5.40 The ratio between the heating capacity of the space heating gas cooler unit during operation in the SH mode and the combined mode at optimum-high side pressure.

The heating capacity of the space heating gas cooler was considerably larger during operation in the SH mode than in the combined mode due to the higher CO_2 inlet temperature. The ratio between the heating capacities dropped off when the set-point for the hot water temperature was increased, since the reduced water flow rate resulted in less cool-down of the CO_2 flow in the DHW reheating gas cooler. The ratio was also heavily affected by the supply/return temperatures in the space heating system, since the higher the temperature level, the higher the DHW heating capacity ratio.

The Heating Capacity of the DHW Gas Cooler Units

Figure 5.41 shows the ratio between the total heating capacity of the two DHW gas cooler units during operation in the DHW mode and the combined mode at optimum high-side pressure and varying set-point temperatures. The measuring data at 80ºC hot water temperature were not included, since the optimum high-side pressure in the DHW mode was not found due to motor load limitations.

The heating capacity of the DHW gas cooler units was considerably larger during operation in the DHW mode than in the combined mode, since no heat was given off to the space heating system, and the fact that the discharge gas temperature was higher and the temperature approach was lower at equal set-points for the hot water temperature. The ratio dropped off when the supply/return temperatures in the space heating system was increased from 33/28 to 40/35ºC, due to the considerable rise in the DHW heating capacity ratio.

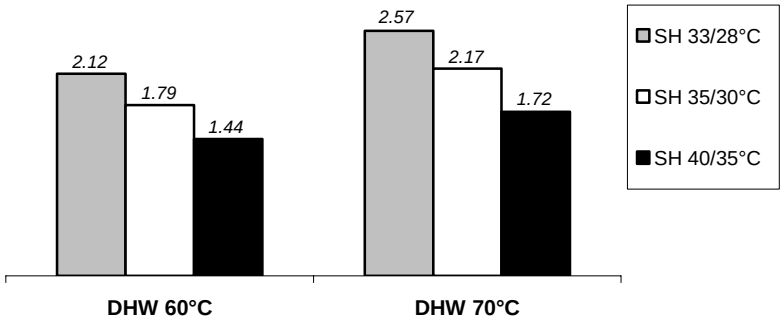

Figure 5.41 The ratio between the total heating capacity of the DHW gas cooler units during operation in the DHW mode and the combined mode at optimum high-side pressure.

5.1.3.6 Compressor Performance

Power Input

Figure 5.42 shows the relationship between the measured *power input* and the gas cooler (high-side) pressure at constant inlet conditions for the prototype rolling piston CO_2 compressor. The evaporation temperature was -5ºC (3.046 MPa), the suction gas superheating was 2.4 K ±0.6 K and the CO_2 mass flow rate was 1.42 kg/min ±2%.

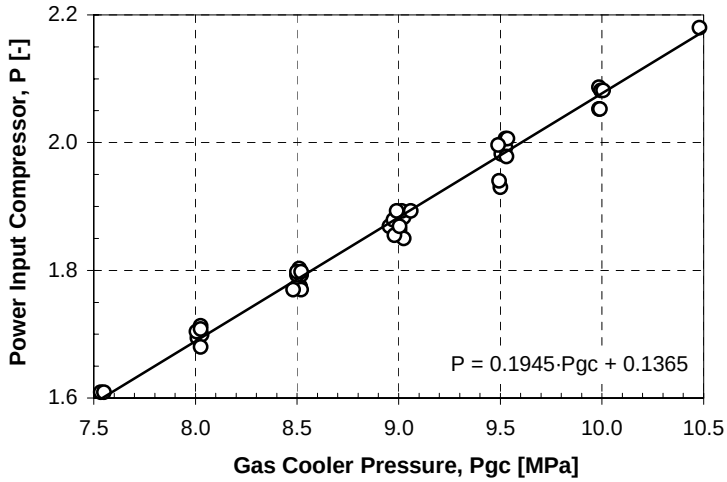

Figure 5.42 The measured power input for the prototype CO_2 compressor as a function of the gas cooler pressure at constant inlet conditions (approximately 3.046 MPa, -2.5ºC).

At the actual pressure levels, which corresponded to *a pressure ratio in the range from 2.5 to 3.4*, the power input to the compressor was more or less proportional to the discharge pressure. The minor variations were a result of the uncertainty in the pressure and power measurements as well as the variations in the isentropic efficiency, the heat loss from the compressor shell, the mass flow rate and the superheating of the suction gas.

Overall Isentropic Efficiency and Relative Heat Loss

Figure 5.43 shows the estimated *overall isentropic efficiency* for the prototype compressor as a function of the pressure ratio. The operating conditions were the same as in Figure 5.41, and the figures were calculated on the basis of the suction gas pressure and temperature, the discharge pressure, the power input to the compressor and the net CO_2 mass flow rate. The estimated oil discharge rate for the compressor, which ranged from about 6 to 9% of the total mass flow rate at varying pressure atios (ref. Table 4.2, Section 4.1.2.2, *The Compressor*), was measured in another project.

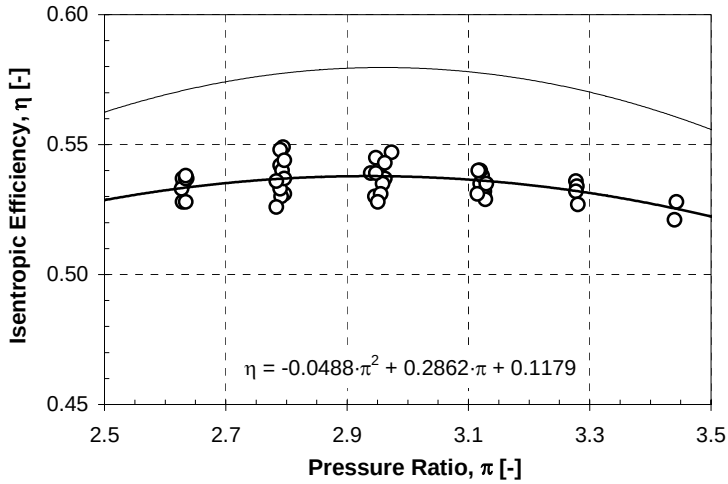

Figure 5.43 The estimated overall isentropic efficiency for the prototype compressor as a function of the pressure ratio at constant inlet conditions (approximately 3.046 MPa, -2.5ºC).

The measured overall isentropic efficiency, which did not change much with the pressure ratio within the narrow operating range, should only be regarded as *a rough estimate* due to the considerable uncertainty in the oil discharge rate as well as the unknown effect of the oil on the power consumption of the compressor. The upper solid-drawn line in Figure 5.43 represents the estimated isentropic efficiency at zero oil discharge rate.

The *relative heat loss* for the compressor is defined as the ratio between the heat loss from the compressor shell and the compressor power input. Figure 5.44 displays the estimated relative heat loss as a function of the pressure ratio. The operating conditions were the same as in Figure 5.42, and the calculations were performed by using the previously described measuring values as well as the discharge gas temperatures.

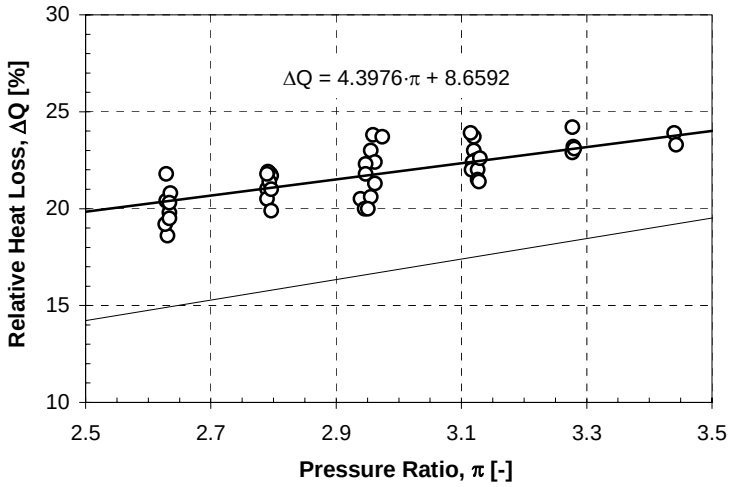

Figure 5.44 The estimated relative heat loss from the prototype compressor as a function of the pressure ratio at constant inlet conditions (approximately 3.046 MPa, -2.5ºC).

The relative heat loss, which ranged from about 17 to 24%, should only be regarded as a *rough estimate* due to the large uncertainty in the oil discharge rate. The lower solid-drawn line represents the estimated relative heat loss at zero oil discharge rate. The relatively large heat loss was partly a result of the cooling effect of a small fan, which was installed in order to keep the shell temperature below the maximum allowable level.

5.1.3.7 Evaporator Performance

Heat Transfer Efficiency

The tube-in-tube evaporator was not instrumented for measuring the local heat transfer coefficient for the flow boiling CO_2. However, by using the temperature and pressure measurements at the inlet and outlet of the evaporator as well as the measured mass flow rates of the CO_2 and the brine, it was possible to estimate the inlet vapour fraction, the evaporator capacity, the LMTD and consequently *the mean overall heat transfer coefficient* (U-value) at varying operating conditions. With reference to

Eqs. 6.21 through 6.26 in Section 6.1.3.3, *Heat Transfer Correlations*, the mean convective heat transfer coefficient for the brine-side h_o was estimated using the Gnielinski correlation for single-phase flow (VDI, 1993). Hence, by rearranging Eq. 6.10 in Section 6.1.3.2, *Energy Equations*, the mean heat transfer coefficient h_i for the CO_2 was calculated as follows:

$$\dot{Q} = U_i \cdot A_i \cdot LMTD \tag{5.1}$$

$$h_i = \frac{U_i}{1 - \left(\frac{U_i \cdot A_i \cdot \ln(d_o / d_i)}{2 \cdot \pi \cdot k \cdot L} \right) - \left(\frac{U_i \cdot A_i}{A_o \cdot h_o} \right)} \tag{5.2}$$

Figure 5.45 displays the estimated mean heat transfer coefficient for the flow boiling CO_2 as a function of the inlet vapour fraction at varying heat flux. The evaporation temperature was -5ºC ±0.1ºC, the CO_2 mass flux was 470 kg/(m^{2}s) ±2% whereas the calculated mean overall heat transfer coefficient ranged from about 1600 to 2100 W/(m^{2}K).

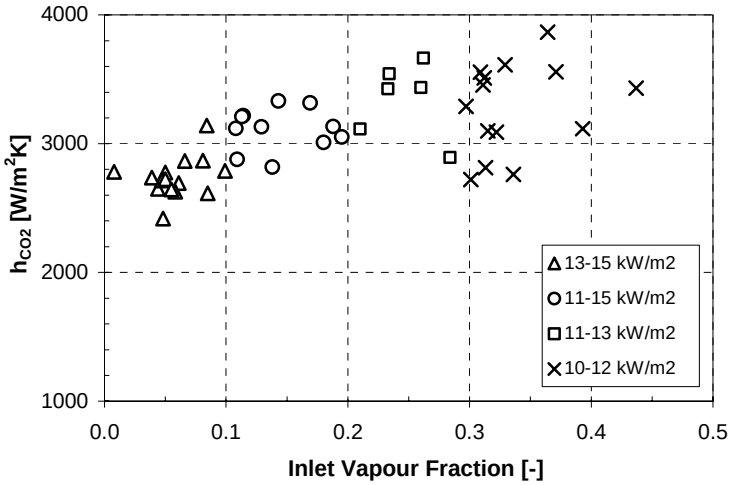

Figure 5.45 The estimated mean heat transfer coefficient (U-value) for the flow boiling CO_2 at -5℃ evaporation temperature and varying inlet vapour fraction and heat flux.

The estimated mean heat transfer coefficient for the CO_2 ranged from about 2500 to 4000 W/(m^{2}K) at inlet vapour fractions between 0.01 and 0.44. Bredesen et al. (1997) measured local heat transfer coefficients and pressure drop for flow boiling pure CO_2 in an ID 7 mm round tube at varying evaporation temperature, mass flux and heat flux (ref. Appendix

A1.6, *Heat Exchanger Performance*). At -10ºC, 400 kg/(m^{2}s) and 9000 W/m^2, which are virtually the same operating conditions as for the prototype CO_2 heat pump unit, the heat transfer coefficients ranged from 10 000 to 12 000 at increasing vapour fraction. Due to the relatively high mass flux, convective evaporation was the predominant boiling regime at vapour qualities above approximately 0.2 to 0.3

The estimated mean CO_2-side heat transfer coefficient was about 3 times lower than that of the heat transfer coefficients measured by Bredesen et al. The dramatic difference was most likely a result of the 6 to 9 weight% lubricant in the CO_2 flow. Both nucleate boiling and convective evaporation is considerably hampered by large oil concentrations in the flow, since it increases the thermal resistance of the liquid boundary layer and more or less offsets the advantage of the very low viscosity and surface tension of the CO_2. The latter property is of particular importance when it comes to nucleate boiling, and the formation and growth of vapour bubbles at low vapour qualities and low mass fluxes.

If the local heat transfer coefficient for the flow boiling CO_2 in the prototype evaporator had been in the same order of magnitude as measured by Bredesen et al., the mean overall heat transfer coefficient would have risen in average by roughly 80%.

Pressure Drop

The total pressure drop at the CO_2-side of the evaporator was measured at varying operating conditions. The pressure drop ranged from typically 25 to 45 kPa at varying inlet vapour qualities, which corresponds to a mean pressure drop gradient of about 2100 to 3800 Pa/m. Bredesen et al. measured a mean pressure drop gradient of about 2700 Pa/m at -10°C evaporation temperature and a mass flux of 400 kg/(m^{2}s).

5.1.3.8 Performance and Main Operating Characteristics of the Tripartite Gas Cooler

Heat Transfer Efficiency

The tube-in-tube tripartite gas cooler was not instrumented for measuring the local convective heat transfer coefficient for the supercritical CO_2. In contrary to the evaporator, it was not possible to estimate the mean heat transfer coefficient h_i for the CO_2 by means of the temperature measurements at the inlet and outlet of the gas cooler units and the mass flow rates

for the water and the CO_2. The reason was that the application of the logarithmic temperature difference (LMTD) in Eq. 5.1 for each gas cooler unit presupposes constant specific heat capacity for both fluids. Whereas the specific heat capacity (c_p) of water is practically invariable between 5 and 90ºC, i.e. 4.192 kJ/(kgK) ±0.5%, the specific heat capacity of supercritical CO_2 is heavily affected by changes in the high-side pressure and the temperature as shown in Figure 5.46.

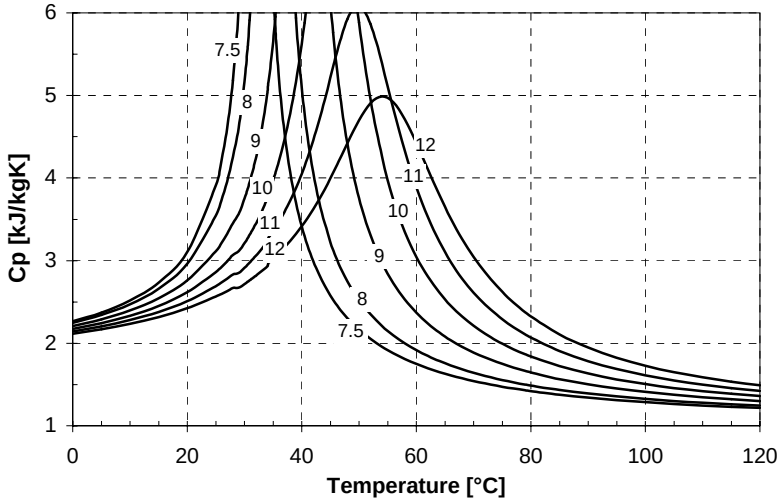

Figure 5.46 The specific heat capacity of supercritical CO_2 at varying temperatures and high-side pressures (RnLib, 2003).

During the design of the tripartite gas cooler, the Gnielinski correlation for single-phase flow (VDI, 1993) was used to calculate the convective heat transfer coefficient for the supercritical CO_2. Figure 5.47 presents the results at the actual operating range for the prototype CO_2 heat pump unit, i.e. 5 to 115ºC fluid temperature, 8 to 11 MPa high-side pressure and a CO_2 mass flux of 840 kg/(m^2s).

Zingerli and Groll (2000) measured the impact of oil on the heat transfer coefficient and the pressure drop during in-tube cooling of supercritical CO_2 (ref. Appendix A1.6). The ID of the test tube was 6.35 mm and the mass flux was 950 kg/(m^2s). A 5% oil concentration reduced the convective heat transfer coefficient on average by 25%, but the maximum value at each high-side pressure still occurred at the pseudocritical temperature. Consequently, since the tube dimensions and the operating conditions of the prototype CO_2 heat pump unit were virtually the same, it is reasonable to conclude that the drop in heat transfer efficiency in comparison to operation with pure CO_2 was in the same order of magnitude.

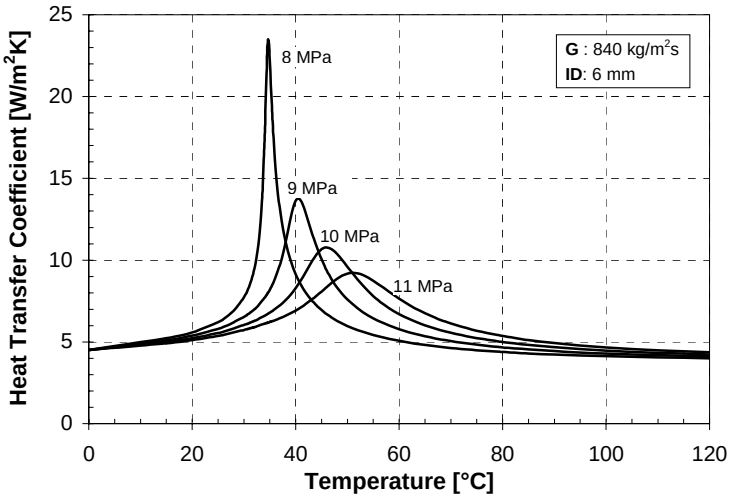

Figure 5.47 The convective heat transfer coefficient during in-tube cooling of supercritical CO_2 calculated by means of the Gnielinski correlation for single-phase flow (VDI, 1993).

The mean water-side convective heat transfer coefficient for the three gas cooler units for each measuring series was calculated using the Gnielinski correlation (VDI, 1993). The results are presented in Figure 5.48.

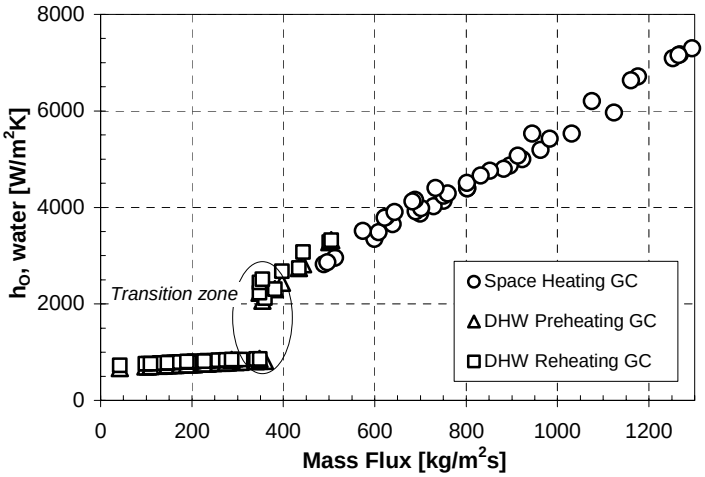

Figure 5.48 The water-side convective heat transfer coefficient for the tripartite gas cooler calculated by means of the Gnielinski correlation for single-phase flow (VDI, 1993).

The relatively high mass flux led to turbulent flow and excellent heat transfer efficiency for the space heating gas cooler in the combined mode and the SH mode (h_i~2800 to 7300 W/(m^{2}K)). Owing to the considerable temperature difference in the hot water circuit, the water flow rate for the DHW gas cooler units was about 5 to 30 times lower than that of the space heating gas cooler at optimum high-side pressure. During operation in the combined mode, low Reynolds numbers in most of the experiments resulted in laminar flow and poor heat transfer (h_i~700 to 850 W/(m^{2}K)). In the DHW mode, however, the water flow rate was roughly twice as high as in the combined mode, which led to turbulent flow and a considerable rise in the convective heat transfer coefficient (h_i~2000 to 3300 W/(m^{2}K)).

During operation in the combined mode, the water-side heat transfer resistance for the DHW gas cooler units constituted about 80 to 85% of the total heat transfer resistance. Hence, the presumed 25% drop in the convective heat transfer coefficient for the CO_2 caused by the 6 to 9% oil concentration in the flow, had only a marginal influence on the overall heat transfer coefficient. For the space heating gas cooler as well as for the DHW gas cooler units during operation in the DHW mode, the presence of oil reduced the U-value by roughly 10 to 15%.

Pressure Drop

The pressure drop for the supercritical CO_2 was measured for each gas cooler unit. The total pressure drop for the tripartite gas cooler in the combined mode, the DHW mode and the SH mode ranged from about *130–200 kPa*, *95–155 kPa* and *85–100 kPa*, respectively. Figures 5.49 to 5.51 show the mean pressure drop gradients in kPa/m for the gas cooler units in the three operating modes.

Since the mass flow rate of the supercritical CO_2 and the lubricant was virtually constant (1.42 kg/min ±2%), the differences and variations in the mean pressure drop gradients for the three gas cooler units were merely a result of the considerable impact of the temperature and the high-side pressure on the density and the dynamic viscosity of the supercritical CO_2. With reference to Figures A4 and A5 in Appendix A1.6, *Heat Exchanger Performance*, both the density and the dynamic viscosity drop off at increasing fluid temperature and rise when the high-side pressure is increased.

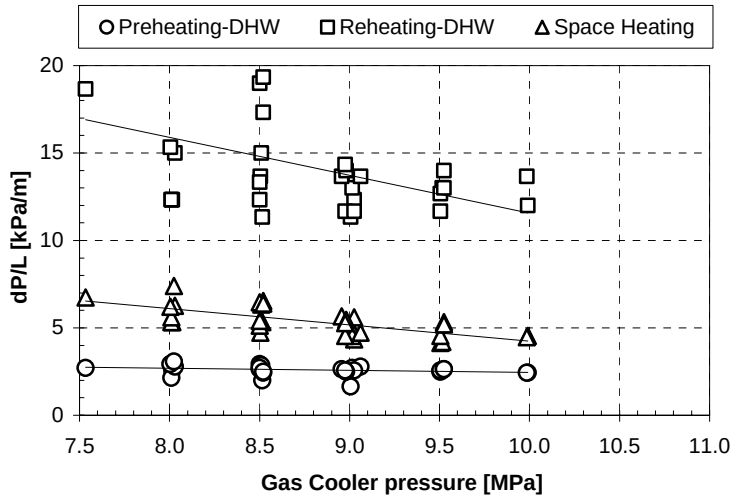

Figure 5.49 The measured mean pressure drop gradient for the gas cooler units in the combined mode.

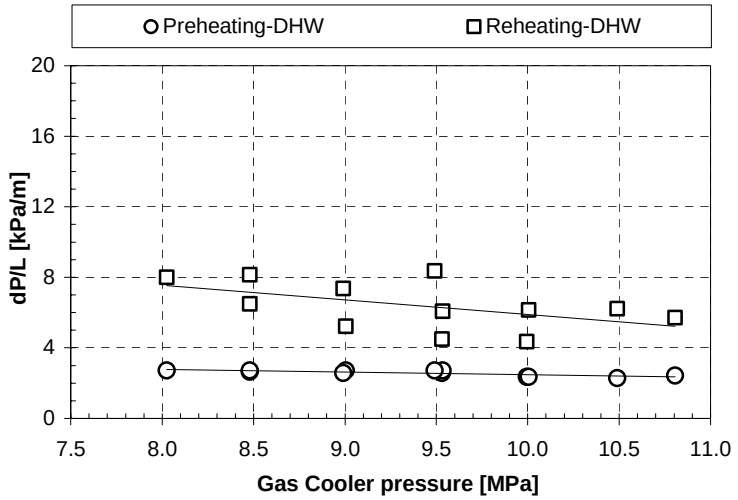

Figure 5.50 The measured mean pressure drop gradient for the gas cooler units in the DHW mode.

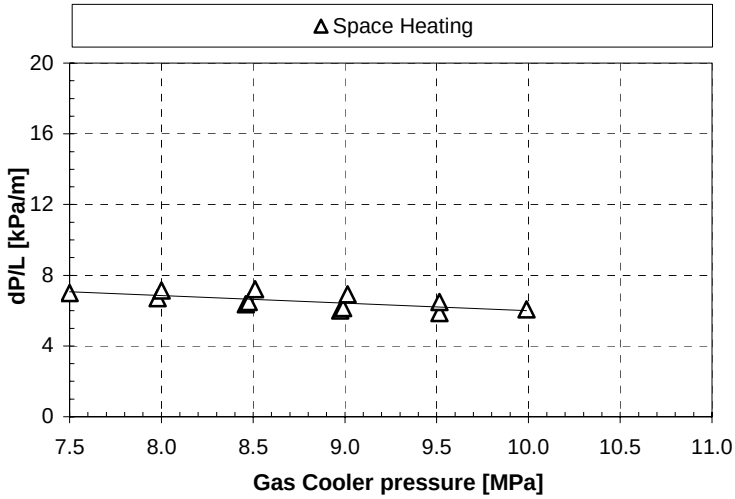

Figure 5.51 The measured mean pressure drop gradient for the single gas cooler unit in the SH mode.

With reference to Eq. 6.28 in Section 6.1.3.4, *Pressure Drop Correlations*, the local pressure loss gradient for (single-phase) supercritical CO_2 is proportional to the density and the square of the average fluid velocity at the cross-section of the tube. By substituting the fluid velocity v with the ratio between the mass flux and the density (G/ρ), the mean pressure drop gradient for a gas cooler unit can be expressed as:

$$\frac{\Delta p}{L} = \zeta \cdot \left(\frac{G^2}{2 \cdot d_h} \right) \cdot \left(\frac{1}{\rho} \right) \tag{5.3}$$

where ΔP is the total pressure drop, L is the tube length, d_h is the inner diameter of the tube, ζ is the friction factor, G is the mass flux and ρ is the weighted average density of the supercritical CO_2. Hence, Eq. 5.3 demonstrates that *the mean pressure drop gradient will be inversely proportional to the density of the supercritical CO_2* (Incropera and DeWitt, 2001).

Figure 5.52 shows the density of supercritical CO_2 at varying high-side pressures and temperatures, and the dashed lines indicate the temperature ranges for the gas cooler units in the combined mode.

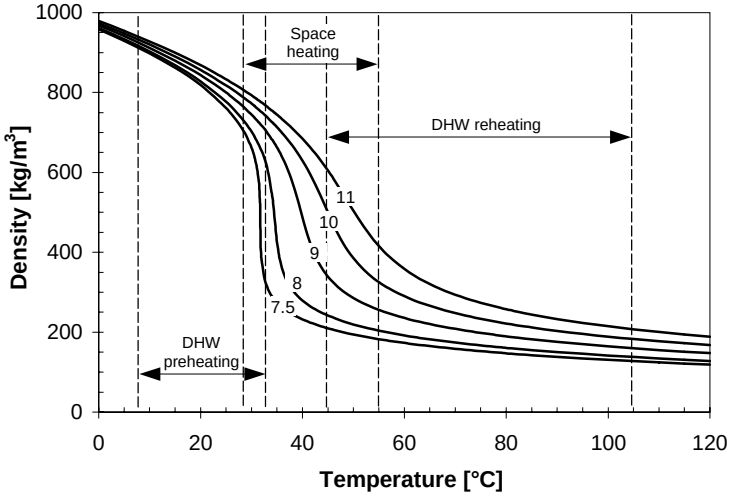

Figure 5.52 The density of supercritical CO_2 at high-side pressures ranging from 7.5 to 11 MPa (RnLIb, 2003).

During operation in the *combined mode* (Figure 5.49), the DHW preheating gas cooler had the lowest average pressure drop gradient. According to Eq. 5.3 and Figure 5.52, this was mainly a result of the large average density of the supercritical CO_2 and the consequent low fluid velocity. Owing to the considerably lower average CO_2 density in the DHW reheating gas cooler unit, the average pressure drop gradient was roughly 5 times higher than that of the DHW preheating gas cooler unit. For the same reason, the measured mean pressure drop gradient for the space heating gas cooler was higher than that of the DHW preheating gas cooler unit and lower than that of the DHW reheating gas cooler unit.

According to Figures 5.50 and 5.51, the differences in the measured average pressure drop gradients during operation in the *DHW mode* and the *SH mode* can also be explained by the large variations in the average fluid density. The temperature ranges for the DHW reheating and DHW preheating gas cooler units during operation in the DHW mode were about 7 to 65ºC and 50 to 110ºC, respectively, while the inlet and outlet CO_2 temperatures for the gas cooler unit ranged from about 28 to 100ºC during operation in the SH mode.

5.1.3.9 Comparison of the Measurements from the Water Circuits and the CO_2 Circuit

With reference to Sections 5.1.3.2 through 5.1.3.4, the heating capacity and the COP of the prototype CO_2 heat pump unit were based on measure-

ments of temperatures and mass flow rates in the secondary (water) circuits. The heat pump performance was also calculated by measuring the mass flow rate as well as the inlet and outlet temperatures and pressures of the supercritical CO_2 in the tripartite gas cooler. The percentage differences between the measurements for the secondary (water) circuits and the CO_2 circuit was calculated as:

$$\Delta\dot{Q}_{rel} = \left(\frac{\dot{Q}_W - \dot{Q}_{CO2}}{\dot{Q}_W} \right) \cdot 100\% \qquad (5.4)$$

where $\dot{Q}_W$ and $\dot{Q}_{CO2}$ represent the measured heating capacity in the water circuits and the CO_2 circuit, respectively.

The results from the calculations are presented in Figure 5.53.

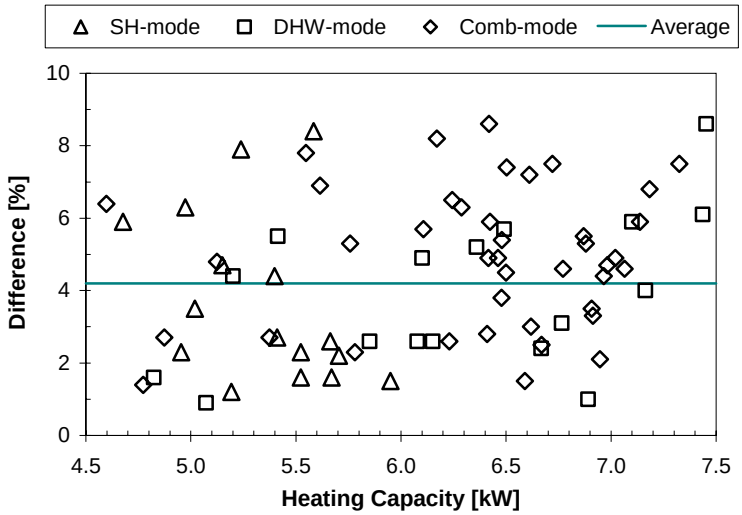

Figure 5.53 The percentage differences between the total heating capacity of the tripartite gas cooler based on measurements from the secondary (water) circuits and the CO_2 circuit.

With reference to Section 4.1.4.6, *Uncertainty of the Computed Values*, the average percentage difference in the calculated heating capacity was considerably larger than estimated in the uncertainty analysis. This deviation may be explained by the fact that the enthalpy calculations were based on thermodynamic data for pure CO_2, and not for a mixture of CO_2 and lubricant. The relatively large oil concentration may also have affected the accuracy of the Coriolis-type CO_2 mass flow meter.

5.2 Testing of a DHW Tank and a Movable Insulating Plate

5.2.1 Testing of a Single-Shell DHW Tank

5.2.1.1 Transient Temperature Drop

In these experiments the transient temperature drop in the 200 litre DHW tank insulated with a 40 mm glass-wool mat, was measured under various operating conditions. With reference to Section 6.2, *Modelling of Single-Shell DHW Tanks*, the results were used to estimate the U-value for the DHW tank. The experimental set-up, the instrumentation and the experimental procedures are described in Section 4.2.1, *Construction of the Test Rig*, and Section 4.2.2.2, *Transient Temperature Drop in a DHW Tank.*

Figure 5.54 shows the measured transient temperature profiles at the centre of the DHW tank. The initial water temperature was 56.2ºC, and the average room temperature was approximately 22ºC during the 24 hour test period. The vertical position of the temperature sensors refers to the distance above the bottom of the tank.

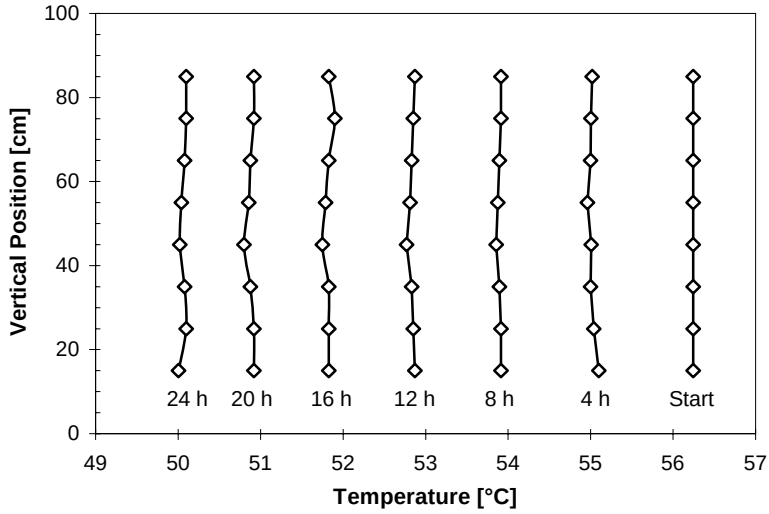

Figure 5.54 The measured temperature profile at the centre of the 200 litre DHW tank insulated with 40 mm glass-wool. The initial water temperature was 56.2ºC, and the average room temperature during the test period was 22ºC.

Figure 5.55 shows the measured mean temperature development at the centre of the DHW tank. The data are from Figure 5.54.

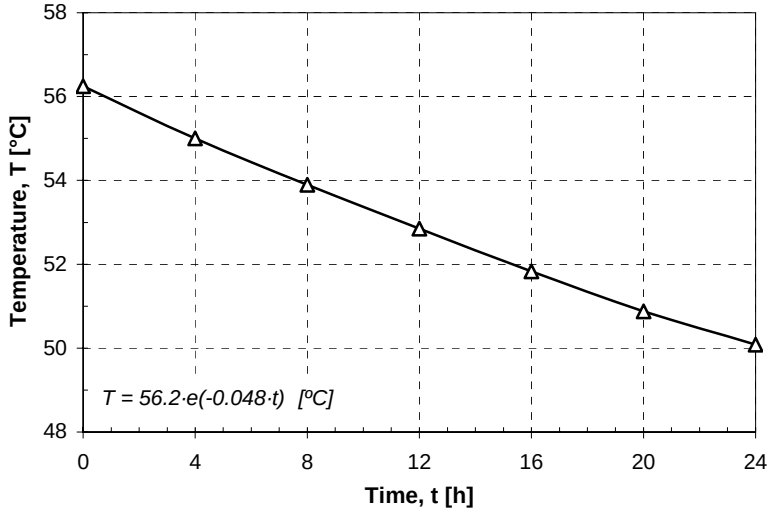

Figure 5.55 The measured transient temperature drop at the centre of the 200 litre DHW tank insulated with 40 mm glass-wool. The data are from Figure 5.54.

The experimental results can be summarized as follows:

- The average temperature drop for the DHW tank during the 24 hour test period was 0.26ºC/h.
- The measured maximum temperature difference between the centre and the inner wall of the DHW tank during the entire test period was less than 0.2 K, i.e. a negligible radial temperature gradient.

5.2.1.2 Transient Temperature Gradients in a DHW Tank Filled with Hot and Cold Water

Details regarding the instrumentation and the experimental procedures are found in Section 4.2.2.3, *Transient Temperature Gradients in a DHW Tank Filled with Hot and Cold Water*.

Static Mode (Static Thermocline)

In these experiments the transient temperature gradient (*thermocline*) between a hot and a cold water volume in the 200 litre DHW tank was measured. With reference to Section 6.2, the results were used to document the effect of internal conductive heat transfer in a DHW tank as well as to verify the transient two-dimensional heat conduction model for cylindrical single-shell DHW tanks.

Figure 5.56 shows the measured thermocline between the hot and cold water reservoirs in the DHW tank. The initial temperatures of the water reservoirs were 53.2 and 4.8ºC, respectively, and the average room temperature during the 12 hour test period was 22.5ºC. The vertical position of the temperature sensors refers to the distance between the sensors and the stainless steel plate that separated the water reservoirs in the tank (ref. Section 4.2.2.3).

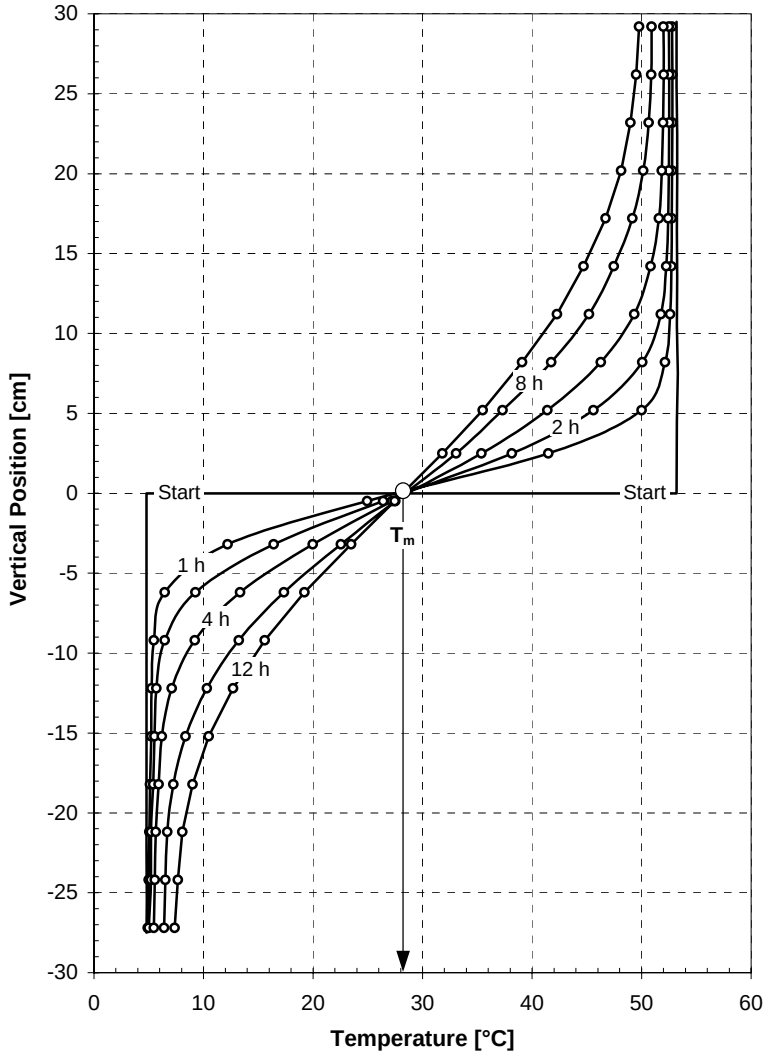

Figure 5.56 The measured thermocline in the 200 litre DHW tank. The initial water temperatures were 53.2 and 4.8ºC, and the average room temperature during testing was 22.5ºC.

By using the temperature measurements from Figure 5.56, the volume of the thermocline zone was calculated according to Eq. (3.27) in Section 3.3.3.3, *Conductive Heat Transfer Inside the DHW Tank*. The cross-sectional area of the tank was 0.196 m^2. The results are presented in Figure 5.57.

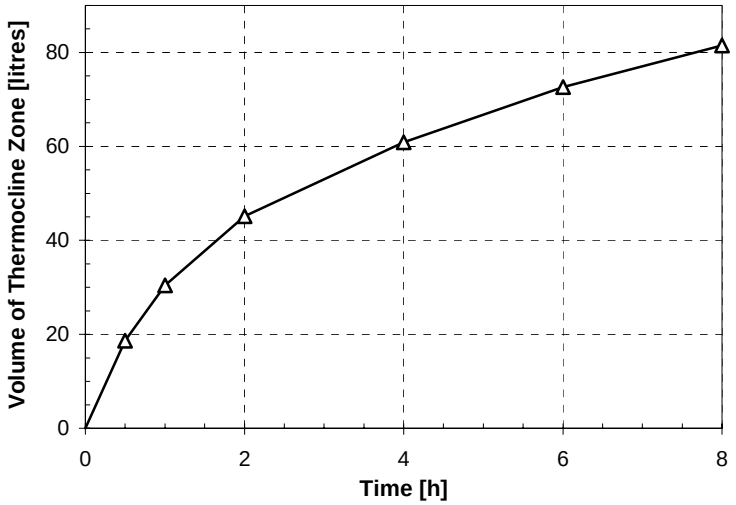

Figure 5.57 The estimated development of the thermocline zone volume during a period of 8 hours. The calculations were based on the experimental data in Figure 5.56.

Figure 5.58 shows the development of the average temperature for the thermocline zones above and below the steel plate as well as the average temperature of the entire thermocline zone. The estimated temperatures were based on the experimental data presented in Figure 5.56.

The experimental results can be summarized as follows:

- The considerable temperature change in the hot and cold water reservoirs during the test period was mainly due to the conductive heat transfer between the reservoirs, and the heat transfer through the tank walls played a minor role.
- After 30 minutes, the thermocline comprised as much as 20 litres of water. That clearly demonstrates that even at moderate temperature differences (50 K) and relatively short tapping/charging periods, the conductive heat transfer between the water reservoirs will lead to a noticeable increase in the average outlet temperature from the tank during the charging period, which in turn will reduce the COP of a CO_2 heat pump (ref. Section 3.3.3, *Exergy Losses in the DHW Tank*).

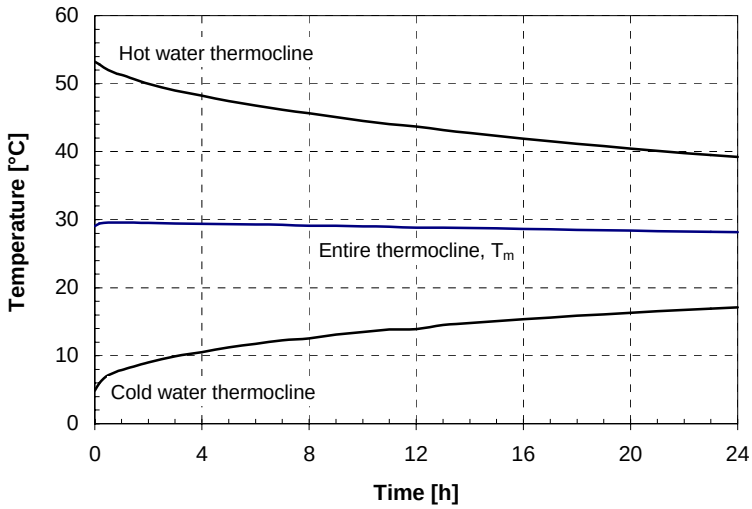

Figure 5.58 The measured average temperature for the thermocline zones above and below the steel plate as well the average temperature for the entire thermocline zone. The experimental data are from Figure 5.56.

- The growth rate of the thermocline zone ($\partial H_{TC}/\partial t$) decreased gradually during the test period. This was expected since the heat flux between the reservoirs is roughly inversely proportional to the extent of the thermocline zone (ref. Section 3.3.3.3). As an example, the growth rate at 30 minutes, 1 hour, 2 hours and 4 hours was about 35, 25, 15 and 10 litres/h, respectively.

- The average water temperature (T_m) for the entire thermocline was virtually identical to the arithmetic mean of the initial hot and cold water temperatures (~29ºC). This was expected since the variations in the thermal conductivity, specific heat capacity and density of water at the actual temperature range are quite small (NIST, 2002).

Charging Mode (Dynamic Thermocline)

In these experiments the outlet water temperature from the bottom of the 200 litre DHW tank, which was filled with 80 litres of cold city water and 120 litres of hot water, was measured at varying water flow rates.

Figure 5.59 shows the measured outlet water temperature from the 200 litre DHW tank as well as the average temperature of the dynamic thermocline zone. The initial city water temperature was approximately 4.8ºC, the initial hot water temperature ranged from 54.7 to 56.7ºC, and

the average room temperature during testing was about 21ºC. The water flow rate from the tank ranged from about 0.6 to 2.5 l/min, which corresponds to a gas cooler heating capacity in the range from approximately 2.1 to 8.7 kW at 50 K temperature difference for the water.

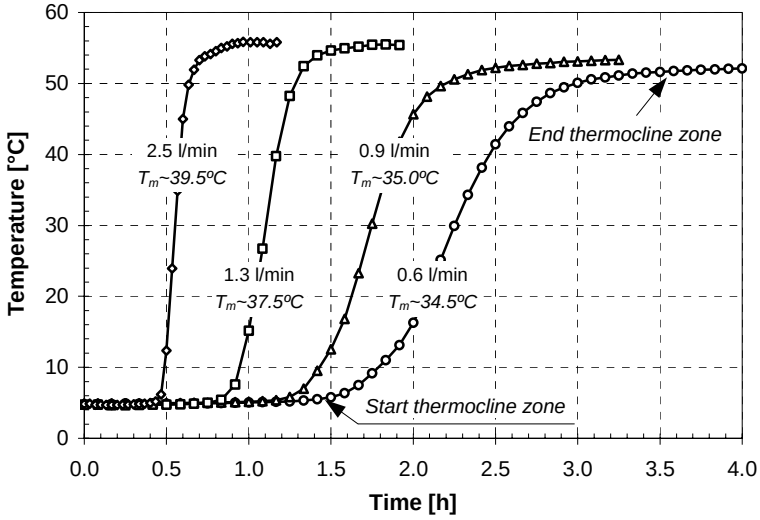

Figure 5.59 The measured outlet water temperature from the 200 litre DHW tank during the charging mode at various water flow rates. The initial cold water volume was 80 litres, and the initial water temperatures were about 5 and 56ºC.

The measurements gave the outlet water temperature from the bottom of the tank, which may represent the inlet water temperature to the DHW preheating gas cooler unit during the charging period.

The measured average temperature (T_m) for the dynamic thermoclines in Figure 5.59 was higher than that of the static thermoclines in Figure 5.58. This was a result of mixing of water at different temperature levels at the tube inlet at the bottom of the tank due to the relatively high water velocity (0.15 to 0.55 m/s) through the ID 10 mm pipeline. The higher the velocity, the higher the average temperature of the thermocline zone.

5.2.2 Testing of a Movable Insulating Plate

One way to reduce the internal conductive heat transfer and eliminate the mixing of hot and cold water in circular DHW tanks, is to separate the water volumes by means of a movable plate with low thermal conductivity. Details concerning the experimental set-up, the instrumentation as

well as the experimental procedures for measuring the thermal performance and functionality of the two prototype insulating plates are presented in Section 4.2.2.4, *Thermal Performance of an Insulating Plate* and Section 4.2.3, *Flow Studies*.

5.2.2.1 Thermal Performance

Figure 5.60 shows the measured transient temperature profiles above and below the 50 mm extruded polystyrene (XPS) plate, which was placed in the middle of the 200 litre tank. The initial water temperatures were 6.2ºC and 54.9ºC, and the average room temperature during the 12 hour test period was about 22.5ºC. The vertical position in the figure refers to the distance between the temperature sensors and the plate surface (20 to 180 mm).

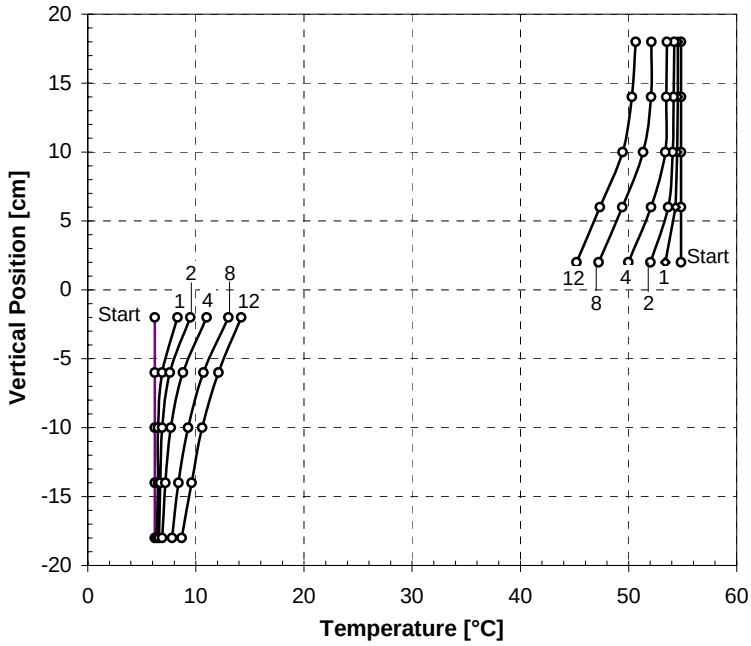

Figure 5.60 The measured temperature gradients above and below the 50 mm XPS plate. The initial water temperatures were 6.2 and 54.9ºC, and the average room temperature was 22.5ºC.

The experimental results can be summarized as follows:

- The measured temperature differences between the centre and the rim of the insulating XPS plate were less than 0.3 K, i.e. a negligible radial temperature gradient.

- The transient temperature development in the water reservoirs near the insulating plate was a result of radial heat transfer between the water and the tank wall as well as axial heat transfer across the insulating plate. Despite the larger initial temperature difference at the hot water side of the plate, the temperature gradient changed more rapidly at the cold water side during the first hour of operation. This was due to the fact that the thermal diffusivity of the stainless steel balancing weight was about 6 times higher than that of the XPS plate. The growth rate at each side of the insulating plate decreased gradually during the test period (ref. Figure 5.57).

- In comparison with the static thermocline experiment (ref. Figure 5.56), the application of an insulating plate resulted in a considerable reduction in both the extent and the average temperature change for the thermocline zones. As an example, after a detention period of 4 hours, the transferred energy between the hot and cold water reservoirs for the two experiments was approximately 2100 kJ and 400 kJ, respectively, which means that *the insulating plate reduced the average heat transfer rate by roughly 80%*. In a real DHW tank, the movable insulating plate will contribute to a further reduction of the thermodynamic losses, since it will eliminate the mixing of hot and cold water during the tapping mode.

- In the experiments, the initial temperature of the insulating plate was about 20ºC. However, for a real DHW tank equipped with a movable insulating plate, the initial surface temperature at the hot water side of the plate will be in the region of the hot water temperature, whereas the surface temperature at the cold water side will be determined by the thermal resistance of the plate, the hot water temperature and the previous heat transfer process. By alternatively *mounting the balancing weight at the upper side of the plate*, the temperature changes at both sides of the plate will be reduced, since the thermal diffusivity of the balancing weight is about 5 to 10 times higher than that of the insulating plate.

5.2.2.2 Hydrostatic Balance and Functionality

The two insulating XPS plates, which were tested in the transparent 200 litre ID 500 mm tank, had a thickness of 50 mm and a diameter of 490 and 495 mm. Although the mass and volume of the balancing weights were accurately tuned, it was necessary to make minor weight adjustments in order to compensate for the effects of water absorption, thermal expansion

and formation of air bubbles at the underside of the plates. The latter phenomena had a large impact on the hydrostatic balance of the plates during the tapping mode, since numerous air bubbles were formed in the diffuser. Figure 5.61 shows an example of how the small air bubbles formed a sheet of air at the underside of the flat plate.

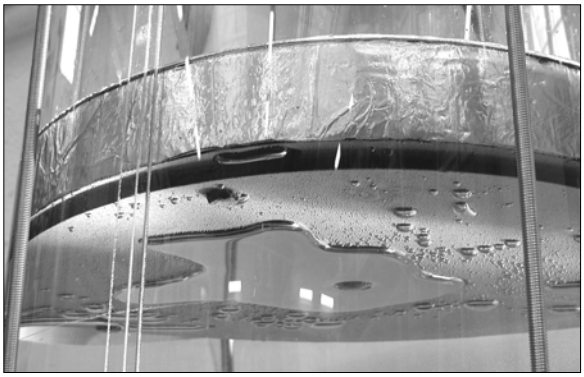

Figure 5.61 Large air bubbles were formed at the underside of the insulating plate during the tapping mode.

It was necessary to rebuild the test rig several times and to carry out a large number of preliminary tests before the different flow experiments could be performed as planned.

The experimental results can be summarized as follows:

- *Tapping Test Mode – Open Tank*

  Both insulating plates performed satisfactorily during testing, and no water leakage was observed across the narrow cylindrical gap between the plate and the tank wall at the highest flow rate (36 l/min). The different diameters did not affect the practical performance of the plates. Figure 5.62 demonstrates how the insulating plates separated the dyed hot water reservoir and the cold water reservoir in the tank.

- *Tapping Test Mode - Closed, Slightly Pressurised Tank*

  At water flow rates below approximately 0.2 l/s (12 l/min), both insulating plates performed satisfactorily, and there was no cold water flow through the gap between the plate and the tank wall. However, at higher flow rates, the plates got stuck and cold water streamed rapidly to the hot water reservoir. This is illustrated in Figure 5.63.

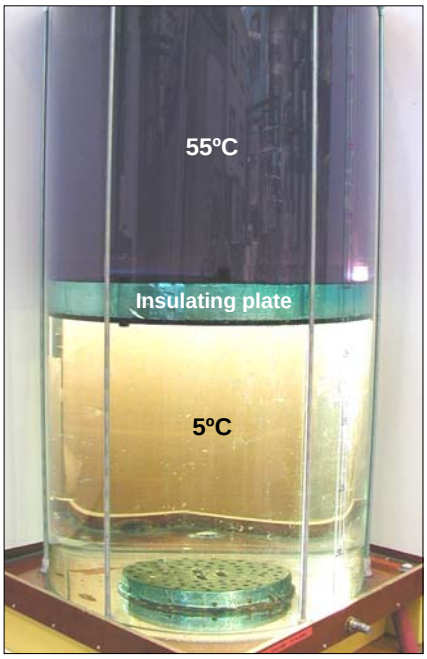

Figure 5.62 *At atmospheric tank pressure (open tank), the movable insulating plates provided perfect separation of the hot and cold water reservoirs during the tapping mode.*

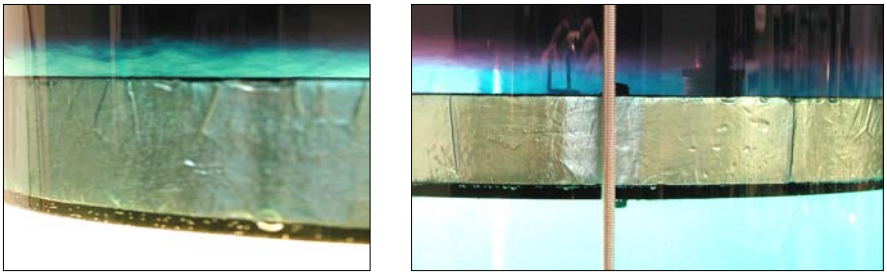

Figure 5.63 *Mixing of hot and cold water during testing of the insulating plates in the tapping mode when using a closed, slightly pressurized tank.*

The plates got stuck as a result of the increased static pressure, which deformed the thin-walled polycarbonate tank and made it slightly oval. *Due to the operating limitations of the test rig, further testing at pressurized conditions (4 to 6 bar) in an unvented steel tank is required in order to prove the functionality of a movable insulating plate under real operating conditions*.

- *Charging Test Mode – Open Tank*

  Both insulating plates performed well during the 8 to 11 hour test periods, and no mixing of the hot and cold water was observed.

- *Static Test Mode – Open Tank*

  The plate did not move during the 8 hour test period, and no mixing of hot and cold water was observed. The separation of the hot and cold water reservoirs in the tank during the static mode is illustrated in Figure 5.64.

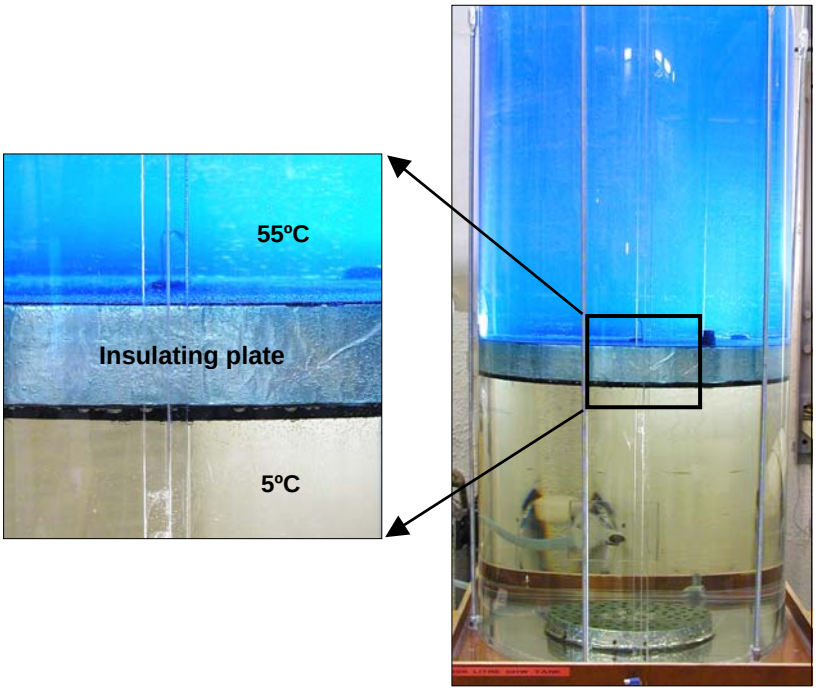

Figure 5.64 *The position of the insulating plate remained constant, and no mixing of hot and cold water was observed during the static test mode.*

6 Modelling

This section describes the thermodynamic background and mathematical basis, and presents selected simulation results for two computer models that were developed to:

- Calculate the heating capacity and COP as well as to study the system characteristics of residential CO_2 heat pump units equipped with a tripartite tube-in-tube counter-flow CO_2 gas cooler for combined space heating and hot water heating.
- Calculate transient temperature profiles and heat losses for cylindrical single-shelled DHW tanks caused by heat transfer through the walls and by conductive heat transfer between the hot and cold water volumes inside the tank.

The computer models were verified with measurements from two prototype test rigs, which are presented in Sections 4.1/5.1, *Testing of a Residential Brine-to-Water CO_2 Heat Pump Unit*, and Sections 4.2/5.2, *Testing of a DHW Tank and a Movable Insulating Plate*.

6.1 Modelling of CO_2 Heat Pumps Using a Tripartite Gas Cooler

6.1.1 Introduction

A steady-state computer model for a CO_2 heat pump using a tripartite counter-flow tube-in-tube gas cooler was developed in order to supplement and analyse the measurements from the prototype CO_2 heat pump test rig. The model also made it possible to provide a more general analysis on how the performance of the CO_2 heat pump unit will be affected by the operating conditions and the gas cooler design.

Since the main focus was on the design and performance of *the tripartite gas cooler*, the computer model was limited to include a hermetic compressor to determine the inlet conditions for the gas cooler, and three gas cooler units for preheating of hot water (*GC A*), space heating (*GC B*) and reheating of hot water (*GC C*). Figure 6.1 shows the principle of the modelled system.

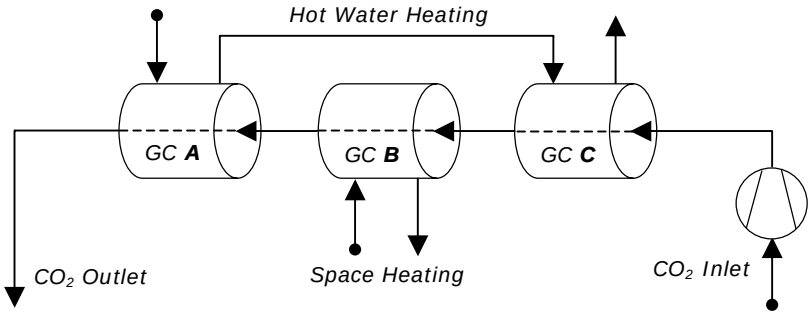

Figure 6.1 Configuration of the CO_2 heat pump model.

6.1.2 The Compressor Model

The simple compressor model calculated the CO_2 mass flow rate, the discharge temperature and the net power consumption of the hermetic compressor. The input parameters were as follows:

- The evaporation pressure p_0
- The suction gas temperature, T_{SG} (or superheating)
- The swept volume at actual rpm, $\dot{V}$
- The isentropic efficiency, η_{is} and the volumetric efficiency, η_{vol}
- The relative heat loss, β_{HL} [-]
- The discharge pressure, p_{GC}

The mass flow rate $\dot{m}$ and the power consumption of the compressor P_C were calculated as shown in Eqs. (6.1) and (6.2):

$$\dot{m} = \left(\frac{\dot{V}}{v_1} \right) \cdot \eta_{vol} \tag{6.1}$$

$$P_C = \dot{m} \cdot (h_2 - h_1) \tag{6.2}$$

where v_1 is the specific volume of the suction gas, and h_1 and h_2 are the specific enthalpy of the suction and discharge gas, respectively. The latter was calculated as:

$$h_2 = h_1 + \left(\frac{h_{is} - h_1}{\eta_{is}} \right) \cdot (1 - \beta_{HL}) \tag{6.3}$$

The subscript *is* refers to isentropic compression of the gas. The discharge temperature from the compressor was computed on the basis of the discharge pressure and the specific enthalpy of the discharge gas.

For most of the simulations, the volumetric and isentropic efficiencies as well as the relative heat loss from the compressor were based on measurements from the prototype CO_2 compressor (ref. Section 5.1.3.6, *Compressor Performance*).

6.1.3 The Tripartite Gas Cooler Model

6.1.3.1 Introduction

The tripartite CO_2 gas cooler was modelled as three single-pass counter-flow tube-in-tube heat exchanger units, where the CO_2 was flowing in the inner tube and water in the annulus. Figure 6.2 sketches the principle of the cross-section of one of the gas cooler units.

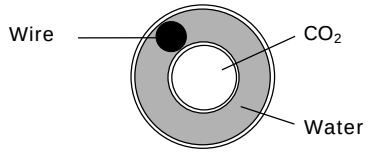

Figure 6.2 Principle of the cross section of a gas cooler unit.

The input parameters for the tripartite gas cooler were as follows:

- Detailed tube geometries
- The CO_2 inlet pressure, p_{GC}
- The CO_2 inlet temperature, T_{GC}
- The CO_2 mass flow rate, $\dot{m}$
- The inlet water temperatures
- The water flow rates

6.1.3.2 Energy Equations

Each gas cooler unit was divided into a fixed number of sub-sections, and the thermophysical properties of the fluids were treated as constant within each sub-section. Figure 6.3 sketches the principle of the inlet and outlet conditions for one gas cooler sub-section. The subscripts *H* and *C* refers to the hot flow (CO_2) and cold flow (water), *in* and *out* refer to the inlet and outlet of the sub-section, whereas *T* is the temperature and *CP* is the product of the mass flow rate $\dot{m}$ and the specific heat capacity c_p (ref. Eq. A5, Appendix A2.4).

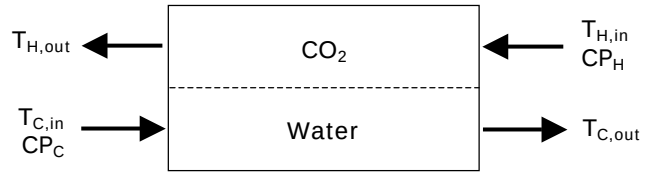

Figure 6.3 Principle of a gas cooler sub-section.

The thermodynamic and transport properties of pure CO_2 were supplied by the library *xlco2lib.dll* (Skaugen 2002), where the data are based on correlations from Span and Wagner (1996), Vesovic et al. (1990) and Fenghour et al. (1998). The thermodynamic and transport properties of water were based on data from the VDI Heat Atlas (1993).

Since the specific heat capacity of the fluids within each gas cooler sub-section was considered as constant, *the UA-LMTD method* was used for calculating the energy equations (Stoecker, 1989):

$$\dot{Q}_H = CP_H \cdot \left(T_{H,in} - T_{H,out}\right) \tag{6.4}$$

$$\dot{Q}_C = CP_C \cdot \left(T_{C,out} - T_{C,in}\right) \tag{6.5}$$

$$\dot{Q}_{tot} = U \cdot A_i \cdot LMTD \tag{6.6}$$

where:

$$CP_H = \left(\dot{m} \cdot c_p\right)_H \tag{6.7}$$

$$CP_C = \left(\dot{m} \cdot c_p\right)_C \tag{6.8}$$

$$LMTD = \frac{\left(T_{H,in} - T_{C,out}\right) - \left(T_{H,out} - T_{C,in}\right)}{\ln \frac{\left(T_{H,in} - T_{C,out}\right)}{\left(T_{H,out} - T_{C,in}\right)}} \tag{6.9}$$

In Eq. (6.6), which describes the energy balance in the each sub-section of the gas cooler unit, the subscript *i* refers to the inside of the CO_2 tube whereas *LMTD* is the logarithmic mean temperature difference between the supercritical CO_2 and the water.

The overall heat transfer coefficient U_i [W/(m^{2}K)] for each sub-section is expressed as follows when referring to the inner heat transfer surface A_i:

$$U_i = \frac{1}{\left(\frac{1}{h_i}\right) + \left(\frac{A_i \cdot \ln\left(d_o / d_i\right)}{2 \cdot \pi \cdot k \cdot L}\right) + \left(\frac{1}{h_o} \cdot \frac{A_i}{A_o}\right)} \tag{6.10}$$

where *L* is the length of the sub-section, *h* is the convective heat transfer coefficient, and *k* is the thermal conductivity of the CO_2 tube. The subscripts *i* and *o* refer to the inside and outside surface of the CO_2 tube, respectively.

Since the modelled tube-in-tube heat exchanger was made of smooth cylindrical tubes, the overall heat transfer coefficient per unit length of the tube *U** [W/(mK)] was expressed as (Kreith, 1980):

$$U^* = \frac{1}{\left(\frac{1}{h_i \cdot \pi \cdot d_i}\right) + \left(\frac{\ln\left(d_o / d_i\right)}{2 \cdot \pi \cdot k}\right) + \left(\frac{1}{h_o \cdot \pi \cdot d_o}\right)} \tag{6.11}$$

Consequently, an alternative form of Eq. (6.10) was used:

$$\dot{Q} = U^* \cdot L \cdot LMTD \tag{6.12}$$

With reference to Eqs. (6.4) through (6.6), the energy balance for each sub-section was expressed as:

$$\dot{Q}_H = \dot{Q}_C = \dot{Q}_{tot} \tag{6.13}$$

With reference to Eqs. (6.4) through (6.8), the following equations were derived to estimate the outlet temperature of CO_2 and water from each sub-section when the inlet CO_2 temperature and the inlet water temperature were known (Stoecker, 1989):

$$T_{H,out} = T_{H,in} - \left(T_{H,in} - T_{C,in}\right) \cdot \left(\frac{1 - e^{X_H}}{\frac{CP_H}{CP_C} - e^{X_H}} \right) - \Delta T_H \tag{6.14}$$

$$T_{C,out} = T_{C,in} - \left(T_{C,in} - T_{H,in}\right) \cdot \left(\frac{1 - e^{X_C}}{\frac{CP_C}{CP_H} - e^{X_C}} \right) \tag{6.15}$$

where:

$$X_H = U \cdot A_i \cdot \left[\left(\frac{1}{\dot{m} \cdot c_p} \right)_H - \left(\frac{1}{\dot{m} \cdot c_p} \right)_C \right] \tag{6.16}$$

$$X_C = U \cdot A_i \cdot \left[\left(\frac{1}{\dot{m} \cdot c_p} \right)_C - \left(\frac{1}{\dot{m} \cdot c_p} \right)_H \right] \tag{6.17}$$

In Eq. (6.14), ΔT_H represents the temperature drop of the supercritical CO_2 gas due to pressure loss in the sub-section, i.e:

$$\Delta T_H = \left(\frac{\partial T}{\partial p} \right)_v \cdot \Delta p \tag{6.18}$$

6.1.3.3 Heat Transfer Correlations

The convective heat transfer coefficients *h* in terms of the Nusselt number (*Nu*) for single-phase turbulent tube flow can generally be expressed as a function of the Reynolds number (*Re*) and the Prandtl number (*Pr*), i.e.:

$$Nu = f(Re, Pr) \tag{6.19}$$

Since the gas coolers were modelled as a tube coils, the change-over from laminar to turbulent flow will occur at higher Reynolds number than that of straight tubes. According to Schmidt (VDI, 1993), the critical Reynolds number Re_{crit} for single-phase flow in a tube coil can be expressed as:

$$\mathrm{Re}_{\mathrm{crit}} = 2300 \cdot \left[1 + 8.6 \cdot \left(\frac{d}{D} \right)^{0.45} \right] \qquad (6.20)$$

where D is the average diameter of the tube coil, and d is the diameter of the tube. Figure 6.4 shows an example of how the critical Reynolds number varies at different tube and coil dimensions.

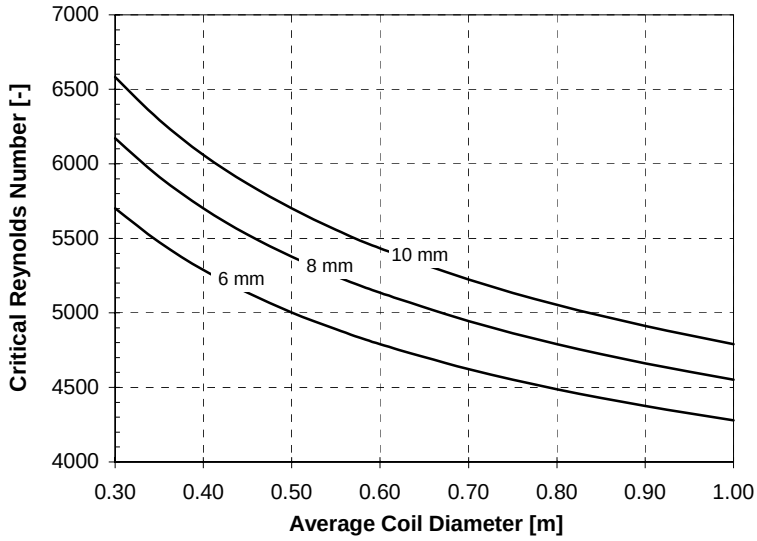

Figure 6.4 The Critical Reynolds number for different coil geometries.

The centrifugal forces caused by fluid flow through a tube coil give rise to a secondary current, which improves the heat transfer and increase the pressure drop compared to a straight tube (VDI, 1993).

Since the heat transfer process in the water-cooled CO_2 gas cooler only involved single-phase fluids, the commonly used *Gnielinski correlation* (VDI, 1993) was applied to estimate the convective heat transfer coefficients. Although the Gnielinski correlation is originally developed for flow in circular tubes, it can also be applied with good accuracy for annulus flow, when the geometric diameter is replaced with the hydraulic diameter of the annulus (Adriansyah, 2001).

The following Gnielinski correlations for laminar and turbulent flow as well as for flow in the transition zone, conforms with a deviation of ±15% with experimental data (VDI, 1993):

Laminar flow (i.e. $Re \leq Re_{crit}$):

$$Nu_L = \left(3.66 + 0.08 \cdot \left[1 + 0.8 \cdot \left(\frac{d_h}{D} \right)^{0.9} \right] \cdot Re^m \cdot Pr^{1/3} \right) \cdot \left(\frac{Pr_b}{Pr_w} \right)^{0.14} \quad (6.21)$$

where:

$$m = 0.5 + 0.2903 \cdot \left(\frac{d_h}{D} \right)^{0.194} \quad (6.22)$$

The subscript *h* refers to the hydraulic diameter of the tube or annulus, whereas *w* and *b* refer to the properties of the fluid at wall and bulk temperature, respectively.

Turbulent flow (i.e. $Re \geq 22\,000$):

$$Nu_T = \left(\frac{\frac{f}{8} \cdot Re \cdot Pr}{1 + 12.7 \cdot \left(\frac{f}{8} \right)^{0.5} \cdot \left(Pr^{2/3} - 1 \right)} \right) \cdot \left(\frac{Pr_b}{Pr_w} \right)^{0.14} \quad (6.23)$$

where:

$$f = \frac{0.3164}{Re^{0.25}} + 0.03 \cdot \left(\frac{d_h}{D} \right)^{0.5} \quad (6.24)$$

Transition zone (i.e. $Re_{crit} < Re < 22\,000$) – linear interpolation:

$$Nu_{TR} = \gamma \cdot Nu_L \left(\text{at } Re = Re_{crit} \right) + \left(1 - \gamma \right) \cdot Nu_T \left(\text{at } Re = 22\,000 \right) \quad (6.25)$$

where:

$$\gamma = \left(\frac{22\,000 - Re}{22\,000 - Re_{crit}} \right) \quad (6.26)$$

The subscripts *L* and *T* refer to laminar and turbulent flow, respectively.

The correction factor in Eqs. (6.21) and (6.23), takes into account the variations in the Prandtl number from the tube wall temperature T_w to the bulk temperature T_b. The wall temperature is defined as:

$$T_w = T_b - \left(\frac{\dot{Q}}{h \cdot A} \right) \tag{6.27}$$

When the convective heat transfer coefficient *h* increases, the wall temperature will approach the bulk temperature of the fluid, and the correction factor will approach 1.

Calculations showed that the variations in the correction factor for the CO_2 flow typically would range from about 0.5 to 5% at 8 to 10 MPa gas cooler pressure and temperatures between 5 to 110°C. Regarding the water flow, the estimated variations ranged from about 0.5 to 2% at temperatures from 5 to 90ºC. The variations in the correction factor were regarded as small enough to be neglected in Eqs. (6.21) and (6.23).

6.1.3.4 Pressure Drop Correlations

The pressure drop for the single-phase supercritical CO_2 as well as the water in each sub-section of the tripartite gas cooler was calculated from the following general equation (Incropera and DeWitt, 2001):

$$\Delta p = \zeta \cdot \left(\frac{L}{d_h} \right) \cdot \left(\frac{\rho \cdot v^2}{2} \right) \tag{6.28}$$

where ζ is the friction factor, *L* the length of the sub-section, and ρ and *v* the density and mean velocity of the fluid, respectively.

The following correlations from *Gnielinski* were used to calculate *the friction factor* for laminar and turbulent flow, respectively (VDI, 1993):

$$\zeta_L = \frac{64}{Re} \cdot \left[1 + 0.033 \cdot \left[\log_{10} \left(Re \cdot \sqrt{\frac{d_h}{D}} \right) \right]^{4.0} \right] \tag{6.29}$$

$$\zeta_T = \frac{0.3164}{Re^{0.25}} \cdot \left[1 + 0.095 \cdot \sqrt{\frac{d_h}{D}} \cdot Re^{0.25} \right] \tag{6.30}$$

Owing to the curvature (d_h/D) of tube-in-tube heat exchangers and the consequent centrifugal forced that are initiated, the pressure drop will be greater than that of straight tubes.

6.1.3.5 Programming Language and Model Structure

The computer model was programmed in *Microsoft Excel/Visual Basic*.

Based on former experiences with computer simulation of counter-flow CO_2 gas coolers (Adriansyah, 2001), each gas cooler unit was divided into 20 sub-sections. Within each sub-section the thermophysical properties of the fluids were calculated on the basis of the arithmetic mean temperature. Table 6.1 shows the calculated length of the gas cooler sub-sections and the maximum CO_2 temperature gradient within each section, when the gas cooler geometry and the operating conditions were the same as for the prototype CO_2 heat pump unit presented in Sections 4.1 and 5.1, *Testing of a Residential Brine-to-Water CO_2 Heat Pump Unit*.

Table 6.1 The maximum CO_2 temperature gradient for the gas cooler sub-sections in the computer model when using data for the prototype CO_2 heat pump unit (ref. Sections 4.1 and 5.1).

Ranges		**DHW Preheating**	**Space Heating**	**DHW Reheating**
Total length [m]		14	15	3
Sub-section (cell) length [m]		0.70	0.75	0.15
Comb. mode:	Max. temp. range [ºC]	5–30	28–60	40–100
	Max. temp.grad. [K/cell]	**1.3**	**1.6**	**3.0**
DHW mode:	Max. temp. range [ºC]	5–70	*	50–120
	Max. temp.grad. [K/cell]	**3.8**	*	**3.5**
SH mode:	Max. temp. range [ºC]	*	28–100	*
	Max. temp.grad. [K/cell]	*	**3.0**	*

Figure 6.5 illustrates the structure of the modelled tripartite gas cooler including the internal connection between the sub-sections. The most important input and output variables are also displayed. The subscripts *SH* and *DHW* refer to the space heating and hot water circuits, respectively.

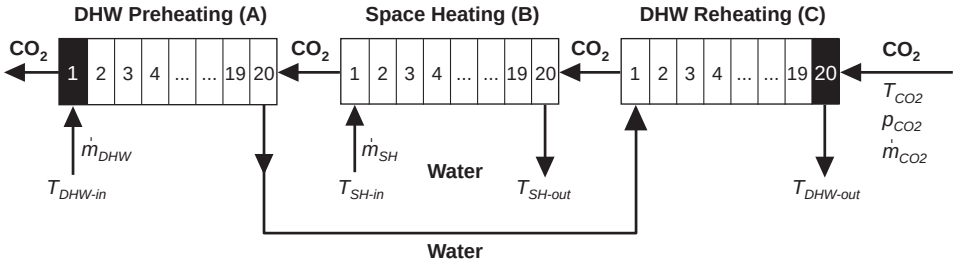

Figure 6.5 Principle showing the structure of the modelled tripartite counter-flow tube-in-tube CO_2 gas cooler.

Since the tripartite gas cooler was of a counter-flow type, initial linear temperature profiles based on the known inlet CO_2 and water temperatures were established by running an integral Visual Basic subroutine. The iteration process was then started in sub-section no. 20 for the DHW reheating gas cooler. The sequential calculation of the inlet and outlet variables for each sub-section was repeated until the difference between the heat flow at the CO_2-side and water-side of sub-section no. 10 for each gas cooler unit was less than 1 W. This convergence criterion constituted less than 2% of the heat flow for the sub-sections in the different gas cooler units.

The results from the simulations were presented as shown in Figure 6.6 and by means of various types of diagrams.

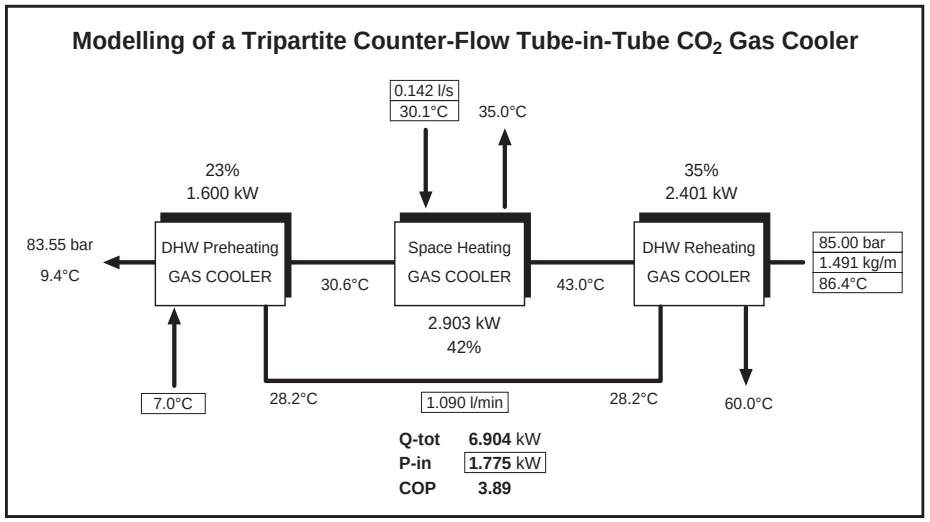

Figure 6.6 Presentation of the main results from the tripartite gas cooler simulation programme (Microsoft Excel/VBA).

6.1.3.6 Verification of the Simulation Model

The simulation model for the tripartite gas cooler was tested and verified by means of experimental data from the CO_2 heat pump unit (ref. Section 5.1). Table 6.2 shows the percentage deviation between the simulation results and the measurements with regard to the main temperatures (*Temp.*), the total heating capacity (Q_{tot}) and the COP. The left-hand column shows the set-points for the space heating (SH) and hot water (DHW) systems. The middle column displays the required adjustment of the CO_2 mass flow rate (Δm_{CO2}) and the tube length of the DHW reheating gas cooler ($\Delta L_{DHW\text{-}R}$) in order to keep the deviation of Q_{tot} and COP within ±1% from the measured values.

Table 6.2 The deviation between the simulation results for the tripartite gas cooler model and the experimental results from the CO_2 heat pump unit (ref. Section 5.1).

Temp. Set-points		Corrections		Deviation		
SH [°C]	**DHW [°C]**	**Δm_{CO2} [%]**	**$\Delta L_{DHW\text{-}R}$ [%]**	**Temp. [°C]**	**Q_{tot} [%]**	**COP [%]**
33/28	60	+4.6	+14	±0.2	+0.2	+0.3
33/28	80	+8.6	0	±0.3	-1.0	-1.0
35/30	60	+3.5	0	±0.3	-0.6	-0.6
35/30	80	+5.9	+14	±0.3	+0.6	+0.7
40/35	60	+5.9	+14	±0.3	+0.5	+0.5
40/35	80	+4.5	+10	±0.2	+0.1	0
*	70	+8.6	+20	±0.3	+0.6	+0.6
35/30	*	+2.6	*	±0.1	-1.0	-1.0

Due to the relatively large oil concentration in the CO_2 flow for the prototype heat pump unit, the CO_2 mass flow rate in the simulations were increased as much as the ratio between the measured heating capacity in the water circuits and CO_2 circuit (ref. Figure 5.53, Section 5.1.3.9, *Comparison of the Measurements from the Water Circuits and the CO_2 Circuit*). For most of the simulations the tube length of the DHW reheating gas cooler unit had to be increased by about 10 to 20% in order to comply with the measured heating capacity and outlet temperatures. Nevertheless, Table 6.2 demonstrates that the simulation model predicted the performance of the tripartite counter-flow tube-in-tube CO_2 gas cooler with satisfactorily accuracy.

6.1.4 Simulation Results

6.1.4.1 The Specific Heat Capacity Ratio

Figure 6.7 shows, as an example, the simulated variations in the c_p-ratio[1] during heat rejection in the tripartite gas cooler in the combined mode. The high-side pressure was 8.5 MPa, and the hot water temperature and the supply/return temperatures in the space heating system were 60ºC and 35/30ºC, respectively. The gas cooler geometry and the operating conditions were the same as for the prototype CO_2 heat pump unit.

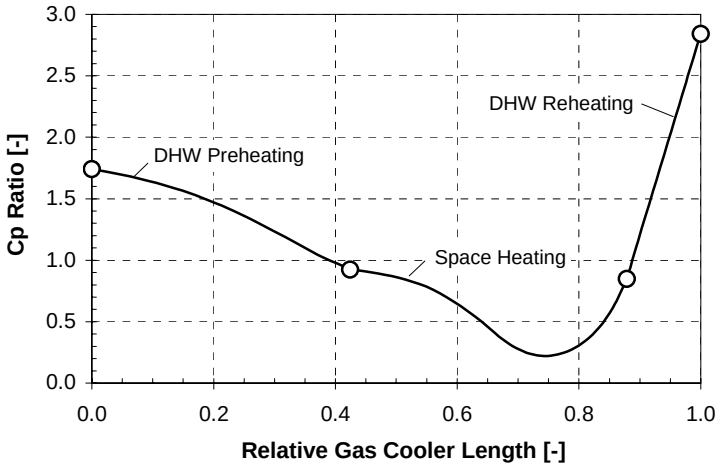

*Figure 6.7 The simulated specific heat capacity ratio for the CO_2 heat pump unit at 8.5 MPa high-side pressure in the combined mode at **35/30ºC** (SH) and **60ºC** (DHW).*

Due to the considerable temperature dependency of the specific heat capacity of the supercritical CO_2, the c_p-ratio ranged from about 0.2 in the space heating gas cooler to 2.8 in the DHW reheating gas cooler.

6.1.4.2 Gas Cooler Temperature Profiles

Simultaneous Space Heating and Hot Water Heating (Combined Mode)

Figures 6.8 through 6.13 present the simulated temperature profiles of the supercritical CO_2 and the water flows in the tripartite gas cooler at optimum high-side pressure in the combined mode. The gas cooler geometry and the operating conditions were the same as for the prototype CO_2 heat pump unit (ref. Sections 4.1 and 5.1).

[1] *The ratio between the specific heat capacity of water and supercritical CO_2.*

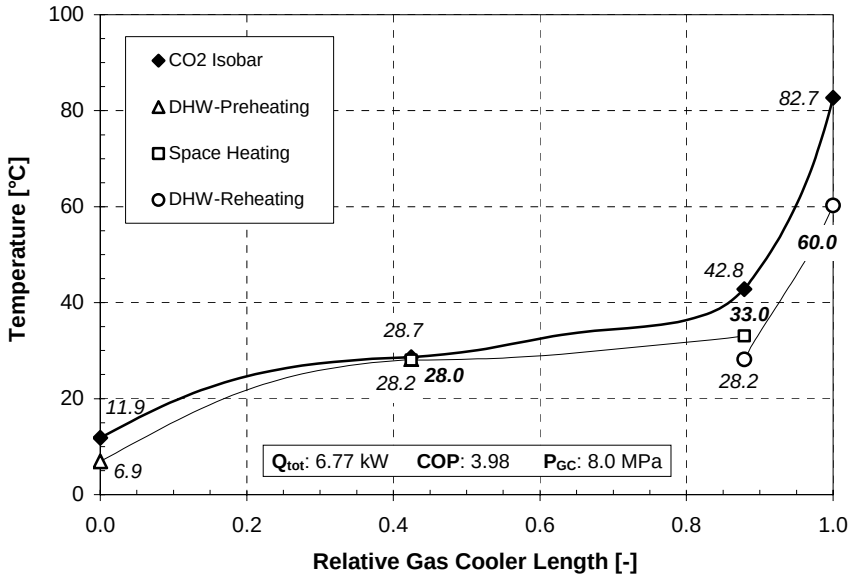

Figure 6.8 *The simulated temperature profiles for the tripartite CO_2 gas cooler at optimum high-side pressure, **33/28ºC** (SH) and **60ºC** (DHW) in the combined mode.*

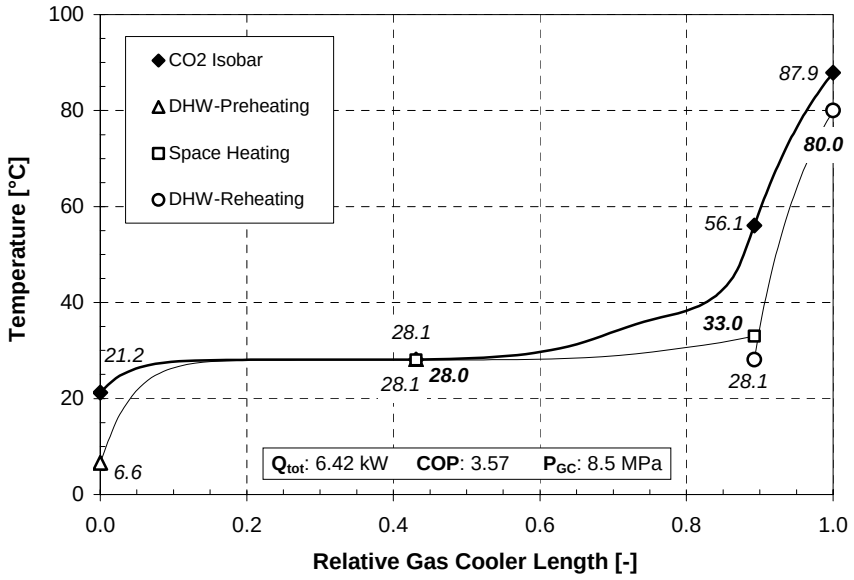

Figure 6.9 *The simulated temperature profiles for the tripartite CO_2 gas cooler at optimum high-side pressure, **33/28ºC** (SH) and **80ºC** (DHW) in the combined mode.*

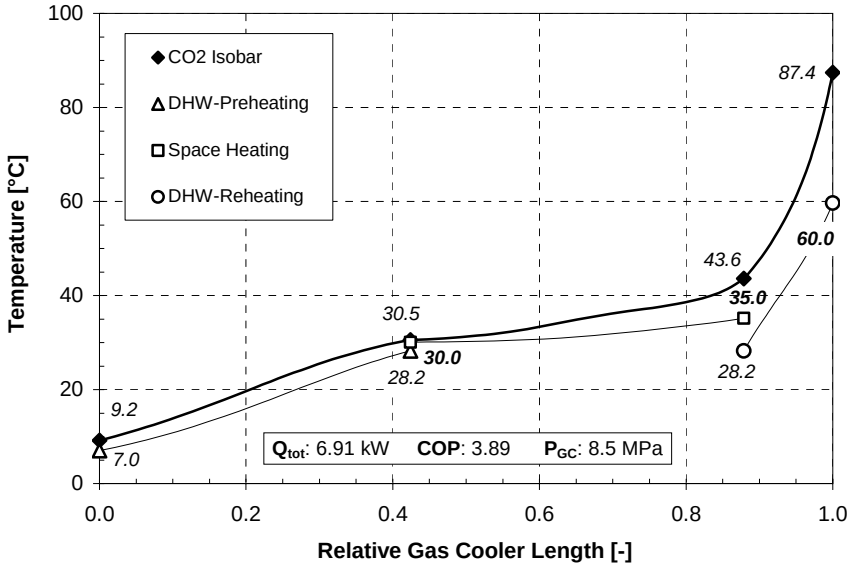

*Figure 6.10 The simulated temperature profiles for the tripartite CO_2 gas cooler at optimum high-side pressure, **35/30ºC** (SH) and **60ºC** (DHW) in the combined mode.*

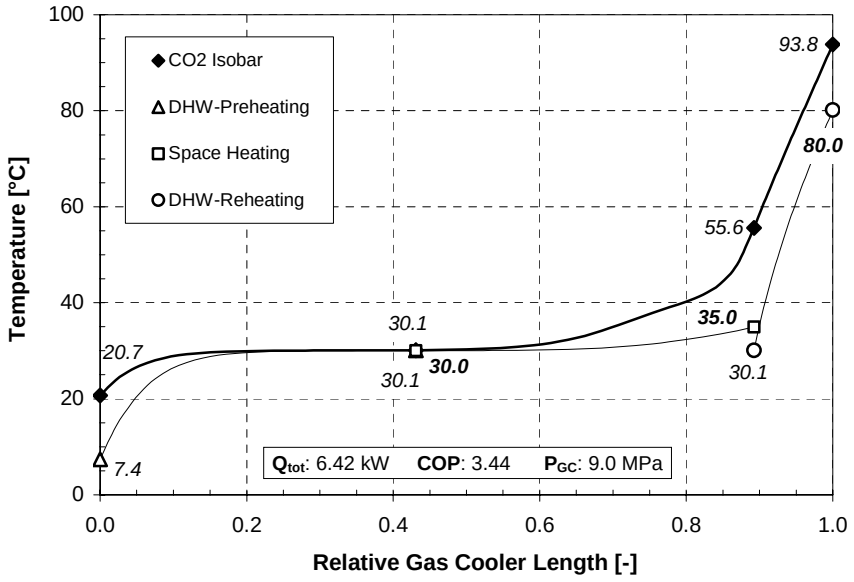

*Figure 6.11 The simulated temperature profiles for the tripartite CO_2 gas cooler at optimum high-side pressure, **35/30ºC** (SH) and **80ºC** (DHW) in the combined mode.*

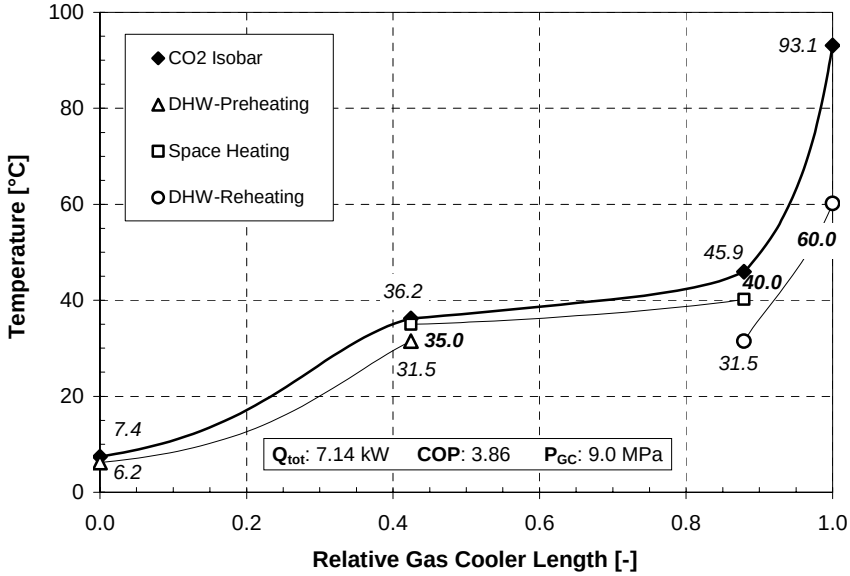

*Figure 6.12 The simulated temperature profiles for the tripartite CO_2 gas cooler at optimum high-side pressure, **40/35ºC** (SH) and **60ºC** (DHW) in the combined mode.*

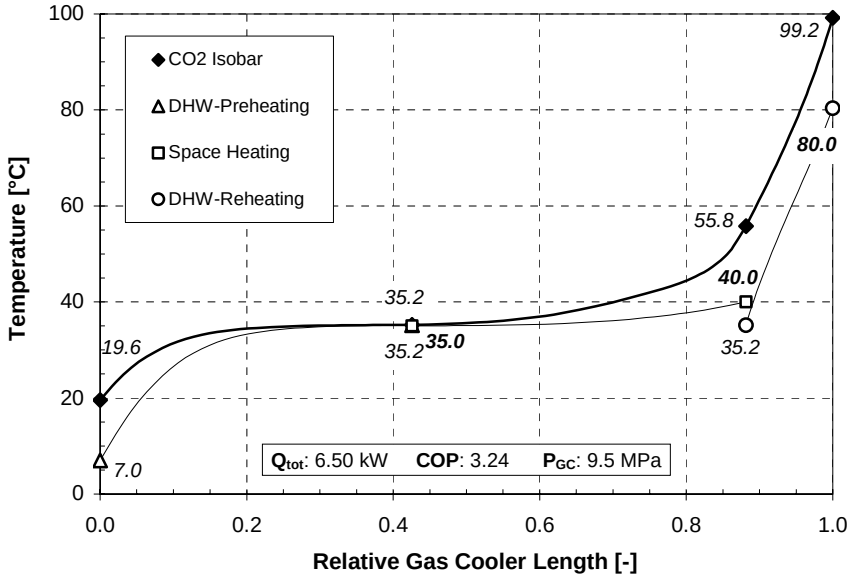

*Figure 6.13 The simulated temperature profiles for the tripartite CO_2 gas cooler at optimum high-side pressure, **40/35ºC** (SH) and **80ºC** (DHW) in the combined mode.*

With reference to Section 5.1.3.2, *Simultaneous Space Heating and Hot Water Heating*, the DHW heating capacity ratio at optimum high-side pressure during operation in the combined mode increased when the temperature level in space heating system was increased or the set-point temperature for the hot water was reduced.

At 60°C hot water temperature and 33/28ºC supply temperature in the space heating system (Figure 6.8), the temperature curves for the CO_2 and the water converged at the hot end of *the DHW preheating gas cooler*. However, by changing the supply/return temperature to 40/35ºC (Figure 6.12), the water flow rate increased and the temperature profiles became divergent. By increasing the hot water temperature to 80ºC, the water flow rate dropped off by about 50%, and only 30 to 60% of the heat transfer surface for the DHW preheating gas cooler was actually used for heat transfer (Figure 6.9, 6.11 and 6.13).

The temperature profiles for the CO_2 and the water in *the DHW reheating gas cooler* were also greatly influenced by the operating conditions. At 60°C hot water temperature (Figures 6.8, 6.10 and 6.12), the temperature curves diverged at the hot end of the gas cooler, and the higher the temperature level in the space heating system, the more pronounced the divergence. At 80°C hot water temperature, the situation was quite different due to the 50% reduction in the water flow rate. Whereas the curves were convergent at 33/28 and 35/30ºC supply/return temperatures in the space heating system (Figures 6.9 and 6.11), the curves were virtually parallel at 40/35ºC (Figure 6.13).

Regarding *the space heating gas cooler*, the average temperature difference during heat rejection at optimum high-side pressure dropped off quite rapidly when the temperature level in the space heating system was increased. This was the main reason for the considerable reduction in the heating capacity at high supply/return temperatures in the space heating system. Due to the relatively large heat transfer surface and the fact that the CP-value of the water flow was larger than that of the CO_2 flow during all operating conditions, the temperature curves were convergent at the cold side of the gas cooler. It should also be noted that *the temperature approach* for the space heating gas cooler unit was also affected by the outlet water temperature from the DHW preheating gas cooler. As a general rule, the larger the water flow rate in the hot water circuit, the lower the temperature approach.

Hot Water Heating Only (DHW Mode)

Figure 6.14 shows the simulated temperature profiles of the supercritical CO_2 and the water flows in the tripartite gas cooler at optimum high-side pressure in the DHW mode. The gas cooler geometry and the operating conditions were the same as for the prototype CO_2 heat pump unit (ref. Sections 4.1 and 5.1).

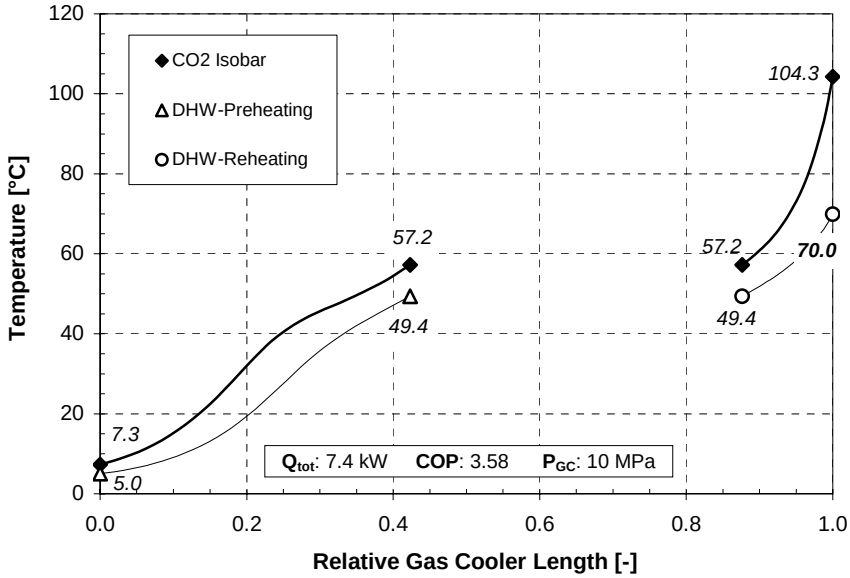

*Figure 6.14 The simulated temperature profiles for the tripartite CO_2 gas cooler at optimum high-side pressure and **70°C** hot water temperature in the DHW mode.*

Due to the relatively large high-side pressure, there was no pinch-point[2] inside the gas cooler units that hampered the heat transfer process, and the temperature approach at the cold end of the DHW preheating gas cooler unit was about 2.3 K. The temperature curves were diverging at the hot end of the DHW reheating gas cooler, since the CP-value of the water flow was larger than that of the CO_2 flow. Despite the relatively small heat transfer surface, about 30% of the heat was given off in the DHW reheating gas cooler unit. This was a result of the larger mean temperature difference than that of the DHW preheating gas cooler unit.

[2] *The minimum temperature difference between the hot and the cold flow in a counter-flow gas cooler occurs at the pinch point.*

Space Heating Only (SH Mode)

Figure 6.15 shows the simulated temperature profiles of the supercritical CO_2 and the water flows in the tripartite gas cooler at optimum high-side pressure in the SH mode. The gas cooler geometry and the operating conditions were the same as for the prototype CO_2 heat pump unit (ref. Sections 4.1 and 5.1).

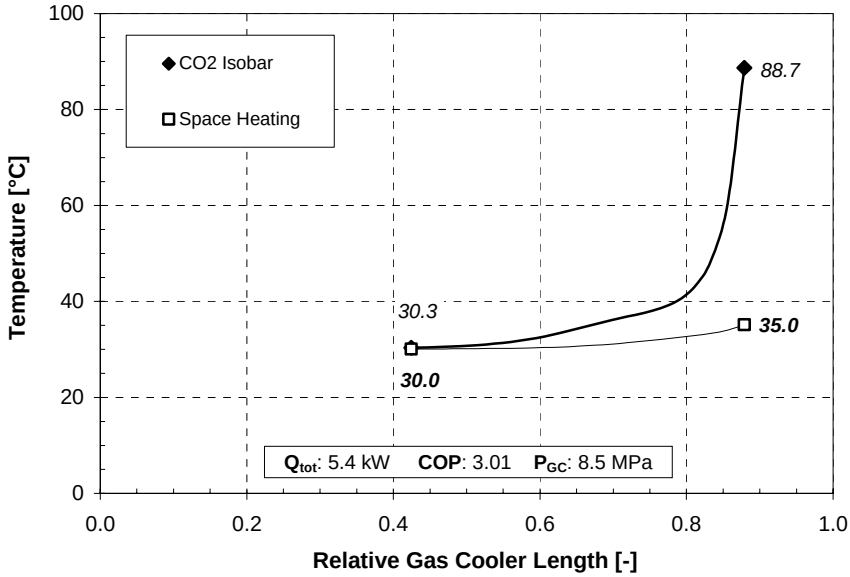

*Figure 6.15 The simulated temperature profiles for the tripartite CO_2 gas cooler at optimum high-side pressure and **35/30ºC** supply/return temperature in the SH mode.*

The characteristic temperature profile of the CO_2 flow was mainly a result of the roughly 10 times higher mass flow rate for the water flow as well as the considerable variations in the specific heat capacity of the CO_2 during heat rejection.

6.1.4.3 The Effect of the Inlet Water Temperature

The inlet (city) water temperature to the DHW preheating gas cooler unit during testing in the combined mode and the DHW mode ranged from about 5 to 7.4°C (ref. Section 5.1). Since the design of the test rig did not enable testing at higher inlet water temperatures, a number of simulations were carried out in order to document the effect of varying inlet water temperature on the COP.

Simultaneous Space Heating and Hot Water Heating (Combined Mode)

Figure 6.16 shows the simulated *relative COP* for the prototype CO_2 heat pump unit in the combined mode at varying inlet water temperature. The supply/return temperature for the space heating system was 35/30 or 40/35°C, the hot water temperature was 60 or 80°C and the high-side pressure for each series was kept constant at the measured optimum high-side pressure. The COP of the CO_2 heat pump unit at 5ºC inlet water temperature was used as the reference (i.e. COP_{rel}=1.0).

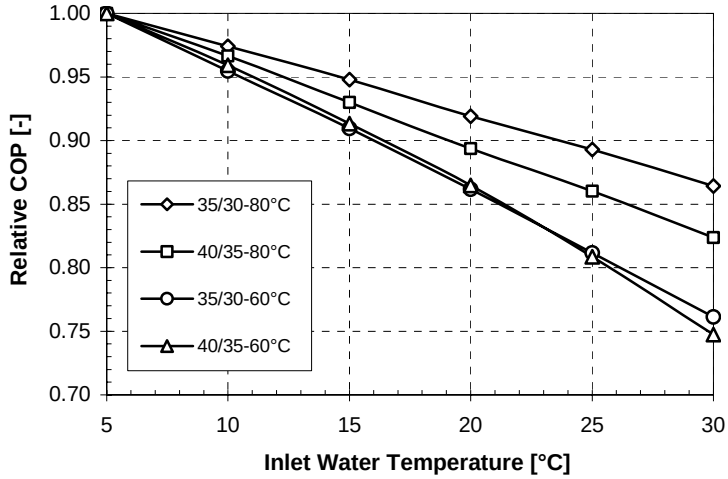

Figure 6.16 The simulated relative COP in the Combined heating mode as a function of the inlet water temperature and varying set-point temperatures for the SH and DHW systems.

Figure 6.16 clearly demonstrates that *the COP was very sensitive to variations in the inlet water temperature*. As an example, by increasing the inlet water temperature from 5 to 10ºC, the COP dropped off by about 5% at 35/30ºC supply/return temperature and 60ºC hot water temperature, whereas the COP was reduced by 14 and 24% at 20 and 30ºC inlet water temperature, respectively. At 80ºC hot water temperature the relative COP for the CO_2 heat pump unit was less influenced by variations in the inlet water temperature due to the considerably lower water flow rate in the hot water circuit.

Hot Water Heating Only (DHW Mode)

Figure 6.17 shows the simulated *relative COP* for the integrated CO_2 heat pump unit in the DHW mode at varying inlet water temperature and 60 and 80ºC hot water temperature.

The COP of the CO_2 heat pump unit at 5ºC inlet water temperature was used as the reference (i.e. COP_{rel}=1.0).

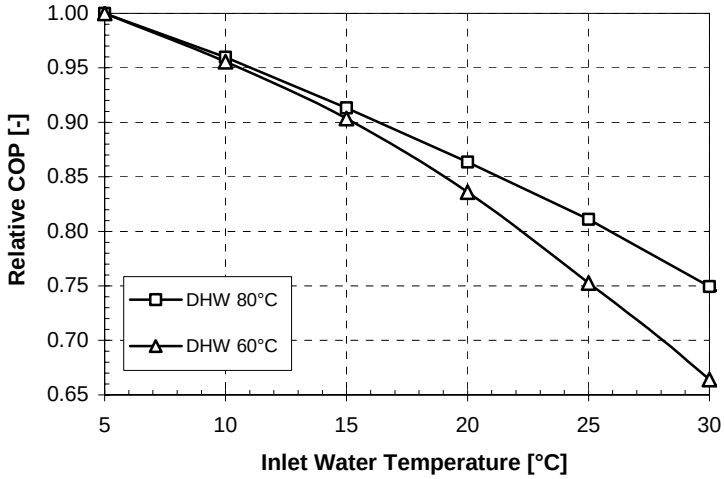

Figure 6.17 The simulated relative COP in the DHW heating mode as a function of the inlet water temperature. The set-points for the hot water temperature were 60 and 80ºC.

The COP was even more sensitive to variations in the inlet water temperature in the DHW mode than in the combined mode, since the entire heating capacity of the CO_2 heat pump unit was used for hot water production. As an example, by increasing the inlet water temperature from 5ºC to 20 and 30°C, the relative COP was reduced by 17 and 34%, respectively. This was approximately 3 and 10% percentage points higher than that in the combined mode.

6.2 Modelling of Cylindrical Single-Shell DHW Tanks

6.2.1 Introduction

The extensive theoretical and experimental work of Abdoly and Rapp (1982) has been an important contribution to the understanding of the general heat transfer mechanisms and transient temperature development in cylindrical single-shell tanks filled with hot water or with hot and cold water. Oppel et al. (1986), Homan et al. (1996), Rodriguez et al. (2002), Yoon et al. (2003) and Shin et al. (2003) developed different computer models in order to study the thermal stratification mechanism in storage tanks, and thereby determine the optimum design and operating conditions. However, since the aim of their work was to investigate thermal storage tanks used in thermal solar systems, the results were not directly applicable when analysing the hot water system for a residential CO_2 heat pump. *A transient two-dimensional heat conduction model*, also termed the tank model, was therefore developed in order to enable tailor-made calculations to be done for actual DHW tank designs, temperature levels, hot water demands and gas cooler heating capacities.

Most of the calculations were carried out for a static system without inlet and outlet water flows, and the DHW tank was either filled with hot water or with equal volumes of hot water and cold city water. The outlet water temperature from the bottom of the tank was also simulated during operation in the charging mode.

The computer model was verified by means of experimental data from a test rig. The design and operation of the test rig as well as the experimental results are presented in Sections 4.2 and 5.2, respectively.

6.2.2 The Computer Model

6.2.2.1 Reasons for Model Simplifications

The transient computer model was limited to calculate the impact of *heat conduction* inside the tank and between the water and the ambient. Consequently, the simulation results represented the minimum temperature change in the tank, and with that *the minimum exergy loss*. If convection as well as mixing caused by the inlet and outlet water flows had been taken into account, the model would have become considerably more complex. Also the results would have been inevitably linked to specific

design parameters such as detailed tank and pipeline/diffuser geometries. Abdoly and Rapp (1982) demonstrated, that as long as the inlet pipelines are equipped with adequate diffusers that reduce the water velocities to a low level, the conductive heat transfer will be the dominating factor that determines the temperature development in the tank. Reference is made to Section 3.3, *The Hot Water System*, for details regarding the design and operation of DHW tanks as well as typical mass flow rates during the tapping and charging periods.

6.2.2.2 Conductive Heat Transfer Equations

The general two dimensional Fourier's law of heat conduction in cylindrical coordinates is expressed as (Kreith, 1980):

$$\frac{1}{r} \cdot \frac{\partial}{\partial r}\left(r \cdot \frac{\partial T}{\partial r} \right) + \frac{\partial T^2}{\partial z^2} = \left(\frac{\rho \cdot c_p}{k} \right) \cdot \frac{\partial T}{\partial t} \qquad (6.31)$$

where T is the water temperature at time t, and r and z represent the radial and vertical location in the tank, respectively. Here c_p is the specific heat capacity, ρ is the density and k is the thermal conductivity of water.

Abdoly and Rapp (1982) found that the radial variations in temperature in well insulated tanks are quite small. These results were verified by own experiments, which proved that the temperature difference between the centre and the wall of a standard insulated cylindrical DHW tank with 55ºC water and 20ºC ambient air temperature was less than 0.2 K (ref. Section 5.2.1.1, *Transient Temperature Drop*).

Since the radial temperature gradient was neglected in the tank model, the tank was divided vertically into n different sub-volumes or nodes, where the temperature at each node i represented the average temperature of the sub-volume (bulk temperature). Figure 6.18 shows the principle of the tank model, displaying the nodes in a coordinate system as well as important input parameters such as the radius (r) and the height of the tank (H), the ambient temperature (T_A) as well as the overall heat transfer coefficient for the tank walls (U).

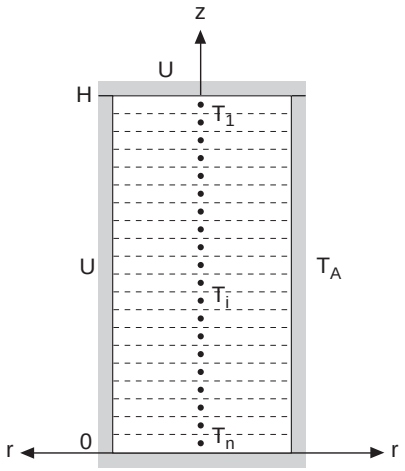

Figure 6.18 Principle of the tank model.

Figure 6.19 shows the principle of the node network, where the thermal resistances *R1* [K/W] and thermal masses *C* [J/K] for water were located between and at the nodes, respectively. The thermal resistances *R2* for the insulation, which were used to calculate the radial heat flux, were located perpendicular to each node. The node distance was determined by the height of the tank and the number of nodes.

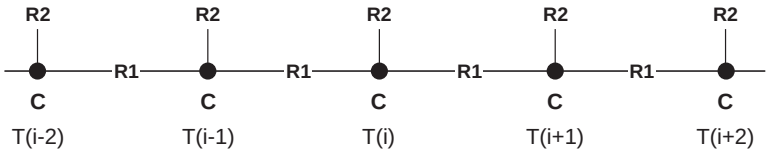

Figure 6.19 Principle of the node network for modelling of transient heat conduction in cylindrical DHW tanks.

When both the axial and radial heat transfer rates were taken into account, the energy balance at each node for ($1 < i < n$) was expressed as:

$$\rho \cdot c_p \cdot \left(\frac{\pi \cdot D_i^2 \cdot dx}{4} \right) \cdot \frac{\partial T}{\partial t} = k \cdot \left(\frac{\pi \cdot D_i^2}{dx \cdot 4} \right) \cdot \left[T(i-1) - T(i) \right] + \tag{6.32}$$

$$k \cdot \left(\frac{\pi \cdot D_i^2}{dx \cdot 4} \right) \cdot \left[T(i+1) - T(i) \right] + \left(\pi \cdot D_o \cdot dx \cdot U \right) \cdot \left[T_A - T(i) \right]$$

where n is the total number of nodes, i is the node number, dx is the node distance, D_i and D_o are the inner and outside diameters of the DHW tank, respectively, T_A is the ambient temperature, and U is the overall heat transfer coefficient of the tank wall (ref. D_o).

For node $i=1$ and $i=n$, the heat transfer rate through the top and the bottom of the tank was added to the right-hand side of Eq. (6.32).

$$\dot{Q}_{TB} = \left(\frac{\pi \cdot D_i^2}{4} \right) \cdot U \cdot \left[T_A - T(i) \right] \tag{6.33}$$

6.2.2.3 Incorporating Mass Transfer in the Tank Model

Since it proved to be impossible to combine the equations for transient heat conduction and mass transfer in the selected programming tool (ref. Section 6.2.2.4, *Programming Tools and Input Parameters*), an indirect method was used when computing the outlet water temperature from the DHW tank during operation in the charging (heating) mode.

By selecting the number of nodes in the tank model in accordance with Eq. (6.34), the mass of water that entered each sub-volume or node during each time step equalled the total mass of the sub-volume.

$$n = \left(\frac{V \cdot \rho}{\dot{m} \cdot t} \right) \tag{6.34}$$

where $\dot{m}$ is the water flow rate through the tank, t is the time step, V is the total water volume in the tank and ρ is the average density of the water. The required number of nodes were calculated for the lowest gas cooler heating capacity (e.g. 0.5 kW), since this corresponded to the lowest water flow rate in the hot water circuit. The latter was calculated as follows:

$$\dot{m} = \frac{\dot{Q}_{GC}}{(T_{out} - T_{in}) \cdot c_p} \tag{6.35}$$

where the subscripts *in* and *out* refer to the inlet and outlet of the gas cooler, $\dot{Q}_{GC}$ is the heating capacity of the gas cooler and c_p is the average specific heat capacity of the water.

For each simulation series, the temperature profiles in the DHW tank at each time step *t* were displayed as shown in Figure 6.20, where the numbers represent the temperatures at the individual nodes from *i=1 to i=n*. The temperature at node no. 1 was kept constant, since the node represented the hot water inlet from the CO_2 gas cooler.

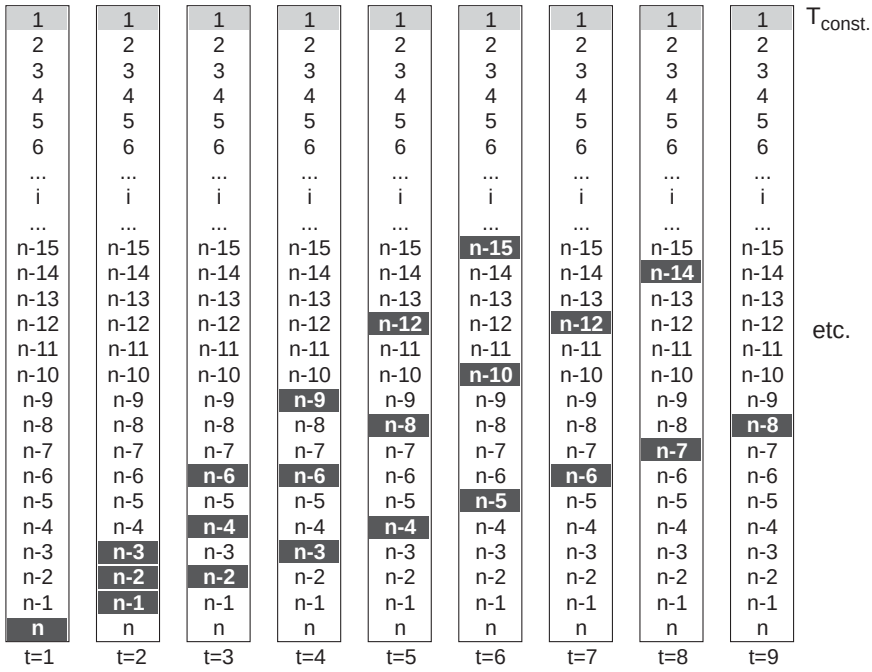

Figure 6.20 Illustration of the principle for reading the outlet water temperatures from the tank when using an indirect method for incorporating mass flow in the tank model.

For the lowest water flow rate, the numbers in the bottom cross row in the output file corresponded to the outlet water temperature from the tank at each time step *t*, i.e. n, n-1, n-2, n-3. n-4 etc. The numbers in the second and third cross rows likewise represented the outlet water temperature from the tank when the water flow rate was twice and three times as high, i.e. n, n-2, n-4, n-6, n-8 etc. and n, n-3, n-6, n-9, n-12 etc.

6.2.2.4 Programming Tools and Input Parameters

The tank model was established in *the Neutral Model Format*, NMF (Sahlin, 1996) and *IDA* (Equa Simulation Technology Group, 1996). The differential equations as well as definition of variables and parameters

were included in the NMF file, whereas the IDA file contained the input parameters, the simulation conditions and the description of the output data files. The NMF file was translated to C/C++ and subsequently to a DLL format (Dynamic Linkable Library) by the *IDA NMF Translator*. The DLL file was then treated by the *IDA Solver* simulation tool, which solved the differential equations and calculated the node temperatures. The NMF and IDA files as well as the procedure for establishing, converting and running the files are presented in Appendix I, *The Transient Two-Dimensional Tank Model*.

The input parameters for the tank model were as follows:

- The tank dimensions (diameters, height)
- The average U-value of the tank
- The ambient air temperature
- The number of nodes
- The initial temperature profile for the water (separate def-file)

6.2.2.5 Verification of the Tank Model

The tank model was verified by means of experimental data from the DHW tank test rig (ref. Section 5.2).

Uniform Initial Hot Water Temperature

In the tank model, the 200 litre DHW tank (ID 500 mm, H 1020 mm) was divided into 200 nodes, which corresponded to a node distance of 5 mm and a water volume of 1 litre for each node. By using the measured initial temperatures for the water (56.2ºC) and the ambient air (22ºC), the simulated temperature drop at varying U-values was compared with the measured temperature drop. The simulated and the measured temperatures in the tank were identical at a U-value of 1.05 W/m^2K. When neglecting the thermal resistance in the water and the thermal resistance between the water and the inner tank wall, this U-value corresponded to 40 mm glasswool insulation (k=0.043 W/(mK)) and a convective heat transfer coefficient between the outer tank wall and the ambient air of 10 W/m^2K.

Static Thermocline

The measured temperature gradients (ref. Figure 5.56, Section 5.2.1.2, *Transient Temperature Gradients in a DHW Tank Filled with Hot and Cold Water*) and the simulated temperature gradients for the static thermocline, were compared by using the U-value from the simulated hot water tank (1.05 W/(m^{2}K)) and the measured initial temperatures for the water (53.2/4.8°C) and the ambient air (22.5°C) in the tank model. The results are presented in Figure 6.21.

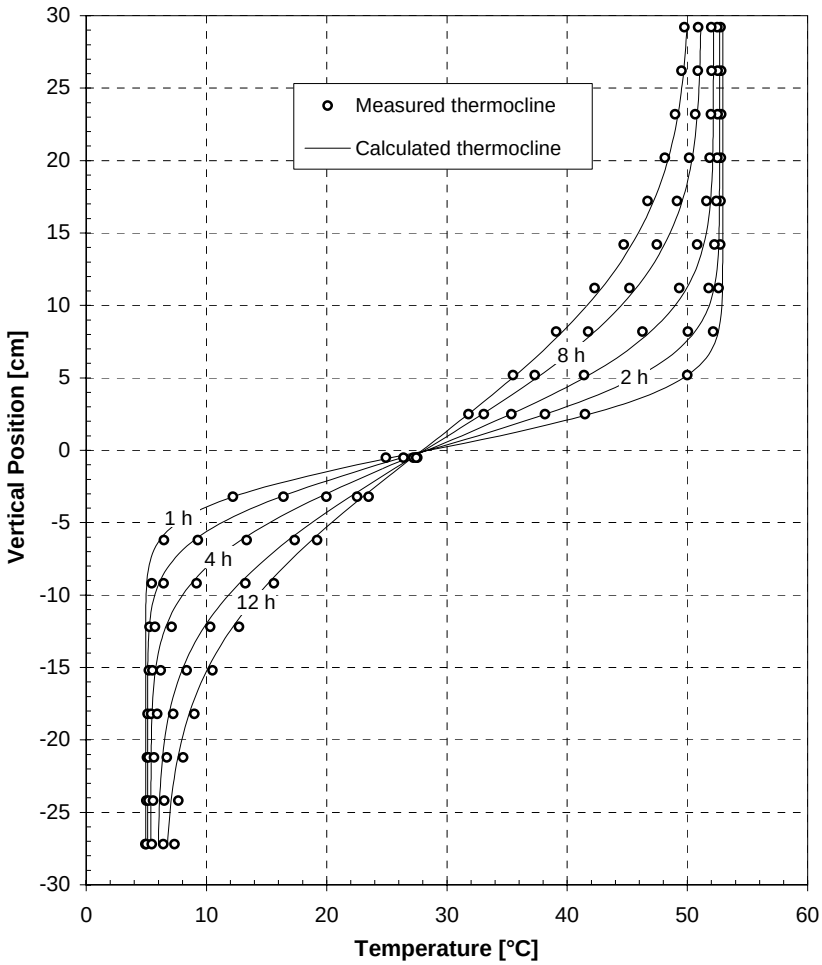

Figure 6.21 Comparison of the measured (Figure 5.56) and simulated transient temperature gradients (thermoclines) between the hot and the cold water reservoirs in the 200 litre tank. The initial water temperatures were 53.2 and 4.8°C, and the average ambient air temperature was 22.5°C.

After a period of 12 hours, the maximum deviation between the measured and simulated temperatures was less than 0.6 K. When taking into account the uncertainty in the temperature measurements and the placement of the temperature sensors, the tank model proved satisfactorily accuracy when calculating transient static thermoclines in cylindrical DHW tanks.

6.2.3 Simulation Results

6.2.3.1 The Static Thermoclines

Figure 6.22 shows the simulated static thermoclines between the hot and the cold water reservoirs in the DHW tank during a period of 12 hours. The initial water temperatures were 70 and 10ºC, the ambient air temperature was 20ºC, whereas the U-value for the tank wall was 1.05 W/(m^{2}K).

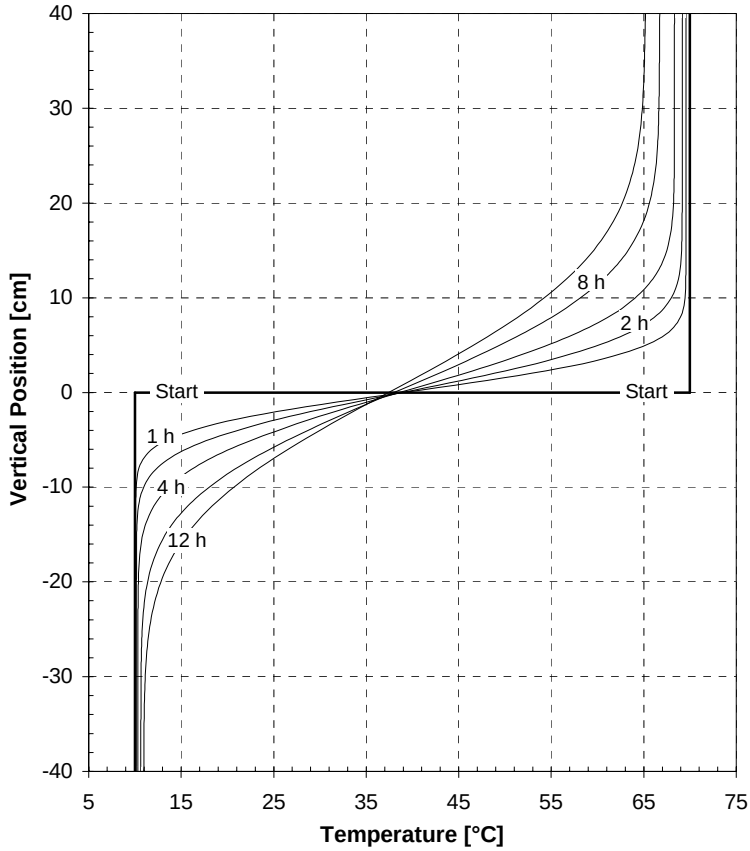

Figure 6.22 The simulated thermocline in the 200 litre DHW tank at 70ºC and 10ºC initial temperatures. The ambient air temperature was 20ºC, and the U-value was 1.05 W/(m^{2}K).

The simulated temperature gradients or thermoclines represent the minimum temperature change in the reservoirs and with that the minimum possible exergy loss in the DHW tank (ref. Section 3.3.3, *Exergy Losses in the DHW Storage Tank*). In a practical system, however, the inlet and outlet water flow will lead to mixing of the water at different temperature levels, and thereby increase the thermodynamic losses.

6.2.3.2 The Water Volume of the Thermocline Zone

The total water volume of the thermocline zone[3] was determined by analysing the thermoclines at varying temperature conditions. Figure 6.23 shows an example of the estimated thermocline volume for the simulated DHW tank at 60/10ºC and 80/10ºC initial water temperatures.

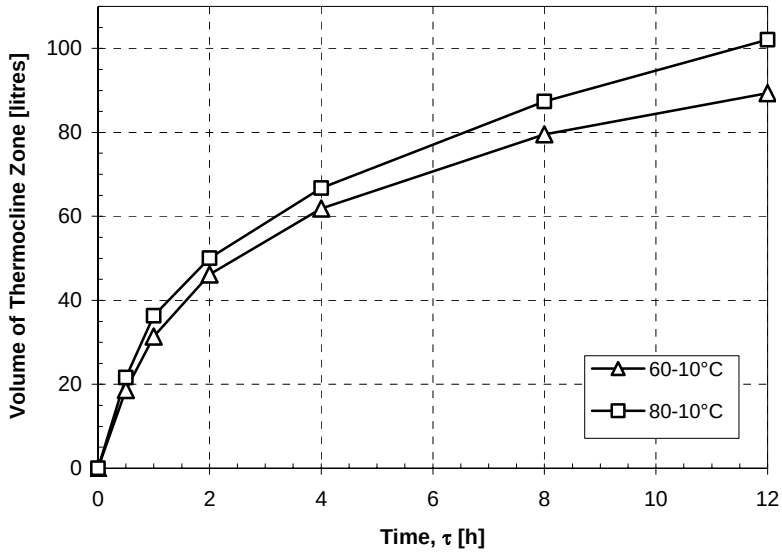

Figure 6.23 The estimated volume of the thermocline zone at 60/10ºC and 80/10ºC initial water temperatures, 20ºC ambient air temperature and a U-value of 1.05 W/(m²K).

The total volume of the thermocline zone V_{TC} could be expressed as a logarithmic function of the retention time τ, i.e. $V_{TC} = [22.9 \cdot \ln(\tau)+30.9]$ ±1.5%. *The weighted mean temperature* of the thermocline zone was roughly the arithmetic mean of the initial water temperatures.

[3] *The water volume in the DHW tank where the temperature has changed due to conductive heat transfer between the hot and the cold water reservoirs (ref. Section 3.3.3.3)*

With reference to Figure 3.28 in Section 3.3.3.3, *Conductive Heat Transfer Inside the DHW Tank*, the growth rate of the thermocline zones ($\partial H_{TC}/\partial\tau$) decreased gradually since the heat flux between the "undisturbed" hot and cold water reservoirs was roughly proportional to the extent of the thermocline zone.

6.2.3.3 The Outlet Water Temperature from the Tank

Figure 6.24 and Figure 6.25 exemplify the simulated outlet water temperatures from the DHW tank during the charging mode at 70/10ºC initial water temperatures, 60 or 120 litres charging volumes and a constant water flow rate ranging from 29 to 72 l/h. The selected water flow rates corresponded to a gas cooler heating capacity in the range from 2 to 5 kW at the actual temperature conditions.

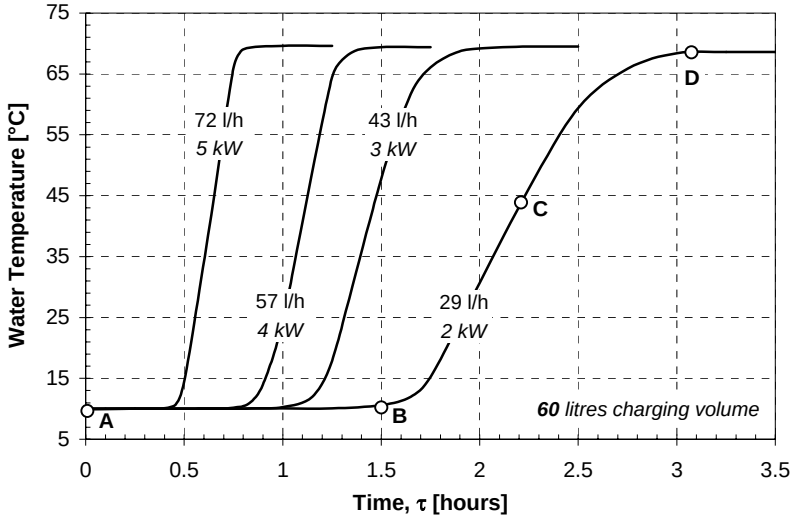

Figure 6.24 The simulated outlet water temperature from the 200 litre DHW tank at 70/10ºC initial water temperatures, 60 litres charging volume and varying water flow rates.

The conductive heat transfer resulted in a considerable rise in the average outlet temperature from the tank and prolonged the charging period. At the lowest water flow rate of 29 l/h, the total thermocline zone *B–D* comprised the heated city water (*B–C*) and the cooled hot water (*C–D*), whereas the extra charging period was equal to $\Delta\tau = (\tau_D - \tau_C)$. The mean outlet water temperature from the tank was about 30ºC, and it was virtually the same at a water flow rate of 72 l/h.

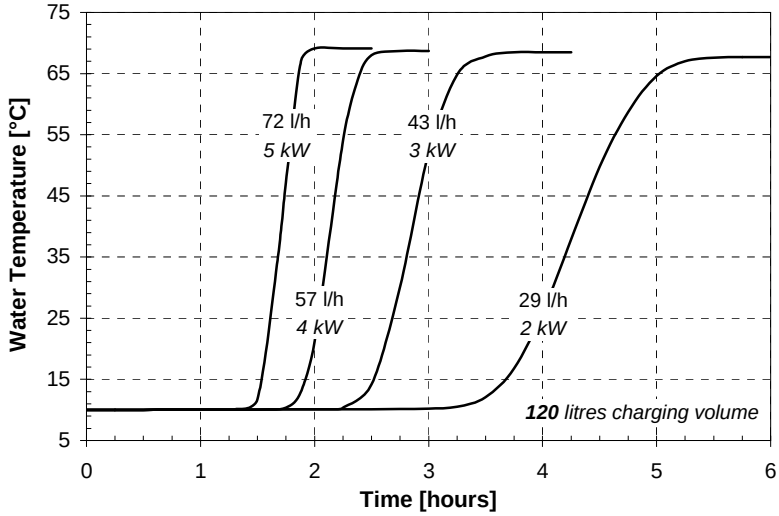

Figure 6.25 *The simulated outlet water temperature from the 200 litre DHW tank at 70/10ºC initial water temperatures, 120 litres charging volume and varying water flow rates.*

Figure 6.26 shows the estimated water volume of the thermocline zone at varying water flow rates. The calculations have been based on the simulation results from Figure 6.24 and 6.25.

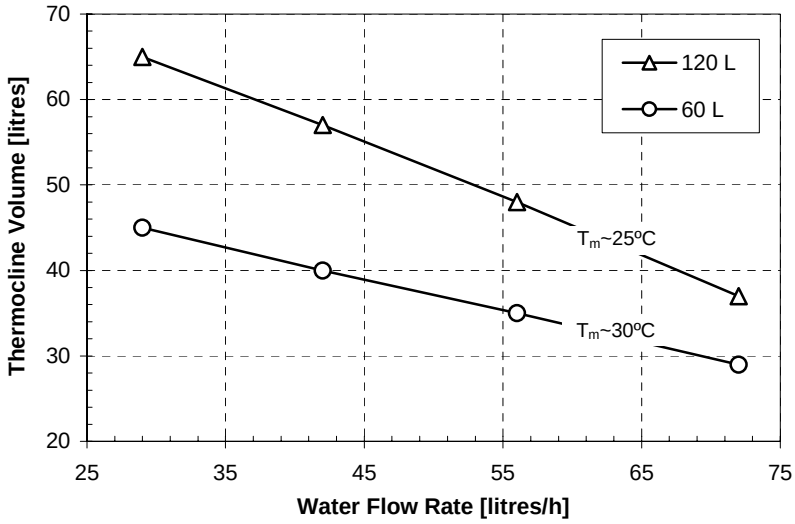

Figure 6.26 *The estimated water volume of the thermocline zone at varying water flow rates and a charging volume of 60 and 120 litres. The calculations have been based on the simulations results presented in Figure 6.24 and 6.25.*

According to Figure 6.26, the mean outlet temperature (T_m) dropped from about 30ºC to 25ºC when the city water volume was increased from 60 to 120 litres. On the other hand, the total volume of the thermocline zone rose about 30 to 45% at water flow rates in the range from 72 to 29 l/h.

The simulations demonstrated that *the smaller the charging volume and the lower the heating capacity of the gas cooler, the larger the relative effect of the conductive heat transfer between the hot and cold water reservoirs*. When the volume of the thermocline zone has been estimated, the average COP for a CO_2 heat pump during the charging period can be estimated by means of Eq. (3.26) in Section 3.33. The water volume and the mean temperature of the thermocline zone correspond to the minimum possible exergy loss in the DHW tank. In a practical system the mixing of hot and cold water during the tapping and charging periods may increase the exergy loss in the tank considerably.

7 Discussion and Analysis

Following on from the work presented in Chapters 5 and 6, this chapter provides an overview and discussion of the most important findings from the experiments and the computer simulations for the integrated brine-to-water CO_2 heat pump unit for space heating and hot water heating, the standard-sized cylindrical domestic hot water (DHW) tank and the movable insulating plate. The final part of the chapter presents a thermodynamic (exergy) analysis for the prototype CO_2 heat pump system as well as an estimate of the seasonal performance factor (SPF) for two CO_2 systems and a state-of-the-art residential brine-to-water heat pump system.

7.1 Main Findings from the Experiments and the Simulations

7.1.1 Introduction

The integrated brine-to-water CO_2 heat pump unit for combined space heating and hot water heating was tested in three different operating modes:

- Simultaneous space heating and hot water heating (*combined mode*)
- Hot water heating only (*DHW mode*)
- Space heating only (*SH mode*)

Virtually all of the 80 tests were carried out at an evaporation temperature of -5ºC, since this represents a typical temperature level for a ground-coupled heat pump operating in a cold climate. The heat pump unit gave off heat to a low-temperature floor heating system at 33/28, 35/30 or 40/35ºC supply/return temperatures. In the combined mode and the DHW mode, the set-point for the DHW temperature was 60, 70 or 80ºC.

7.1.2 Energy Efficiency

7.1.2.1 The COP vs. the Temperature Levels in the Space Heating and DHW Systems

The coefficient of performance (COP) of an integrated brine-to-water CO_2 heat pump unit for combined space heating and hot water heating is strongly affected by the temperature levels in the space heating (SH) system and the domestic hot water (DHW) system. The experimental and simulation results regarding the impact of the temperature levels on the COP of the prototype CO_2 heat pump unit, can be summarized as follows:

Simultaneous Space Heating and Hot Water Heating (Combined Mode)

- The highest COP, approx. **4.0**, was measured at 33/28°C supply/-return temperatures for the SH system, 60°C DHW temperature, 7ºC city water temperature and 8 MPa high-side pressure.
- At 60, 70 and 80ºC DHW temperature, the COP dropped off by approximately 3, 6 and 9%, respectively, when the supply/return temperatures in the SH system was increased from 33/28 to 40/35ºC.
- At 33/28, 35/30 and 40/35ºC supply/return temperatures in the SH system, the COP dropped off by approximately 10, 12 and 16% when the DHW temperature was altered from 60 to 80ºC.
- At 60°C DHW temperature and 35/30 to 40/35ºC supply/return temperatures for SH system, the COP dropped off by approximately 0.8% per ºC rise in the inlet water temperature for the DHW pre-heating gas cooler. At 80ºC DHW temperature, the corresponding figures were about 0.5% and 0.6%, respectively.

Hot Water Heating Only (DHW Mode)

- The highest COP, approx. **3.8**, was measured at 60°C DHW temperature, 5.5ºC city water temperature and 9 MPa high-side pressure.
- The COP dropped off by approximately 6% when the set-point was altered from 60 to 70ºC (i.e. ~0.6% per °C). The maximum COP at 80ºC was not found due to operational limitations of the test rig.
- At 60ºC and 80ºC DHW temperature, the COP dropped off in average by approximately 1.1% and 0.8% per ºC rise for the inlet water temperature to the DHW preheating gas cooler.

Space Heating Only (SH Mode)

- The highest COP, approx. **3.15**, was measured at 33/28ºC supply/-return temperatures for the SH system and 8 MPa high-side pressure.
- The COP dropped off by approximately 4 and 12% when the supply/return temperatures were increased from 33/28ºC to 35/30ºC and 40/35ºC, respectively (i.e. ~1.8% per ºC).

All Modes

- The COP in *the combined mode* at 33/28ºC supply temperature was approximately 5 to 10% higher than that of *the DHW mode*, and the higher the DHW temperature the larger the relative difference. At 35/30 and 40/35ºC supply/return temperatures and 60 to 70ºC DHW temperature, the COPs were virtually identical.
- The COP in *the SH mode* was 12 to 28% lower than that of *the combined mode*, and the lower the DHW temperature and the higher the temperature level in the SH system, the larger the relative difference.

The experimental results clearly demonstrated, that for all operating modes a reduction in the temperature level(s) for the SH system and/or the DHW system would lead to a higher COP for the CO_2 heat pump unit. During operation in the combined mode and DHW mode, it was observed that the lower the inlet water temperature to the DHW preheating gas cooler unit, the higher the COP. Hence, an integrated CO_2 heat pump unit should preferably supply heat to a low-temperature space heating system (ref. Section 2.3, *Hydronic Heat Distribution Systems*), and the set-point temperature for the DHW system should not exceed the minimum national temperature requirement (ref. Section 2.4.2.3, *Examples of System Designs*). The highest COP will be achieved in regions having a relatively low city water temperature, and when the thermodynamic losses in the DHW tank due to conductive heat transfer and mixing of hot and cold water has been minimized by means of adequate measures (ref. Section 7.1.2.4).

Since the supercritical CO_2 rejects heat at a gliding temperature in a counter-flow tripartite gas cooler, it is mainly *the return temperature* in the SH system that affects the COP of the heat pump unit in the combined mode and the SH mode, and not the supply temperature. The reason is that the return temperature represents the theoretical minimum CO_2 inlet temperature for the DHW preheating gas cooler unit, and the lower the temperature level, the larger the possible cool-down of the CO_2 before throttling.

Hot water heating has been regarded as one of the most energy efficient applications for the transcritical CO_2 heat pump process due to the virtually perfect temperature fit between the supercritical CO_2 and the water, and the consequent low exergy loss during heat rejection. When heat is given off at three different temperature levels in a tripartite gas cooler, the same temperature approach can be achieved but at a lower high-side pressure. Consequently, at low return temperatures in the SH system, *the COP in the combined mode can be even higher than that of the DHW mode*.

The COP of the CO_2 heat pump unit during operation in the SH mode was considerably less than that of the other modes. This was mainly the result of the bad temperature fit between the CO_2 and the water, and the relatively high CO_2 temperature before the throttling valve. In the SH mode, an integrated CO_2 heat pump unit will generally benefit less from a low temperature level in the SH system than that of conventional heat pump units, where heat is given off by means of condensation of the working fluid.

7.1.2.2 The COP vs. the Evaporation Temperature

The evaporation temperature affects the heating capacity of the tripartite gas cooler, the input power to the compressor and consequently the COP of the heat pump unit. The experimental results regarding the impact of the evaporation temperature on the COP of the prototype CO_2 heat pump unit can be summarized as follows:

- In *the combined mode* and *the DHW mode*, the COP dropped off by approximately 6 and 10%, respectively, when the evaporation temperature was reduced from -5 to -10ºC.
- In *the SH mode*, the COP dropped off and rose by approximately 7.5 and 5.5%, respectively, when the evaporation temperature was altered from -5 to -10ºC and from -5 to 0ºC.

The experiments were carried out at 35/30ºC supply/return temperatures for the SH system and 60ºC DHW temperature. Assuming a linear relationship between the evaporation temperature and the COP, the prototype CO_2 heat pump unit would have achieved a COP of approximately 4.2 and 4.1 in the combined mode and the DHW mode, respectively, if the evaporation temperature had been increased from -5 to 0ºC.

7.1.2.3 The COP vs. the DHW Heating Capacity Ratio

During operation in the combined mode, the DHW heating capacity ratio, which is defined as the ratio of the heating capacity for the DHW gas cooler units and the total heating capacity for the tripartite gas cooler, was heavily affected by the temperature levels in the SH and DHW systems. As shown in Figure 7.1, there was also a correlation between the DHW heating capacity ratio and the COP of the prototype CO_2 heat pump unit.

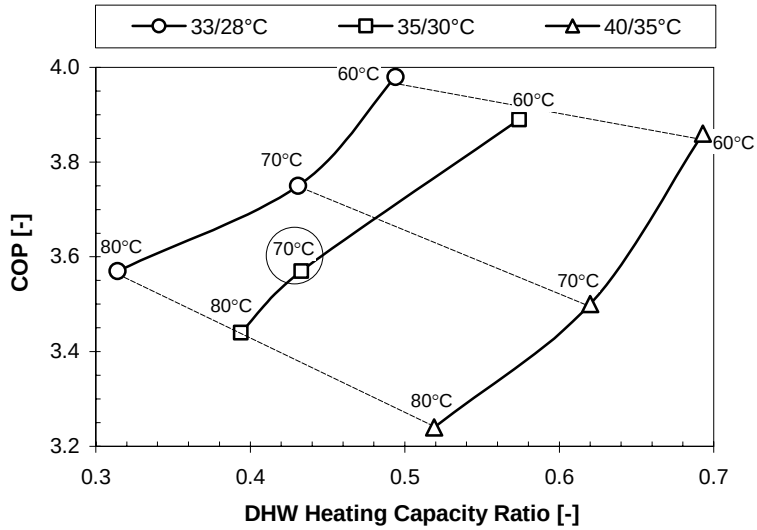

Figure 7.1 The relationship between the COP and the DHW heating capacity ratio for the prototype CO_2 heat pump unit at varying temperature levels in the SH and DHW systems.

The experimental result can be summarized as follows:

- At constant temperature level in the SH system, the DHW heating capacity ratio dropped off in average by approx. 18 percentage points when the DHW temperature was increased from 60 to 80ºC.
- At constant DHW temperature, the DHW heating capacity ratio dropped off in average by approx. 18 percentage points when the supply/return temperature for the SH system was increased from 33/28 to 40/35ºC.

The experimental results demonstrated that the higher the temperature level for the SH system and the lower the set-point temperature for the DHW system, the larger the DHW heating capacity ratio for the prototype CO_2 heat pump unit. At 40/35ºC supply/return temperature for the SH

system and 60ºC DHW temperature, the DHW heating capacity ratio was almost 70%, which means that the prototype CO_2 heat pump unit practically operated as a heat pump water heater. At 33/28ºC supply/return temperature and 80ºC DHW temperature, the DHW heating capacity ratio was about 30%, and most of the heat was rejected to the SH system.

At constant temperature level in the SH system, both the DHW heating capacity ratio and the COP for an integrated CO_2 heat pump unit will diminish at elevated DHW temperatures due to the reduced water flow rate in the DHW circuit and the consequent less cool-down of the CO_2 in the DHW preheating gas cooler unit. The compressor power input will also affect the COP, since the optimum high-side pressure increases slightly when the DHW temperature is increased. The higher the DHW temperature, the larger the relative drop-off in the DHW heating capacity ratio.

At constant DHW temperature, the COP for an integrated CO_2 heat pump will diminish whereas the DHW heating capacity ratio will increase when the temperature level in the SH system is increased. The latter can be explained by the lowered mean temperature difference between the CO_2 and the water in the SH gas cooler, and the consequent reduction of the heating capacity. Although the total heating capacity of the tripartite gas cooler will increase due to a larger water flow rate in the DHW circuit, the rise in the optimum high-side pressure will lead to a drop in the COP.

Figure 7.2 shows the measured relative heating capacities for the three gas cooler units at optimum high-side pressure and varying temperature levels in the SH system and the DHW system.

The COP and the relative heating capacities at 35/30ºC supply/return temperatures for the SH system and 70ºC DHW temperature did not follow the general trends in Figures 7.1 and 7.2. This was because the pressure measurements were carried out at 0.5 MPa intervals, and that the optimum high-side pressure was between 8.5 and 9.0 MPa. Hence, at the real optimum high-side pressure, the DHW heating capacity ratio and the COP would most likely have been around 0.48 and 3.65, respectively.

The heat pump unit was designed for 35/30ºC supply/return temperatures for the SH system and 60ºC DHW temperature. When the heat pump unit was tested at the other temperature programs, the measured COP at the optimum high-side pressure was the highest possible COP that could be obtained with the actual gas cooler design. Thus, if the tripartite gas cooler had been redesigned and optimized for each temperature program, both the COP and the DHW heating capacity ratio would have increased.

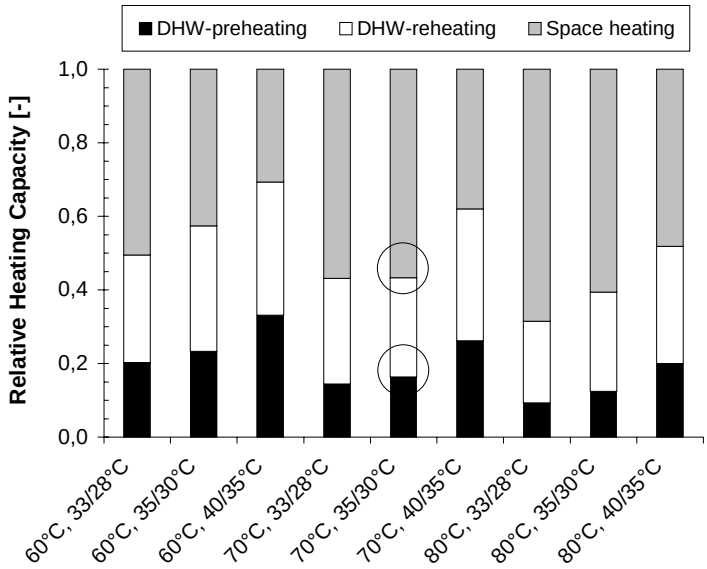

Figure 7.2 *The measured relative heating capacity for the three gas cooler units at optimum high-side pressure and varying temperature levels in the SH and DHW systems.*

As described in Section 2.2, *Heating Demands in Houses*, the annual DHW demand typically constitutes 10 to 15% of the total heating demand in existing residences and about 20 to 45% in new houses and so-called low-energy houses. Consequently, in order to obtain a high COP and at the same time limit the DHW heating capacity ratio for an integrated CO_2 heat pump, *the return temperature for the SH system* should be as low as possible.

7.1.2.4 The COP vs. the Thermodynamic Losses in the DHW Tank

The COP vs. the Inlet Water Temperature

The inlet water temperature for the DHW preheating gas cooler will have a significant impact on the COP for an integrated CO_2 heat pump unit during operation in the combined mode and DHW mode, since it governs the maximum possible cool-down of the CO_2 in the DHW preheating gas cooler unit (ref. Section 6.1.4.3, *The Effect of the Inlet Water Temperature*). The simulation results regarding the impact of the inlet water temperature on the COP of the prototype CO_2 heat pump unit can be summarized as follows:

- *The combined mode*: At 60ºC DHW temperature and 35/30 to 40/35ºC supply/return temperatures for SH system, the COP for the prototype CO_2 heat pump unit decreased by 0.8% per °C rise in the inlet water temperature. This corresponds to a drop in the COP of approx. 4 to 16%, when the inlet water temperature is increased by 5 to 20 K.

- *The DHW mode*: At 60ºC DHW temperature, the COP for the prototype CO_2 heat pump decreased by 1.1% per °C rise in the inlet water temperature. This corresponds to a drop in the COP of approximately 6 to 22%, when the inlet water temperature is increased by 5 to 20 K.

The Impact of Conductive Heat Transfer Inside the DHW Tank

The theoretical evaluation (Section 3.3.3, *Exergy Losses in the DHW Storage Tank*), the experimental results (Section 5.2.1.2, *Transient Temperature Gradients in a DHW Tank*) and the computer simulations (Section 6.2.3, *Simulation Results*), demonstrated that the conductive heat transfer between the hot and cold water in the DHW tank will lead to a rise in the mean inlet water temperature for the DHW preheating gas cooler unit during the charging period. Table 7.1 presents, as an example, a *rough estimate* of the COP and the relative COP reduction for the prototype CO_2 heat pump unit when including the impact of the conductive heat transfer inside the DHW tank. The calculations were based on the estimated volume of the thermocline zone (Figure 6.23, Section 6.2.3.2, *The Water Volume of the Thermocline Zone*), Eq. (3.26) in Section 3.3.3 and the fact that the average temperature of the thermocline zone is virtually identical to the arithmetic mean of the initial water temperatures in the tank (Section 6.2.3.2). The boundary conditions were as follows:

- DHW tank — Standard design, 200 litres, ID 500 mm
- City water — 10ºC
- Charging periods — 0.5, 1, 2 and 4 hours
- Combined mode — COP = *3.89* at 35/30ºC and 60ºC
2 kW DHW heating capacity
- DHW mode — COP = *3.80* at 60ºC
4 kW DHW heating capacity

With reference to Section 6.2.3.2, the estimated volume of the thermocline zone V_{TC} was a logarithmic function of the retention time τ in the DHW tank, i.e. $V_{TC}= [22.9 \cdot \ln(\tau)+30.9] \pm 1.5\%$. Consequently, *the smaller the*

charging volume, the higher the relative reduction in the COP for the integrated CO_2 heat pump unit. In addition, the inlet water flow during the tapping period will lead to inevitable mixing of DHW and city water, and further increase in the thermodynamic losses

Table 7.1 Estimated COP and relative COP reduction (ΔCOP) for the prototype CO_2 heat pump, when including the impact of the conductive heat transfer inside the DHW tank.

Charging Period [h]	Initial Temp. [°C]	Combined Mode			DHW Mode		
		Charging Volume [l]	COP	ΔCOP	Charging Volume [l]	COP	ΔCOP
0.5	60/10	17	2.98	*-23%*	34	3.32	*-13%*
1.0	60/10	34	3.23	*-17%*	69	3.42	*-10%*
2.0	60/10	69	3.46	*-11%*	138	3.53	*-7%*
4.0	60/10	138	3.64	*-9%*	276	3.61	*-5%*

Application of a Movable Insulating Plate

One possible way to reduce internal conductive heat transfer and eliminate the mixing in cylindrical single-shell DHW tanks is to separate the hot water and the city water volumes by means of a movable insulating plate. The experiments (Section 5.2.2, *Testing of a Movable Insulating Plate*) demonstrated that a 50 mm XPS plate will contribute to a reduction in the heat transfer rate between the reservoirs by roughly 80%. The functionality of the movable plate was completely satisfactory at atmospheric test conditions, but it was impossible to test the plate at pressurized conditions (4 to 6 bar) since the DHW tank was made of polycarbonate plates. However, according to theory (Section 3.3.4, *Application of a Movable Insulating Plate Inside the DHW Tank*), pressurized operating conditions should not affect the functionality of the plate, since the small gap between the plate and the tank wall will lead to a uniform static pressure in the tank.

The concept of a movable insulating plate for reduction of the thermodynamic losses in single-shell cylindrical DHW tanks seems promising, but definite conclusions regarding the optimum design, functionality and thermal performance can only be drawn after full-scale testing has been carried out at real operating conditions in an unvented DHW tank. First-costs as well as the long-term reliability of the insulating plate are also important issues that need to be further addressed.

7.1.3 High-Side Pressure Control

7.1.3.1 The Optimum High-Side Pressure

At each temperature program and operating mode for the prototype CO_2 heat pump unit, there was a maximum COP which corresponded to an optimum high-side pressure (ref. Section 5.1.3.5, *Comparison of the Measurements in the Different Heating Modes*). The experimental results regarding the optimum high-side pressure can be summarized as follows:

- *The combined mode* – At constant DHW temperature and 33/28ºC, to 40/35ºC supply/return temperatures in the SH system, the optimum high-side pressure ranged from approximately 8.0 to 9.0 MPa (60ºC), 8.5 to 9.5 MPa (70ºC) and 8.5 to 9.5 MPa (80ºC).

- *The combined mode* – At constant supply/return temperatures in the SH system and 60 to 80ºC DHW temperature, the measured optimum high-side pressure ranged from approximately 8.0 to 8.5 MPa (33/28ºC), 8.5 to 9.0 MPa (35/30ºC) and 8.5 to 9.5 MPa (40/35ºC).

- *The DHW mode* – The optimum high-side pressure rose from 9 to 10 MPa when the DHW temperature was incresaed from 60 to 70ºC.

- *The SH mode* – The optimum high-side pressure increased from 8 to 9.5 MPa when the supply/return temperatures in the SH system was altered from 33/28 to 40/35ºC.

The experimental results demonstrated that the higher the temperature level in the SH system and the higher the DHW temperature, the larger the optimum high-side pressure. *In the combined mode, the temperature level in the SH system had a greater impact on the optimum high-side pressure than the DHW temperature*, i.e. 0.14 MPa/°C vs. 0.03 MPa/ºC. This was due to the fact that the SH gas cooler unit gave off heat in the pseudocritical region, where the specific heat capacity of the CO_2 reach large peak values, and the temperature glide for the CO_2 is relatively moderate during heat rejection (ref. Appendix A2.1, *Temperature Gradients During Heat Rejection*). As a consequence, even small variations in the high-side pressure had a considerable impact on the temperature difference between the CO_2 and the water, and with that the heating capacity of the counterflow gas cooler unit. Figure 7.3 shows the correlation between the pressure and the pseudocritical temperature for supercritical CO_2 (RnLib, 2003).

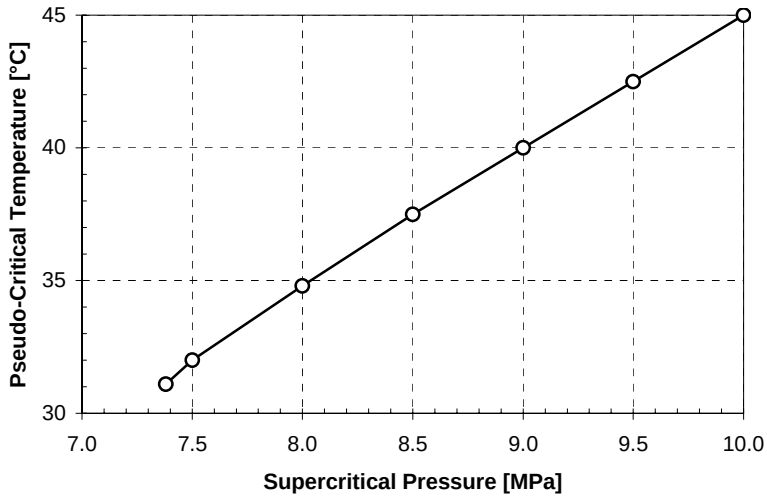

Figure 7.3 The correlation between the pressure and the pseudo-critical temperature of supercritical CO_2 (RnLib, 2003).

7.1.3.2 Constant or Variable High-Side Pressure?

From an economical point of view, it would be a great advantage if the integrated CO_2 heat pump unit could be operated at a constant high-side pressure and still achieve more or less the same COP as a system using high-side pressure control. The experimental results regarding the benefit of high-side pressure control can be summarized as follows:

- As long as the entire DHW heating demand was covered by operation in the combined mode, and the temperature levels in the SH and DHW systems remained constant, it was possible to operate the CO_2 heat pump at *the same high-side pressure* in the combined mode and the SH mode and still achieve the maximum COP.
- *At 60ºC DHW temperature*, the COP was about 5% (combined mode), 0% (DHW mode), and 7.5% (SH mode) less than the maximum COP, when CO_2 heat pump unit was run at a constant high-side pressure of *9 MPa*.
- *At 70ºC DHW temperature* and 35/30 to 40/35ºC supply/return temperature in the SH system, the COP was approximately 3% (combined mode), 7% (DHW mode), and 6% (SH mode) less than the maximum COP, when the CO_2 heat pump unit was run at a constant high-side pressure of *9.5 MPa*.

- *At 80ºC DHW temperature*, the difference between the average COP at varying temperature levels in the SH system and the maximum COP was approximately 7% (combined mode), 10% (DHW mode) and 18% (SH mode), when the CO_2 heat pump unit was run at a constant high-side pressure of *10 MPa*.

Due to the relatively flat maximum points of the COP curves at 60 and 70°C DHW temperature, the COP of the prototype CO_2 heat pump unit was only 5% less than the maximum COP when operating at constant high-side pressures. At 80ºC DHW temperature, the drop in the COP was considerably larger. Consequently, *at moderate DHW temperatures, an integrated CO_2 heat pump unit can be operated at constant high-side pressure in all three modes with only a minor reduction in the COP*.

7.1.4 Design of the Tripartite Gas Cooler

7.1.4.1 The Total and the Relative Heating Capacities

The experimental results for the prototype CO_2 heat pump unit regarding the heating capacities of the three gas cooler units during operation in the different modes, can be summarized as follows:

- Despite the relatively large variations in the set-point temperatures for the SH and DHW systems, *the total heating capacity* of the tripartite gas cooler at optimum high-side pressure was relatively invariable (6.8 kW ±6%) during operation in the different modes.

- The ratio of *the heating capacity for the SH gas cooler* during operation in the SH mode and the combined mode ranged from about 1.2 to 2.6, and the higher the temperature level in the SH system and the lower the DHW temperature, the larger the ratio.

- The ratio of *the heating capacity for the DHW gas cooler units* during operation in DHW mode and the combined mode ranged from about 1.4 to 2.6, and the higher the DHW temperature and the lower the temperature level in the SH system, the larger the ratio.

- The heat transfer surface of *the DHW reheating gas cooler unit* constituted less than 10% of the total heat transfer area of the tripartite gas cooler, but covered about 22 to 36% of the total DHW heat load during operation in the combined mode. This was due to the relatively large average temperature difference in the heat exchanger.

7.1.4.2 Design Considerations

Section 3.2.4, *Application of a Tripartite Gas Cooler*, provides a general description of the operational characteristics and design parameters for a counter-flow tripartite CO_2 gas cooler. Based on the experimental results, the following general considerations regarding the design of the tripartite gas cooler can be presented:

- *The SH gas cooler unit* should be designed for a relatively small temperature approach (e.g. ΔT_A<0.2 K) during operation in the combined mode, since the required heat transfer area in the combined mode will be larger than that of the SH mode.
- *The DHW gas cooler units* should be designed for a relatively low temperature approach (e.g. ΔT_A<2 K) during operation in the DHW mode, since the required heat transfer area in the DHW mode will be larger than that of the combined mode.
- In the combined mode, the heat transfer surface of *the DHW reheating gas cooler unit* and the inlet CO_2 temperature (i.e. the high-side pressure) govern the water flow rate in the DHW circuit. The larger the surface, the larger the DHW water flow rate.
- Due to the relatively large mean temperature difference between the CO_2 and the water in *the DHW reheating gas cooler unit*, even small changes in the heat transfer surface will have a major impact on the heating capacity and the water flow rate in the DHW circuit.
- The higher the DHW temperature, the larger the optimum heat transfer surface for *the DHW reheating gas cooler unit*.
- In the combined mode, the heat transfer surface of *the DHW preheating gas cooler unit* governs the cool-down of the CO_2 after the SH gas cooler unit.
- The lower the temperature level in the space heating system, the smaller the DHW heating capacity ratio during operation in the combined mode.
- The lower the temperature level in the DHW system, the larger the DHW heating capacity ratio during operating in the combined mode. In other words, the larger the water flow rate in the DHW circuit, the smaller the approach temperature at the cold end of *the DHW preheating and reheating gas cooler units*, and the larger the DHW heating capacity ratio.

7.2 Exergy Analysis of the Prototype CO_2 Heat Pump System

The prototype CO_2 heat pump system was analysed by means of the exergy method (ref. Section 3.2.5, *Exergy Analysis*). The main intention of the analysis was to get a better understanding of the CO_2 heat pump process and to reveal the possibilities for efficiency improvements. The exergy analysis was based on experimental data at -5ºC evaporation temperature, 33/28ºC and 40/35ºC supply/return temperatures for the space heating (SH) system and a DHW temperature of 60 and 80ºC.

The total exergy balance for the prototype CO_2 heat pump system (ref. Eq. 3.14, Section 3.2.5), showed that the total heat loss from tubing, heat exchangers and other components excluding the compressor typically ranged from 80 to 160 W. The heat loss depended on the operating mode and the average temperature level during heat rejection.

7.2.1 The Combined Mode

Figure 7.4 shows the exergy losses for the CO_2 heat pump system during operation in the combined mode at optimum high-side pressure and temperature programmes 33/28-60ºC and 40/35-80ºC. The numbers at the top of the bars represent the measured COP of the heat pump unit.

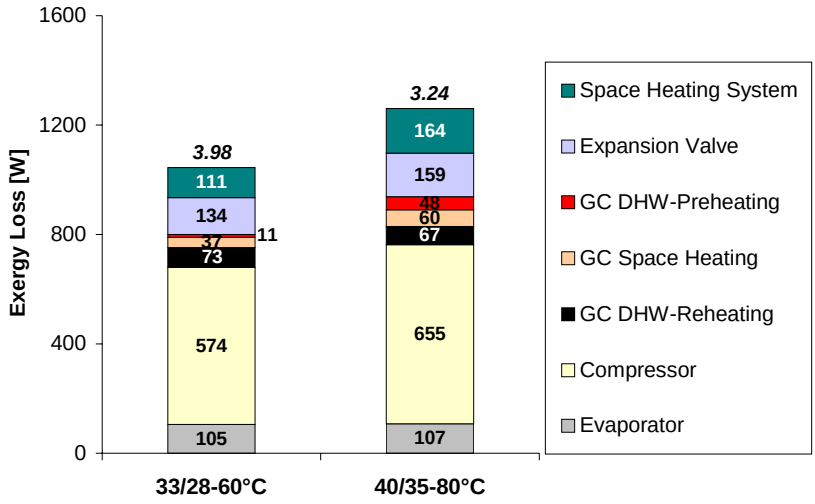

Figure 7.4 *The exergy losses for the prototype CO_2 heat pump system at optimum high-side pressure during operation in the combined mode at 33/28-60ºC and 40/35-80ºC (SH-DHW).*

- The exergy loss for *the compressor* was totally dominant, and constituted about 52 to 55% of the total exergy loss for test series. For high-efficiency state-of-the-art residential brine-to-water heat pumps, the relative compressor loss will typically be around 35 to 40% (ref. simulations with Coolpack; Rasmussen, 2001).

- The moderate exergy loss for *the expansion valve* (13%) was a result of the relatively low outlet temperature from the DHW preheating gas cooler unit (*9.8ºC* at 33/28-60ºC, *19.0ºC* at 40/35-80ºC).

- The total exergy loss for *the tripartite gas cooler* was in the same order of magnitude as the exergy loss for the expansion valve and the space heating system. The exergy loss increased by approximately 45% when the temperature program was altered from 33/28-60ºC to 40/35-80ºC. This was due to the larger mean temperature difference and the higher mean temperature level during heat rejection.

7.2.2 The DHW Mode

Figure 7.5 shows the exergy losses for the prototype CO_2 heat pump system during operation in the DHW mode at optimum high-side pressure and 60 and 80ºC DHW temperature. The numbers at the top of the bars represent the measured COP of the heat pump unit.

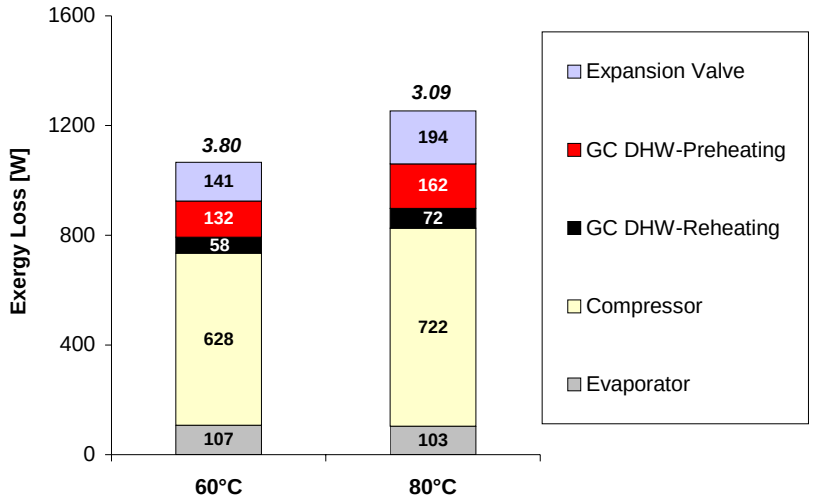

Figure 7.5 *The exergy losses for the prototype CO_2 heat pump system at optimum high-side pressure during operation in the DHW mode at 60ºC and 80ºC hot water temperature.*

- Owing to the higher discharge pressure, the exergy loss for *the compressor* was even larger than in the combined mode (approx. 58%).
- The total exergy loss for *the DHW gas cooler units* was about 15 to 55% higher than that of the combined mode. This was due to the larger mean temperature difference and the higher mean temperature level during heat rejection.
- The moderate exergy loss for *the expansion valve* (14%) was a result of the relatively low outlet temperature from the DHW preheating gas cooler unit (*8.3ºC* at 60°C DHW, *12.0ºC* at 80ºC DHW).

7.2.3 The SH Mode

Figure 7.6 shows the exergy losses for the prototype CO_2 heat pump system during operation in the SH mode at optimum high-side pressure and supply/return temperatures of 33/28ºC and 40/35ºC. The numbers at the top of the bars represent the measured COP of the heat pump unit.

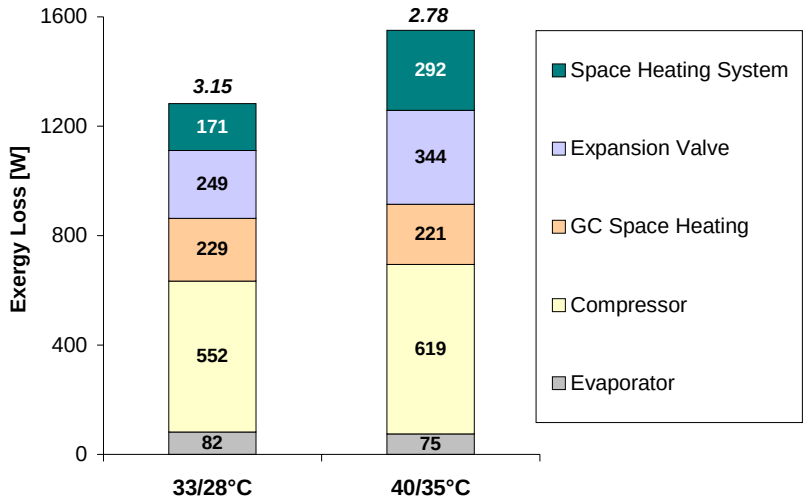

Figure 7.6 *The exergy losses for the prototype CO_2 heat pump system at optimum high-side pressure during operation in the SH mode at 33/28 and 40/35ºC supply/return temperatures.*

- The absolute exergy loss for *the compressor* was almost the same as in the combined mode due to identical discharge pressures at the same supply/return temperatures in the SH system, i.e. 8.0 MPa at 33/28-60ºC and 33/28ºC, and 9.5 MPa at 40/35-80ºC and 40/35°C.

- The relatively large exergy loss for *the expansion valve* (approx. 19 to 22%) was a result of the high outlet temperature from the SH gas cooler unit (*28.2ºC* at 33/28ºC, *35.1ºC* at 40/35ºC).
- Owing to the bad temperature fit between the supercritical CO_2 and the water, the exergy loss in *the SH gas cooler unit* was relatively large (approx. 14 to 18%). The higher the temperature level in the SH system, the larger the exergy loss.
- The relative exergy loss for *the SH system* ranged from 13 to 19%, and the higher the temperature level, the larger the exergy loss.

7.2.4 Possibilities of Efficiency Improvements

7.2.4.1 The Compressor

The exergy analysis clearly demonstrated that the prototype compressor had the largest relative exergy loss, and therefore represented the component with the largest potential for efficiency improvement. The isentropic efficiency of the prototype compressor ranged from approximately *0.52 to 0.55*, whereas the relative heat loss ranged from about *18 to 24%* (ref. Section 5.1.3.6, *Compressor Performance*). However, these values only represent rough estimates due to the large uncertainty in the oil discharge rates and the unknown effect of the oil on the power consumption.

The most energy efficient residential brine-to-water heat pumps on the market in the capacity range from about *5 to 7 kW* achieve a COP of about *4.6* and *3.3* at 0/35ºC and 0/50ºC, respectively (ref. Appendix B, *Performance Testing of Residential Brine-to-Water and Water-to-Water Heat Pumps*). By using the analysis tool *CoolPack* (Rasmussen, 2001), the isentropic efficiency of the compressor was estimated. The design parameters and the boundary conditions for the brine-to-water heat pump unit in the simulations were as follows:

- Evaporator: LMTD 3.5 K, inlet/outlet brine temperature 0/-3ºC
- Condenser: LMTD 3.5 K, inlet/outlet water temperature 25/35ºC
- Superheat: 5 K superheating of the suction gas
- Heat loss: 10% relative heat loss from the compressor
- SGHC: Suction gas heat exchanger, 70% thermal efficiency
- $\Delta T_{SL\text{-}DL}$: 0.5 K temperature drop in the suction/discharge lines

The calculated evaporation and condensation temperature was -5ºC and 35.5ºC, respectively, whereas the isentropic efficiency of the compressor was about *0.67*. The latter was approximately 12 to 14 percentage points higher than the estimated efficiency of the prototype CO_2 compressor.

The simulation model described in Section 6.1, *Modelling of CO_2 Heat Pumps Using a Tripartite Gas Cooler*, was used to calculate the COP of the prototype CO_2 heat pump unit when the isentropic efficiency was increased by 5 percentage points, and the heat loss from the compressor was reduced to 10%. The simulation results are presented in Table 7.2.

Table 7.2 The estimated COP of the prototype CO_2 heat pump unit at 5% percentage points higher isentropic efficiency and 10% relative heat loss from the compressor.

Mode – Temperature Program		Measured COP	Calculated New COP	Relative Difference
Combined mode	**35/30-60ºC**	3.89	**4.35**	|
DHW mode	**60ºC**	3.80	**4.24**	12%
SH mode	**35/30ºC**	3.01	**3.37**	|

The higher isentropic efficiency reduced the power input to the compressor, whereas the lower heat loss from the compressor shell resulted in a higher CO_2 inlet temperature for the tripartite gas cooler. All in all the improved compressor performance led to approximately 12% higher COP for the integrated CO_2 heat pump in all operating modes.

The exergy analysis and the computer simulations clearly demonstrated that *it is of particular importance for an integrated CO_2 heat pump unit to apply a high-efficiency compressor*.

7.2.4.2 The Tripartite Gas Cooler

During operation in the combined mode, the relative exergy losses for the tripartite gas cooler was as low as 12 to 14%, and increased heat transfer surfaces would only had a minor impact on the losses. This was also the case during operation in the DHW and SH mode, due to the low temperature approaches. Consequently, under the prevailing operating conditions, the tripartite gas cooler was a component with minimal potential for efficiency improvements.

7.2.4.3 The Expansion Valve

The relative exergy loss for the expansion valve during operation in the SH mode was nearly twice as high as in the combined mode and the DHW mode. This was mainly a result of the 10 to 25 K higher CO_2 outlet temperature from the tripartite gas cooler. However, at higher inlet water temperatures for the DHW preheating gas cooler unit, the relative expansion loss will be significant even in the combined mode and the DHW mode.

In addition to an optimum gas cooler design resulting in a minimum temperature approach, Lorentzen (1994) stated that methods of current interest for reducing the expansion loss in CO_2 heat pump and air conditioning systems include multiple compression and expansion, recovery of expansion work by means of an expansion turbine and installation of *a suction gas heat exchanger* (internal heat exchanger). From an economical and technical point of view, only the latter alternative represents a viable option in residential CO_2 heat pump systems.

A suction gas heat exchanger increases the temperature of the suction and discharge gas of the compressor, reduces the CO_2 mass flow rate due to lower vapour density at the compressor inlet and lessens the optimum high-side pressure. As a consequence, there will be a drop in both the gas cooler heating capacity and the compressor power input. The CO_2 heat pump simulation model (ref. Section 6.1) was used to calculate the COP of the prototype CO_2 heat pump unit during operation in the SH mode at 35/30ºC supply/return temperatures and varying suction gas temperatures. The simulations showed that *increasing superheat had a negligible effect on the COP (<1%).* Consequently, for integrated brine-to-water CO_2 heat pumps, a suction gas heat exchanger should only be installed as long as the system is equipped with a low-pressure receiver (LPR), and it is considered as necessary to evaporate the liquid droplets in the suction line. Reference is made to Appendix A2.2, *Methods of Controlling the High-Side Pressure*, for further details on LPR systems.

7.2.4.4 The Space Heating System

The exergy loss for the space heating system can only be reduced by lowering the average temperature level during heat rejection. This implies that low-temperature heat distribution systems, such as hydronic floor heating systems, fan-coils and convectors, should be used instead of radiators and other high-temperature systems (ref. Section 2.3, *Hydronic Heat Distribution Systems*).

7.3 Calculation of the Seasonal Performance Factor

7.3.1 Introduction

The seasonal performance factor (SPF) is the key parameter when evaluating the energy efficiency of residential brine-to-water and water-to-water heat pump systems for combined space heating and hot water heating. The SPF, which is defined as the ratio of the annual heat supply from the heat pump *system* and the total energy supplied, depends on a number of factors, including:

- The annual space heating and domestic hot water (DHW) demands, the maximum heat loads and load variations over the day/year.
- The sizing of the heat pump unit in relation to the maximum space heating load (monovalent/bivalent), and the requirement for supplementary heating by means of a peak load unit/system (ref. Section 2.4.2, *Design of the Heat Pump System*).
- The capability of the heat pump unit for heating DHW to the required temperature level, and the requirement for reheating of DHW (ref. Section 2.4.2).
- The coefficient of performance (COP) for the heat pump unit at varying operating conditions.
- The variations in the supply (set-point) temperature for the space heating system during the heating season.
- The set-point temperature for the DHW system.
- The temperature variations for the heat source.
- The energy consumption of pumps and auxiliary equipment.
- The control system.

The SPFs for the prototype brine-to-water CO_2 heat pump and a high-efficiency state-of-the-art residential brine-to-water R-407C/R-410A heat pump unit were estimated on the basis of constant temperature conditions for the evaporator, the space heating system and the hot water system during the heating season. With reference to Section 7.2.4.1, an improved CO_2 heat pump system with 10% higher COP than that of the prototype CO_2 system was also investigated in order to demonstrate the future potential of the integrated CO_2 heat pump system.

7.3.2 Basis of Calculations

The SPF for a monovalent or bivalent heat pump system (ref. Section 2.1, *Classification of Residential Heat Pump Systems*) is calculated as follows:

$$SPF = \frac{Q_{SH} + Q_{DHW}}{\left[Q \cdot \left(\frac{HP}{COP} + \frac{PL}{\eta}\right)\right]_{SH} + \left[Q \cdot \left(\frac{HP}{COP} + \frac{PL}{\eta}\right)\right]_{DHW}} \quad (7.1)$$

where the subscripts *SH* and *DHW* refer to the SH mode and the DHW mode, respectively, *Q* is the total annual heating demand of the residence, *PL* and *HP* represent the share of the total annual heating demand that is covered by the peak load unit and the heat pump unit, respectively (i.e. HP+PL = 1), *COP* is the average COP for the heat pump unit, and η is the average efficiency for the peak load unit(s). In a *monovalent* heat pump system, the heat pump unit covers the entire space heating demand, and auxiliary heating is not required (i.e. PL_{SH}=0).

The SPFs for the heat pump systems were calculated on the basis of *relative values* for the heating demands, and the results were presented as a function of *the seasonal DHW heating capacity ratio*. The latter is defined as the ratio of the annual heat delivered for DHW production and the total heat delivered from the heat pump unit/system.

The boundary conditions for the heat pump systems were as follows:

- Heat source — 0ºC inlet brine temperature for the evaporator
- SH system — *35/30ºC* supply/return temperature (constant)
  Bivalent system – electric peak load unit (η=1.0)
- DHW system — *10/60ºC* city water/DHW temperature (constant)
  Reheating with electric immersion heater (η=1.0)
- DHW ratio — 0 to 50%
- Peak load — The annual heat production constituted 10% of the annual space heating demand (bivalent systems)
- Pumps — Annual energy consumption not included

The measured and calculated COPs for the heat pump systems at the selected boundary conditions are presented in Table 7.3.

Table 7.3 The measured/calculated COPs for the three heat pump systems at the selected boundary conditions.

CO_2 Heat Pump Unit – Prototype[1]		
COP_{SH}	Approx. *3.0*	Space heating (SH) mode at 0/35ºC
COP_{DHW}	Approx. *3.8*	Hot water (DHW) mode at 60ºC No reheating of DHW required
COP_{COMB}[5]	Approx. *3.9*	Combined mode at 0/35ºC and 60ºC
CO_2 Heat Pump Unit – Improved Prototype[2]		
COP_{SH}	Approx. *3.3*	Space heating (SH) mode at 0/35ºC
COP_{DHW}	Approx. *4.2*	Hot water (DHW) mode at 60ºC No reheating of DHW required
COP_{COMB}[5]	Approx. *4.3*	Combined mode at 0/35ºC and 60ºC
High-Efficiency State-of-the-Art Heat Pump Unit (R-407C or R-410A)[3]		
System design	System with shuttle valve and prioritized DHW heating[4]	
COP_{SH}	Approx. *4.6*	Space heating (SH) mode at 0/35ºC
COP_{DHW}	Approx. *3.0*	Hot water (DHW) mode at 0/55ºC DHW reheating required, 13% (from 53 to 60ºC)

1) Ref. Section 5.1.3, Experimental Results

2) Ref. Section 5.1.3 and Section 7.2.4, Possibilities for Efficiency Improvements

3) Ref. Appendix B, Performance Testing of Residential Brine/Water-to-Water Heat Pumps

4) Ref. Figure 2.4, Section 2.4.2.3, Examples of System designs

5) DHW heating capacity ratio during the combined mode approx. 0.55 (ref. Figure 5.11)

In the calculations it was presupposed that the inlet water temperature to the DHW preheating gas cooler unit for the CO_2 heat pumps was identical to the city water temperature. This implies that the effect of the thermodynamic losses in the DHW tank during the tapping and charging periods was not taken into account (ref. Section 7.1.2.4).

7.3.3 Results

The estimated SPFs for the three heat pump systems during *monovalent* and *bivalent* operation are presented as a function of the seasonal DHW heating capacity ratio in Figures 7.7 and 7.8.

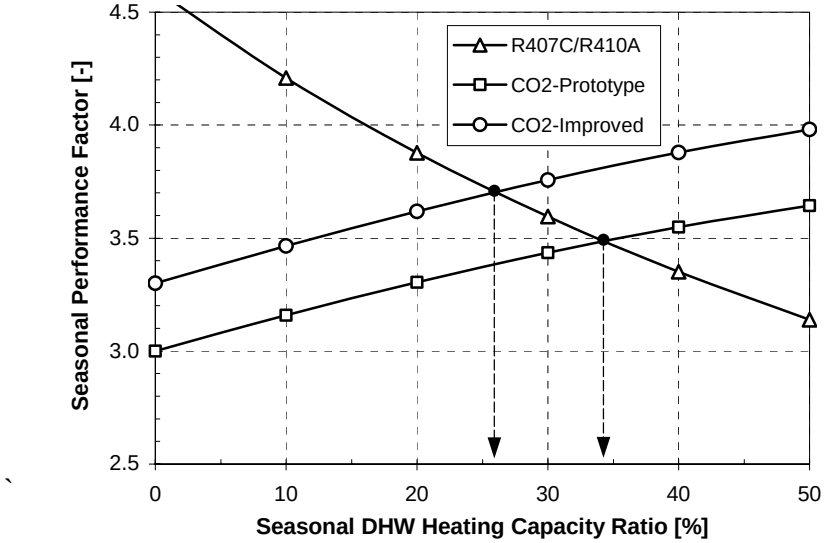

Figure 7.7 *The estimated SPF at **monovalent** operation for the high-efficiency residential state-of-the-art brine-to-water heat pump system, the prototype CO_2 heat pump system and the improved CO_2 heat pump system.*

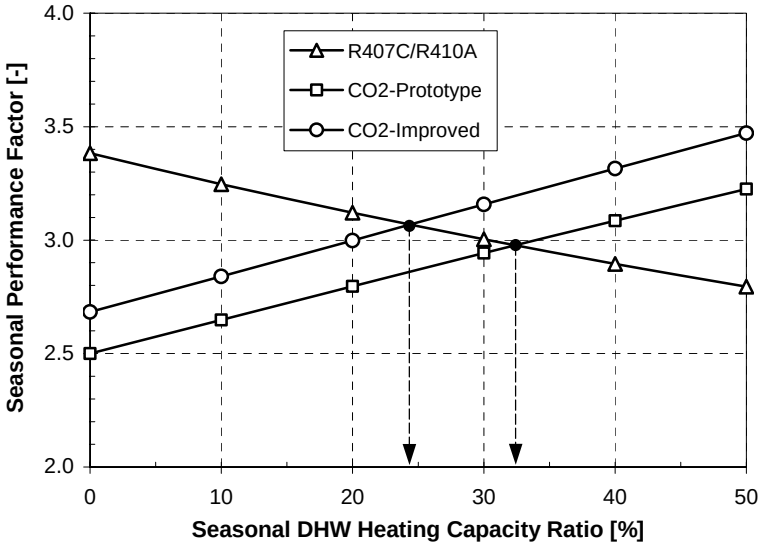

Figure 7.8 *The estimated SPF at **bivalent** operation for the high-efficiency residential state-of-the-art brine-to-water heat pump system, the prototype CO_2 heat pump system and the improved CO_2 heat pump system.*

It is important to emphasize that the SPF calculations for heat pump systems only should be regarded as rough estimates due to the simplified calculation method and the fixed boundary conditions.

At low seasonal DHW heating capacity ratios, the state-of-the-art heat pump system was considerably more energy efficiency than that of the CO_2 systems due to the poor COP of the CO_2 system during operation in the SH mode. At increasing seasonal DHW heating capacity ratios, the seasonal performance of the CO_2 systems was gradually improved, since an increasing part of the heating demand was covered by operation in the combined mode and the DHW mode. On the other hand, the SPF of the state-of-the-art heat pump systems dropped off quite rapidly at increasing seasonal DHW heating capacity ratios, since the COP during operation in the DHW mode was about 30% lower than that of the SH mode.

At the actual operating conditions, *the break-even for the prototype CO_2 system* occurred at a seasonal DHW heating capacity ratio around 35%, whereas *the break-even for the improved and more energy efficient CO_2 system* was about 10 percentage points lower. Consequently, in existing houses where the DHW ratio typically ranges from 10 to 15% (ref. Section 2.2, *Heating Demands in Houses*), a state-of-the-art brine-to-water heat pump system will be considerably more energy efficient than a brine-to-water CO_2 heat pump system for combined space heating and hot water heating. However, in new houses or in so-called low-energy houses, where the DHW ratio typically ranges from 20 to 45% (ref. Section 2.2), an optimised CO_2 heat pump system may achieve the same or higher SPF than that of the most energy efficient state-of-the-art brine-to-water heat pump systems. However, the latter presupposes that:

- The CO_2 heat pump unit covers the entire DHW heating demand, and the annual heat delivered for DHW production is minimum 25 to 30% of the total annual heat delivered from the heat pump unit.
- The CO_2 heat pump is operated in the combined heating mode when there is a simultaneous space heating and DHW heating demand.
- The CO_2 heat pump delivers heat to a space heating system with a relatively low return temperature (about 30ºC or lower).
- The city water temperature is relatively low (about 10ºC or lower), and the mixing of hot and cold water as well as the conductive heat transfer inside the DHW tank is at a low level.

8 Conclusions and Suggestions for Further Work

8.1 Conclusions

A number of conclusions can be drawn from the theoretical and experimental investigation of residential brine-to-water and water-to-water CO_2 heat pump systems for combined space heating and hot water heating – so-called integrated CO_2 heat pump systems.

8.1.1 The CO_2 Heat Pump Unit

- Residential CO_2 heat pump systems for combined space heating and hot water heating may achieve the same or higher seasonal performance factor (SPF) than the most energy efficient state-of-the-art brine-to-water heat pumps as long as:
  - The CO_2 heat pump unit covers the entire DHW heating demand, and the annual heat delivered for DHW production is minimum 25 to 30% of the total annual heat delivered from the heat pump.
  - The CO_2 heat pump unit is operated in the combined heating mode when there is a simultaneous space heating and DHW heating demand.
  - The return temperature in the hydronic space heating system is about 30ºC or lower.
  - The city water temperature is about 10ºC or lower.
  - The thermodynamic losses in the DHW storage tank are low, i.e. negligible mixing losses and minimum conductive heat transfer between the hot and cold water during tapping and charging.

- In contrary to conventional heat pump systems for combined space heating and DHW heating, the integrated CO_2 heat pump system achieves the highest COP in the combined heating mode and the DHW heating mode, and the lowest COP in the space heating mode. Hence, the larger the annual DHW heating demand, the higher the SPF of the integrated CO_2 heat pump system.

- The lower the return temperature in the space heating system and the lower the DHW storage temperature, the higher the COP of the integrated CO_2 heat pump. A low return temperature in the space heating system also results in a moderate DHW heating capacity ratio, which means that a relatively large part of the annual space heating demand can be covered by operation in the combined heating mode, where the COP is considerably higher than in the space heating mode.

- During operation in the combined heating mode and the DHW heating mode, the COP of the integrated CO_2 heat pump is heavily influenced by the inlet water temperature for the DHW preheating gas cooler unit. The lower the inlet temperature, the higher the COP. The CO_2 system will therefore achieve the highest COP at low city water temperatures, and when there is negligible mixing and minimum conductive heat transfer between the hot and cold water in the DHW tank during the tapping and charging periods.

- The COP for the integrated CO_2 heat pump is generally more sensitive to variations in the compressor efficiency than that of conventional brine/water-to-water heat pump systems. It is therefore of particular importance to apply a high-efficiency compressor.

- At each operating mode and temperature programme, there will be an optimum gas cooler (high-side) pressure that leads to a maximum COP for the integrated CO_2 heat pump. However, at moderate DHW temperatures, the heat pump can be operated at constant high-side pressure in all heating modes with only a minor reduction in the COP. This is favourable, since it simplifies the operation of the system and reduces the first cost.

- During operation in the combined heating mode, the COP for the integrated CO_2 heat pump may be higher than in the DHW heating mode due to similar temperature approaches at the cold outlet of the gas coolers and lower optimum high-side pressure. The higher the DHW temperature, the larger the COP difference for the operating modes.

- The integrated CO_2 heat pump system will be more complex than the state-of-the art residential heat pump systems due to the requirement for a tripartite gas cooler, extra valves and tubing for by-pass of fluids, an inverter controlled pump in the DHW circuit as well as an especially designed DHW storage tank. The application of optimum high-side pressure control will further increase the technical and operational complexity of the system.

8.1.2 The Domestic Hot Water Tank

- Conductive heat transfer between the DHW and the cold city water in the storage tank during the tapping and charging periods may result in a considerable increase in the inlet water temperature for the DHW preheating gas cooler. This will in turn reduce the COP of the integrated CO_2 heat pump. The thermodynamic losses are highest at large initial temperature differences for the DHW and the city water, small charging volumes and low gas cooler heating capacities. Inevitable mixing of hot and cold water in the tank will lead to further increase in the thermodynamic losses for the CO_2 heat pump system.

- One possible way to reduce internal conductive heat transfer and avoid the mixing in cylindrical single-shell DHW storage tanks, is to separate the DHW and the city water by means of a movable plate with low thermal conductivity. The concept proved to give satisfactory thermal performance and functionality at atmospheric operating conditions. However, definite conclusions regarding the functionality, thermal performance and optimum design can only be drawn after full-scale testing has been carried out in a pressurised tank. First-costs as well as the long-term reliability of the insulating plate are also important issues that need to be further addressed.

8.2 Suggestions for Further Work

On the basis of the results and conclusions from this thesis, the suggestions for further work are as follows:

- To develop a steady-state computer model for in-depth analyses and optimisation of integrated CO_2 heat pump systems, incl. calculation of the seasonal performance factor (SPF) based on hourly time steps.
- To analyse the economic viability for an integrated brine-to-water CO_2 heat pump system for residential use.
- To study the operational characteristics and performance of an integrated CO_2 heat pump system using ambient air as the heat source.
- To develop a low-cost and high-efficiency tripartite gas cooler.
- To carry out further analyses and testing of a movable insulating plate for cylindrical single-shell tanks.

Nomenclature

Symbol	Description	Unit
A	Area – heat transfer surface	m^2
C	Thermal mass ($m \cdot c_p$)	J/K
c_p	Isobaric specific heat capacity	J/(kgK)
COP	Coefficient of Performance	-
CP	Heat capacity flow rate	W/K
d	Differential	-
d, D	Diameter	m
$\dot{E}$	Exergy	W
E	Exergy	J
F	Force	N
f	Friction factor	-
g	Acceleration due to gravity	m/s^2
G	Mass flux (mass velocity)	$kg/(m^2s)$
h	Convective heat transfer coefficient	$W/(m^2K)$
h	Specific enthalpy	J/kg
H	Height	m
i	Integer number	-
k	Thermal conductivity	W/(mK)
L	Length, thickness	m
$LMTD$	Logarithmic mean temperature difference	K
M	Mass	kg
$\dot{m}$	Mass flow rate	kg/s
n	Integer number, number of moles	-
p	Pressure	Pa
P	Electric or thermal power	W
q	Heat flux	W/m^2
Q	Quantity of heat, heating demand, heat delivered	J
$\dot{Q}$	Heat flow, heat load, heating capacity	W
r	Radius	m

R	Thermal resistance	K/W
R	Universal gas constant	Nm/(g·mole·K)
s	Specific entropy	J/(kgK)
SPF	Seasonal Performance Factor	-
t	Period of time, time step	s
T	Temperature	°C, K
U	Overall heat transfer coefficient (per unit area)	$W/(m^2K)$
U^*	Overall heat transfer coefficient (per unit length)	W/(mK)
v	Specific volume	m^3/kg
v	Velocity	m/s
V	Volume	m^3
$\dot{V}$	Swept volume (compressor)	m^3/s
VRC	Volumetric refrigerating capacity	J/m^3
w	Specific compressor work	J/kg
x	Direction (x axis)	-
X	Dimensionless variable	-
y	Direction (y axis)	-
z	Direction (z axis)	-
Z	Compressability factor	-

Greek Letters

α	Thermal diffusivity	m^2/s
β	Ratio, variable	-
Δ	Difference	-
∂	Partial derivative	-
δ	Differential	-
ξ	Friction factor, ratio	-
η	Efficiency	-
θ	Temperature difference	K
γ	Dimensionless factor	-
κ	Exponent	-
μ	Dynamic viscosity	Pa·s
ν	Kinematic viscosity	m^2/s
π	Pressure ratio, 3.14	-
ρ	Density	kg/m^3
Σ	Sum	-
τ	Period of time	s

Dimensionless Numbers		
Nu	Nusselt number	-
Pr	Prandlt number	-
Re	Reynolds number	-

Subscripts	
0	Evaporator state, outdoor (air)
1	Suction state (compressor)
2	Discharge state (compressor)
A	Approach, ambient
b	Bulk
BW	Balancing weight
C	Compressor, cold fluid flow
CO2	Carbon dioxide (CO_2)
crit	Critical
CW	City water
DHW	Domestic hot water
E	Evaporator
EX	Expansion valve
GC	Gas cooler
h	Hydraulic
H	Hot fluid flow
HC	Heating capacity
HD	Heating demand
HL	Heat loss, heat load
HP	Heat pump
i	Inside, internal
in	Inlet
IP	Insulating plate
is	Isentropic
L	Laminar flow
LZ	Lorentz
m	Mean/average, minimum
M	Mixing
n	Integer number
o	Outside
opt	Optimum
out	Outlet

P	Preheating
R	Reheating
rel	Relative
S	Storage (temperature)
SG	Suction gas
SH	Space heating
T	Turbulent flow, tapping, tank
TB	Top-bottom
TC	Thermocline
Tot	Total
TR	Transition
vol	Volumetric
w	Wall
W	Water
Superscripts	
m	Exponent
n	Exponent

References

Aarlien, R., 2001: *On the Design, Efficiency, and Market Potential of Residential Air Conditioning and Heat Pump Units with CO_2 as Working Fluid*. Doctoral thesis at the Norwegian University of Science and Technology (NTNU), Faculty of Mechanical Engineering, Department of Refrigeration and Air Conditioning.

Abdoly M.A., Rapp, D., 1982: *Theoretical and Experimental Studies of Stratified Thermocline Storage of Hot Water*. Energy Conservation Mgmt. Vol. 22, pp. 275-285.

Adriansyah, W., 2001: *Combined Air-Conditioning and Tap Water Heating Plant Using CO_2 as Refrigerant for Indonesian Climate Condition.* Doctoral thesis at the Norwegian University of Science and Technology (NTNU), Faculty of Mechanical Engineering, Department of Refrigeration and Air Conditioning.

Afjei,T., 1997: *Low-Cost Low-Temperature Heating with Heat Pump Systems*. IEA Heat Pump Centre Newsletter, Vol. 15, No. 3/1997. pp. 26-28.

Banks, R.E., Sharratt, P.N., 1996: *Environmental Impacts of the Manufacture of HFC-134a*. Department of Chemistry and Department of Chemical Engineering, UMIST, Manchester, United Kingdom.

Brandes, B., Kruse, H., 2000: *High Temperature Residential Heat Pump with CO_2 as Working Fluid.* KI Luft- og Kältetechnik 7/2000. pp. 311-315.

Bredesen, A., Aflekt, K., Pettersen, J., Hafner, A., Nekså, P., Skaugen. G., 1997; *Studies of CO_2 Heat Exchangers and Heat Transfer*. IIR / IEA Heat Pump Centre workshop "CO_2 Technology in Refrigeation, Heat Pump and Air Conditioning Systems". Trondheim, Norway, May 13-14. Report HPC/WR-19, pp. 329-358.

Bredesen, A., Hafner, A., Pettersen, J., Nekså, P., Aflekt, K., 1997: *Heat Transfer and Pressure Drop for In-Tube Evaporation of CO_2.* Int. Conference on Heat Transfer Issues in Natural Refrigerants, College Park, Maryland, USA, 6-7 Nov, pp 1-15.

Breembroek, G., Dieleman, M., 2001: *Domestic Heating and Cooling Distribution and Ventilation Systems and their Use with Residential Heat Pumps*. IEA Heat Pump Centre Analysis Report HPC-AR8. ISBN 90-72741-40-8.

Bouma, J., 2002: *Heat Pumps Better by Nature, Report on the 7th IEA Heat Pump Conference, Beijing, China*. IEA Heat Pump Centre Newsletter, Vol. 20, No. 2/2002. pp. 10-27.

Dang, C., Hihara, E., 2002: *Heat Transfer Coefficient of Supercritical Carbon Dioxide*. 5th IIR-Gustav Lorentzen Conference on Natural Working Fluids. Guangzhou, China, Sept. 17-20. pp. 100-107. Preliminary proceedings.

Doorn, J.v., Oostendorp, P., 1997: *Heat Pump Competition in the Netherlands Finalised*. IEA Heat Pump Centre Newsletter, Vol. 15, No. 3/1997. pp. 16-19.

EN255-2, 1997: European Standard: *Air Conditioners, Liquid Chilling and Heat Pumps with Electrically Driven Compressors – Heating Mode – Part 2: Testing and Requirements for Marking for Space Heating Units*. European Committee for Standardisation (CEN).

Equa Simulation Technology Group, 1996: *IDA NMF Translator / IDA Solver Version 8.07.6*. Sundbyberg, Sweden.

Erb, M., Hubacher, P., 2001: *Field Analysis of Swiss Heat Pump Installations*. IEA Heat Pump Centre Newsletter, Vol. 19, No. 1/2001. pp. 15-17.

Fenghour, A., Wakeman, W., Vesovic, V., 1998: *The Viscosity of Carbon Dioxide*. J.Phys. Chem. Ref. Data 27(1), pp. 31-44.

Gilli, P.V., Streicher, W., Halozan, H., 1999: *Environmental Benefits of Heat Pumping Technologies*. IEA Heat Pump Centre Analysis Report no. HPC-AR6. ISBN 90-72741-33-5.

Gosney, W.B., 1982: *Principles of Refrigeration*. Press Syndicate of the University of Cambridge. ISBN 0-521-23671-1.

Halozan, H., Ritter, W., 1994: *Transcritical CO_2 – a New Cycle*. Austrial proposal for the working COHEPS Meeting, Trondheim, Norway.

Halozan, H., 1997: *Residential Heat Pump Systems and Controls*. IEA Heat Pump Centre Newsletter, Vol. 15, No. 3/1997. pp. 19-21.

Haukås, H.T., 1992: *Compression Cycles for Environmentally Acceptable Refrigeration, Air Conditioning and Heat Pump Systems – Thermodynamic Analysis of Heat Pumping Systems*. International Institute of Refrigeration (IIR/IIF). ISBN 2-903-633-60-6. pp. 27-64.

Hihara, E., Tanaka, S., 2000: *Boiling Heat Transfer of Carbon Dioxide in Horisontal Tubes*. 4th IIR-Gustav Lorentzen Conference on Natural Working Fluids at Purdue. July 25-28, Purdue University, Indiana, USA. pp. 290-296. ISBN 2-913149-16-2.

Homan, K.O., Sohn, C.W., Soon, S.I., 1996: *Thermal Performance of Stratified Chilled Water Storage Tanks*. HVAC&R Research. Vol. 2, No. 2, pp. 158-169.

Hubacher, B., Groll, E.A., 2002: *Measurement of Performance of Carbon Dioxide Compressors*. ARTI report no. ARTI-21CR/611-10070-01. Prepared at the Ray W. Herrick Laboratories, USA.

Hwang, Y., Radermacher, T., 1998: *Experimental Evaluation of a CO_2 Water Heater*. IIR/IIF Conference ”Natural Working Fluids ’98”. Oslo, Norway, June 2-5. pp. 368-375. ISBN 2-903633-97-5.

Høiax AS, 2003. Product information from a Norwegian manufacturer of domestic hot water tanks. *www.hoiax.no*.

Incropera, F.P., DeWitt, D.P., 2001: *Introduction to Heat Transfer*. 4th edition. John Wiley & Sons, New York. ISBN 0-471-38649-9.

Kerherve, B., Clodic, D., 2002: *Energy Efficiency Comparisons for Heat Pump Working with CO_2 and R-407C*. 5th IIR-Gustav Lorentzen Conference on Natural Working Fluids. Guangzhou, China, Sept. 17-20. pp. 237-244. Preliminary proceedings.

Klöcker, K., Flacke, N., Schmidt, E.L., 1998: *Energetische Bewertung konventioneller und transcritischer Kaltdampfkompressionsprozesse*. Report - Kohlendioxid, Besonderheiten und Einsatzchancen als Kältemittel, Statusbericht des DKW No. 20, Germany, pp. 88-100. ISBN 3-932715-00-4.

Kreith, F., Black, W.Z., 1980: *Basic Heat Transfer*. Harper & Row Publishers, New York. ISBN 0-700-22518-8.

Kruse, H., Heidelck, R., Süss, J., 1999: *The Application of CO_2 as Refrigerant*. Review article in the IIR/IIF (International Institute of Refrigeration) Bulletin 99.1.

Linnhoff, B., Townsend, D.W., Boland, D., Hewitt, G.F., Thomas, B.E.A., Guy, A.R., Marsland, R.H., 1984: *A User Guide in Process Integration for the Efficient Use of Energy*. The Institution of Chemical Engineers, England. ISBN 0-85295-156-6.

Lorentzen, G., 1990: *Trans-Critical Vapour Compression Cycle Device*. International Patent Publication WO 90/07683.

Lorentzen, G., Pettersen, J., 1993: *A New, Efficient and Environmentally Benign System for Car Air Conditioning*. International Journal of Refrigeration. Vol. 16, No. 1, pp. 4-12, 1993.

Lorentzen, G., 1994: *Revival of Carbon Dioxide as a Refrigerant*. International Journal of Refrigeration. Vol. 17, No. 5, pp.292-301.

Melinder, Å., 1997: *Thermophysical Properties of Liquid Secondary Refrigerants*. International Institute of Refrigeration.

Nekså, P., Rekstad, H., 1998: *CO_2 Heat Pump Prototype System – Experimental Results.* IIR / IEA Heat Pump Centre workshop "CO_2 Technology in Refrigeration, Heat Pump and Air Conditioning Systems". Trondheim, Norway, May 13-14. Report HPC/WR-19, pp. 201-216.

Nekså, P., Rekstad, H., Zakeri, G.R., Schiefloe, P.A., 1998: *CO_2 Heat Pump Water Heaters – Characteristics, System Design and Experimental Results*. International Journal of Refrigeration. Vol. 21, No. 3, pp. 172-179.

NIST – National Institute of Standards and Technologies, 2000: *Thermophysical Properties of Fluid Systems.* Gaithersburg, USA.

Novakovic, V., 1996: *Energy Conservation in Buildings – Efficient Use of Energy*. 2nd ed. Universitetsforlaget, Oslo. ISBN 82-00-42307-7.

Nowacki, J.E., 2002: *Single-Room Heat Pumps for Cold Climates*. IEA Heat Pump Centre Analysis Report. no. HPC-AR14. ISBN 90-73741-46-7.

Nozomi, I., 1986: *Temperature Stratification Type Heat Storage Tank*. Japanese patent JP61066088.

Oostendorp, P., Traversari, R., 2000: *Improving Heat Pump System Quality in the Netherlands*. IEA Heat Pump Centre Newsletter, Vol. 19, No. 2/2000. pp. 13-15.

Oppel, F.J., Ghajar, A.J., Moretti, P.M., 1986: *Computer Simulation of Stratified Heat Storage*. Applied Energy. Vol. 21, pp. 205-224.

Oso Hotwater, 2003. *Product information*, http://www.oso-hotwater.com/.

Pettersen, J., Skaugen, G., 1994: *Operation of Trans-Critical CO_2 Vapour Compression Circuits in Vehicle Air Conditioning*. IIR/IIF Conference "New Applications of Natural Working Fluids in Refrigeration and Air Conditioning". Hannover, Germany, May 10-13. pp. 495-505. ISBN 2-903-633-68-1.

Pettersen, J., Aarlien, R., 1997: *Progress in CO_2 Vapour Compression Systems*. 45th Oji International Seminar – New Approach Towards Low Temperature Thermal Engineering without Fluorocarbon Refrigerants. Tamakomai, Hokkaido, Japan.

Pettersen, J., Hafner, A., Skaugen, G., 1998: *Development of Compact Heat Exchangers for CO_2 Air Conditioning Systems*. International Journal of Refrigeration. Vol. 21, No. 3, pp. 180-193.

Pettersen, J., Hafner, A., Brånås, M., 2000: *Some Safety Aspects of CO_2 Vapour Compression Systems*. IEA Heat Pump Programme Annex 27. Workshop on Selected issues on CO_2 as Working Fluid in Compression Systems. Trondheim, Norway, Sept. 19-20.

Pettersen, J., Rieberer, R., Munkejord, S.T., 2000: *Heat Transfer and Pressure Drop Characteristics of Evaporating Carbon Dioxide in Microchannel Tubes*. 4th IIR-Gustav Lorentzen Conference on Natural Working Fluids at Purdue. July 25-28, Purdue University, Indiana, USA. pp. 324-332. ISBN 2-913149-16-2.

Pettersen, J., 2002: *Flow Vaporisation of CO_2 in Microchannel Tubes. Part 2: Heat Transfer, Pressure Drop and Correlations*. 5th IIR-Gustav Lorentzen Conference on Natural Working Fluids. Guanzhou, China, Sept. 17-20. pp. 84-91. Preliminary proceedings.

Pitla, S.S., Groll, E.A., Ramadhyani, S., 2000: *New Correlation for the Heat Transfer Coefficient During In-Tube Cooling of Turbulent Supercritical Carbon Dioxide*. 4th IIR-Gustav Lorentzen Conference on Natural Working Fluids at Purdue. July 25-28, Purdue University, Indiana, USA. pp. 270-278. ISBN 2-913149-16-2.

Poulsen, C.S., 2001: *CO_2 as Refrigerant in Heat Pumps*. 16th Nordic Refrigeration Conference and 9th Nordic Heat Pump Days. Copenhagen, Denmark.

Rasmussen, B.D., 2001: *Coolpack version 1.46* – A collection of simulation programs for designing, dimensioning, analysing and optimising refrigerating and heat pump plants. The Technical University of Denmark, Department of Mechanical Engineering.

Richter, M.R., Song, S.M., Yin, J.M., Kim, H., Bullard, C.W., Hrnjak, P.S., 2000: *Transcritical CO_2 Heat Pump for Residential Application*. 4th IIR-Gustav Lorentzen Conference on Natural Working Fluids at Purdue. July 25-28, Purdue University, Indiana, USA. pp. 59-67. ISBN 2-913149-16-2.

Rieberer, R., Halozan, H., 1997: *CO_2 Heat Pump Water Heater, Simulation and Test Results*. IIR/IIF Conference in Graz, Austria.

Rieberer, R., Kasper, R., Halozan, H., 1997: *CO_2 – A Chance for Once-Through Heat Pump Heaters*. IIR / IEA Heat Pump Centre workshop "CO_2 Technology in Refrigeration, Heat Pump and Air Conditioning Systems". Trondheim, Norway, May 13-14. Report HPC/-WR-19, pp. 193-200.

Rieberer, R., Halozan, H., 1997: *Design of Heat Exchangers for CO_2 Heat Pump Water Heaters*. International Conference on Heat Transfer Issues in Natural Refrigerants, College Park, Maryland, USA, 6-7 Nov, pp 75-82.

Rieberer, R., Halozan, H., 1998: *CO_2 Heat Pumps in Controlled Ventilation Systems*. IIR/IIF Conference "Natural Working Fluids '98". Oslo, Norway, June 2-5. pp. 212-222. ISBN 2-903633-97-5.

Rieberer, R., Nekså, P., Aarlien, R., 1998: *Heat Pumps* - Report - Kohlendioxid, Besonderheiten und Einsatzchancen als Kältemittel, Statusbericht des DKW No. 20, Germany, pp. 195-206.

Rieberer, R., Gassler, M., Halozan, H., 2000: *Control of CO_2 Heat Pumps*. 4th IIR-Gustav Lorentzen Conference on Natural Working Fluids at Purdue. July 25-28, Purdue University, Indiana, USA. pp. 109-116. ISBN 2-913149-16-2.

RnLib, 2003: *Thermodynamic and Transport Properties of Refrigerants and Refrigerant Mixtures*. SINTEF Energy Research, Department of Energy Processes, Norway.

Rodriguez, I., Consul, R., Oliva, A., 2002: *Thermal Optimisation of Storage Tanks by Means of Three-Dimensional CFD Simulations*. International Forum for Renewable Energy. Tétouan, Marocco.

Saikawa, M., Hashimoto, K., 2000: *Development of Prototype CO_2 Heat Pump Water Heater for Residential Use*. 4th IIR-Gustav Lorentzen Conference on Natural Working Fluids at Purdue. July 25-28, Purdue University, Indiana, USA. pp. 97-108. ISBN 2-913149-16-2.

Sahlin, P., 1996: *NMF Handbook – An Introduction to the Neutral Model Format*. ASHRAE RP-839. KTH, Stockholm, Sweden.

Shin, M.S., Kim, H.S., Jang, D.S., Lee, S.N., Lee, Y.S., Yoon, H.G., 2003: *Numerical and Experimental Study on the Design of Stratified Thermal Storage Systems*. Applied Thermal Engineering. Vol. 24, No. 1, pp. 17-27.

Skaugen, G., 2002: *Investigation of Transcritical CO_2 Vapour Compression Systems by Simulation and Laboratory Experiments*. Doctoral thesis at the Norwegian University of Science and Technology (NTNU), Faculty of Engineering Science and Technology, Department of Energy and Process Engineering.

Span, R., Wagner, W., 1996: *A New Equation of State for Carbon Dioxide Covering the Region from the Triple-Point Temperature to 1100 K at Pressures up to 800 MPa*. Journal of Physical Chemistry. Ref. Data 25 (6), pp. 1509-1596.

Stene, J., 1998: *Guidelines for Design and Operation of Compression Heat Pump, Air-Conditioning and Refrigerating Systems with Natural Working Fluids – Section 6, Carbon Dioxide as Working Fluid*. IEA Heat Pump Programme Report No. HPP-AN22-4. ISBN 90-73741-31-9.

Stoecker, W.F., 1989: *Design of Thermal Systems, 3rd edition*. McGraw-Hill, Inc. ISBN 0-07-061620-5.

Sun, Z., Groll, E.A., 2002: CO_2 *Flow Boiling Heat Transfer in Horizontal Tubes. Part II – Experimental Results*. 5th IIR-Gustav Lorentzen Conference on Natural Working Fluids. Guanzhou, China, Sept. 17-20. pp. 127-141. Preliminary proceedings.

Süss, J., Kruse, H., 1998: *Efficiency of the Indicated Process of CO_2-Compressors*. International Journal of Refrigeration. Vol. 21, No. 3, pp. 194-201.

Tadano, M., Ebara, T., Oda, A., Susai, T., Takizawa, K., Izaki, H. Komatsubara, T., 2000: *Development of the CO_2 Hermetic Compressor (Sanyo)*. 4th IIR-Gustav Lorentzen Conference on Natural Working Fluids at Purdue. July 25-28, Purdue University, Indiana, USA. pp. 335-342. ISBN 2-913149-16-2.

Thomas, G.B., Finney, R.L., 1982: *Calculus and Analytical Geometry*. Addison-Wesley Publishing Company Ltd. ISBN 0-201-07523-7.

UNEP – United Nations Environment Programme, 1998: *Montreal Protocol on Substances that Deplete the Ozone Layer – 2003 Report of the Refrigeration, Air Conditioning and Heat Pumps Technical Options Committee*.

USHA - United Department of Labour, Occupational Safety & Health Accumulation, 2003: *http://www.osha.gov/SLTC/etools/legionnaires/hotwater.html.*

Van Doorn, J., Oostendorp, P., 1997: *Heat Pump System Competition in the Netherlands Finalised*. IEA Heat Pump Centre Newsletter, 3/1997, pp 16-19.

VDI Heat Atlas (VDI Värme Atlas), 1993: VDI-verlag GmbH, Düsseldorf. ISBN 3-18-400915-7.

Vesovic, V., Wakeham, W., Olchowy, G., Sengers, J., Watson, J., Millat, J., 1990: *The Transport Properties of Carbon Dioxide*. J. Phys. Chem. Ref. Data 19 (3), pp. 763-808.

Woodson, R.D., 1999: *Radiant Floor Heating.* McGraw-Hill. ISBN 0-07-134786-0.

Yanagisawa, T., Fukuta, M., 2000: *Basic Operating Characteristics of Reciprocating Compressor of CO_2 Cycle (Denso)*. 4th IIR-Gustav Lorentzen Conf. on Natural Working Fluids at Purdue. July 25-28, Purdue University, Indiana, USA. pp. 343-349. ISBN 2-913149-16-2.

Yin, J., Park, Y.C., Boewe, D., McEnaney, R. Beaver, A., Bullard, C.W., Hrnjak, P.S, 1998: *Experimental and Model Comparison of Transcritical CO_2 Versus R-134a and R-410 System Performance*. IIR/IIF Conference ”Natural Working Fluids ’98”. Oslo, Norway, June 2-5. pp. 376-389. ISBN 2-903633-97-5.

Yoon, S.H., Kim, J.H, Hwang, J.H., Kim, M.S., Min, K., Kim, Y., 2003: *Heat Transfer and Pressure Drop Characteristics During In-Tube Cooling Process of Carbon Dioxide in the Supercritical Region*. International Journal of Refrigeration. Vol. 26, pp. 857-864.

Yun, R., Choi, C., Kim, Y., 2002: *Convective Boiling Heat Transfer of Carbon Dioxide in Horizontal Small Diameter Tubes*. 5th IIR-Gustav Lorentzen Conference on Natural Working Fluids. Guanzhou, China, Sept. 17-20. pp. 299-308. Preliminary proceedings.

Zingerli, A.P., Groll, E.A., 2000: *Influence of Refrigeration Oil on the Heat Transfer and Pressure Drop of Supercritical CO_2 During In-Tube Cooling*. 4th IIR-Gustav Lorentzen Conference on Natural Working Fluids at Purdue. July 25-28, Purdue University, Indiana, USA. pp. 279-289. ISBN 2-913149-16-2.

APPENDICES

Appendix A

CO_2 as a Working Fluid in Heat Pumps

Appendix B

Performance Testing of Residential Brine-to-Water and Water-to-Water Heat Pumps

Appendix C

Test Results for the Prototype CO_2 Heat Pump

Appendix D

Uncertainty Analysis of the Measurements for the Prototype CO_2 Heat Pump

Appendix E

Photos of the Prototype CO_2 Heat Pump

Appendix F

Characteristic Properties of DHW Systems

Appendix G

Application of a Movable Insulating Plate in Cylindrical Single-Shell DHW Tanks

Appendix H

Test Conditions for the Prototype Movable Insulating Plates

Appendix I

The Transient Two-Dimensional Tank Model

Appendix A
CO_2 as a Working Fluid in Heat Pumps

The physical and thermophysical properties of the working fluid are of vital importance when designing the next generation of energy efficient and environmentally friendly residential heat pump systems. The properties affect the selection of the thermodynamic process, component and system design, control strategies as well as issues related to the local safety of the installation.

This appendix provides a presentation on the use of *carbon dioxide* (CO_2, R-744) as a working fluid in heat pumps. Important physical and thermophysical properties of CO_2 are discussed, focusing on the main design parameters, operational characteristics as well as compressor and heat exchanger performance for residential systems. The last part of the appendix elaborates on the supercritical heat rejection process in the gas cooler, where the high-side pressure plays a key role regarding the heating capacity and the coefficient of performance (COP) of the heat pump.

All calculations in the appendix have been performed by means of Microsoft Excel. The Span and Wagner (1996) equation of state was used for the thermodynamic properties of CO_2, whereas the thermal conductivity and dynamic viscosity were calculated from Vesovic et al. (1990) and Fenghour et al. (1998), respectively.

A1 Physical and Thermophysical Properties

CO_2 is an environmentally friendly[1] working fluid with unique physical and thermophysical properties, which has been identified as an interesting long-term alternative to conventional working fluids (Lorentzen and Pettersen, 1993). Table A1 shows some important physical and thermophysical properties of CO_2, propane (R-290) and HFCs that are commonly used in residential heat pumps.

[1] *CO_2 is a non-flammable and non-toxic substance. CO_2 does not deplete the ozone layer (i.e ODP = 0), and the Global Warming Potential (GWP) is zero since it is surplus CO_2 from industry that is being used as a working fluid (i.e. no generation of CO_2).*

Table A1 Important physical and thermophysical properties of CO_2, propane (R-290) and selected HFCs (RnLib, 2003).

Property	**CO_2**	**R-290**	**R-407C[3]**	**R-410A**	**R-134a**
Molar mass [kg/kmol]	*44.01*	44.10	86.20	72.59	102.03
Normal boiling point [ºC]	*-78.4[1]*	-42.1	-43.8	-51.6	-26.2
Critical temperature [ºC]	*31.1*	96.8	87.3	72.5	101.1
Critical pressure [MPa]	*7.38*	4.25	4.63	4.95	4.07
Saturation pressure at 0ºC [MPa]	*3.49*	0.48	0.57	0.80	0.29
Δh at 0ºC [kJ/kg][2]	*231*	375	209	221	199
Density, sat. liquid at 0ºC [kg/m^3]	*928*	493	1237	1171	1295
Density, sat. vapour at 0ºC [kg/m^3]	*97.8*	10.3	19.7	30.5	14.4

1) *Sublimation temperature. Triple point at -56.6 ºC and 0.518 MPa*
2) *Specific enthalpy of evaporation*
3) *The mean of the bubble point and dew point has been used as the datum temperature*

A1.1 High Operating Pressure

CO_2 has an especially high critical pressure and low critical temperature. As a consequence, the operating pressure in CO_2 heat pump systems will typically be 5 to 10 times higher than that of plants using propane or HFCs. This is demonstrated in Figure A1 on the following page, which compares the pressure-enthalpy diagrams of CO_2 and HFC-134a. At 4.07 MPa, which is the critical pressure or HFC-134a, the saturation temperature of CO_2 is only 5.3ºC.

A1.2 Heat Rejection at Supercritical Pressure

Due to the low critical temperature (31.1ºC), most CO_2 heat pumps will have to operate in a so-called *transcritical cycle* (Lorentzen, 1990). This means that the CO_2 absorbs heat from the heat source at *subcritical* pressure, and gives off heat above the critical point at *supercritical* pressure (high-side pressure). Unlike conventional subcritical heat pump cycles, the heat is not given off by means of condensation of the fluid in a condenser but by cooling of the high-pressure CO_2 gas in a *gas cooler*. The temperature drop for the CO_2 gas during heat rejection is denoted *the temperature glide*.

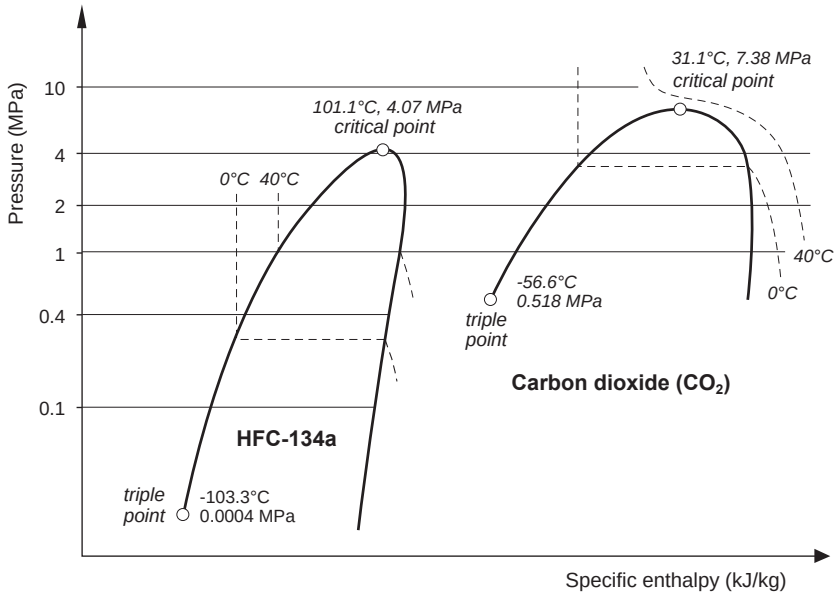

Figure A1 Comparison of the pressure-enthalpy diagrams for R-134a (HFC-134a) and CO_2 (RnLib, 2003).

Figure A2 illustrates the transcritical CO_2 heat pump cycle in a pressure-enthalpy diagram.

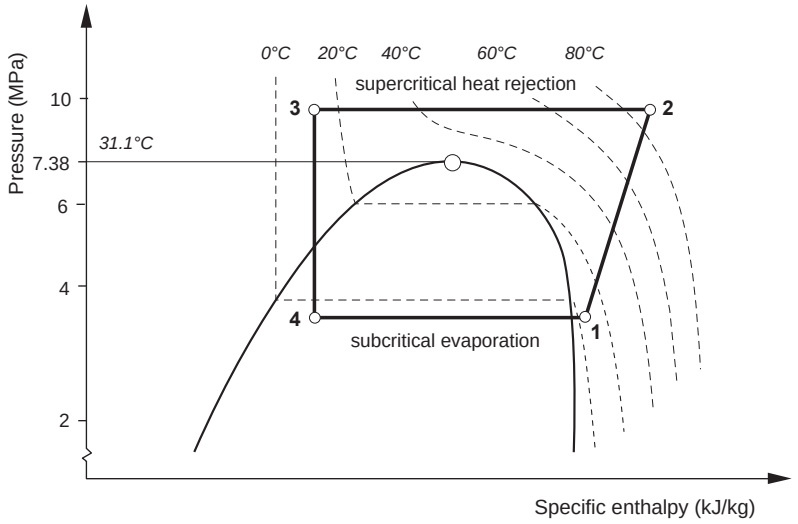

Figure A2 Principle of the transcritical CO_2 cycle: 1-2 compression, 2-3 supercritical heat rejection with temperature glide, 3-4 throttling, and 4-1 subcritical evaporation.

A1.3 Mass Flow Rate and Pressure Drop vs Dimensions of Pipelines and Components

The mass flow rate in a heat pump system, which affects the required dimensions of components and piping, is inversely proportional to the specific enthalpy of evaporation of the working fluid. Since CO_2 has a relatively large specific enthalpy of evaporation (Table A1), the required mass flow rate in a CO_2 heat pump at 0ºC evaporation temperature is about 5 to 15% lower than that of plants using HFCs. The moderate mass flow rate in combination with the steep saturation pressure curve (Section A1.6) leads to higher optimum flow velocities and smaller dimensions of components and pipelines than that of heat pump systems using HFC working fluids. This is also the case when comparing a CO_2 system to a propane system, since the considerably steeper saturation pressure curve of CO_2 is dominant to the roughly 60% lower mass flow rate in the propane system.

A1.4 Required Compressor Volume

The required compressor volume to produce a certain refrigerating or heating capacity is roughly inversely proportional to the suction pressure (Lorentzen and Pettersen, 1993). Due to the very high vapour density of CO_2, the volumetric refrigerating capacity VRC (Gosney, 1982) is considerably higher than that of propane and the HFCs. As an example, the required swept volume for a reciprocating CO_2 compressor at 0ºC suction gas temperature is in the order of 35 to 85% lower than that of compressors designed for propane and HFC working fluids.

A1.5 Compressor Performance

Compressors in CO_2 heat pump systems will operate at high mean pressures with large pressure differentials, and the latter will typically range from 5 to 10 MPa. However, the pressure ratio, which heavily affects the volumetric and energy efficiencies of the compressor, will be lower than that of conventional working fluids. Table A2 shows, as an example, typical pressure ratios for CO_2, propane and selected HFCs at -10 and 0ºC evaporation temperature and 35 and 50ºC condensation temperature. The high-side pressures for the CO_2 system are 9 and 11 MPa (RnLib, 2003).

Table A2 Pressure ratios for CO_2, propane and some HFCs at various evaporation and condensation temperatures (RnLib, 2003).

T_0	T_C	CO_2	R-290	R-407C	R-410A	R-134a
-10°C	35ºC	*3.4 (9 MPa)*	3.6	4.2	3.7	4.4
-10°C	50ºC	*4.2 (11 MPa)*	5.0	6.2	5.3	6.6
0°C	35ºC	*2.6 (9 MPa)*	2.6	2.9	2.7	3.0
0°C	50ºC	*3.2 (11 MPa)*	3.6	4.3	3.8	4.5

Süss and Kruse (1998) concluded that the heat transfer and pressure losses in reciprocating CO_2 compressors have a negligible influence on the volumetric and isentropic efficiencies due to the low pressure ratio, and that internal leakages caused by the considerable pressure differentials could be reduced to a low level by means of appropriate design.

Pettersen and Aarlien (1997) found that a reciprocating car air-conditioning CO_2 compressor typically obtained 10 to 15 percentage points higher isentropic efficiency than an R-134a compressor at equal operating conditions. Tadano et al. (2000), Yanagisawa and Fukuta (2000), and Hubacher and Groll (2002) demonstrated by means of measurements the superior performance of several types of CO_2 compressors for residential use.

A1.6 Heat Exchanger Performance

Pressure Drop

CO_2 has a considerably steeper saturation pressure curve than that of the commonly used working fluids. Figure A3 shows the slope of the saturation pressure curve ($\partial T/\partial p$) for CO_2, propane and selected HFCs. As a result, the optimum mass flow rate in CO_2 heat exchangers will be higher than that of equipment designed for propane or HFCs.

Evaporation

Table A3 shows thermophysical properties for CO_2, propane and selected HFCs that are important for the convective evaporation and nucleate boiling processes (RnLib, 2003). The data are presented as average relative values for the temperature range from -10 to +10ºC, and CO_2 is the reference (=1.0). Since the data are provided for a 20 K temperature span they should only be regarded as approximate values.

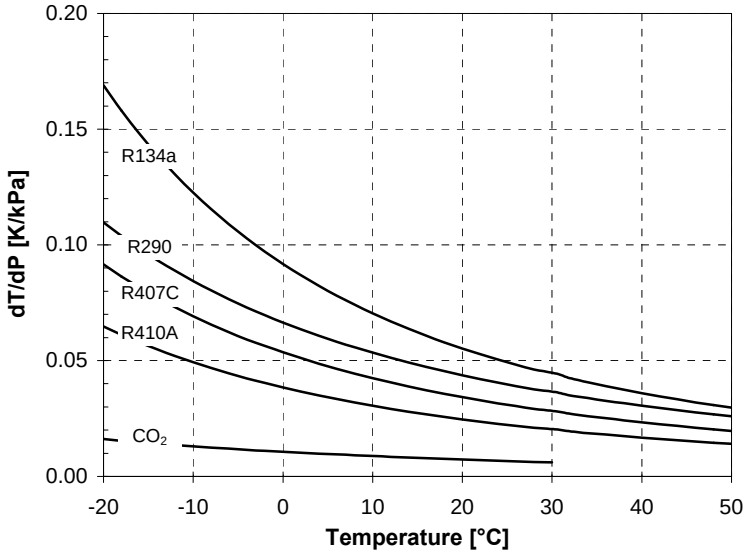

Figure A3 The slope of the saturation pressure curve ($\partial T/\partial p$) for CO_2, propane and selected HFCs (RnLib, 2003).

Table A3 Average relative values of thermophysical properties at saturated state for CO_2, propane (R-290) and selected HFCs for the temperature range from -10 to +10ºC (RnLIb, 2003).

Property		**CO_2**	**R-290**	**R-407C**	**R-410A**	**R-134a**
Thermal conductivity	liquid	*1.0*	0.95	0.87	0.90	0.86
	vapour	*1.0*	0.72	0.59	0.61	0.53
Dynamic viscosity	liquid	*1.0*	1.24	1.98	1.59	2.65
	vapour	*1.0*	0.53	0.81	0.82	0.88
Specific heat capacity	liquid	*1.0*	1.01	0.56	0.60	0.51
	vapour	*1.0*	0.83	0.42	0.56	0.46
Density	liquid	*1.0*	0.53	1.33	1.27	1.40
	vapour	*1.0*	0.10	0.19	0.31	0.15
Ratio of liquid/vapour density		*1.0*	5.04	6.98	4.08	9.58
Surface tension	liquid	*1.0*	1.92	1.82	1.60	2.04

Table A4 presents some examples of measured heat transfer coefficients for flow boiling CO_2 in horizontal round tubes (RT) and microchannel tubes (MPE) for automotive and *residential applications*.

Table A4 Measured heat transfer coefficients (h_{CO2}) for flow boiling CO_2 in horizontal round tubes (RT) and microchannel tubes (MPE) at various operating conditions.

Authors	ID Tube [mm]	T_0 [°C]	M [kg/(m²s)]	q [kW/m²]	h_{CO2} 1) [kW/(m²K)]
Hihara/Tanaka (2000)	1 (RT)	15	360-1440	9-15	8-23
Bredesen et al. (1997)	2 (RT)	-10 to 5	200-400	6 – 9	6-16
Yun et al. (2002)	1-2 (RT)	0 to 10	500-3570	7-48	10-20
Sun/Groll (2002)	4.5 (RT)	-2 to 10	500-1670	10-50	6-11
Bredesen et al. (1997)	7 (RT)	-25 to 5	200-400	3-9	4-14
Pettersen (2002)	0.8 (MPE)	0 to 25	190-570	5-20	8-25

1) Pre dry-out heat transfer coefficients. Post dry-out heat transfer coefficients typically ranged from 1500 to 3000 W/(m²K).

The following observations and conclusions can be drawn with reference to Tables A3 and A4:

- The flow boiling heat transfer coefficient for pure CO_2 typically ranged from 6 to 20 kW/(m²K), and the smaller the tube diameter the higher the value. However, the effects of lubricant on heat transfer needs to be further investigated since lubricant may have considerable influence on the convective evaporation and nucleate boiling processes (Pettersen, 2002).

- Due to the small surface tension of pure CO_2, *nucleate boiling* was the dominating heat transfer mechanism at low and moderate vapour fractions ($x<0.5$). Hence, the heat transfer coefficient was mainly a function of the heat flux and the evaporation temperature rather than variations in the mass flux and the vapour fraction.

- For the small diameter tubes (ID<4.5 mm), the average heat transfer coefficients were significantly affected by the existence of a *liquid film dry-out*. The probable reason for the dry-out phenomena is that the liquid film breaks down due to the low surface tension and the increased vapour velocity, and the liquid becomes entrained as droplets in the gas core of the flow (Pettersen, 2002).

- The *critical vapour quality* where dry-out occurred, typically ranged from 0.3 to 0.6 for the small diameter tubes, and the critical quality was strongly dependent on the mass flux. For the test with the ID 7 mm tubes, the critical vapour quality was about 0.9.
- The post *dry-out heat transfer coefficients* were typically 5 to 10 times lower than the pre dry-out values, i.e. 1000 to 3000 W/(m^2K).
- Pettersen (2002) recommended that compact evaporators (MPE) for unitary applications should be designed for a low mass flux, since increased mass flux leads to an early dry-out and does not improve heat transfer in the pre dry-out region.

Supercritical Heat Rejection

At supercritical pressures, the thermophysical properties of CO_2 have a strong temperature and pressure dependency, which in turn affects the Reynolds and Prandtl numbers and because of that the local single-phase heat transfer coefficient in the gas cooler. Figure A4 shows the specific heat capacity and the density of CO_2 at supercritical pressures ranging from 8 to 12 MPa, whereas Figure A5 shows the dynamic viscosity and the thermal conductivity at the same pressure levels (RnLib, 2003).

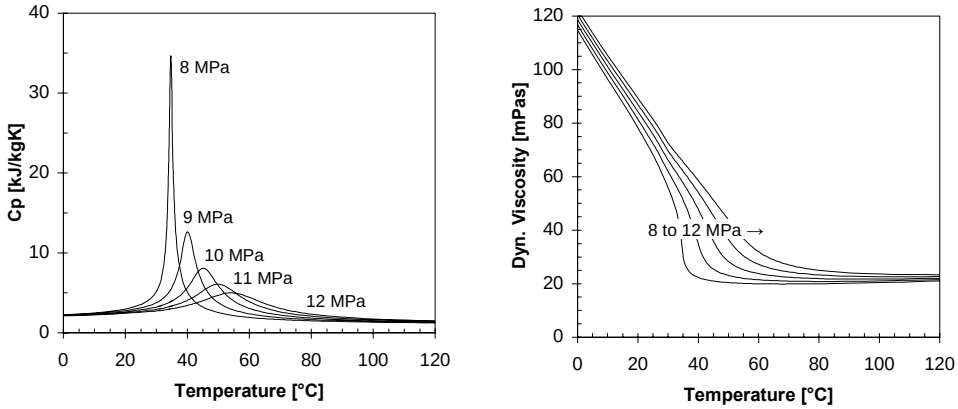

Figure A4 The specific heat capacity and density of CO_2 at supercritical pressures ranging from 8 to 12 MPa (RnLib, 2003).

Figure A6 shows, as an example, the calculated convective heat transfer coefficient for in-tube cooling of supercritical CO_2 in an ID 6 mm round tube. The calculations are based on the commonly used Gnielinski correlation for single-phase flow (VDI, 1993), and the mass fluxes are 900 and 1200 kg/(m^2s). The effects of lubricant are not included.

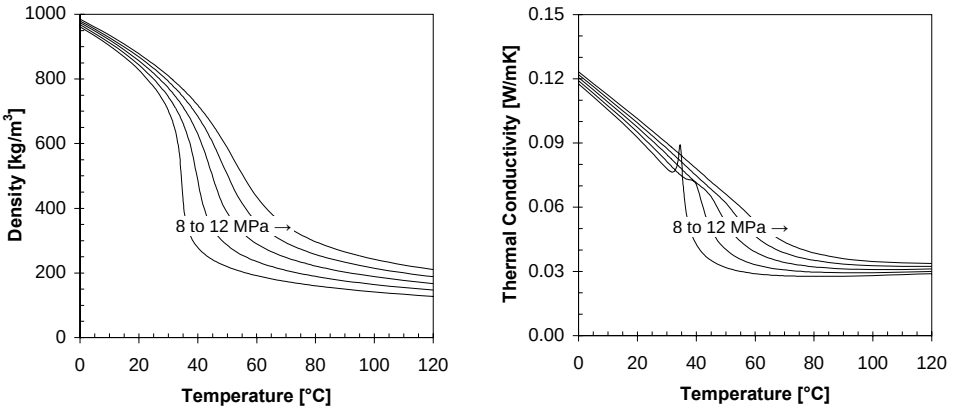

Figure A5 *The dynamic viscosity and thermal conductivity of CO_2 at supercritical pressures ranging from 8 to 12 MPa (RnLib, 2003).*

The peak values of the convective heat transfer coefficient occur at the pseudo-critical temperature, where the specific heat capacity reaches its maximum (ref. Figure A4). Figure A6 clearly demonstrates that a higher mass flux results in a higher heat transfer coefficient.

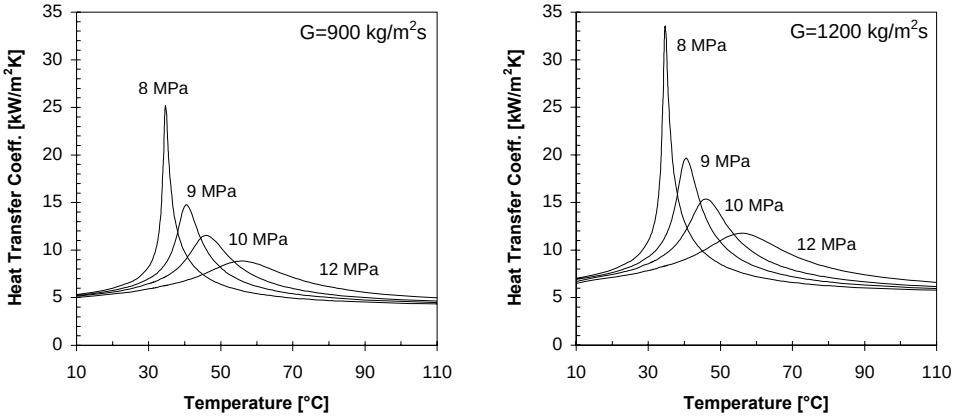

Figure A6 *The convective heat transfer coefficient for in-tube cooling of supercritical CO_2 in an ID 6 mm round tube, calculated by means of the Gnielinski correlation (VDI, 1993).*

Table A5 presents some examples of measured convective heat transfer coefficients during in-tube cooling of pure supercritical CO_2 in round tubes (RT) and microchannel tubes (MPE) for automotive and *residential applications*.

Table A5 Measured heat transfer coefficients (h_{CO2}) for in-tube cooling of pure supercritical CO_2 in round tubes (RT) and micro-channel tubes (MPE) at various operating conditions.

Authors	ID Tube [mm]	M [kg/(m²s)]	p [MPa]	T [°C]	h_{CO2} [kW/(m²K)]
Zingerli and Groll (2000)	6.4 (RT)	930	8-12	20-95	5-35
Dang and Hihara (2002)	6.4 (RT)	950	8-10	15-80	3-14
Yoon et al. (2003)	7.7 (RT)	225-450	7.5-8.8	30-65	2-21
Pettersen et al. (2000)	0.8 (MPE)	600-900	8-10	15-70	3-17.5

Zingerli and Groll (2000) showed that 2 and 5% oil concentration in the supercritical CO_2 reduced the heat transfer coefficient on average by 15 and 25%, respectively.

Since a high pressure drop can be tolerated in the gas cooler and a high mass flux is beneficial for the heat transfer efficiency, Pettersen et al. (1998) concluded that air-cooled gas coolers can have mass fluxes typically ranging from 600 to 1200 kg/(m²s). Rieberer and Halozan (1997) recommended a mass flux of 1500 kg/(m²s) or even higher for water-cooled tube-in-tube gas coolers.

A2 The Transcritical CO_2 Heat Pump Cycle

A2.1 Temperature Gradients During Heat Rejection

Assuming isobaric conditions during the transcritical heat rejection, the heating capacity of the gas cooler is calculated as:

$$\dot{Q} = \dot{m} \cdot \int_{T2}^{T3} c_p \, dT = \dot{m} \cdot (h_2 - h_3) = H_2 - H_3 \qquad \text{(A1)}$$

where $\dot{m}$ is the CO_2 mass flow rate and c_p is the isobaric specific heat capacity. Subscripts *2* and *3* refer to the inlet and outlet of the gas cooler.

As previously illustrated in Figure A4, the specific heat capacity of supercritical CO_2 is virtually independent of temperature at high and low operating pressures. However, at pressures and temperatures close to the critical point, the property reaches tremendous values. As a consequence, there will be considerable variations in the temperature gradient for the CO_2 gas during heat rejection at relatively low supercritical pressures.

Figure A7 displays constant pressure lines (isobars) for supercritical CO_2 in a temperature-enthalpy diagram. Since the slope of the isobars $(\partial T/\partial h)_p$ is the inverse of the isobaric specific heat capacity $(\partial h/\partial T)_p$, the diagram reflects the variations in the specific heat capacity under supercritical conditions.

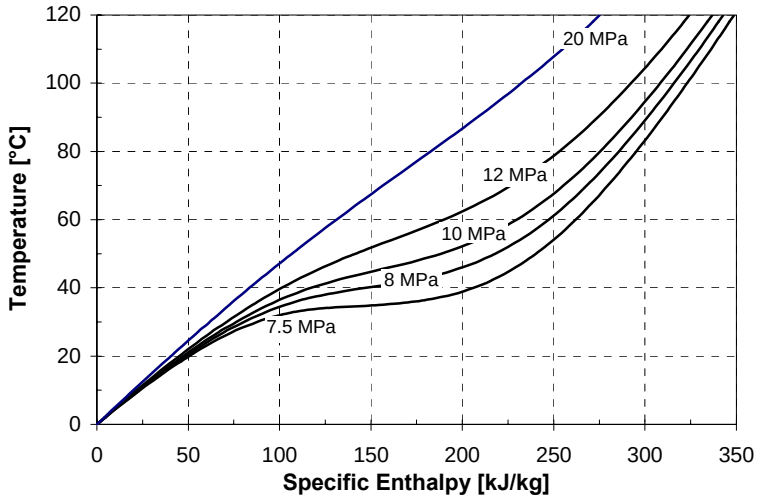

Figure A7 Supercritical isobars for CO_2 (RnLib, 2003).

At pressures and temperatures close to the critical point, the isobars are virtually horizontal. This indicates that the temperature will be almost constant during heat rejection, and the temperature development will be rather similar to a process with subcritical condensation of the working fluid. On the other hand, at high operating pressures or at temperatures below the critical point and above roughly 40 to 50ºC, there will be a considerable temperature drop during heat rejection.

A2.2 Methods of Controlling the High-side Pressure

In a conventional subcritical heat pump process, the saturation pressure of the working fluid during heat rejection is inevitably linked to the saturation temperature, which in turn is determined by the heat balance in the condenser. In a transcritical CO_2 system, however, the gas cooler (high-side) pressure and the temperature are independent variables, and the pressure can be calculated using the real gas equation:

$$p \cdot V = n \cdot R \cdot T \cdot Z \qquad \text{(A2)}$$

where p is the absolute pressure, V is the internal volume of components and tubing, n is the number of moles, R is the universal gas constant, T is the absolute temperature and Z is the compressibility factor. Eq. (A2) shows that the supercritical pressure is determined by the internal volume and the momentary CO_2 charge in the high-pressure side of the system, when assuming constant average temperature in components and tubing.

The most commonly used method to control the high-side pressure in a transcritical CO_2 heat pump system is to use *a low-pressure receiver* (LPR) installed at the evaporator outlet (Lorentzen, 1990). Figure A8 shows the principle of the LPR system.

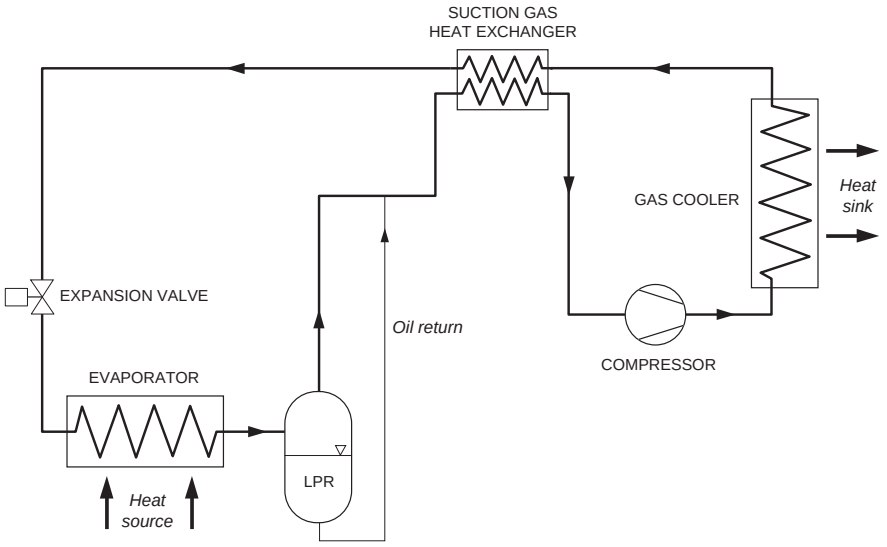

Figure A8 Principle of a CO_2 heat pump system equipped a low-pressure receiver (Lorentzen, 1990).

The high-side pressure is controlled by adjusting the opening of *the expansion valve*, thus temporarily changing the balance between the mass flow rate in the compressor and the valve. By reducing the valve opening, more CO_2 will accumulate in the gas cooler and piping, and the high-side pressure will rise until a new balance point for the mass flow rate in the compressor and the valve has been reached. The extra CO_2 charge needed to increase the pressure is boiled off and transferred from the liquid reservoir in the receiver. When reducing the opening of the expansion valve, the high-side pressure will be reduced, and the surplus CO_2 is stored as liquid in the receiver.

The low-pressure receiver should be designed to prevent possible liquid droplets from entering the suction line, as well as to provide sufficient volume to avoid excessive pressures if the system is inoperative at high ambient temperatures. It is important to ensure that *the total CO_2 charge* in the system, and with that the initial liquid volume in the receiver, is sufficient to provide adequate pressure control at all operating conditions. If the CO_2 charge is too small, the receiver will be emptied and the evaporator will be underfed at high operating pressures. This will in turn result in excessive superheating and reduced evaporation temperature, and as a consequence poor system performance.

An oil return system can be arranged by bleeding off lubricant and possible CO_2 liquid from the bottom of the receiver, as illustrated in Figure A9. However, this requires that the lubricant is fully miscible with the CO_2, or that the density of the immiscible lubricant is higher than that of liquid CO_2. Depending on the CO_2 flow rate in the oil return pipeline, the flow from the evaporator will either be saturated vapour or a mixture of vapour and liquid droplets. *A suction gas heat exchanger* (internal heat exchanger) may be used to evaporate the liquid droplets in the suction line. The influence of a suction gas heat exchanger on the system performance for CO_2 heat pumps is discussed in Section A2.3 and Section 7.2.4, *Possibilities of Efficiency Improvements*.

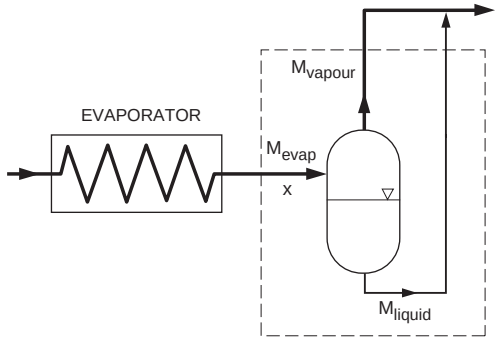

$\underline{CO_2 \text{ mass flow rates}}$

$M_{evap} = M_{vapour} + M_{liquid}$

$M_{liquid} \approx 0 \rightarrow x \approx 1$

$M_{liquid} > 0 \rightarrow x < 1$

Figure A9 The CO_2 mass balance of the LPR and the oil return system.

Lorentzen (1990) and Pettersen and Skaugen (1994) have discussed several alternative concepts for controlling the supercritical pressure including high-side volume control and systems using a medium-pressure receiver. Rieberer et al. (2000) analysed the operating characteristics of CO_2 heat pump systems using a thermostatic expansion valve for controlling the CO_2 liquid feed to the evaporator.

A2.3 Optimum High-side Pressure at Constant CO_2 Outlet Temperature from the Gas Cooler

Both the heating capacity and the coefficient of performance (COP) of a transcritical CO_2 heat pump cycle are affected by the high-side pressure (Lorentzen and Petttersen, 1993). In Figure A10, the transcritical cycle is illustrated in a temperature-enthalpy diagram for high-side pressures ranging from 8 to 11 MPa. The evaporation temperature is -5ºC, the superheating is 5 K, the isentropic compressor efficiency is 60%, and the CO_2 outlet temperature from the gas cooler is kept constant at 35ºC.

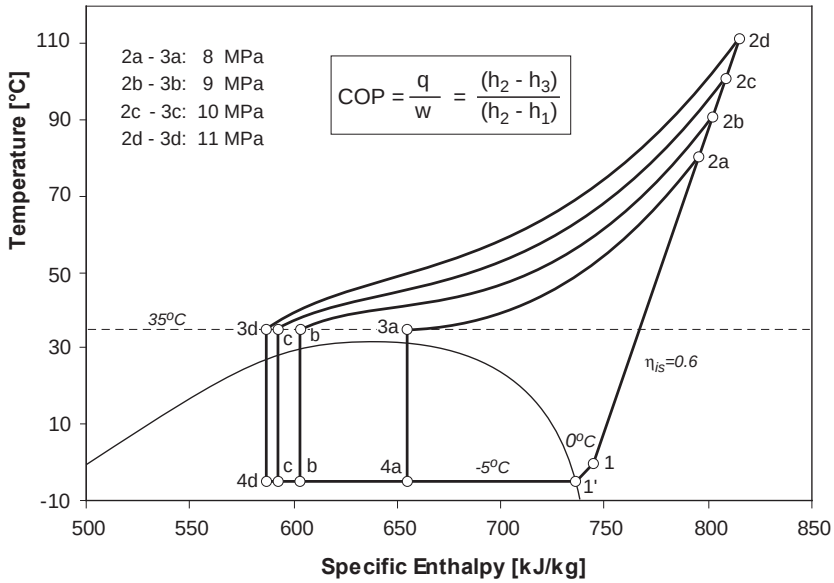

Figure A10 The transcritical CO_2 heat pump cycle operated at four different high-side pressures. The CO_2 outlet temperature from the gas cooler is assumed to be constant at 35ºC.

With reference to Figures A7 and A10, the inlet enthalpy to the gas cooler increases and the outlet enthalpy decreases when the high-side pressure is raised. Due to the great variations in the specific heat capacity at pressures and temperatures above and near the critical point, the slope $(\partial T/\partial h)_p$ is not constant and the isobars are not parallel. As a consequence, the change in the specific enthalpy difference in the gas cooler is not proportional to the change in the specific compressor work, and for each fixed outlet temperature from the gas cooler there will therefore be an optimum high-side pressure leading to a maximum COP.

Figure A11 illustrates the relationship between the specific heating capacity (q), the specific compressor work (w) and the COP for a transcritical heat pump cycle. The boundary conditions are the same as in Figure A10.

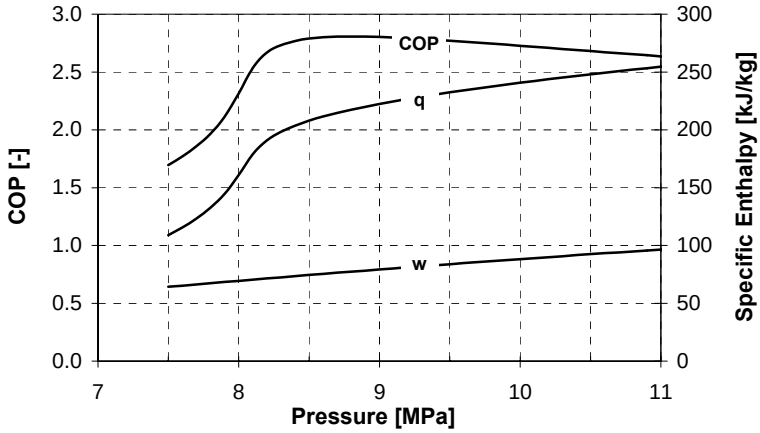

Figure A11 The relationship between the specific heating capacity (q), the specific compressor work (w) and the COP for a CO_2 heat pump at varying high-side pressures. The boundary conditions are as in Figure A10.

Pettersen and Skaugen (1994) presented a simplified differential expression for the optimum pressure of a transcritical CO_2 refrigeration or air conditioning process. The same type of expression can be derived for a heat pump system. The COP of a transcritical CO_2 heat pump is defined as:

$$\varepsilon_{HP} = \frac{q}{w} = \frac{h_2 - h_3}{h_2 - h_1} \tag{A3}$$

where the subscripts *1*, *2* and *3* refer to the compressor inlet, the compressor outlet (gas cooler inlet) and the gas cooler outlet, respectively.

At constant CO_2 outlet temperature from the gas cooler, the maximum COP is found for $(\partial \varepsilon_{HP}/\partial p)=0$, which gives the following equation assuming constant inlet conditions for the compressor (i.e. h_1=constant) and isentropic compression.

$$\left(\frac{\partial h_3}{\partial p}\right)_T = -(\varepsilon_{HP} - 1) \cdot \left(\frac{\partial h_2}{\partial p}\right)_s \tag{A4}$$

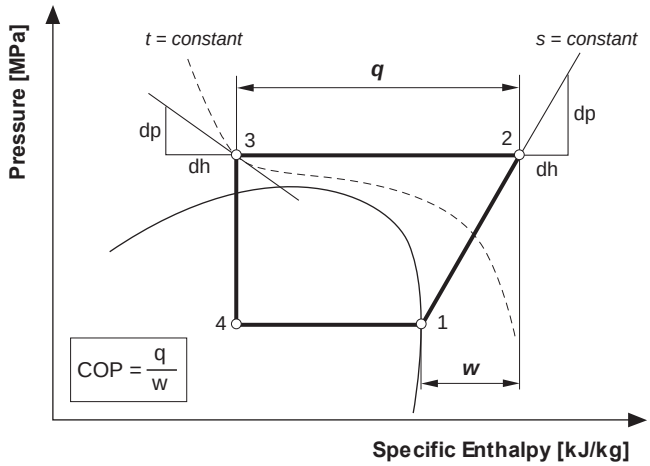

Figure A12 Principle of a simplified differential method for finding the optimum high-side pressure for a transcritical CO_2 heat pump cycle.

Consequently, as a rough estimate, the optimum COP is found at the high-side pressure where the marginal increase in the specific outlet enthalpy in the gas cooler equals (ε_{HP}-1) times the marginal increase in the specific compressor work.

In addition to the CO_2 outlet temperature from the gas cooler, the most important parameters that determine the optimum high-side pressure in a transcritical process are (Skaugen, 2002):

- the evaporation temperature
- the superheating of the suction gas
- the volumetric and isentropic compressor efficiency

The volumetric efficiency affects the mass flow rate, and with that the absolute compressor work and the heating capacity of the gas cooler. The other parameters have an impact on the specific compressor work and the inlet specific enthalpy for the gas cooler.

Figure A13 shows the calculated COP of a transcritical CO_2 heat pump as a function of the high-side pressure at -5ºC evaporation temperature, 5 K suction gas superheat and 60% isentropic efficiency for the compressor (ref. Figure A10 and A11).

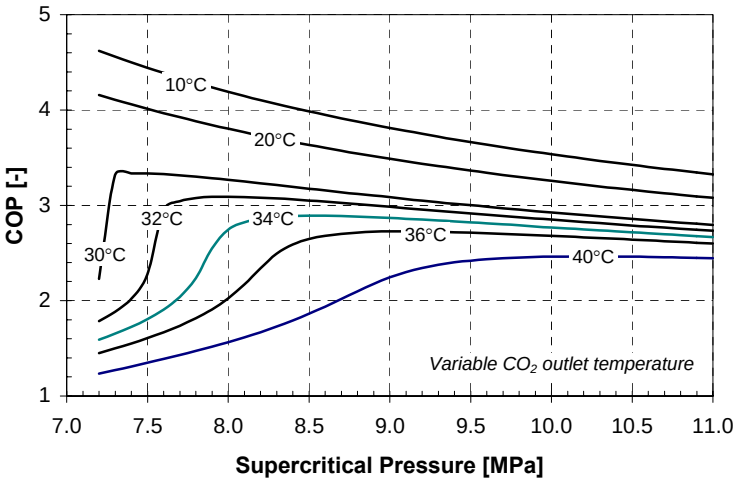

Figure A13 The calculated COP for a transcritical CO_2 heat pump cycle as a function of the high-side pressure and the CO_2 outlet temperature from the gas cooler. The boundary conditions are as in Figure A10.

Figure A14 shows the optimum high-side pressure at varying evaporation temperatures. The boundary conditions are the same as in Figures A10 and A11, with the exception that the isentropic compressor efficiency is a function of the pressure ratio (i.e. real compressor data).

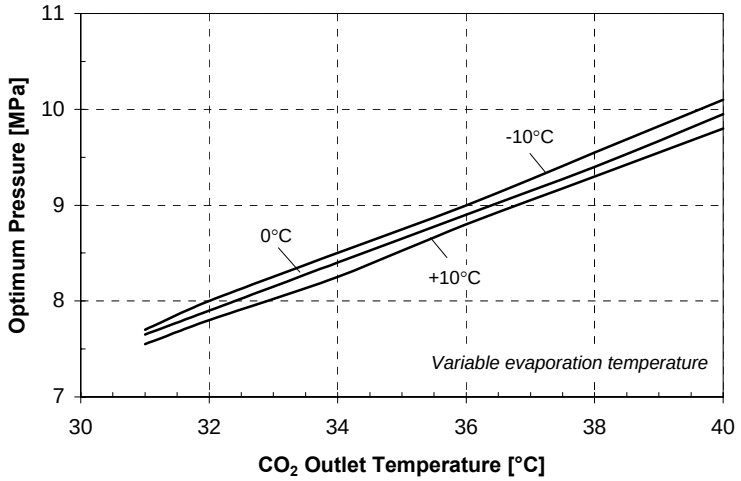

Figure A14 The calculated optimum high-side pressure for a transcritical CO_2 heat pump cycle as a function of the CO_2 outlet temperature from the gas cooler and the evaporation temperature. The boundary conditions are as in Figure A10.

With reference to Figure A13 and A14 it can be concluded that:

- The optimum high-side pressure rises almost linearly from about 7.5 MPa and 31ºC CO_2 outlet temperature to about 10 MPa at 40ºC. Consequently, *the higher the CO_2 outlet temperature from the gas cooler, the higher the optimum high-side pressure*.
- The COP drops off quite rapidly when the high-side pressure is below the optimum value, particularly at CO_2 outlet temperatures near and above the critical temperature. Conversely, the COP is quite invariable when the high-side pressure is above the optimum value. As a result, *the high-side pressure for a CO_2 heat pump cycle should be kept at or slightly above the optimum value*.
- At CO_2 outlet temperatures above the critical temperature, the optimum high-side pressure is virtually independent of *the evaporation temperature* (maximum ±1.5% variance).
- When the CO_2 outlet temperature drops below approximately 30ºC, there is no optimum high-side pressure since the isobars are virtually coincident (ref. Figure A7). However, *this is only true as long as the CO_2 outlet temperature is constant when varying the high-side pressure*. This topic is elaborated in Section A2.4.
- At high-side pressures above the optimum value, a deviation in the order of 0.1 to 0.3 MPa from the optimum value will not reduce the COP by more than a few percent. Hence, the influence of *the pressure drop* in the gas cooler can be neglected when calculating the optimum high-side pressure.
- In bivalent space heating systems (ref. Section 2.1), the optimum high-side pressure providing *the maximum COP for the total heating system*, will in most cases be higher than that of monovalent systems. The reason is that the heating capacity of the heat pump unit can be increased by raising the high-side pressure, thus reducing the need for supplementary heating (Richter et al., 2000 and Aarlien, 2002). The heat from the heat pump will in any case be delivered at a higher energy efficiency that that of the peak load unit.

Skaugen (2002) investigated a transcritical CO_2 air conditioning system, and concluded that *superheating of the suction gas* by using an internal (suction gas) heat exchanger slightly decreased the optimum high-side pressure. Only at an evaporation temperature of 20ºC, a significant improvement of the maximum COP could be achieved by introducing superheat.

Consequently, in brine-to-water and water-to-water heat pump systems operating with moderate CO_2 outlet temperatures from the gas cooler, the use of a suction gas heat exchanger will only marginally improve the COP.

A2.4 Optimum High-Side Pressure when Incorporating Real Gas Cooler Performance

In the previous section it was presupposed that the CO_2 outlet temperature from the gas cooler was constant when varying the high-side pressure. However, in a real gas cooler the high-side pressure may have a considerable impact on the CO_2 outlet temperature, which in turn will change the heating capacity of the system and alter the optimum high-side pressure.

Pinch Point in the Gas Cooler

The minimum temperature difference ΔT_m between the hot CO_2 flow (H) and the cold water or air flow (C) in a counterflow gas cooler occurs at *the pinch point*. When the pinch point occurs inside the gas cooler it will represent a constraint for the heat transfer process, and therefore affect the heating capacity and the CO_2 outlet temperature from the gas cooler. For a given gas cooler design, the temperature profiles and the location of the pinch point are determined by the inlet temperatures, the local heat capacity flow rates (CP-values) and the local heat transfer coefficient (U-value). *The heat capacity flow rate* is defined as (Linnhoff et al., 1984):

$$CP \equiv \dot{m} \cdot c_p \tag{A5}$$

where $\dot{m}$ is the mass flow rate and c_P the local value of the specific heat capacity of the fluid. The temperature-heat (T-Q) diagram is suitable to represent the thermal characteristics for the hot and cold flows in the gas cooler. With reference to Eq. (A2), the slope of the curves in the T-Q diagram is expressed as:

$$\frac{dT}{dH} = \frac{1}{\dot{m} \cdot c_p} = \frac{1}{CP} \tag{A6}$$

A low CP value leads to a steep T-Q curve and vice versa. Due to the considerable variations in the specific heat capacity of supercritical CO_2 at relatively low high-side pressures, the isobars will appear as curves with a sway-backed shape. On the other hand, the T-Q curves for water and air (heat sink) will be more or less linear, since their specific heat capacities are virtually constant in the temperature range from 0 to 100ºC (±0.4%).

The thermal drawback caused by a pinch point inside the heat exchanger is illustrated in the T-Q diagram in Figure A15. In this example water is heated from 25°C to 50°C (set-point), and the initial high-side pressure in the gas cooler is 7.5 MPa. The diagram does not show the actual temperature profiles for the flows as a function of the relative gas cooler length.

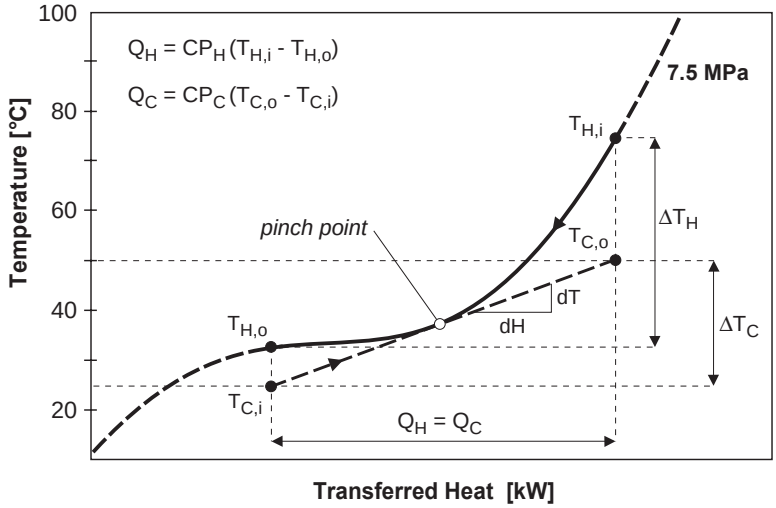

Figure A15 Illustration of the thermal drawback caused by a pinch point inside the gas cooler, when water is to be heated from 25ºC to 50ºC, and the high-side pressure is 7.5 MPa.

The inverse slope of the T-Q curve for the water (broken line) represents the theoretical maximum CP value for the flow, since it is tangent to the CO_2 isobar at the pinch point. Above the pinch $CP_H < CP_C$, and $CP_H > CP_C$ below the pinch. If the water flow rate is increased above this maximum value, the outlet water temperature will drop below the set-point, which is normally undesirable. By increasing the high-side pressure, the isobar will become straighter and the water flow rate can theoretically be increased until the T-Q curve for the water becomes tangential to the CO_2 isobar. The increased water flow rate will in turn reduce the CO_2 outlet temperature from the gas cooler and increase the heating capacity of the heat pump.

Nekså et al. (1998), Rieberer et al. (1998), Saikawa and Hashimoto (2000) and Adriansyah (2001) discussed the existence of a gas cooler pinch point and the effect of high-side pressure control for CO_2 heat pump water heaters. Figure A16 illustrates the result of increasing the high-side pressure from 8 to 11 MPa for a CO_2 heat pump water heater. The city water temperature is 5ºC and the set-point for the hot water is 70ºC.

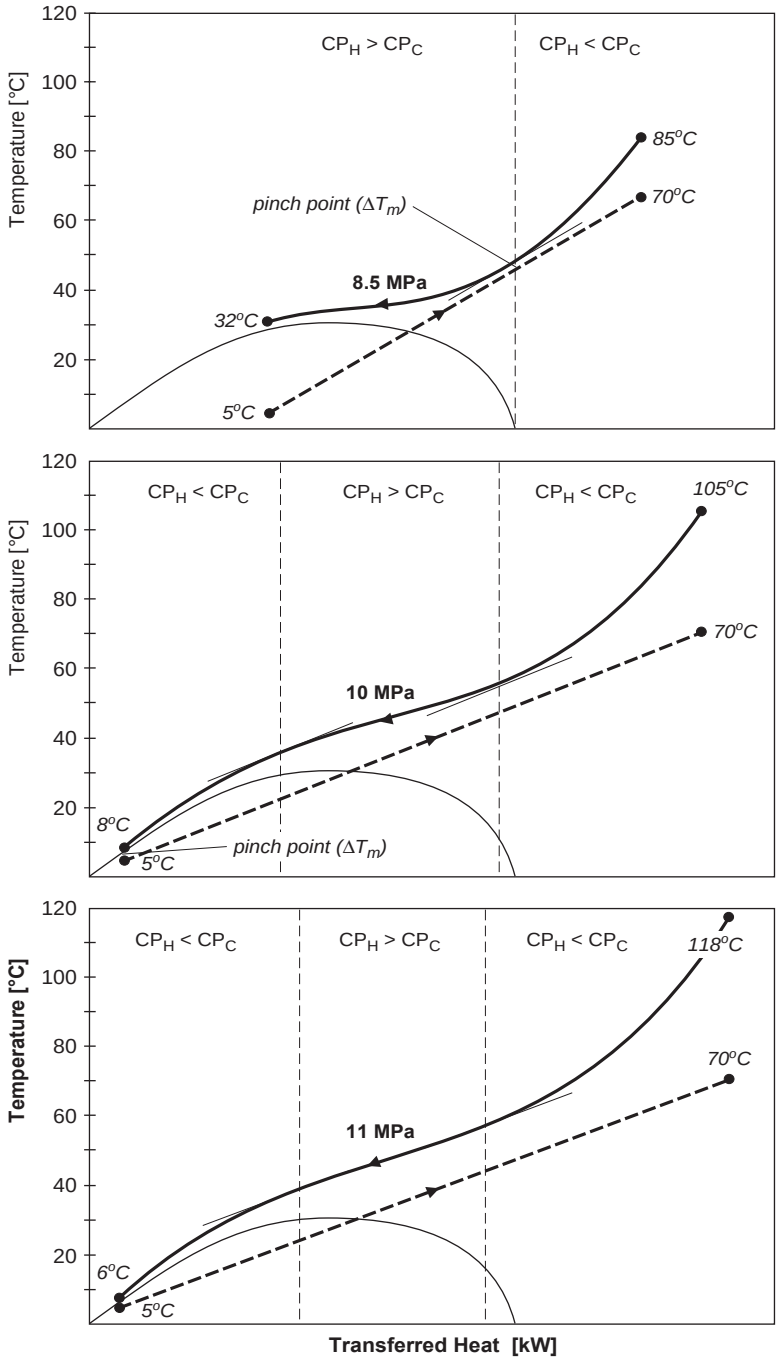

Figure A16 Illustration of the tight dependency between the high-side pressure, the pinch point and the CO_2 outlet temperature from the gas cooler for a CO_2 heat pump water heater.

At 8.5 MPa high-side pressure, there is a pinch point inside the gas cooler (ΔT_m), which leads to a high CO_2 outlet temperature from the gas cooler. Despite the moderate input power to the compressor, the COP will be relatively low due to the limited heating capacity of the heat pump.

By increasing the high-side pressure to 10 MPa, the CO_2 isobar becomes more linear, and the outlet temperature from the compressor increases. Due to the improved temperature fit between the fluids, there is no pinch inside the gas cooler that hampers the heat transfer process, and the minimum temperature difference ΔT_m is now identical to the temperature approach ΔT_A at the hot outlet of the gas cooler. Since the marginal increase in the heating capacity is considerably larger than the marginal increase in the power input to the compressor, the COP increases.

At 11 MPa high-side pressure, there is only a marginal change in the heating capacity of the heat pump, and due to the relatively larger increase in the input power to the compressor, the COP is lower than at 10 MPa. Consequently, 10 MPa is the optimum high-side pressure that leads to a *maximum COP* for the CO_2 heat pump water heater at the actual operating conditions (5/70ºC).

Heat Transfer Coefficients

The thermophysical properties of CO_2 exhibit large variations at supercritical pressures (ref. Section A1.6), which will affect the local heat transfer coefficients in the gas cooler. Due to this fact, variations in the high-side pressure influences the heat transfer process and consequently the CO_2 outlet temperature from the gas cooler.

Appendix B

Performance Testing of Residential Brine-to-Water and Water-to-Water Heat Pumps

B1 Prevailing Test Standards for Brine-to-Water and Water-to-Water Heat Pumps

The following standards are dealing with performance testing and rating of residential brine-to-water and water-to-water heat pumps:

- **EN 255-2** (1997): Air conditioners, liquid chilling packages and heat pumps with electrically driven compressors – Heating mode – Part 2: Testing and requirements for marking for space heating units.
- **EN 255-3** (1997): Air conditioners, liquid chilling packages and heat pumps with electrically driven compressors – Heating mode – Part 3: Testing and requirements for marking for sanitary hot water units.
- **ISO 13256-2** (1998): Testing and rating for performance - Part 2: Water-to-water and brine-to-water heat pumps.
- **ANSI-ASHRAE 37** (1988): Methods of testing for rating unitary air-conditioning and heat pump equipment including water-to-water and brine-to-water heat pumps.

B2 Available Test Results

Several European heat pump test stations are testing residential brine-to-water and water-to-water heat pumps in accordance with *EN 255-2*:

- TNO-MEP (the Netherlands)
- Technischer Überwachungs-Verein, TÜV (Germany)
- WPZ Töss – Heat Pump Test Centre (Switzerland)
- Laboratory of Industrial Energy at EPFL (Switzerland)
- Arsenal Research Heat Pump Test Centre (Austria)
- The Swedish National Testing and Research Institute (Sweden)

WPZ Töss is the only European test station that presents updated test results at their Internet homepage (*www.wpz.ch*). Figure B1 shows the range of the measured coefficient of performance (COP) at various operating conditions for brine-to-water (B/W) and water-to-water (W/W) heat pumps with heating capacities between 5 and 10 kW. The temperatures before and after the slash represent the inlet fluid temperature to the evaporator and the outlet water temperature from the condenser, respectively.

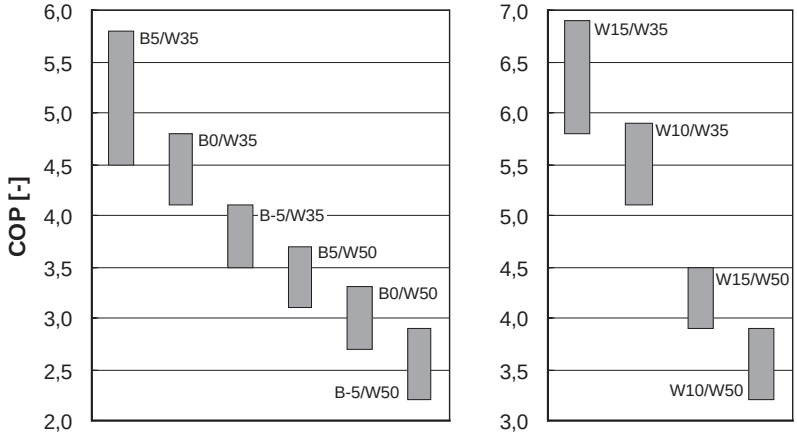

Figure B1 *COP for residential brine-to-water (B-W) and water-to-water (W-W) heat pumps tested at WPZ Töss.*

The highest COPs are achieved for the heat pump units having a heating capacity between 8 and 10 kW.

Oostendorp and Traversari (2000) have compared the COP for residential brine-to-water and water-to-water heat pumps tested at TNO-MEP during the period 1998 to 2000. The results are presented in Figure B2 and B3.

The test results from WPZ Töss and TNO-MEP demonstrates that the most energy efficient residential brine-to-water heat pumps on the market in the capacity range from about *5 to 7 kW* achieve a COP of about *4.6* and *3.3* at B/W 0/35ºC and 0/50°C, respectively.

There exists no standards or acknowledged guidelines for estimating the seasonal performance factor (SPF) of residential brine-to-water and water-to-water heat pump systems. However, some research organisations have developed software to predict the SPF of various types of heat pump systems. As an example, TNO-MEP have made a dynamic heat pump

model that predicts the performance of a heat pump system by simulating the interaction between inhabitants, installations, building and outdoor climate during a shortened reference year (Doorn and Oostendorp, 1997).

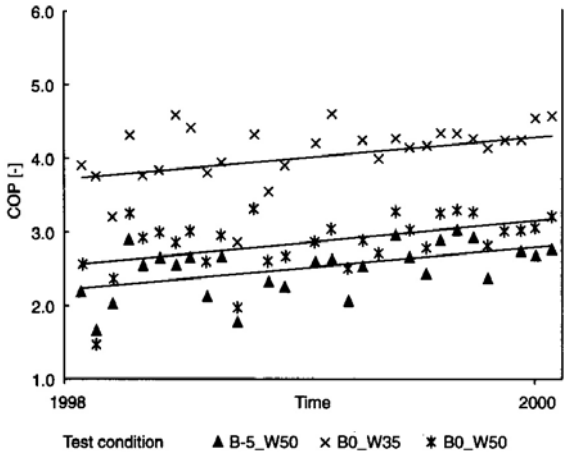

Figure B2 *COP for residential brine-to-water heat pumps tested at TNO-MEP (Oostendorp and Traversari, 2001).*

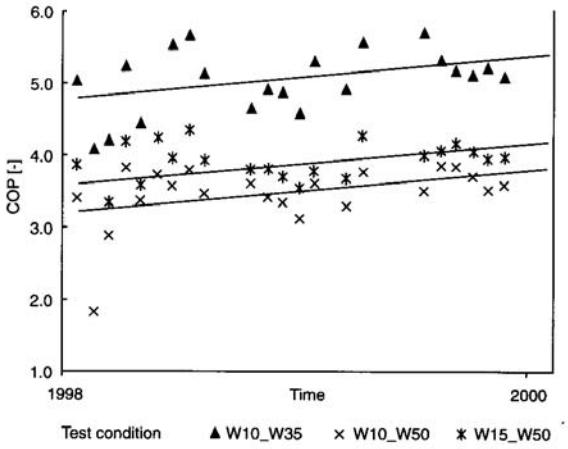

Figure B3 *COP for residential water-to-water heat pumps tested at TNO-MEP (Oostendorp and Traversari, 2001).*

Appendix C

Test Results for the Prototype CO_2 Heat Pump

Reference is made to Section 5.1.3, *Experimental Results*, regarding a detailed presentation and analysis of the test results for the prototype brine-to-water CO_2 heat pump unit.

C1 CO_2 Heat Pump Unit – Combined Heating Mode

T_E [°C]	p_{GC} [bar]	T_{CO2} [°C]	M_{CO2} [kg/m]	Q_{TOT} [W]	T_{SH} [°C]	Q_{SH} [W]	T_{DHW} [°C]	Q_{DHW-P} [W]	Q_{DHW-R} [W]	P [W]	COP [-]
-5.1	75.34	76.6-27.6	1.440	5415	28.1-33.1	2557	6.9-60.2	1303	1555	1609	3.36
-5.0	**80.15**	**81.7-12.3**	**1.445**	**6771**	**28.0-33.1**	**3423**	**6.9-60.1**	**1373**	**1975**	**1701**	**3.98**
-5.0	85.15	85.7-9.8	1.445	6965	28.1-33.1	3204	6.9-60.1	1363	2398	1775	3.92
-5.1	90.05	90.2-8.3	1.420	7183	28.0-33.0	2984	6.6-60.2	1351	2849	1864	3.85
-5.0	80.10	82.2-20.4	1.420	6243	28.1-33.1	3939	7.3-70.5	797	1507	1694	3.68
-4.9	**85.20**	**87.3-15.8**	**1.415**	**6720**	**28.0-33.1**	**3821**	**7.2-70.3**	**972**	**1927**	**1793**	**3.75**
-5.0	90.25	92.7-12.4	1.410	6869	28.1-33.1	3423	7.4-70.0	1108	2338	1883	2.65
-4.9	95.05	97.4-10.1	1.405	7020	28.0-33.1	3110	7.1-70.1	1182	2728	1977	3.55
-5.1	80.10	80.6-26.7	1.405	5615	28.0-33.0	4795	6.5-80.1	233	586	1647	3.41
-5.0	**85.05**	**86.9-21.1**	**1.418**	**6419**	**28.0-33.1**	**4400**	**6.6-80.1**	**595**	**1423**	**1798**	**3.57**
-5.0	90.15	91.5-18.2	1.417	6610	28.0-33.0	4107	6.4-80.3	742	1761	1893	3.49
-5.1	95.15	97.6-15.1	1.405	6880	28.1-33.1	3766	6.5-80.4	913	2202	1987	3.40
-5.0	75.50	75.5-30.5	1.436	4722	30.1-35.2	1911	7.4-59.7	1298	1513	1609	2.93
-5.1	80.30	81.6-18.0	1.440	6230	30.2-35.2	2728	7.4-60.7	1674	1828	1699	3.67
-5.1	**85.00**	**86.4-9.8**	**1.441**	**6907**	**30.1-35.1**	**2942**	**7.0-59.8**	**1608**	**2357**	**1775**	**3.89**
-5.0	89.80	90.6-8.5	1.442	6947	30.0-35.0	2596	6.7-59.7	1550	2801	1878	3.70
-5.1	80.05	81.1-26.1	1.445	5758	29.9-35.0	3421	7.0-71.3	929	1408	1704	3.38
-4.9	**85.00**	**86.1-17.7**	**1.455**	**6410**	**30.2-35.1**	**3635**	**6.7-70.0**	**1046**	**1729**	**1793**	**3.57**
-5.0	90.60	91.0-13.5	1.440	6668	30.1-35.1	3202	7.1-69.7	1253	2212	1893	3.52
-5.0	95.05	95.5-10.5	1.425	6913	30.1/35.0	2994	6.4-70.4	1358	2561	1992	3.47
-5.0	80.25	81.4-29.3	1.442	5547	30.0-35.1	4085	7.5-79.3	508	954	1713	3.24
-4.9	85.10	85.5-24.2	1.460	6106	30.1-35.1	4196	7.4-80.1	614	1297	1803	3.39
-5.1	**89.55**	**91.8-20.1**	**1.420**	**6423**	**30.0-35.0**	**3895**	**7.4-80.0**	**797**	**1731**	**1869**	**3.44**
-5.1	95.00	96.3-17.6	1.390	6462	30.1-35.1	3548	7.5-80.7	905	2010	1930	3.35
-5.1	99.85	103-14.7	1.380	6618	29.9-35.0	3243	8.0-80.7	996	2379	2053	3.22
-5.1	80.25	81.7-31.3	1.445	5125	35.0-39.7	1313	7.0-60.4	2043	1768	1708	3.00
-5.1	85.20	87.2-16.2	1.425	6478	35.3-40.2	1656	6.4-60.4	2711	2111	1770	3.66
-4.9	**90.25**	**92.1-8.1**	**1.410**	**7137**	**35.0-40.2**	**2190**	**6.2-60.4**	**2364**	**2583**	**1850**	**3.86**
-4.9	94.95	96.0-7.5	1.405	7325	35.0-40.0	2086	6.1-60.4	2091	3148	1940	3.78
-5.0	85.00	86.4-29.6	1.430	5374	35.1-40.0	2117	6.4-70.0	1550	1707	1798	2.99
-5.1	89.80	92.4-17.7	1.400	6480	35.1-40.0	2669	6.7-70.3	1766	2045	1855	3.49
-5.0	**95.25**	**97.7-11.2**	**1.410**	**6982**	**35.0-40.0**	**2652**	**6.7-70.6**	**1827**	**2503**	**1992**	**3.50**
-5.0	99.90	99.7-9.5	1.410	7064	35.0-39.9	2450	6.6-70.4	1810	2803	2053	3.44
-5.0	85.20	86.7-33.7	1.435	4873	35.1-40.2	2745	6.9-79.3	874	1254	1798	2.71
-5.1	89.75	94.0-25.4	1.395	5780	34.9-39.9	2937	6.6-80.0	1142	1700	1879	3.08
-5.0	**95.25**	**98.2-19.7**	**1.420**	**6500**	**35.0-40.0**	**3129**	**7.0-80.4**	**1300**	**2071**	**2006**	**3.24**
-5.0	99.85	103.7-15.5	1.400	6589	35.0-40.0	2913	6.6-80.6	1406	2269	2087	3.16
-10.1	74.84	84.0-30.1	1.235	4598	30.0-35.0	1558	7.1-60.4	1385	1655	1619	2.84
-10.1	**79.90**	**87.7-12.3**	**1.227**	**6171**	**30.0-34.9**	**2529**	**6.6-59.8**	**1742**	**1900**	**1690**	**3.65**
-10.1	84.95	94.1-7.4	1.200	6288	30.0-34.9	2404	5.9-59.8	1434	2449	1756	3.58
-10.1	90.00	100.1-7.1	1.205	6502	29.9-35.0	2220	6.1-60.4	1341	2941	1878	3.46

Variables: T=temperature [°C], p=pressure [bar], M=mass flow rate [kg/min], Q=heating capacity [W], P=electric power input [W]

Subscripts: E=evaporator, GC=gas cooler, TOT=total, SH=space heating, DHW=hot water, DHW-P= preheating, DHW-R=reheating

C2 CO_2 Heat Pump Unit – DHW Heating Mode

T_E [°C]	p_{GC} [bar]	T_{CO2} [°C]	M_{CO2} [kg/m]	Q_{TOT} [W]	T_{SH} [°C]	Q_{SH} [W]	T_{DHW} [°C]	Q_{DHW-P} [W]	Q_{DHW-R} [W]	P [W]	COP [-]
-5.1	80.25	82.3-29.1	1.425	5413	-	-	6.0-60.4	3873	1540	1680	3.22
-5.0	84.80	87.0-18.1	1.397	6150	-	-	5.7-59.9	4385	1766	1732	3.55
-5.0	**90.05**	**92.6-8.3**	**1.400**	**7100**	**-**	**-**	**5.4-59.7**	**4796**	**2304**	**1869**	**3.80**
-5.0	95.30	96.6-6.9	1.405	7163	-	-	5.4-60.2	4431	2732	1978	3.62
-5.0	84.80	87.6-33.0	1.400	4823	-	-	6.1-69.8	3550	1274	1770	2.73
-5.1	89.90	93.8-24.9	1.400	5851	-	-	6.0-69.7	4180	1671	1893	3.09
-5.0	95.35	98.2-14.2	1.415	6677	-	-	5.0-70.1	4730	1946	2006	3.33
-5.0	**99.95**	**103.3-8.6**	**1.390**	**7453**	**-**	**-**	**5.0-70.0**	**5036**	**2417**	**2082**	**3.58**
-5.1	104.80	107.8-6.9	1.390	7436	-	-	5.0-70.1	4695	2741	2180	3.41
-5.1	94.90	96.6-33.8	1.405	5072	-	-	6.4-80.0	3783	1289	1996	2.54
-5.1	100.05	105.1-24.2	1.380	6077	-	-	6.5-80.1	4386	1691	2096	2.90
-5.0	104.90	109.3-16.8	1.405	6764	-	-	6.4-80.3	4779	1984	2229	3.03
-5.0	108.05	112.1-12.2	1.395	6891	-	-	6.2-79.8	4744	2147	2229	3.09
-10.0	79.80	91.3-25.7	1.225	5.178	-	-	6.9-60.5	3605	1573	1770	2.93
-10.0	85.20	97.9-11.3	1.200	6.103	-	-	6.9-60.5	4034	2069	1864	3.27
-10.0	**89.90**	**103.0-8.1**	**1.200**	**6.363**	**-**	**-**	**6.9-60.5**	**3910**	**2453**	**1959**	**3.25**
-10.1	95.00	109.4-7.5	1.190	6.492	-	-	6.9-60.0	3355	3137	2073	3.13

C3 CO_2 Heat Pump Unit – Space Heating Mode

T_E [°C]	p_{GC} [bar]	T_{CO2} [°C]	M_{CO2} [kg/m]	Q_{TOT} [W]	T_{SH} [°C]	Q_{SH} [W]	T_{DHW} [°C]	Q_{DHW-P} [W]	Q_{DHW-R} [W]	P [W]	COP [-]
-4.9	74.99	79.7-30.5	1.452	4590	28.1-33.0	4590	-	-	-	1607	2.86
-4.9	**79.80**	**86.2-28.7**	**1.440**	**5344**	**28.0-32.9**	**5344**	**-**	**-**	**-**	**1697**	**3.15**
-5.1	84.60	88.9-28.2	1.452	5663	28.0-33.0	5663	-	-	-	1797	3.15
-5.1	89.75	94.3-28.0	1.448	5705	28.0-33.0	5705	-	-	-	1898	3.01
-5.0	80.00	83.5-31.8	1.450	5019	30.1-35.1	5019	-	-	-	1697	2.96
-5.0	**84.75**	**88.7-30.5**	**1.451**	**5411**	**30.1-35.1**	**5411**	**-**	**-**	**-**	**1797**	**3.01**
-5.0	89.80	93.5-30.1	1.450	5523	30.1-35.0	5523	-	-	-	1893	2.92
-5.0	95.15	98.2-30.0	1.451	5670	30.1-35.1	5670	-	-	-	2003	2.83
-5.0	85.10	90.1-35.9	1.451	4030	35.1-39.9	4030	-	-	-	1817	2.22
-5.0	90.15	95.1-35.7	1.451	4954	35.0-40.0	4954	-	-	-	1927	2.57
-5.1	**95.15**	**99.5-35.0**	**1.452**	**5585**	**34.9-40.0**	**5585**	**-**	**-**	**-**	**2012**	**2.78**
-5.1	99.90	104.0-35.0	1.452	5399	35.1-40.2	5399	-	-	-	2104	2.57
-10.0	79.85	91.2-31.3	1.224	4677	30.1-35.0	4677	-	-	-	1708	2.74
-9.9	**84.65**	**96.0-30.3**	**1.216**	**4973**	**30.2-35.1**	**4973**	**-**	**-**	**-**	**1798**	**2.78**
-10.0	90.20	103.1-29.9	1.205	5239	30.0-35.1	5239	-	-	-	1907	2.75
-10.0	95.15	109.6-30.0	1.190	5151	30.1-35.1	5151	-	-	-	1992	2.59
0.1	79.90	77.6-32.4	1.632	5193	30.1-35.1	5193	-	-	-	1661	3.12
0.2	85.20	82.2-30.7	1.635	5523	30.2-35.1	5523	-	-	-	1770	3.13
0.2	**90.05**	**86.4-30.1**	**1.637**	**5949**	**30.0-35.1**	**5949**	**-**	**-**	**-**	**1874**	**3.18**
0.1	95.05	91.8-30.1	1.625	5926	30.1-35.1	5926	-	-	-	1977	3.00

Variables: T=temperature [°C], p=pressure [bar], M=mass flow rate [kg/min], Q=heating capacity [W], P=electric power input [W]

Subscripts: E=evaporator, GC=gas cooler, TOT=total, SH=space heating, DHW=hot water, DHW-P= preheating, DHW-R=reheating

Appendix D

Uncertainty Analysis of the Measurements for the Prototype CO_2 Heat Pump

Reference is made to Table 4.11 in Section 4.11, *Instrumentation*, regarding the uncertainties of the sensor/instruments that measured temperature, CO_2 pressure, CO_2 mass flow rate, water volume flow rate and electric power for the prototype brine-to-water CO_2 heat pump unit.

D1 Principles of Uncertainty Analysis

R represents a quantity which by means of an equation is computed from a set of measurements, where X_i to X_n represent independent variables.

$$R = R(X_1, X_2, X_3, ..., X_n) \tag{D1}$$

The absolute uncertainty δR in the computed result *R*, can be estimated by using a root-sum-square combination of the effects of the individual measurements (propagation analysis), and is defined as:

$$\delta R = \left[\sum_{i=1}^{n} \left(\frac{\partial R}{\partial X_i} \cdot \delta X_i \right)^2 \right]^{0.5} \tag{D2}$$

δX_i is the uncertainty in the variable X_i, and the partial derivative is the sensitivity coefficient for the result R with respect to the measurement X_i. Each term in the equation represents the contribution made by the uncertainty in one variable to the absolute uncertainty of the result (δR). The equation is valid as long as each of the measurements are independent, repeated observation of each measurement would display Gaussian distribution, and the uncertainty in each measurement is expressed with the same confidence level.

The relative uncertainty αR in the computed result is defined as:

$$\alpha R = \left(\frac{\delta R}{R} \right) \cdot 100\% \tag{D3}$$

D2 Uncertainty in the Evaporation Temperature

Each test series for the integrated CO_2 heat pump unit was carried out at a constant evaporation temperature, and the evaporation temperature *T* was based on a pressure measurement *p* at the evaporator outlet. The uncertainty in the saturation temperature was calculated from the uncertainty in the absolute pressure measurement:

$$\delta T = \left(\frac{\partial T}{\partial p} \right)_{sat} \cdot \delta p \tag{D4}$$

The uncertainty in the pressure measurements was ±12 kPa. Table D1 shows the computed absolute uncertainties in the evaporation temperature at the temperature levels that were used in the tests.

Table D1 The absolute uncertainty in the evaporation temperature.

T [°C]	-10	-5	0
δT [K]	±0.16	±0.14	±0.13

D3 Uncertainty in the Gas Cooler Heating Capacity

D3.1 Water Circuit Measurements

The total heating capacity of the CO_2 heat pump for space heating (SH) and hot water heating (DHW) is given by the following equation:

$$\dot{Q} = \left[\dot{V} \cdot \rho \cdot c_p \cdot \left(T_{out} - T_{In} \right) \right]_{SH} + \left[\dot{V} \cdot \rho \cdot c_p \cdot \left(T_{out} - T_{In} \right) \right]_{DHW} \tag{D5}$$

where $\dot{V}$ is the water flow rate [m^3/s], T_{in} and T_{out} the inlet and outlet water temperatures [°C], and ρ and c_p the density [kg/m^3] and the specific heat capacity [J/kgK] of water, respectively.

According to Eq. D2, the absolute uncertainty in the total heating capacity is:

$$\delta \dot{Q} = \left[\begin{array}{l} \left[\rho \cdot c_p \cdot \left(T_{out} - T_{In} \right) \cdot \delta \dot{V} \right]_{SH}^2 + \left[2 \cdot \dot{V} \cdot \rho \cdot c_p \cdot \delta T \right]_{SH}^2 + \\ \left[\rho \cdot c_p \cdot \left(T_{out} - T_{In} \right) \cdot \delta \dot{V} \right]_{DHW}^2 + \left[2 \cdot \dot{V} \cdot \rho \cdot c_p \cdot \delta T \right]_{DHW}^2 \end{array} \right]^{0.5} \tag{D6}$$

The calculation of the density and the specific heat capacity of water were based on the average water temperature for each system, i.e. $(T_{out}+T_{in})/2$. The uncertainty in the temperature measurements was ±0.085°C, and the uncertainty in the volume flow rates was 0.5% of the measured value.

Table D2 shows the absolute and relative uncertainty in the total heating capacity of the CO_2 heat pump during operation in the three different operating modes, when the compressor was running at 6000 rpm (100 Hz), the set-point for the hot water temperature was 70°C and the supply, and return temperatures in the space heating system were 35/30°C.

Table D2 The absolute and relative uncertainty in the total heating capacity for the CO_2 heat pump unit based on measurements from the water circuits.

	SH	**DHW**	**SH + DHW**
δQ [W]	±155	±65	±80
αQ [%]	±2.5	±1.0	±1.3

SH=Space heating mode DHW=hot water heating mode SH+DHW=combined mode

D3.2 CO_2 Circuit Measurements

The total heating capacity of the CO_2 heat pump is:

$$\dot{Q}_{GC} = \dot{m}_{CO2} \cdot \left(h_{CO2-in} - h_{co2-out}\right) \tag{D7}$$

where $\dot{V}$ is the CO_2 mass flow rate [kg/s], and $h_{CO2\text{-}in}$ and $h_{CO2\text{-}out}$ the specific enthalpy [kJ/kg] of the CO_2 at the gas cooler inlet and outlet, respectively. Since the specific enthalpy *h* of the supercritical gas is a function of the pressure and the temperature, the uncertainty in the specific enthalpy according to Eq. D2 is:

$$\delta h = \left[\left(\frac{\partial h}{\partial p}\cdot\delta p\right)^2 + \left(\frac{\partial h}{\partial T}\cdot\delta T\right)^2\right]^{0.5} \tag{D8}$$

The uncertainty in the total heating capacity is:

$$\delta\dot{Q} = \left[\left((h_2 - h_1)\cdot\delta\dot{m}\right)^2 + \left(\dot{m}\cdot\delta h_2\right)^2 + \left(\dot{m}\cdot\delta h_1\right)^2\right]^{0.5} \tag{D9}$$

The uncertainty in the temperature and pressure measurements was ±32 kPa and ±0.5°C, respectively, whereas the uncertainty in the CO_2 mass flow rate was 0.3% of the measured value when assuming pure CO_2. However, due to the fact that the measured mass flow rate was a mixture of roughly 91 to 93% CO_2 and 6 to 9% lubricant, the uncertainty was set at 2% in the calculations.

Table D3 shows the absolute and relative uncertainty in the total heating capacity of the CO_2 heat pump unit during operation in the three different operating modes, when the compressor was running at 6000 rpm ($\dot{m} \approx 1.45$ kg/min), the set-point for the hot water temperature was 70°C, and the supply and return temperatures in the space heating system were 35/30°C.

Table D3 The absolute and relative uncertainty in the total heating capacity for the CO_2 heat pump unit at different operating modes and gas cooler (high/side) pressures. The calculations are based on measurements from the CO_2 circuit.

Heating Mode	**SH**		**DHW**		**SH + DHW**	
GC Pressure	8 MPa	9 MPa	9 MPa	10 MPa	8 MPa	9 MPa
δQ [W]	±115	±110	±115	±160	±115	±130
αQ [%]	±2.2	±2.0	±2.4	±2.0	±1.9	±1.9

SH=Space heating mode DHW=hot water heating mode SH+DHW=combined mode

D4 Uncertainty in the COP

The Coefficient of Performance (COP) of a heat pump unit is defined as:

$$COP = \frac{\dot{Q}}{P} \tag{D10}$$

where $\dot{Q}$ is the total heating capacity of the gas cooler(s) [W] and P is the power consumption of the compressor [W]. According to Eq. D2, the absolute uncertainty for the total heating capacity is:

$$\delta COP = \left[\left(\frac{\delta \dot{Q}}{P} \right)^2 + \left(-\frac{\dot{Q}}{P^2} \cdot \delta P \right)^2 \right]^{0.5} \tag{D11}$$

D4.1 Water Circuit Measurements

The uncertainty in the watt meter that measured the power consumption was ±25 W, whereas the uncertainty in the heating capacity is shown in Table D2. Table D4 shows the calculated relative uncertainty in the COP, when the compressor was running at 6000 rpm (100 Hz), the set-point for the hot water temperature was 70°C, and the supply and return temperatures in the space heating system were 35/30°C.

Table D4 The relative uncertainty in the COP for the CO_2 heat pump unit. The heating capacities were based on measurements from the water circuits.

	SH	DHW	SH + DHW
αCOP [%]	±2.8	±1.7	±1.9

SH=Space heating mode DHW=hot water heating mode SH+DHW=combined

D4.2 CO_2 Circuit Measurements

The uncertainty in the wattmeter that measured the power consumption was ±25 W, whereas the uncertainty in the heating capacity is shown in Table D3. Table D5 presents the relative uncertainty in the COP, when the compressor was running at 6000 rpm (100 Hz), the set-point for the hot water temperature was 70°C, and the supply and return temperatures in the space heating system were 35/30°C.

Table D5 The relative uncertainty in the COP for the CO_2 heat pump unit. The heating capacities were based on measurements from the CO_2 circuit.

Heating Mode	**SH**		**DHW**		**SH + DHW**	
GC Pressure	8 MPa	9 MPa	9 MPa	10 MPa	8 MPa	9 MPa
αCOP [%]	±2.6	±2.2	±2.1	±2.6	±2.6	±2.5

SH=Space heating mode DHW=hot water heating mode SH+DHW=combined mode

Appendix E

Photos of the Prototype CO_2 Heat Pump

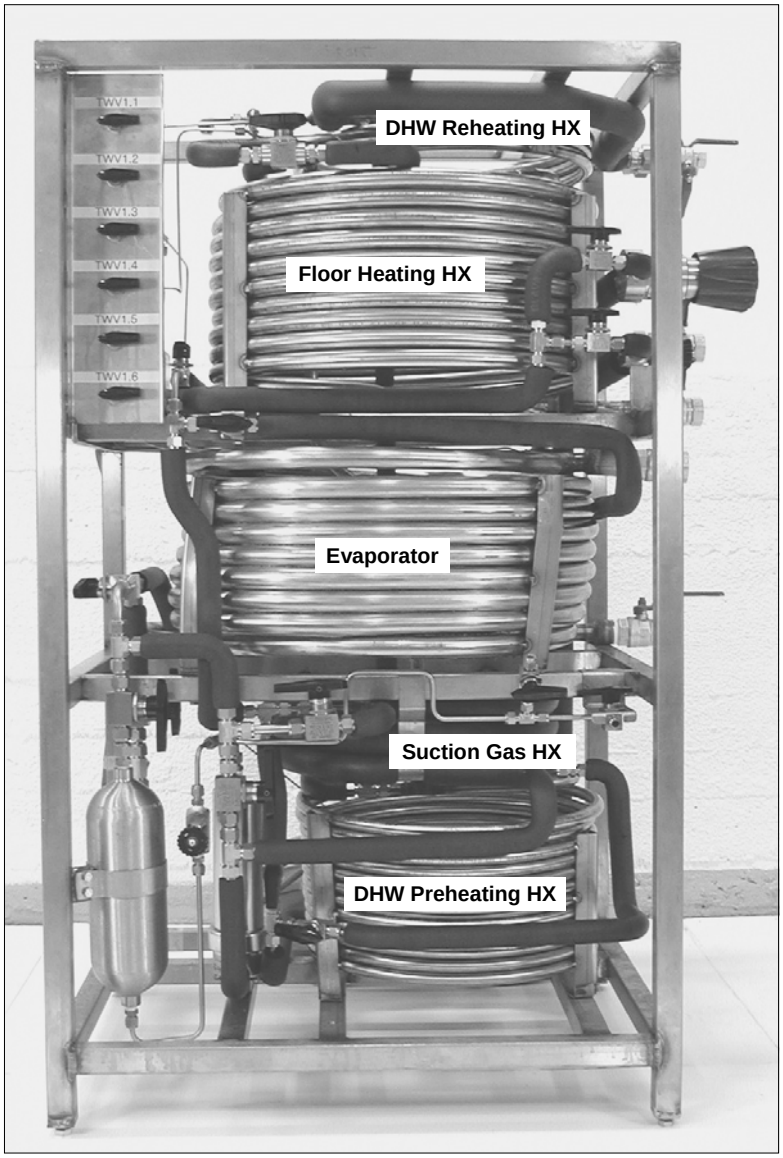

Figure E1 The prototype brine-to-water CO_2 heat pump unit for combined space heating and hot water heating (front view).

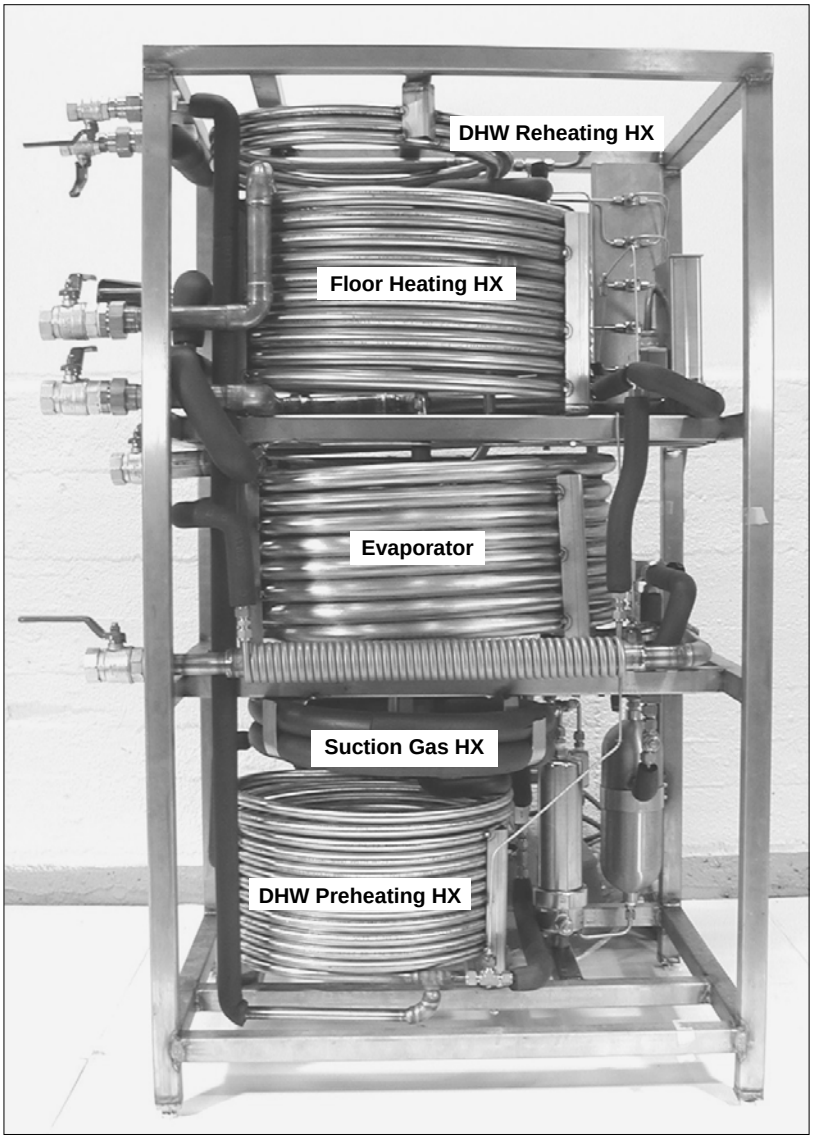

Figure E2 The prototype brine-to-water CO_2 heat pump unit for combined space heating and hot water heating (rear view).

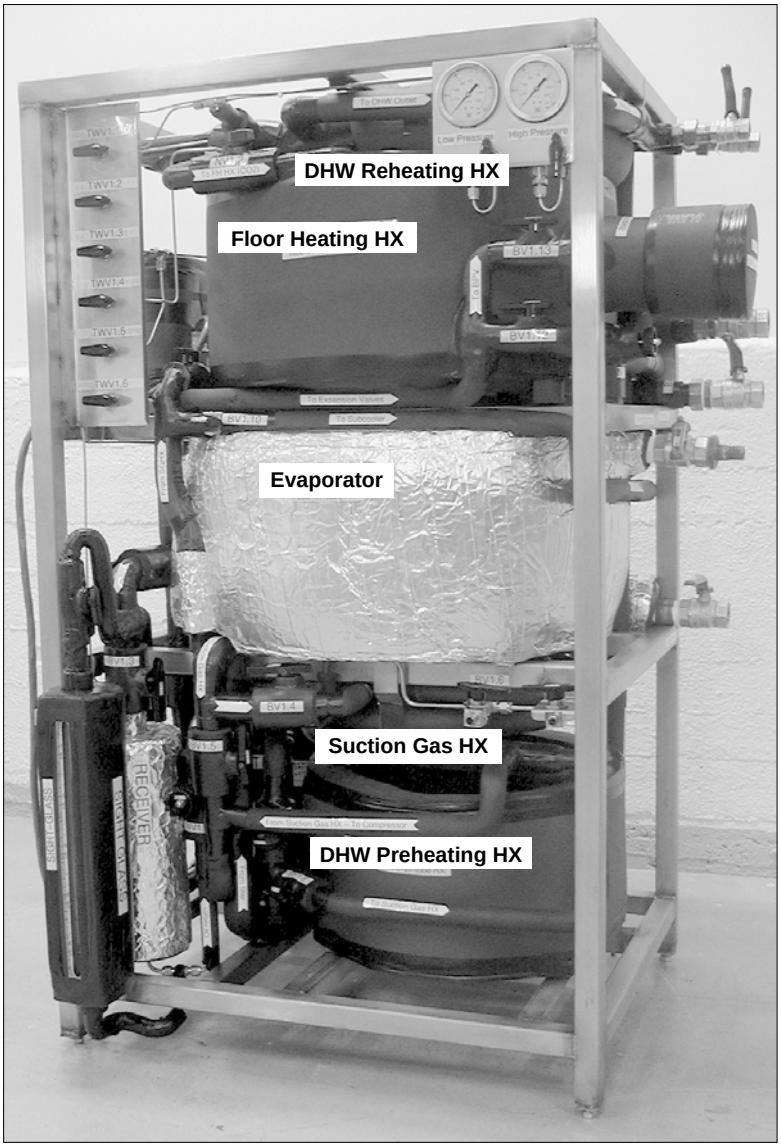

Figure E3 The prototype brine-to-water CO_2 heat pump unit for combined space heating and hot water heating (front view).

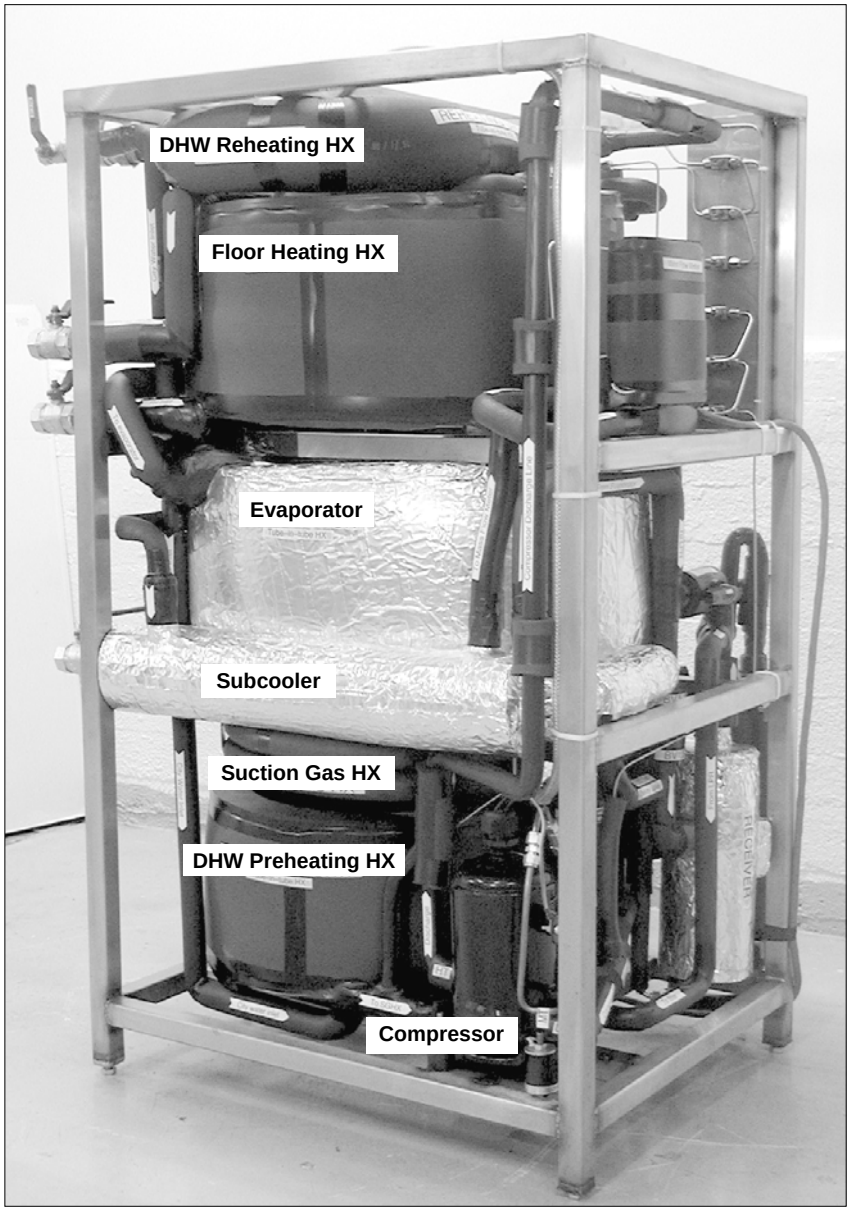

Figure E4 The prototype brine-to-water CO_2 heat pump unit for combined space heating and hot water heating (rear view).

Appendix F

Characteristic Properties of DHW Systems

The annual heating demand for domestic hot water (DHW) in European, US and Canadian homes typically ranges from 3000 to 6000 kWh/family (Breembroek and Dieleman, 2001). Table F1 shows some characteristic parameters for DHW systems in Europe (Novakovic et al., 1996).

Table F1 Characteristic parameters for European domestic hot water (DHW) systems (Novakovic, et al., 1996)

City water temperature	• 5 – 20ºC (cold mains supply)	
Minimum storage temperature	• 55 – 60ºC	
Hot water storage temperature	• 60 – 85ºC	
Hot water user temperature	• 35 – 40ºC (shower, bath-tubs, washbasins)	
	• 60 – 70ºC (washing up)	
Hot water demand – tapping sites	• Bath-tub	100 – 150 litres
	• Shower	50 – 80 litres
	• Washbasin	5 – 10 litres
	• Washing-up	10 – 20 litres
Hot water flow rate	• Bath-tub	0.3 litres/s
	• Shower	0.1 – 0.2 litres/s
	• Washbasin	0.1 litres/s
	• Washing-up	0.2 litres/s

Unvented single-shell and double-shell DHW tanks are usually cylindrical and are made from stainless steel plates and insulated with *40 mm* glass-wool, expanded polystyrene (EPS) or expanded polyurethane. The tank volumes typically range from 100 to 350 litres (ref. Section 2.4.2.2).

TNO-MEP in the Netherlands have developed a protocol for testing heat pump water heaters in accordance with standard daily tapping patterns/-classes (Oostendorp and Traversari, 2000). The heat pumps are tested for classes 3 and 4, which correspond to a daily consumption of 60ºC hot water of 150 and 180 litres. This corresponds to about 250 and 300 litres of 40ºC water at the tapping site.

Appendix G

Application of a Movable Insulating Plate in Cylindrical Single-Shell DHW Tanks

One way to reduce the internal conductive heat transfer and more or less eliminate the mixing in cylindrical single-shell DHW storage tanks, is to separate the hot and cold water volumes by means of a plate with low thermal conductivity – a so called movable insulating plate (ref. Section 3.3.4, *Application of a Movable Insulating Plate Inside the DHW Tank*).

G1 Design of the Balancing Weight

Since the density of the solid insulators of current interest presented in Table G1 on page G3 is in the order of 5 to 50 times lower than that of water, the buoyancy effect will force the insulating plate upwards when the plate is submerged in water. The resulting buoyancy force F on a submerged plate is calculated as:

$$F \approx (\rho_W - \rho_{IP}) \cdot g \cdot V \qquad \text{(G1)}$$

where V is the volume of the plate, g is the acceleration due to gravity and the subscripts W and IP refer to the water and the plate, respectively.

Since the average density of the insulating plate should be lower than that of the city water and higher than that of the hot water, an extra weight has to be attached to the plate in order to counterbalance the buoyancy force. The required mass of the balancing weight (M_{BW}) is calculated on the basis of the mass of the insulating plate (M_{IP}), the density of water (ρ_W) at an intermediate temperature (e.g. 35-40ºC), and the volumes of the insulating plate (V_{IP}) and the balancing weight (V_{BW}):

$$M_{BW} = (V_{IP} + V_{BW}) \cdot \rho_W - M_{IP} \qquad \text{(G2)}$$

where the subscripts BW and IP refer to the balancing weight and the insulating plate, respectively. As an example, a 50 mm XPS plate having a diameter of 495 mm will displace about 9.6 litres of water, and the required mass of the balancing weight will be roughly 10.5 kg.

Due to the relatively small total volume of the insulating plate and the balancing weight, the correct tuning of the mass of the balancing weight becomes very important. Figure G1 shows the weight difference per litre for city water at 5 to 20ºC and hot water at 60 to 85ºC.

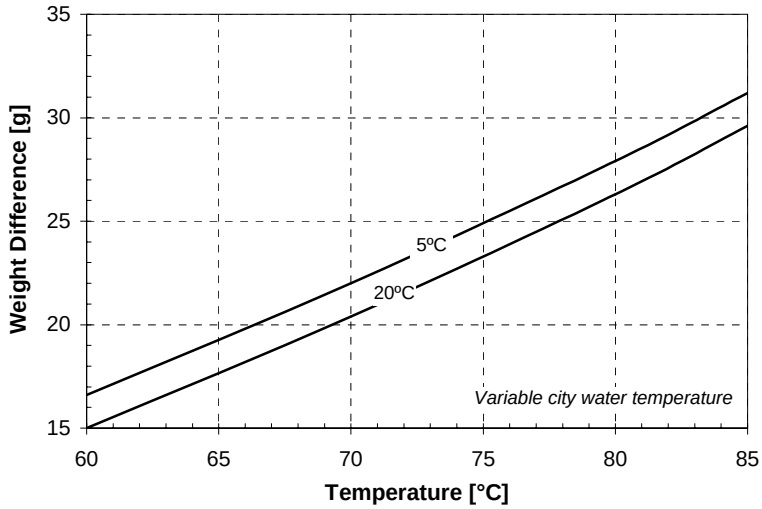

Figure G1 The calculated weight difference per litre for hot water at 60 to 85ºC and city water at 5 to 20ºC.

Figure G1 demonstrates that the tuning of the balancing weight is most critical when operating at relatively low hot water temperatures and relatively high city water temperatures.

G2 Thermal Resistance of the Insulating Plate

The conductive heat flux through a solid insulator is expressed as:

$$q = \frac{\Delta T}{\left(\frac{L}{k}\right)} \qquad \text{(G3)}$$

where ΔT is the temperature difference across the plate, and k and L are the thermal conductivity and the thickness of the plate, respectively. The thermal conductivity of 40ºC water and some solid insulators of current interest is presented in Table G1.

Table G1 The thermal conductivity of selected solid insulators and water at 40ºC.

Fluid / Material	Thermal Conductivity	
	[W/(mK)]	**[%]**
Water at 40ºC	0.628	100
Extruded polystyrene (XPS)	0.030 – 0.040	5 – 6
Cork	0.045 – 0.060	7 – 10
Cellular glass	0.055 – 0.070	9 – 11

Since the use of XPS will lead to roughly 35 to 45% lower heat flux in comparison with cork and cellular glass, XPS appears as a promising material for a movable insulating plate. However, XPS can only be used in DHW systems with storage temperatures below 75ºC.

Figure G2 shows the marginal percentage reduction in the unit thermal conductance and the consequent reduction in the heat flux through an XPS plate, when increasing the plate thickness from 5 to 250 mm. The thermal conductivity of the insulating plate is 0.035 W/(m^{2}K).

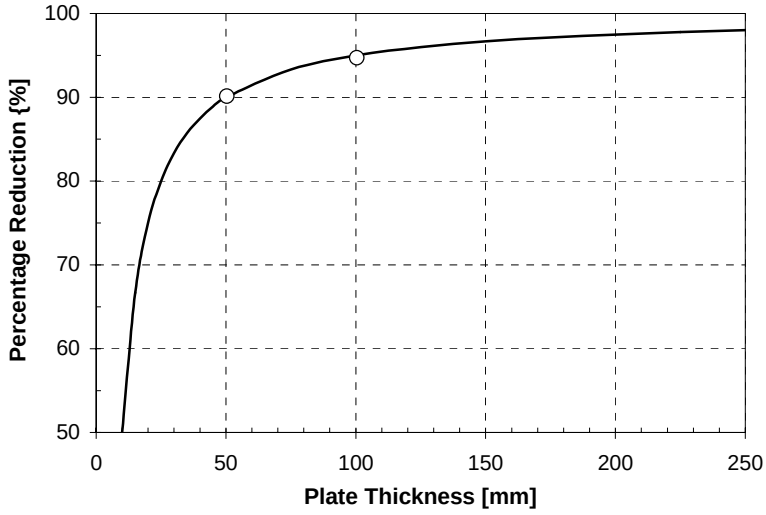

Figure G2 The calculated marginal percentage reduction in the heat flux through a XPS plate as a function of the plate thickness. The reference thickness is 5 mm.

A 50 mm XPS plate will reduce the heat flux by 90% compared to a 5 mm plate. However, by doubling the plate thickness to 100 mm, the marginal reduction in the heat flux is less than 5 percentage points.

Since the optimum thickness of the movable insulating plate depends on many technical and financial parameters, no optimisation has been carried out. However, by employing 50 mm XPS for the insulating plate, the heat flux between the hot and cold water volumes will be in the same order of magnitude as the heat flux between the water and the ambient air. As a consequence, 50 mm XPS was used when testing the hydrodynamic function and thermal performance of a movable insulating plate in a standard-sized DHW tank in the laboratory (ref. Section 4.2, *Testing of a DHW Tank and a Movable Insulating Plate*).

G3 Important Factors Regarding Material Selection and Plate Design

The hydrostatic balance of the insulating plate is affected by the weight of the plate. *If the plate absorbs water*, the average density of the plate and the balancing weight may become larger than the density of the cold water in the tank, and *the plate will sink*. As an example, XPS has an average water absorption of 0.3 volume %. For an insulating plate having a thickness of 50 mm and a diameter of 495 mm, 0.3% water absorption will increase the weight by roughly 30 grams. Consequently, in order to avoid operational malfunction, the insulating material should have a very low water absorption, or the maximum water absorption should be taken into account when calculating the required mass of the balancing weight.

The hydrostatic balance of the insulating plate is affected by the volume of the plate. *If the plate expands* during operation due to the elevated temperature at the upper part of the plate, the displaced water volume will increase and the hydrostatic balance will be altered. Consequently, if the average density of the insulating plate and the balancing weight becomes less than the density of the hot water in the tank, *the plate will move upwards*. For an insulating plate having a thickness of 50 mm and a diameter of 495 mm, 1% thermal expansion will increase the volume of the plate by roughly 0.1 litres, which corresponds to about 100 grams weight difference. Consequently, in order to avoid operational malfunction, the insulating material should have a very low thermal expansion coefficient, or the average thermal expansion should be taken into account when calculating the required mass of the balancing weight.

During the tapping period, cold water flows into the DHW tank below the insulating plate. Depending of the design of the inlet pipeline and diffuser, some of the dissolved air in the water will form *air bubbles* of various sizes at the underside of the plate. Since the bubbles are attached to the surface, they will create an undesirable buoyancy force that will alter the hydrostatic balance of the plate. This problem can be solved, for instance by designing the underside of the plate with a conical shape, and applying a non-wetting surface coating, i.e. a coating that leads to a small contact angle α for the bubbles. Due to the buoyancy force and the slippery surface, the bubbles will slide towards the cylindrical gap between the plate and the tank wall and rise quickly to the top of the tank. Figure G3 shows the principle of water bubbles on non-wetting and wetting surfaces, whereas Figure G4 presents a possible design for a movable insulating plate equipped with a conical balancing weight.

Figure G3 *Principle of water bubbles on a non-wetting (a) and a wetting (b) surface. α is the contact angle of the bubbles.*

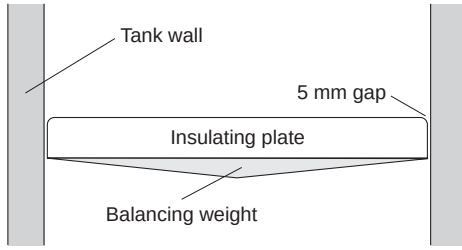

Figure G4 *Possible design of a movable insulating plate equipped with a balancing weight.*

The conical shape and the placement of the balancing weight are favourable for the hydrodynamic stability of the insulating plate, since the centre of gravity will be below the underside of the insulating plate. However, *higher thermal performance will be achieved if the balancing weight is placed at the top of the insulating plate* since the cold city water will not be heated by the balancing weight.

Appendix H

Test Conditions for the Prototype Movable Insulating Plates

With reference to Section 4.2, *Testing of a DHW Tank and a Movable Insulating Plate*, both insulating plates (diameter 490 and 495 mm) were tested in accordance with the test procedures described in Table H1.

Table H1 Test conditions for the movable insulating plates.

Mode [1]	DHW tank [2]	Mass Flow [3]		Visual Observations and Temperature Measurements	
		l/min	cm/min	Type [4]	Flow Control – Comment [5]
Tapping	Open	6	3.0	Dye/obs.	Continuous flow
	Open	12	6.1	Dye/obs.	Continuous flow
	Open	18	9.2	Dye/obs.	Continuous flow
	Open	24	12.2	Dye/obs.	Continuous flow
	Open	30	15.3	Dye/obs.	Continuous flow + frequent start/stop
Tapping	Closed	6	3.0	Dye/obs.	Continuous flow
	Closed	12	6.1	Dye/obs.	Continuous flow
	Closed	18	9.2	Dye/obs.	Failure (leakage) due to stucked plates
	Closed	24	12.2	Dye/obs.	Failure (leakage) due to stucked plates
	Closed	30	15.3	Dye/obs.	Failure (leakage) due to stucked plates
Charging	Open	0.25	3.9/h	Dye/obs.	1 kW electric heater, 60°C hot water
Static	Open	0	0	Dye/obs.	Plate in the middle of the tank – 8 hour test
Static	Open	0	0	Temp.	Plate in the middle of the tank – 24 hour test

1) *Mode:* *Tapping – city water supplied through the diffuser*
Charging – cold water heated to 60℃ and returned at the top of the tank
Static – no water flow through the tank

2) *DHW tank:* *Cover at the top of the tank – open or closed*

3) *Mass flow:* *Mass flow rate through the diffuser or through the entire tank*

4) *Type:* *Dye/obs. = dyed water, observations, Temp. = temp. measurements*

5) *Flow contr.* *Continuous water flow or frequent on/off during testing*

Appendix I

The Transient Two-Dimensional Tank Model

Reference is made to Section 6.2, *Modelling of Single-Shell Cylindrical DHW Tanks*, for a detailed description of the transient two-dimensional heat conduction model, also termed the tank model.

I1 The NMF[1] File for the Tank Model

CONTINUOUS_MODEL Conduct

ABSTRACT
"Calculation of the transient temperature development (static thermocline) of water in circular DHW tanks. The transient, two-dimensional conduction model (tank model) includes conductive heat transfer inside the tank and between the ambient air and the water. The initial temperature profile is set by the user. The thermophysical properties of water (cp, ρ and k), which are from RnLib (2003), are calculated as temperature dependent functions of first and second order."

EQUATIONS

```
/*  Energy balance for each node - axial and radial heat transfer included  */

FOR i=1,n
    IF i==1 then
        (AT-T[1]) * (U*PI*(Di**2)/4 + PI*Dy*dx*U)
    ELSE
        ((PI*(Di**2)/4)*(0.0013*T[i]+0.5731)/dx)*(T[i-1]-T[i])
    END_IF
        +
    IF i==n then
        (AT-T[n]) * (U*PI*(Di**2)/4 + PI*Dy*dx*U)
    ELSE
        ((PI*(Di**2)/4)*(0.0013*T[i]+0.5731)/dx)*(T[i+1]-T[i])+
          PI*Dy*dx*U*(AT-T[i])
    END_IF
        =
        ((PI*(Di**2)/4)*(-0.3975*T[i]+1006)*(0.0144*(T[i]**2)-
          1.2066*T[i]+4202.6*)*dx)*T'[i]
END_FOR;
```

[1] *Neutral Model Format (Sahlin, 1996)*

```
/*  Energy and temperature equations at side a and b of the element  */
    Ta = AT;
    Tb = AT;
    Qa = U2*PI*((D**2)/4)*(AT-T[1]);
    Qb = U2*PI*((D**2)/4)*(AT-T[n]);
```

PARAMETER_PROCESSING

```
/*  Calculations of constants  */
    dx := H/n;
```

LINKS

```
/*  Type      Name      Variables  */
    TQ        a_side    Ta,POS_IN Qa;
    TQ        b_side    Tb,POS_IN Qb;
```

VARIABLES

```
/*  Type      Name    Role  Def  Min  Max  Description  */
    Temp      T[n]    OUT   0                "Temp. at each node"
    Temp      Ta      IN    65               "Temp. for side a of element"
    Temp      Tb      IN    10               "Temp. for side b of element"
    HeatFlux  Qa      OUT   0                "Heat flow rate into side a"
    HeatFlux  Qb      OUT   0                "Heat flow rate into side b"
```

PARAMETERS

```
/*  Supplied parameters  */
/*  Type        Name  Role  Def  Min  Max  Description  */
    HeatCondL   U     S_P   1               "U-value, ref. Dy”
    Length      Di    S_P   1               "Inner diameter - DHW tank"
    Length      Dy    S_P   1               "Outside diameter - DHW tank"
    Length      H     S_P   1               "Height - DHW tank"
    Temp        AT    S_P   1               "Ambient air temperature"

/*  Calculated parameters  */
/*  Type        Name  Role  Def  Min  Max  Description  */
    Length      dx    C_P   0               "Node distance = H/n"
```

MODEL_PARAMETERS

```
/*  Type      Name      Role  Def  Min    Max      Description  */
    INT       n         SMP   10   1      BIGINT   "Number of nodes"
```

END_MODEL

I2 The IDA[2] File for the Tank Model

ABSTRACT
"Calculation of the transient temperature development (static thermocline) of water in circular DHW tanks. The transient, two-dimensional conduction model (tank model) includes conductive heat transfer inside the tank and between the ambient air and the water. The initial temperature profile is set by the user. The thermophysical properties of water (cp, ρ and k), which are from RnLib (2003), are calculated as temperature dependent functions of first and second order.

The output files display the transient temperature profiles in the DHW tank as a function of the time t. The variables and the input parameters are as follows:

T[n], Ta, Tb	Water temperatures	[°C]
AT	Ambient air temperature	[°C]
Qa, Qb	Heat flux from side a and b	[W]
U	U-value for the tank walls, ref. Dy	[W/m2K]
Di	Inner diameter of the DHW tank	[m]
Dy	Outside diameter of the DHW tank	[m]
H	Height of the DHW tank	[m]
n	Number of nodes	[-]
dx	Node distance = H/n	[m]

The water in the DHW tank is treated as a single element with an initial temperature profile (def-file) supplied by the user"

```
! Name of the output file (print-file)
FILES
  OUTPUT OUTPUT1
    PATH DHW70_10.PRN
END_FILES

! Input parameters  for the module
MODULES
    MODULE Water
        TYPE   Conduct
        n      200
        AT     20
        Di     0.50
        Dy     0.58
        H      1.02
        U      1.05
END_MODULES
```

[2] *Equa Simulation Technology Group (1996)*

```
! There are no connections since there is only one module (Water)
CONNECTIONS
END_CONNECTIONS

! Boundary conditions for the element
BOUNDARIES
    Water.Qa 0.0
    Water.Qb 0.0
END_BOUNDARIES

! Initial temperature profile for the water in the DHW tank
START_VALUES
    DEFAULT 0.0
    INCLUDE DHW70_10.def
END_START_VALUES

! Simulation conditions - 43200 sec. (12 h) with varying time step
INTEGRATION
    FROM 0.0
    TO 43200.0
    STEP 60.0
    TOL 0.00001
    TOL_LIM 0.1

! Description of which results that are written to the monitor
LIST
    OUT_ALL
    OUT_TIMES
        0 1 1
    END_TIMES
        Water.T(1)      Water_T1
        Water.T(100)    Water_T100
        Water.T(200)    Water_T200
END
LOG

! Description of which results that are written to files (*.res, *.end, *.prn)
FILE OUTPUT1
    Water.Qa      Water_Qa
    Water.Qb      Water_Qb
    Water.Ta      Water_Ta
    Water.Tb      Water_Tb
    Water.T(1)    Water_T1
    Water.T(2)    Water_T2
    Water.T(3)    Water_T3
    Water.T(4)    Water_T4
    Water.T(5)    Water_T5
```

```
    Water.T(6)    Water_T6
    Water.T(7)    Water_T7
    Water.T(8)    Water_T8
    ……
    Water.T(50)   Water_T50
    ……
    Water.T(100) Water_T100
    ……
    Water.T(150) Water_T150
    ……
    ……
    Water.T(200) Water_T200
    END
END_INTEGRATION
```

I3 Procedures when Establishing, Converting and Running the NMF and IDA Files

- Programme the **NMF-file** (*.nmf)
- Programme the **IDA-file** (*.ida)
- Establish the **DEF-file** (*.def) – displays the initial temperature profile
- Establish the **TYP-file** (*.typ) – lists the active NMF-files in the model
- Start the **IDA NMF translator**
- Select the IDA Options (C/C++, GnuC egcs-1.1.2, numerical Jacobians)
- Activate the TYP-file (Project → New)
- Convert the NMF-file to C/C++ format (Translate Current Project)
- Convert the file in C/C++ format to DLL-format (Project → Make DLL)
- Run simulation (ida i=*.ida) – starts the **IDA solver**
- Display **Results** – the time dependent node temperatures and boundary heat fluxes are displayed in PRN, RES and END-files
- Transfer the PRN-file to **MS Excel** for further processing